

Molecular design and characterization
of glycerol-based thermoresponsive polymers and
coatings for tissue culture applications

Inaugural-Dissertation
to obtain the academic degree
Doctor rerum naturalium (Dr. rer. nat.)

submitted to the Department of Biology, Chemistry, Pharmacy
of Freie Universität Berlin

by

M.Sc. Alexander Schweigerdt

Berlin, July 2024

This work was conducted from February 2019 to July 2024 under the supervision of Prof. Dr. Marie Weinhart at the Institute of Chemistry and Biochemistry of Freie Universität Berlin.

1st reviewer: Prof. Dr. Marie Weinhart

2nd reviewer: Prof. Dr. Rainer Haag

Date of defense: 06.12.2024

Acknowledgements

I would like to warmly thank Prof. Marie Weinhart for the chance to conduct my doctoral research under her supervision, the scientific advice and for being the first reviewer of my thesis. Furthermore, I would like to thank Prof. Rainer Haag for his role as the second reviewer and the possibility to use the build-up infrastructure in the research facilities for my work.

Special thanks go out to Dr. Daniel Stöbener for his constant support and feedback during my work, as well as the helpful discussions and idea exchange, which helped me to grasp the research and background concepts on a profound level and shape my scientific skills and knowledge. I would further like to thank Dr. Laura Elomaa and Ahed Almalla for the nice atmosphere in the office and the inspiring discussions in and out of the work field. I further kindly thank Andrea Cosimi for the mutual support, exchange of the ideas and the first proofreading of my doctoral thesis. I would like to thank Johanna Scholz for taking care of organization and ordering matters and together with Elisa Quaas for the training for cell culture practice. Further thanks go out to Dr. Wiebke Fischer and Kerstin Battermann for having the solution and help to every organizational question.

Big thanks go out to all supervised students, namely Florian Junge, Julian Woelffer, Jenny Stephan, Otto Staudhammer, Wesley Pietsch and Inar Fallaha, which supported the research and development of scientific ideas with their work. Additionally, I would like to thank all other current and former members of the AG Weinhart for the pleasant working atmosphere and scientific exchange. I would further like to thank Dr. Doğuş Işık, Dr. Thi Mai Phuong Neumann-Tran and Cathleen Hudziak for the measurement and evaluation of GPC samples for my work. Additional thanks go out to the NMR Core Facility members for the measurement and evaluation of non-trivial NMR spectra. Furthermore, I would like to thank the Haag group for the relaxed atmosphere in and outside of work and the lovely talks and discussions.

Finally, my gratitude goes towards my friends and family, who always patiently supported me during all challenging times. A special mention goes to my mother. Without her support many things would not have been possible, and I will be always grateful for her unconditional, tireless support to help me achieve my goals and dreams.

Declaration of authorship

I hereby declare that I alone am responsible for the content of my doctoral dissertation and that I have only used the sources or references cited in the dissertation.

Berlin, July 2024

Alexander Schweigerdt

Table of Contents

1.	Introduction.....	1
1.1.	LCST-type polymers for cell culture applications	2
1.2.	Fundamentals of a LCST transition	4
1.3.	Design principles for non-ionic LCST polymers	7
1.4.	Transfer to thermoresponsive surfaces	9
1.4.1.	Grafting-to and grafting-from approaches for brush fabrication.....	10
1.4.2.	RAFT polymerization	14
1.5.	Surface properties and phase transition	16
1.6.	Parameters for successful cell sheet fabrication.....	19
1.7.	Coating translation, sterilization and storage stability	22
2.	Objectives.....	26
3.	Publications and Manuscripts	27
3.1.	Grafting Density-Dependent Phase Transition Mechanism of Thermoresponsive Poly(glycidyl ether) Brushes: A Comprehensive QCM-D Study.....	27
3.2.	Impact of Amphiphilicity Balance in Hydroxy-Functional, Isomeric, Thermoresponsive Poly(meth)acrylates	53
3.3.	Thermoresponsive brush coatings for cell sheet engineering with low protein adsorption below and above the polymers' phase transition temperature	96
4.	Short summary	159
5.	Kurzzusammenfassung	161
6.	Outlook	164
7.	References	165
8.	Publications and conference contributions	174

1. Introduction

Polymeric materials that rapidly respond to external stimuli such as light, mechanic stress, redox potential, pH or temperature are valuable for applications as self-healing surfaces, actuators, biosensors or drug delivery systems.¹⁻⁶ Temperature-induced polymer responses are particularly interesting due to their ease of implementation, relevance to biological processes, and the robustness of many biological systems to moderate temperature variations. Polymers in solutions can respond to temperature shifts by undergoing solvation changes, leading to phase separation into a polymer phase and a solvent phase. Polymers that demix upon rising temperature, thus, exhibit lower critical solution temperature (LCST) behavior, while those that demix upon decreasing temperature exhibit upper critical solution temperature (UCST) behavior.⁷ Technically, the LCST is strictly defined as the minimum of the binodal curve in a phase diagram (Figure 3),⁸ but for the sake of readability, the term is used interchangeably to describe the general phenomenon in the following text, irrespective of the polymer concentration.

Polymers with LCST behavior in aqueous solutions below the human body temperature ($\sim 37\text{ }^{\circ}\text{C}$) are especially relevant in biomedical applications.⁴ As cell culture substrates, thermoresponsive polymers enable temperature-controlled cell detachment. Conceptually, the dehydrated polymer coating is adhesive to proteins and cells above the LCST, allowing cell attachment and proliferation. Reducing the temperature below the LCST then induces coating hydration, making it unfavorable for protein and cell interactions. Consequently, cultured cells detach from the surface, available for tissue replacement, wound healing, or for disease or drug screening models.^{5, 9} A major advantage of this method is the preservation of cell-cell junctions and the extracellular matrix (ECM), providing a viable cell environment. This contrasts with biochemical disruption of cells through trypsinization or physical disruption through scraping, both of which damage cell junctions and the ECM, causing unnecessary stress to cultured cells (Figure 1).^{10, 11}

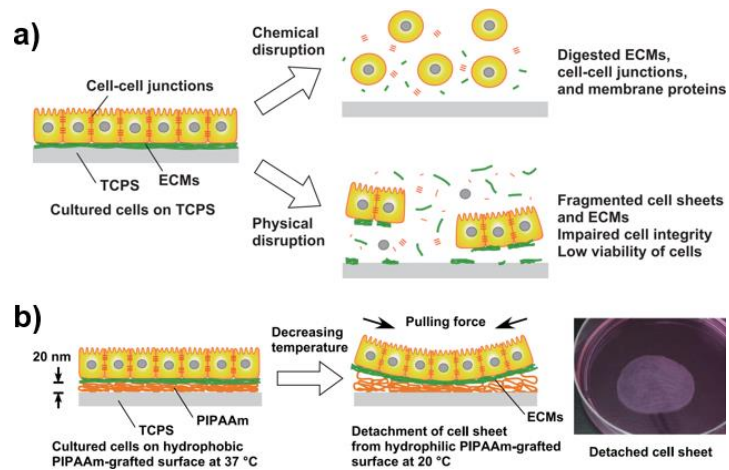


Figure 1. (a) Impact of chemical or physical disruption on cultured cells. (b) Temperature-triggered detachment of a whole cell sheet with intact cell junctions and ECM matrix from a thermoresponsive PIPAAm polymer layer with a photograph of a detached sheet. (a) and (b) adapted with permission from Kobayashi *et al.*¹¹ Copyright 2019 John Wiley and Sons.

In practice, successful utilization of LCST-type polymers as thermoresponsive coatings for reliable cell culture and detachment platforms depends on several polymer properties and optimization steps. The polymer must be biocompatible to avoid cytotoxicity and adverse effects on cell functions like metabolism, proliferation, and gene expression.¹² Parameters such as coating architecture, thickness, grafting or crosslinking density, and surface roughness must be optimized to ensure proper cell adhesion at culture conditions (37 °C) and detachment (usually at room temperature, ~20 °C). These parameters may need further specific adjustment for distinct cell types.^{5, 11, 13} Additionally, the coating must remain stable during application and storage time. Lastly, compatibility with common heat, gas or radiation sterilization techniques is essential for a translation into biomedical field.

1.1. LCST-type polymers for cell culture applications

Although a wide variety of neutral LCST-type polymers has been described in the literature,⁷ only a few polymer classes have been emphasized for cell culture applications. A common feature of these polymers is the structural diversity of the foundational monomers, which allows for fine-tuning of the LCST behavior. The first discovered and most studied LCST-type polymer is poly(*N*-isopropyl acrylamide) (PIPAAM), belonging to the class of poly(acryl amide)s (PAAM).^{8, 9, 14, 15} Thermoresponsive poly(oxazoline)s (POX) are structural isomers of PAAM polymers, with amides incorporated into the polymer backbone.¹⁶ They are furthermore considered a more stable alternative to water soluble poly(ethylene glycol) (PEG) due to the higher oxidation stability of amide bonds compared to ether bonds.¹⁷ Another polymer class that initially emerged as an alternative to PEG is poly(oligoethylene (meth)acrylate) (POEG(M)A). In this group, (meth)acrylic acids esterified with oligoethylene chains, usually

Introduction

comprising one to eight repeating units and terminated either with a hydroxyl or short alkoxy group, enable a wide range of LCST fine-tuning.^{18, 19} Structurally, PEG chains can also be tuned thermoresponsive by incorporating short alkyl chains, e. g., through the incorporation of propylene oxide (PPO)²⁰ or alkoxy side chains on the polyether backbone. The integration of alkoxy groups can be achieved through the polymerization of glycidyl ethers to poly(glycerol ether) (PGE), with different alkoxy chain lengths, guiding the LCST fine-tuning.²¹ Polymer examples used directly for successful cell sheet detachment along with exemplary LCST values are shown in Figure 2.

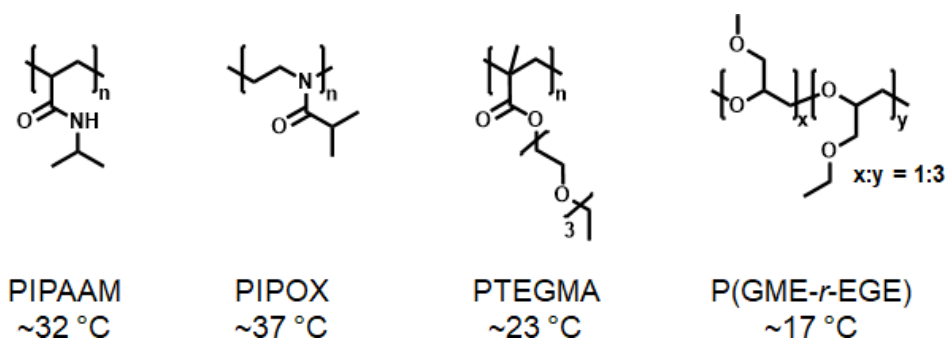


Figure 2. Examples of polymer structures, and their respective LCST values, that have been successfully utilized for cell sheet fabrication, from left to right: PIPAAM, poly(isopropyl oxazoline) (PIPOX), poly(tri(ethylene glycol) monoethyl ether methacrylate) (PTEGMA) and poly(glycidyl methyl ether-*r*-ethyl glycidyl ether) (P(GME-*r*-EGE)).²²⁻²⁵

Several parameters of PIPAAM coatings have been investigated, including substrate type, layer thickness, coating methods and structures.²⁵⁻²⁸ Modifications such as the incorporation of ionic comonomers, cell-adhesive peptides or patterned structures have also been examined.²⁹⁻³¹ Electron beam polymerization of IPAAM monomer on tissue culture polystyrene (TCPS) surfaces, popularized by *Okano* and coworkers, led to the creation of the first commercial thermoresponsive dish for cell culture, UpCell™.^{32, 33} However, the e-beam method requires expensive equipment and can suffer from batch-to-batch reproducibility issues.^{24, 25, 34} Additionally, the extensive literature on PIPAAM surfaces encompasses highly diverse across various substrate types, complicating the extraction of general design guidelines. This issue may stem from the differing requirements of various cell types, such as human umbilical vein endothelial cells (HUVEC) or smooth muscle cells (SMC), which require either specific PIPAAM modifications or alternative coating procedures, thereby limiting the general applicability.^{30, 35, 36}

Research on PIPAAM alternatives has shown that POEGMA polymers often lack intrinsic protein and cell-adhesion properties, thus requiring modification with cell adhesion-enhancing peptides for cell sheet preparation.¹³ Few reports of cell sheet detachment from POX surfaces also rely either on extensive modifications³⁷ or grafting processes in acetonitrile, limiting their

Introduction

applicability on PS, TCPS or PC substrates, due to limited solvent resistance.^{23, 38, 39} In consequence, functional POEGMA or POX coatings on application relevant PS, TCPS, PET or PC substrates or the detachment of different human cell types have not been reported so far.

PGE brush systems on glass, PS, and TCPS surfaces have emerged as a promising platform for versatile cell sheet fabrication.^{40, 41} HUVECs, human aortic SMC and human dermal fibroblasts (HDF) can be cultured on PGE brush coatings immobilized on PS substrates²² and a recent report demonstrated the modulation of dendritic cells for regenerative purposes on unmodified PGE brushes and hydrogels.⁴² The structured approach of grafting well-characterized polymer chains to gold, glass, PS, TCPS, PC and PET surfaces renders PGE brushes a viable candidate for investigating structure-property relationships in thermoresponsive phase transitions.^{43, 44} However, limited long-term stability and susceptibility to degradation under sterilization conditions due to chain oxidation and scissoring, similar to PEG, can limit the translation potential of PGE chains.⁴⁵⁻⁴⁷

A polymer alternative to PGE, designed with temperature transition fundamentals and rational guidelines could provide a more robust cell sheet fabrication platform. Developing a straightforward well-defined coating procedure for cell sheet fabrication, along with thorough characterization in solution and on surfaces would be an important step toward universally functional cell culture substrates for temperature-triggered cell sheet fabrication. Studies of thermoresponsive properties of PGE coatings can furthermore help to identify beneficial traits and provide meaningful comparisons with established and newly designed alternative polymers and coatings, especially when prepared in similar brush systems.

1.2. Fundamentals of a LCST transition

The solubility of a polymer in water can be described thermodynamically using the Gibbs mixing energy (ΔG_m), which includes enthalpic (ΔH_m) and entropic (ΔS_m) contributions, as well as the influence of temperature T , as shown in equation (1).

$$\Delta G_m = \Delta H_m - T \cdot \Delta S_m \quad (1)$$

The polymer becomes soluble when ΔG_m is negative and vice versa. The enthalpic contribution of a LCST-type polymer is usually given through the water interactions with the polymer chain, either through hydrogen bonds with hydrophilic polymer elements (e. g. amides, hydroxyl, carbonyl, or ether groups) or by forming an ordered shell around hydrophobic polymer elements with enhanced water hydrogen bonds. This leads to a negative enthalpic contribution, similar to the dissolution enthalpies of small alkanes in water known as the hydrophobic effect.^{48, 49} However, an entropic penalty for ordered water molecules results in a negative ΔS_m ,

Introduction

as opposed to a pure combinatorial approach for polymer-water mixing, which always results in $\Delta S_m > 0$. Hence, the entropy part of ΔG_m is positive, and with rising temperature, the entropic penalty outweighs the enthalpic contribution, resulting in a positive ΔG_m , the breakup of the ordered water shell and demixing of the polymer solution. At the turning point where ΔG_m equals zero (assuming temperature independent ΔH_m and ΔS_m) the demixing temperature T_m for a specific concentration can be obtained through equation (2).⁵⁰

$$T_m = \Delta H_m / \Delta S_m \quad (2)$$

Thus, the LCST transition is considered entropy-driven, as opposed to UCST transitions.⁵¹ In practice, LCST transitions are often concentration dependent. Determining T_m values with increasing polymer content in the mixture can then be used to create a polymer phase diagram with the binodal curve. The lowest T_m value defines the LCST point with the corresponding value of the lower critical polymer concentration (LCSC) (Figure 3).^{50, 51}

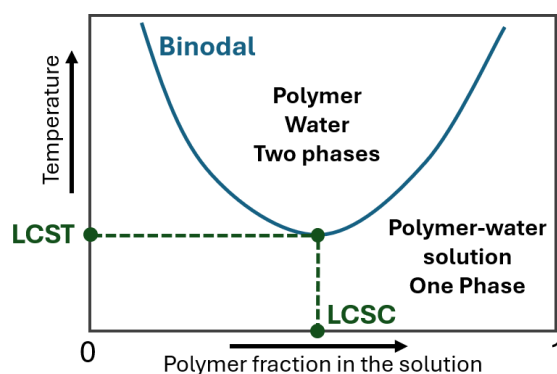


Figure 3. Schematic phase diagram for a polymer-solvent mixture exhibiting LCST behavior.

The determination of T_m values in solution is commonly conducted through turbidimetric UV/Vis measurements, dynamic light scattering (DLS), nuclear magnetic resonance spectroscopy (NMR) or differential scanning calorimetry (DSC), among other techniques. It is important to note that all results also depend on measurement parameters, and measurement conditions should be specified or ideally standardized for meaningful comparison.^{51, 52} Turbidimetry and DLS measurements detect changes in polymer aggregation, providing the cloud point temperatures (T_{cp}), which can be considered as the equivalent to the thermodynamic T_m . DSC measurements detect the endothermic disruption of water-polymer hydrogen bonds during phase separation. However, some thermoresponsive polymers exhibit transitions in turbidimetry, but not in DSC measurements, such as IPAAM copolymers with 2-hydroxyisopropylacrylamide P(IPAAM-co-HIPAAM), as shown in Figure 4.

Introduction

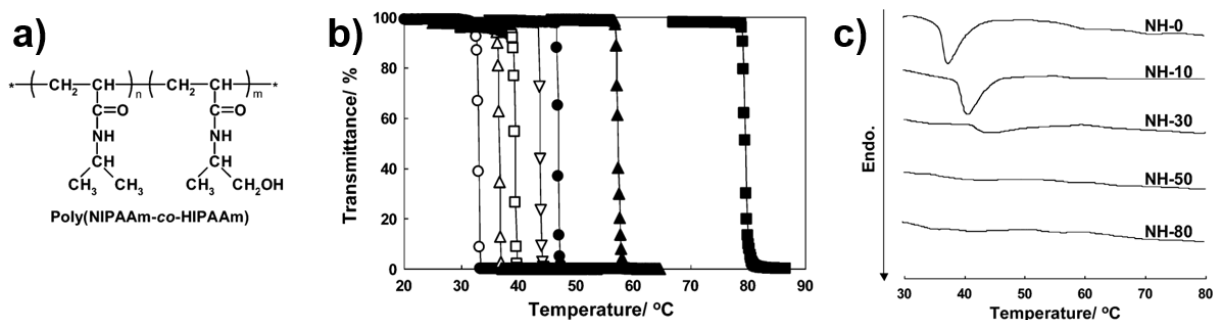


Figure 4. (a) The structure of thermoresponsive P(IPAAM-co-HIPAAm) copolymer with variable comonomer ratio according to n and m . (b) Turbidimetry curves of 1 w/v % copolymers in water with 0, 10, 20, 30, 40, 50 and 80% HIPAAM content (from left to right). (c) DSC diagrams of 10 w/v % copolymers in water with 0, 10, 30, 50 and 80% HIPAAM content (from top to bottom). (a) adapted with permission from *Maeda et al.*⁵³ and (b) and (c) adapted with permission from *Maeda et al.*⁵⁴ All copyrights 2006 American Chemical Society.

DSC analysis shows that the dehydration of the polymer chains decreases with rising HIPAAM content, revealing two different transition types. The first type is the coil-to-globule (CTG) transition (or liquid-solid phase separation), where the hydrated random coil collapses into a compact, water depleted polymer globule upon dehydration. This transition is typical for PIPAAm and also occurs in POX and PGE polymers.^{55, 56} The second type involves the more hydrophilic copolymers with at least 50% HIPAAM content, which undergo a liquid-liquid phase separation (LLPS), forming a coacervate with polymer-rich droplets, which still contain water and a polymer-depleted water phase. This behavior is also observed in PEG-PPO copolymers, several POEGMA polymers and poly(4-hydroxybutyl vinyl ether) polymers.^{20, 57, 58} The crossover from a liquid-solid to a liquid-liquid phase separation type with increasing HIPAAM content is illustrated in Figure 5.

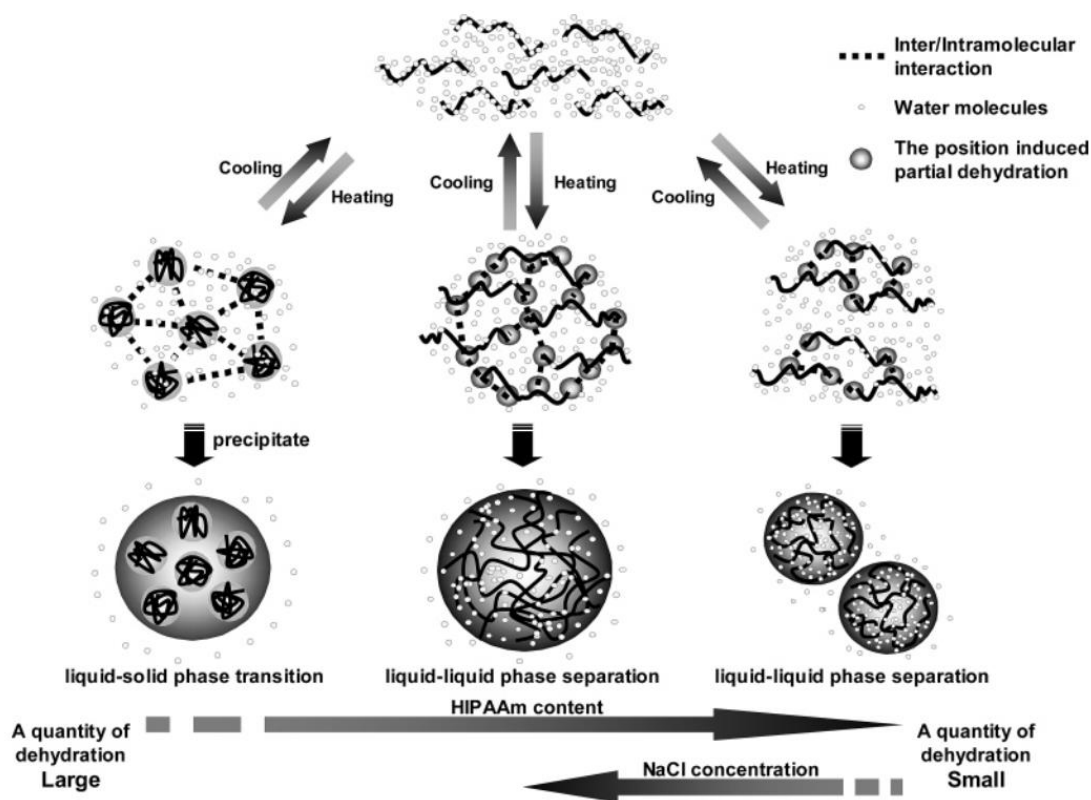


Figure 5. Schematic change of phase transition behavior from liquid-solid to liquid-liquid phase separation of P(IPAAM-co-HIPAAm) copolymers with rising HIPAAm content. Adapted with permission from *Maeda et al.*⁵³ Copyright 2006 American Chemical Society.

It is important to note that the transition type is a spectrum, and therefore polymers can exhibit varying degrees of dehydration upon the LCST transition. Polymers exhibiting LLPS behavior can be utilized in drug delivery and bioseparation applications.⁵⁹⁻⁶¹ However, cell sheet fabrication coatings without additional adhesion-enhancing modifications are usually based on CTG polymer types, such as PIPAAm or PGE, likely due to the inherent hydrophilicity of LLPS type polymers (e. g. POEGMA derivatives) even in the collapsed state, which does not facilitate cell adhesion.^{58, 62}

1.3. Design principles for non-ionic LCST polymers

For the successful design of a LCST polymer, monomer structures with the appropriate amphiphilic balance are essential. Balancing structural elements capable of hydrogen bonding, such as ether, hydroxy, amine, amide or sulfoxide groups, with hydrophobic counterparts leads to the continuous discovery of new thermoresponsive polymers. Some of these polymers also show a dual response to a second trigger, such as oxidative environments or pH changes.⁶³⁻⁶⁶ The quality of the hydrogen donor/acceptor (e. g. hydroxy or ether groups)⁶⁷, the accessibility of the group (e. g. unshielded hydroxy groups in HIPAAm and shielded amide groups in IPAAM or ether groups in PGE) and the quantity (e. g. several ether groups in POEGMA polymers

Introduction

with long side chains) govern the transition type between LLPS and CTG and naturally affect the location of the LCST. These effects can be exemplarily illustrated through isomeric polymer structures, e. g. of PAAM and POX derivatives and POEG(M)A isomers in Figure 6.

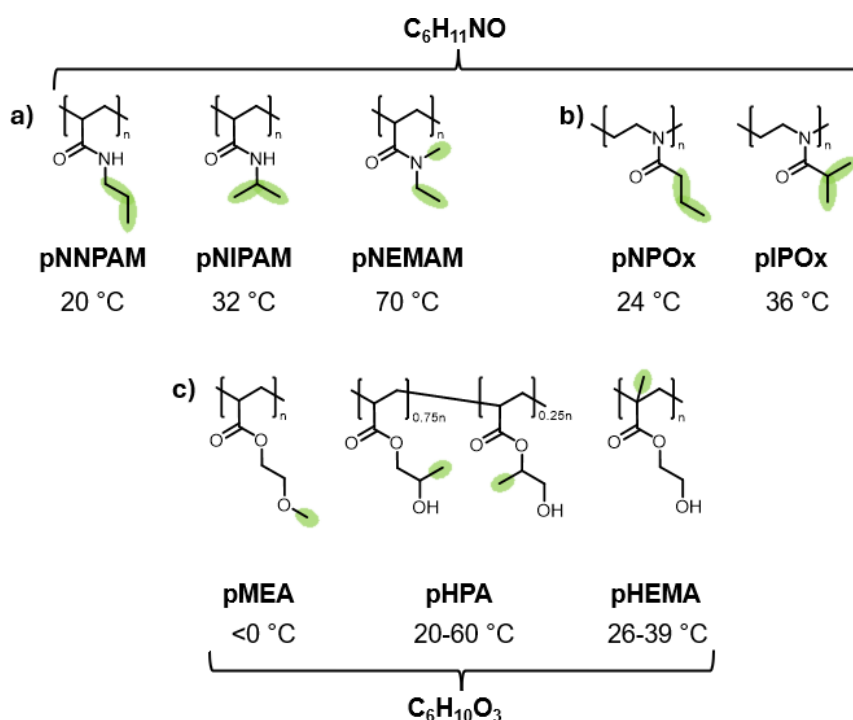


Figure 6. Structures and T_{cp} values of isomeric thermoresponsive PAAM^{8, 68, 69} (a), POX⁷⁰ (b) derivatives and isomeric POEG[M]A^{71, 72} derivatives (c). For PHPA, the most available and researched structure is presented.^{73, 74} Structural isomeric differences are highlighted. (a-c) adapted from Schweigerdt *et al.*⁷⁵ under CC-BY 4.0 license.

The T_{cp} values of PAAM and POX polymers are influenced by varying degrees of hydrophobic shielding of the amide group. In PAAM polymers, the amide groups are shielded by the hydrophobic propyl group and the aliphatic backbone. In contrast, POX polymers have more accessible backbone-incorporated amides, resulting in a T_{cp} increase of $\sim 4\text{ }^{\circ}\text{C}$ in isomeric poly(*N*-*n*-propylacrylamide) (PNNPAM) and poly(*n*-propyl oxazoline) PNPOX as well as PIPAAM and poly(isopropyl oxazoline) (PIPOX).^{8, 68, 70} Smaller hydrophobic moieties, as in poly(*N,N*-ethylmethyl acrylamide) (PNEMAM), significantly increase the LCST due to reduced amide shielding and entropic penalty required to solubilize the small hydrophobic groups and establish amide hydrogen bonds.⁶⁹ The opposite effect is seen when comparing isopropyl to *n*-propyl groups, as branched groups induce a smaller entropic penalty, resulting in higher T_{cp} values.^{48, 50} The difference between a strong (hydroxyl) and moderate (ether) hydrophilic moiety in isomeric polymers is demonstrated between the swellable PMEA and thermoresponsive PHPA and PHEMA polymers. However, T_{cp} values of PHPA between 20-60 $^{\circ}\text{C}$ significantly depend on the concentration and the molecular weight (M).^{73, 74} Similarly PHEMA polymers show a broad transition range for polymers with $M \leq 6\text{ kDa}$ and become

Introduction

insoluble, and thus only swellable, above this molecular weight.⁷¹ Polymers with several ethylene oxide units are in turn more hydrophilic, resulting in thermoresponsive or fully soluble polymers.^{18, 76, 77}

Fine tuning of LCST values is achieved through copolymerization, covering the temperature range between the LCST values of the homopolymers, as demonstrated with groups of POX, POEG(M)A and PGE copolymers.^{19, 76, 78} It is also feasible to use similarly designed monomers, if further functionalization is necessary. For instance, carboxyl groups for possible pH control and post-functionalization of PIPAAm were incorporated through copolymerization with acrylic acid (AA) or 2-carboxyisopropyl acrylamide (CIPAAM), resembling the structure of IPAAm with an additional carboxyl group. Incorporation of 5% AA to PIPAAm resulted in an ~ 10 °C increase of the T_{cp} value, while incorporating 5% CIPAAM did not affect the T_{cp} at physiological conditions (pH = 7.4).²⁹

Further parameters influencing the LCST value include the molecular weight of the polymers and polymer end groups.^{65, 79, 80} Higher molecular weight usually leads to lower LCST values due to higher local polymer concentrations of longer chains, which can enable hydrophobic aggregation at lower temperatures. However, the differences become less pronounced with increasing molecular weight.^{79, 80} Higher molecular weights also diminish the influence of hydrophobic or hydrophilic end groups, which can accordingly decrease or increase the LCST value.^{65, 80}

1.4. Transfer to thermoresponsive surfaces

The first step towards a thermoresponsive surface coating is the choice of an appropriate coating architecture, which then determines the suitable fabrication method. Various coating designs with diversely elaborate procedures have been described, ranging from simply physically adsorbed thermoresponsive polymer layers to hydrogels, brushes, bottlebrushes, and patterned brush architectures (Figure 7). The latter, for example, can allow simultaneous co-culture and harvesting of several cell types.^{24, 31, 81-84}

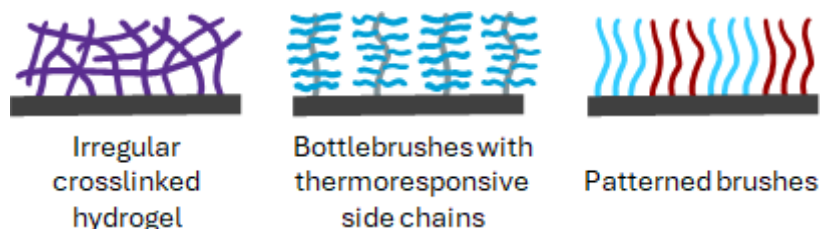


Figure 7. Schematic structures of various coating architectures used for cell sheet fabrication.

Hydrogel formation is a straightforward process, originating directly from monomers crosslinked *via* e-beam, plasma or UV irradiation, or from polymers with statistically

Introduction

copolymerized crosslinkers.^{5, 9, 42, 85, 86} A prominent example is the commercialized PIPAAm-based UpCell™ surface, prepared through e-beam irradiation of IPAAM monomer solution in isopropanol directly on a TCPS surface.⁹ However, these hydrogels often have ill-defined structures due to random crosslinking, leading to batch variation that can hinder proper structure-property relation analysis.²⁵

A more defined approach is provided through surface coatings in the form of brush structures. Brush coatings are primarily characterized by the grafting density (GD) and molecular weight of the polymer chains, which translate to brush length and coating thickness. Control over these parameters helps to optimize the brush coatings systematically on a molecular level, e. g. to achieve optimal antifouling performance or desired cell culture and detachment control.^{40, 87-90} For instance, PIPAAm brushes allow cultivation and detachment of HUVEC cells, while PIPAAm hydrogels only support HUVEC culture after additional modification with cell adhesion enhancing arginyl-glycyl-aspartic acid (RGD) peptide motif.^{30, 36} Optimizing the grafting conditions for PIPAAm brushes helped to identify ideal cell sheet fabrication conditions on glass⁹⁰, while optimizing PGE brush thickness through grafting density has determined the optimal grafting range on PS and TCPS surfaces, avoiding premature or hampered cell detachment.⁴⁰ Structure control further renders brush coatings valuable candidates for structure-property relationship studies of thermoresponsive behavior on surfaces.^{40, 91-93} Thus, parametrized brush functionalization further enhances surface design for an optimal performance.

Copolymerization and patterning techniques allow for defined layer-by-layer structures and multifunctional patterned surface structures.^{94, 95} For example, PIPAAm brushes with patches of *n*-butyl methacrylate (BMA) grafted on PIPAAm chains enabled the simultaneous cultivation of endothelial cells and hepatocytes and lowering the temperature allowed the detachment of the co-cultured cell sheets.³¹

1.4.1. Grafting-to and grafting-from approaches for brush fabrication

Generally, the preparation of brush surfaces can be approached via a grafting-from or grafting-to methods (Figure 8). Grafting-from procedures are mostly performed *via* controlled radical polymerization (CRP) techniques, such as atom transfer radical polymerization (ATRP) or reversible addition fragmentation chain transfer (RAFT),^{96, 97} although examples of free radical polymerization from the surface are also reported.³⁶ For this procedure, an initiator or chain transfer agent is immobilized on the surface and immersed into a monomer solution, which can include additional components, such as copper catalysts for ATRP, to initiate the reaction. Grafting density can be controlled through the degree of initiator immobilization, with high quantity immobilizations enabling grafting densities over 1.0 chains nm⁻² on planar surfaces.⁹⁸

Introduction

⁹⁹ Typical initiators containing alkyl halides for ATRP or di- or trithiocarbonate moieties for RAFT can be fixed on glass, silicon and gold substrates.^{24, 100, 101} Further grafting-from strategies from polymer surfaces, such as PS or PMMA, are also reported.^{25, 36, 102} Polymerization conditions with high monomer concentration or continuous monomer feed can enable brush thicknesses over 100 nm.¹⁰³ The main disadvantage of grafting-from strategies is the limited characterization potential, usually only encompassing surface morphology and layer thickness.⁹⁴ Molecular weight characteristics can be analyzed with chains obtained through cleavable surface linkers, but are instead often approximated from solution-polymerized chains, despite poor comparison potential.¹⁰⁴ Grafting densities are often estimated through initiator density, neglecting the initiator's reaction potential and thus non-activated initiator moieties.^{27, 94}

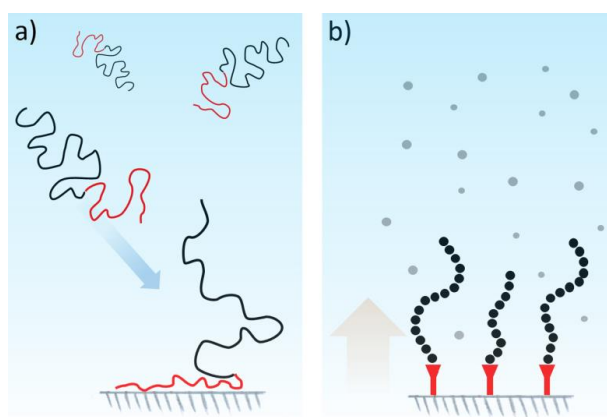


Figure 8. Schematic depiction of a grafting-to procedure via favored surface-anchor interactions (a) and a grafting-from procedure via surface-initiated polymerization process (b). Adapted from *Morgese et al.*, 2017,¹⁰⁵ with permission from Elsevier.

CRP techniques can polymerize (meth)acryl based monomers, rendering them suitable for the fabrication of PIPAAm and POEGMA based brush coatings,⁹⁷ but not for the living polymerization of POX or PGE polymers. However, all these polymers can be used for brush coating fabrication via the grafting-to technique.^{43, 44, 105, 106} As the name indicates, coatings are fabricated through covalent immobilization of polymer chains to the selected surface. Besides polymer versatility, the advantage of this method is that the polymers can be thoroughly characterized for their molecular weight, polydispersity and thermoresponsive behavior prior to immobilization.⁹⁴ After the immobilization process, grafting density can be calculated based on polymer density and coating thickness. However, grafting densities are limited since the polymer chains occupy more space, resulting in lower densities than brushes obtained *via* grafting-from methods at comparable molecular weights. Still, brush coatings with chains stretched above the solvated random coil conformation, are achievable through grafting process optimization, such as multi-step adsorption with flushing procedures and optimized solvation.^{40, 43, 93}

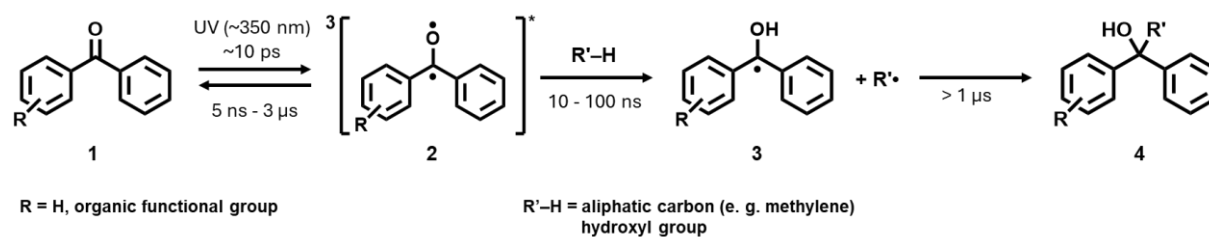
Introduction

The covalent immobilization of polymer chains is accomplished through reactive end groups. An anchoring layer on the surface may be required, necessitating additional modification, or the reactive end group can immobilize through specific surface attraction and suitable reactive pathways. For example, a poly(glycidyl methacrylate) anchoring layer was used to immobilize carboxyl terminated POX polymers of various molecular weights in brush formations.⁹³ It is also possible to graft POX chains directly from the polymerization solution using surface-immobilized termination groups.³⁸ Common immobilization procedures rely on click-chemistry reactions, such as azide-alkyne cycloaddition or thiol-ene reactions.^{107, 108} The latter can be conveniently performed with polymers synthesized *via* RAFT polymerization, followed by cleavage of the transfer agent to obtain the thiol group.¹⁰⁸ No surface modification is required for chemisorption of thiol-terminated polymers on gold surfaces, which creates stable gold-sulfur bonds.¹⁰⁹ Since gold surfaces are otherwise chemically inert and do not readily interact with polymer chains, they can be used as non-interacting substrates for model studies of self-assembly and characterization of brush surfaces,¹¹⁰ e. g. with the surface plasmon resonance (SPR) or quartz crystal microbalance with dissipation monitoring (QCM-D) techniques.^{43, 78, 89,}

108, 111

Another convenient immobilization approach, suitable for unmodified polymer substrates, is the use of photoreactive crosslinkers. Utilizing UV light as an activation source is an effective way to excite electrons and induce reactions, while avoiding thermal exposure. Additionally, hydrophobic reactive molecules can preferably interact with hydrophobic polymer surfaces, allowing directed adsorption or self-assembly. Benzophenone (BP) moieties are frequently used due to their effective excitation wavelength of ~350 nm, which minimizes the adverse effects on DNA, proteins, cells, or polymer structures. In addition, functional groups can be incorporated into the benzophenone structure, allowing it to be integrated into polymer, protein or dye molecules prior to the crosslinking process. Consequently, BP is often used in biological studies for bioconjugation, labeling or mapping molecule-protein interactions.^{112, 113} BP also exhibits good chemical and solvent stability, including polar solvents and water and is non-reactive under ambient light. A common photoinduced reaction pathway of BP, the C-H insertion, is shown in Scheme 1.

Introduction



Scheme 1. C-H insertion with structures of benzophenone (BP) in its ground state (1), biradical triplet state after excitation (2), ketyl radical intermediate after hydrogen abstraction (3) and recombination product with the remaining radical moiety $R'\cdot$ to complete the crosslinking process (4).^{114, 115}

Upon suitable excitation, the $n-\pi^*$ or $\pi-\pi^*$ electron transitions convert the BP moiety (1) into an excited singlet state S_1 or S_2 , respectively. Electrons from S_2 state rapidly undergo an internal conversion to S_1 and the energetically similar triplet states T_2 and T_1 facilitate efficient intersystem crossing into the triplet biradical state (2), which is considered the most reactive of several possible structures (Figure 9).¹¹⁴

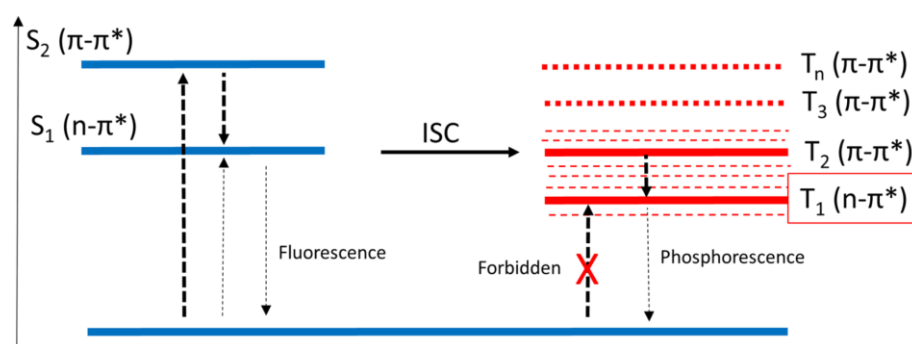


Figure 9. The Jablonski diagram of the photoinitiated electron transitions in benzophenone. Adapted with permission from *Dormán et al.*¹¹⁶ Copyright 2016 American Chemical Society.

Since photorelaxation (phosphorescence) from the T_1 state is “forbidden” by the laws of quantum mechanics, the triplet state can persist up for several μs , depending on the solvent and the type of the R group.^{115, 117} This stability allows for the execution of the C-H insertion (Norrish type II) crosslinking process, which begins with the formation of ketyl radical (3) after rapid hydrogen adsorption from a nearby aliphatic C-H or O-H bond (with a strong preference for C-H bonds). The subsequent recombination of the ketyl radical 3 and remaining radical leads to the comparably slow formation of the crosslinked product 4, as BP must return into a singlet state for the recombination. However, cross recombination occurs an order of magnitude faster than self-recombination with another ketyl radical, ensuring an effective crosslinking pathway.¹¹⁷

Benzophenone can be utilized in several ways to prepare thermoresponsive surfaces. BP adsorbed on poly(dimethyl siloxane) (PDMS) layers was used to fabricate grafted-from PIPAAm hydrogels *via* photoinitiated surface polymerization.¹¹⁸ Similarly, BP adsorbed on PS

Introduction

surfaces induced a grafting-from procedure for PGE-based bottlebrush systems.⁸³ Introducing BP moieties into polymer chains for grafting-to strategies can be achieved through simple copolymerization of suitable benzophenone functionalized monomers (e.g. benzophenone acrylamide with IPAAM)^{86, 119, 120} or through post-functionalization reactions.^{42, 44} Hydrogels of PIPAAM and PGE polymers with incorporated benzophenone groups were fabricated on PS or TCPS substrates *via* spin-coating or adsorption processes and crosslinked through irradiation.^{42, 86, 120} PGE copolymers terminated with short BP-blocks were also successfully selectively adsorbed and grafted to PS, TCPS, poly(ethylene terephthalate) (PET) and polycarbonate (PC) surfaces in brush regime through the design of appropriate BP linkers, which enhanced the affinity to the polymer surfaces.⁴⁴ The visualization of the selectivity approach on PS and TCPS is shown in Figure 10.

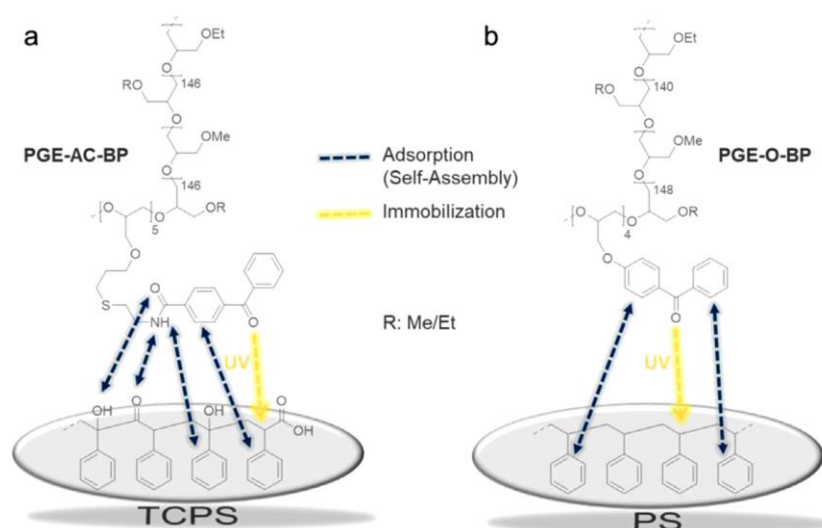


Figure 10. Affinity visualization of tailored BP anchoring units to TCPS (a) and PS (b) substrates for a directed self-assembly of PGE brushes. Adapted from *Stöbener et al.*, 2021,⁴⁰ with permission from Elsevier.

1.4.2. RAFT polymerization

Narrow dispersed polymer chains are required to fabricate homogeneous brush coatings with chains of similar length. The living polymerization procedures of POX and PGE polymers are well suited for narrow dispersed polymer synthesis but are incompatible with IPAAM and other monomers with potential proton donors. The development of CRP techniques, such as ATRP and RAFT, perfectly fills the gap, allowing the synthesis of narrow dispersed polymers from a wide range of monomer types. Both techniques are applied in the development of homogeneous brush layers, with ATRP grafting-from procedures on silicon and glass being particularly popular.⁹⁷ RAFT polymerization, however, supports a wider range of monomers, functional groups and solvents as well as milder conditions, enabling polymerizations at room temperature or in the presence of air.¹²¹⁻¹²³ Furthermore, copper catalysts employed in ATRP

Introduction

procedures can induce toxicity even in small quantities, rendering the polymers less suitable for biomedical applications.¹²⁴ Nevertheless, optimization of polymerization conditions including choice of solvent, temperature and RAFT agent, is required. The mechanism of a general RAFT polymerization procedure is shown in Figure 11.

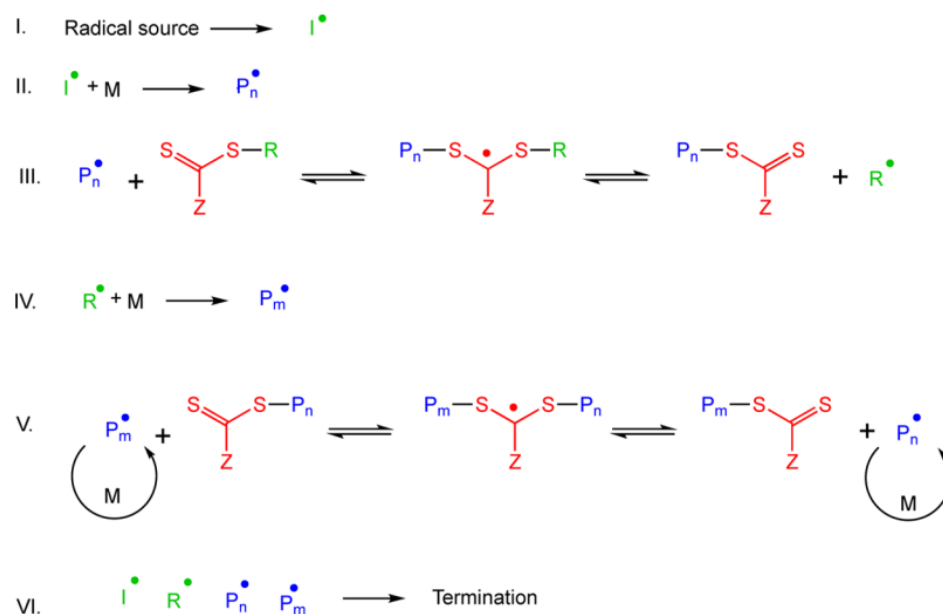


Figure 11. General mechanism of the RAFT polymerization process. Adapted with permission from Perrier *et al.*¹²² Copyright 2017 American Chemical Society.

Controlled radical polymerizations, including RAFT, rely on an equilibrium between active and dormant species to achieve chain growth control.¹²² In RAFT systems, control is obtained through di- and trithiocarbonate species (RAFT agents) that are susceptible to radical addition and fragmentation reactions, hence the name. These agents control the polymerization step and avoid premature chain termination by limiting the number of active species. As the number of radical species remains constant during polymerization, radicals must first be generated, typically *via* thermal radical initiators, such as azobisisobutyronitrile (AIBN) or 4,4'-azobis(4-cyanopentanoic acid) (ACPA) (step I in Figure 11). Once the polymerization is initiated, the radical species P_n^\bullet add to the RAFT agents, releasing the R^\bullet radicals and temporarily deactivating the polymerization, while the R^\bullet group initiates a new polymer chain (steps II-IV). Effective control is achieved through a slightly higher transfer rate than the propagation rate, ensuring that less than one monomer is added per transfer reaction (step V). This results in a similar degree of polymerization for all chains at any given time and can be facilitated by the R^\bullet group, which forms radicals and can be structurally similar to the radical initiator. The Z-group stabilizes the intermediate radical and adjusts the reactivity of the transfer agent to the propagation. A mismatch in reactivity can result in retardation or premature termination of the polymerization with low yields or freely propagating chains, thus limiting the polymerization control.¹²⁵ However, the wide range of available R and Z groups allows for tailored controlled

Introduction

conditions for almost all monomer types.¹²⁵ Termination occurs through the usual recombination or fragmentation reactions known from free radical polymerization (step VI).

As mentioned before, RAFT polymerization can be used to obtain PIPAAM and POEGMA brushes. The synthesized chains were grafted via thiol-gold or thiol-ene reactions to gold and glass surfaces and the surface parameters were comparatively analyzed to evaluate different grafting-to methods.¹⁰⁸ Grafting densities and chain lengths of RAFT grafted-from PIPAAM polymer chains were further systematically analyzed to determine optimal cell sheet detachment conditions.⁹⁰ Additionally, the functionalization of the terminal thiol group obtained from the cleavage of the RAFT agent also elucidated the influence of terminal functionalization on PIPAAM brushes.³⁵

1.5. Surface properties and phase transition

Covalently grafted brush and hydrogel layers are characterized by several properties: thickness values in dry and hydrated states, coating wettability and contact angle, surface morphology and coating density and stiffness, which usually correlate with water content.^{126, 127} Furthermore, protein adhesion is important for coatings designed for cell sheet fabrication. These extrinsic properties can be correlated with intrinsic molecular parameters, such as crosslinking density in hydrogel layers or molecular weight and grafting density in brush layers. For surface-tethered chains, the chain overlap, defined as the ratio of the chain radius ($2R$) to the anchor distance (l), is an important parameter that determines whether the conformation of tethered chains is in a stretched brush regime or in a more spread mushroom regime (Figure 12). The experimental gyration (R_g) or hydrodynamic (R_h) radius can be used for this purpose.^{43, 89} Alternatively, the theoretical Flory radius R_f can estimate the radius under different solvent conditions.^{89, 128}

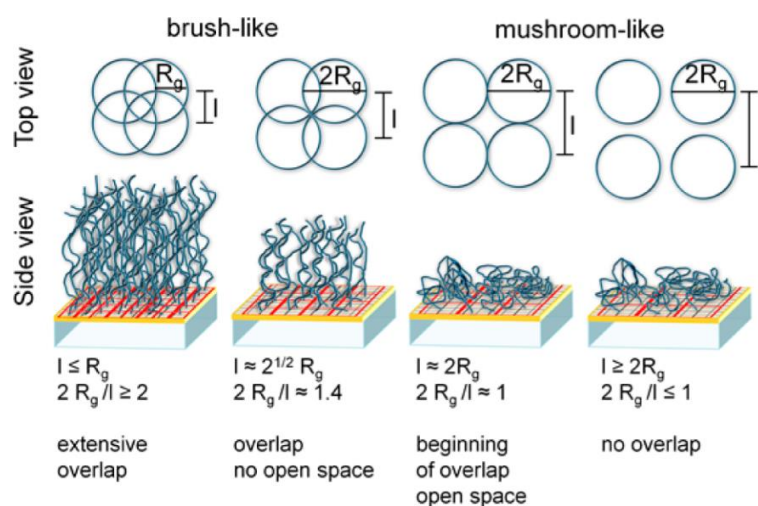


Figure 12. Schematic depiction of the brush or mushroom configuration of surface tethered chains based in the chain gyration radius R_g and anchor distance l . Adapted with permission from *Heinen et al.*⁴³ Copyright 2017 American Chemical Society.

Thermoresponsive brush (and hydrogel) surfaces gradually transition from a well hydrated, stretched, protein-repellent state to a dehydrated, collapsed, protein-adhesive state as temperatures rise. This volume phase transition (VPT) with the corresponding volume phase transition temperature (VPTT) typically occurs over a broad range (> 10 °C) due to the restricted chain movement and high polymer concentration on the surface, which can slow down water diffusion in and out of the layer.^{92, 129} Therefore, VPT detection measurements are often performed under quasi-static conditions to minimize transition lagging. During the transition, vertical phase separation (VPS) of the brush layer can occur, resulting in several vertical layers of different chain hydration, especially at extensive brush overlap regimes.^{91, 92, 130} At intermediate densities, brush radii can decline below the anchor distance value upon dehydration, leading to a brush-to-mushroom transition. Tracking the VPT transition through changes in these properties allows for a meaningful structure-property analysis.

The grafting processes can be monitored through quartz crystal microbalance with dissipation (QCM-D), allowing for direct assessment of polymerization or adsorption kinetics and layer thickness. Thickness buildup of grafted-from PEOGMA brushes was monitored up to 200 nm¹³¹ as well as grafting-to processes of thiolated PGE and PIPAAM brushes on gold with solvated thicknesses up to ~ 15 nm.⁴³ A further grafting-to study of thiolated PIPAAM brushes revealed different adsorption kinetics, depending on the molecular weight.¹¹¹

Characterization in the dry state typically focuses on thickness values, coating morphology and wettability *via* contact angle (CA) measurements. Dry thickness can be determined using spectroscopic ellipsometry, atomic force microscopy (AFM) or x-ray photoelectron spectroscopy (XPS). Ellipsometry is especially popular due to its quick non-invasive process and has been exemplary used to assess thickness values of concentration dependent

Introduction

grafted-to PGE brushes on PS and TCPS surfaces (3-9 nm) or thickness values (7-90 nm) for a series of ATRP grafted-from PIPAAM brushes.^{40, 132} Complementary AFM thickness measurements of identical PIPAAM brushes yielded values between 5-60 nm, due to adhesion between the AFM tip and brushes, inducing a systematic error, but also highlighting the utility of complementary measurements. AFM can also assess morphology differences between non-coated and coated samples to verify the brush presence,⁸³ and roughness differences in water at rising temperatures indicate the VPT.¹³³ Accordingly, wettability changes through rising static or advancing water CA of PGE and PIPAAM brushes between 20 and 37 °C verify the transition process with increasing hydrophobicity.^{40, 132} Differences in protein adsorption can be detected via QCM-D or SPR measurements.^{40, 78, 134} Furthermore, adsorption of common culture medium proteins, such as fibronectin or bovine serum albumin can be further monitored via fluorescent or radioactive labeling.^{17, 28, 135}

Several direct studies of the brush VPT process of PIPAAM, POEGMA, POX and PGE brushes, revealing transition mechanisms, were performed using temperature-dependent QCM-D or ellipsometry measurements in water, or a combination of these techniques. Temperature dependent QCM-D measurements of dense PIPAAM brushes with $M = 93$ kDa and thickness of 41 nm revealed a discontinuous transition process with several distinct steps and VPS of the brush layer.⁹¹ In contrast, identically probed PIPAAM brushes with $M = 12$ kDa and a thickness of 2.7 nm showed a continuous brush-to-mushroom transition process starting at 20 °C, well below the LCST value, and proceeding to 35 °C.¹³⁶ Several further QCM-D and ellipsometry studies with PIPAAM brushes of similar dimensions confirmed the early onset and continuous transition, especially at low grafting densities, revealing the influence of pronounced chain overlap differences.^{93, 137} Densely grafted POEGMA brushes with thickness values of 92 and 135 nm probed *via* QCM-D measurements also showed a VPS mechanism with a transition range of ~25°C, thus confirming the polymer independent occurrence of this effect. Contact angle measurements *via* the captive bubble method further revealed a distinct change in the outermost surface brush layer, complementary to the continuous bulk layer transition (Figure 13).⁹² This phenomenon was further observed on dense PIPAAM brushes.¹³⁸ Transition behavior of POX brushes ($M \sim 50$ kDa, thickness ~9 nm) with varying monomer composition and T_{cp} values was probed *via* complementary ellipsometry and QCM-D measurements and revealed an almost linear continuous transition between 20 and 50 °C, as opposed to similar PIPAAM brushes, which finish the transition process at ~36 °C.⁹³ This difference was attributed to the LCST type 1 behavior of POX polymers, which is more M and concentration dependent compared to the LCST type 2 transition of PIPAAM polymers. QCM-D studies of PGE brushes ($M \sim 28$ kDa) grafted to PS and TCPS substrates with varied grafting densities revealed that the hydrophobic PS substrates induce a “grounded” VPT with an almost

Introduction

completely dehydrated basal layer at all times, while moderately hydrophilic TCPS substrates result in a “cushioned” transition with a hydrated basal layer at all times (Figure 13).⁴⁰

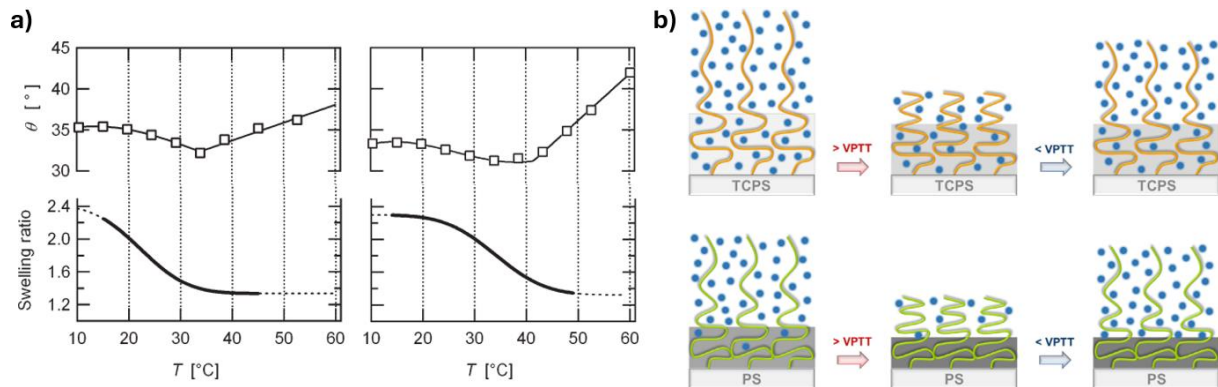


Figure 13. Surface and bulk transition of dense POEGMA brushes indicated through trend change in the captive bubble CA θ (top) and QCM-D-derived swelling ratio (bottom), respectively (a). QCM-D deduced mechanisms of the “cushioned” transition on TCPS (top) and “grounded” transition on PS (bottom) grafted PGE brushes (b). (a) adapted with permission from *Laloyaux et al.*⁹² Copyright 2010 American Chemical Society. (b) adapted from *Stöbener et al.*, 2021,⁴⁰ with permission from Elsevier.

1.6. Parameters for successful cell sheet fabrication

Since most anchorage-dependent cells rely on surface adhesion for regular activity and proliferation *in vitro*, it is necessary to understand the basic parameters and steps of the cell adhesion process (or lack thereof).¹³⁹ The basic stages of cell surface adhesion in serum containing culture medium are presented in Figure 14.

Introduction

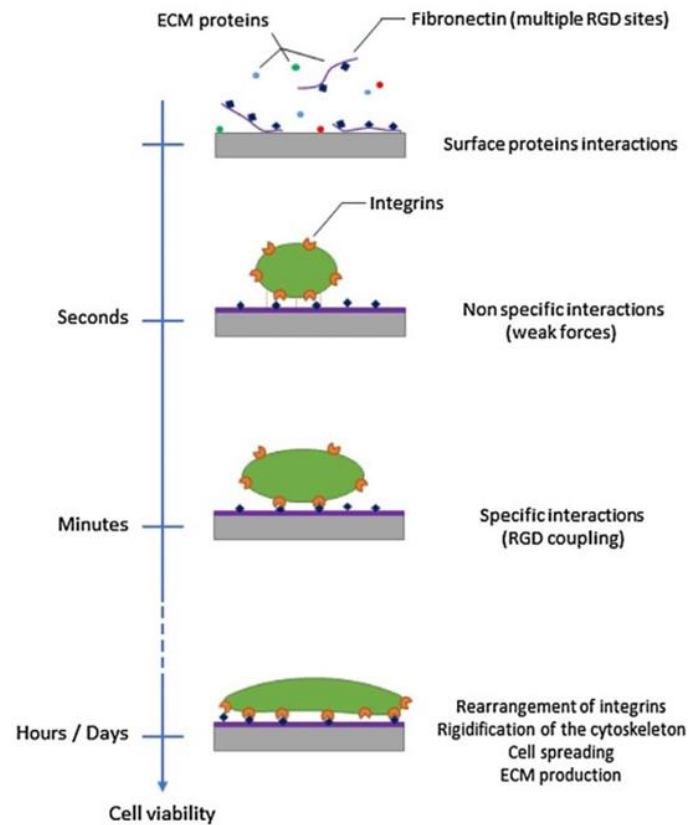


Figure 14. Schematic stages of protein adsorption and cell adhesion. Adapted from *Conzatti et al.*, 2017,¹⁴⁰ with permission from Elsevier.

Upon initial contact with the medium, proteins instantly start to adhere on the surface.¹⁴¹ Protein attachment can be hindered by hydrophilic surfaces with a tightly bound surface water layer, as displacing this layer would be energetically unfavorable.¹⁴² Protein adhesion on hydrophobic surfaces is possible, but can lead to rearrangement of protein segments for enhanced hydrophobic interactions, resulting in denaturation and loss of functionality.¹⁴³ Thus, moderately hydrophobic surfaces, which allow protein adhesion, without interfering with the protein structure, are required.¹⁴³ From the commonly used fetal bovine serum, fibronectin (FN) and vitronectin (VN) are particularly important due to the presence of the adhesion enhancing RGD-motif in their protein structure.¹⁴⁴ Functional integrin proteins, located in the cell membrane, scan their environment for the RGD sequence and couple the cell to this sequence upon sensing it.¹⁴⁴ Subsequently, cells rearrange their cytoskeleton to spread on the surface and start further adhesion and proliferation processes, such as forming focal adhesion points and producing additional ECM components to maintain a well-suited environment.¹⁴⁵ Minimal amounts of proteins can be already sufficient for cell adhesion, as shown by fibroblasts spreading equivalently on surfaces exposed to serum for 10 s or 90 min.¹⁴⁶

Even with protein adsorption and the availability of RGD-motifs, the softness of a substrate can prevent successful cell adhesion, as the forces exerted on protein molecules during the formation of focal adhesion points may lead to insufficient protein adherence on soft

Introduction

surfaces.¹⁴⁷ Surface softness in brush systems can be controlled through brush mobility, with well-solvated and stretched chains leading to increased surface softness and lower protein adhesion.^{148, 149} Parameters resulting in insufficient adhesion can guide the optimization of detachment conditions: thermoresponsive coatings transitioning from a collapsed mushroom state into a soft, well-hydrated brush state during the VPT can facilitate efficient detachment of cultured cells. Interestingly, cell adhesion also occurs on surfaces with wide tethered PHEMA or PEG chains, which have enough space for a mushroom conformation. Gradually increasing grafting density results in more stretched chains and reduced cell adhesion and the tipping points can be used as a blueprint for an optimal brush state under cell culture and cell detachment conditions.^{150, 151}

Initial observations of parameter dependence issues of thermoresponsive coatings were made with PIPAAm based hydrogels. Thickness limits for cell attachment were deduced to be 15-25 nm on TCPS and ~5 nm on hydrophilic glass, as PIPAAm retains considerable amounts of water above the VPT. With increasing substrate hydrophilicity, thicker PIPAAm layers retain too much water, preventing effective protein adsorption and cell adhesion (Figure 15).^{152, 153} Conversely, PIPAAm hydrogels on TCPS with thicknesses below ~15 nm do not induce detachment due to insufficient hydration change upon cooling.²⁸

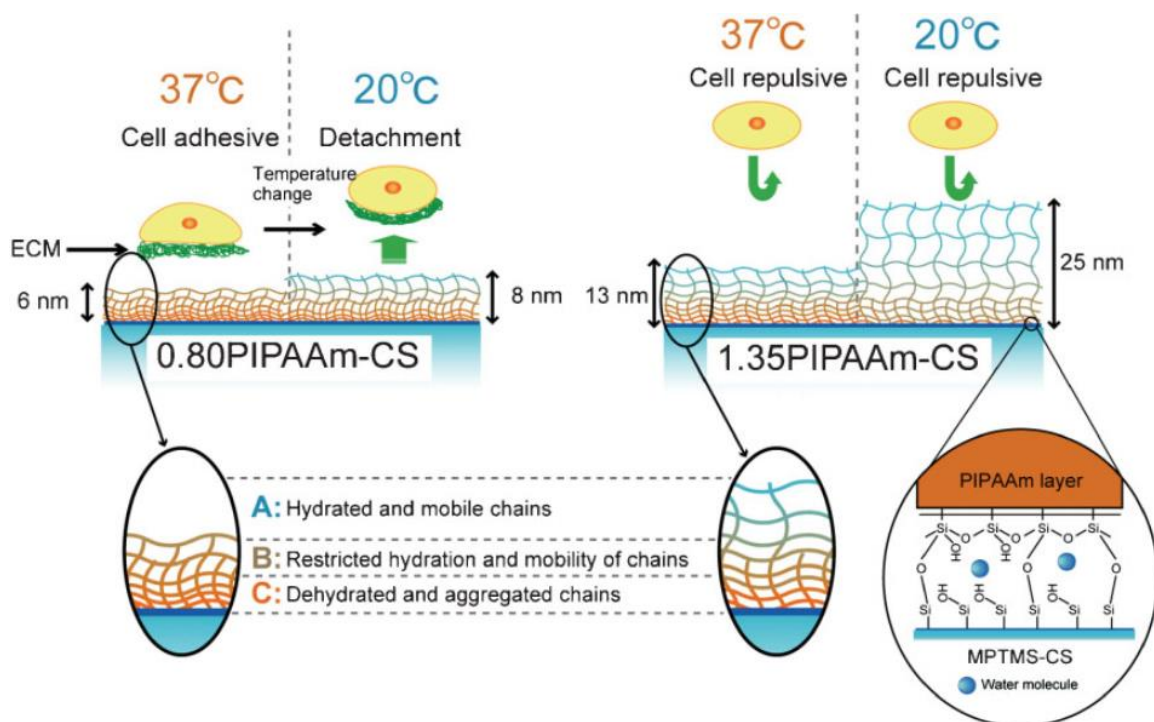


Figure 15. Depiction of hydration levels of PIPAAm hydrogels with different thicknesses on glass surfaces and the following impact on cell adhesion and detachment. Adapted with permission from *Fukumori et al.*¹⁵³ Copyright 2010 John Wiley and Sons.

Introduction

Studies of PIPAAM brushes grafted from PS revealed a similar effect, where the number of adhered cells after 24 h cultivation decreased with increased brush thickness and virtually no adhesion was observed for ~65 nm thick brushes.²⁵ Since the protein adsorption on PIPAAM hydrogels is generally lower than on TCPS surfaces, some cell types, such as HUVECs, could only be cultured after additional modification with RGD sequences, as mentioned before.³⁰ However, parametric studies of PIPAAM brushes grafted from glass substrates revealed enhanced adhesion at medium to low grafting densities and chain lengths.⁹⁰ In a subsequent study, PIPAAM brushes grafted from PS substrates were used to culture and detach bovine arterial endothelial cells, HUVECs and HDFs from the same unmodified PIPAAM surface.³⁶ The aforementioned study of substrate governed phase transition of PGE brushes helped to reveal cell culture trends in a similar way: high grafting densities resulted in mostly premature detachment, while middle to low grafting densities on TCPS resulted in hampered cell detachment due to enhanced protein adsorption at 20 °C and optimum grafting thickness at middle to high densities was established. The more ambiguous detachment trends of PGE brushes on PS surfaces were then linked to different protein adsorption kinetics and used to establish the phase transition mechanisms.⁴⁰

1.7. Coating translation, sterilization and storage stability

It is feasible to translate the optimized surfaces for tissue engineering to other laboratories, enabling research facilities without the capability to manufacture such coatings to benefit from temperature-driven gentle cell detachment, as in the case of UpCell™ dishes. This translation typically occurs through the process of commercialization, with approval steps regulated by international and national agencies, such as the Food and Drug Administration (FDA) in the United States, the European Medicines Agency in the European Union, or the Federal Institute for Drugs and Medical Devices in Germany.

The approval steps ensure device safety and efficacy, demonstrated by the absence of adverse side effects such as toxicity, immunogenicity or carcinogenicity when working with cells, as well as consistent and reliable cell adhesion, proliferation and detachment. The examination usually requires a large number of uniformly prepared samples, to obtain statistically significant data for robust results. As biocompatibility is already partly evaluated through initial cell culture experiments, another crucial aspect is often initially overlooked: the sterilization and storage stability of the coating and the underlying substrate. Storage packaging and conditions should provide physical protection and functionality after prolonged time periods, thus protecting against harmful environmental impacts like oxygen, UV light and heat exposure.¹⁵⁴ Studies indicate that sterile items in hospitals can remain sterile for 12 to 24 months, setting up an expectation range for new products,¹⁵⁵ and Nunc UpCell™ dishes

Introduction

feature a shelf-life of 3 years according to the supplier.¹⁵⁶ Suitable packaging solutions can also be compatible with sterilization methods, allowing direct sterilization of the packaged material.¹⁵⁴

Sterilization, as the final production step, ensures that the device is ready-to-use without the risk of biological contamination. Per definition, sterilization is successful at a sterility assurance level of less than 10^{-6} , meaning there should be less than one unsterile item per million devices.¹⁵⁴ Especially single-use products, such as plastic cell culture dishes, require a high-output sterilization method to process large product batches simultaneously. The most common lab technique for this case is heat-based autoclaving. However, while some polymers, such as polypropylene, can be autoclaved, other polymers such as PS or PET cannot be used afterwards due to potential deformation and degradation.^{157, 158} Other laboratory methods, such as aqueous ethanol disinfection or UV radiation are not suitable for commercial devices and would not meet FDA regulations.¹⁵⁴ Therefore, gas or plasma sterilization with hydrogen peroxide, ethylene oxide (EO) or formaldehyde (FO),¹⁵⁹ or radiation sterilization through gamma (γ) or e-beam (β^-) radiation,¹⁶⁰ standardized to DIN EN ISO 11137, is required. The sterilization mechanism is usually based on the alkylation of reactive groups (EO, FO), or creation of free radicals (γ , β^-), which lead to scission and crosslinking of DNA and protein molecules.^{154, 161} Thus, gas sterilization is considered milder compared to radiation sterilization.

Due to the popularity of PEG, numerous studies on its sterilization and degradation in bulk and as a surface layer can help to estimate the stability of PGE coatings. PEG in bulk (M : 6 kDa) degrades in the presence of air due to autooxidation and chain scission through oxygen, leading to lower M values and higher polydispersities, while PEG supplemented with antioxidants or stored in vacuum did not degrade.⁴⁵ The thickness of self-assembled PEG layers on silicon surfaces (20 nm) in PBS solutions declined ~20% after 7 d.¹⁶² A similar comparative study of PEG and POX brush layers (1.3-2.5 nm) on Nb_2O_5 substrates in HEPES buffer supplied with NaCl revealed a ~20% thickness decline already after ~1 d for PEG and after ~7 d for the POX brushes, demonstrating the comparatively enhanced stability of POX polymers.¹⁶³ EO gas-sterilized PEG bulk hydrogels, brush substrates (~1 nm) and plasma polymerized films (~20 nm) were mostly stable, with minimal changes in swelling ratio and surface morphology after sterilization and no difference in protein or cell repellent properties.^{47, 164, 165} In contrast, sterilization via γ or β^- radiation with a total dose between 20-25 kGy had a severe effect, especially on lightly crosslinked hydrogels and brush systems, by increasing the crosslinking density and lowering the swelling ratio of hydrogels or degrading brush systems, while lowering the protein repellency.^{47, 164} Furthermore, an enhanced number of free radicals, determined by electron spin resonance measurements, was found in the PEG bulk hydrogels, which can lead to long-term oxidation and degradation reactions.⁴⁷ Plasma polymerized films and densely crosslinked hydrogels, however, mostly retained their properties probably due to

Introduction

their already high degree of crosslinking.^{47, 165} In summary, PEG can be sterilized by commercial techniques (e. g. EO gas), but the potential oxidation and chain scission of PEG and similarly designed PGEs needs to be considered, when preparing long-term application samples and these processes can be enhanced through radiation sterilization.

E-beam polymerized PIPAAM gels were sterilized *via* EO, confirming their compatibility with this method.¹⁶⁶ Unfortunately, to our best knowledge there is no published data on the sterilization of PIPAAM or POX surface coatings. However, the radiation results of bulk and aqueous solutions can help to estimate sterilization outcomes of surface layers.¹⁶⁰ PIPAAM (*M*: 20 kDa), poly(2-ethyl-2-oxazoline) (PETOX) (*M*: 20 kDa), and PEG (*M*: 5 kDa) irradiated under argon atmosphere showed only little changes after γ radiation with doses up to 50 kDa and remained soluble afterwards. Thus, inert sterilization might be the key to radiation sterilization of functional polymers, similar to its use for ultra-high molecular weight polyethylene (UHMWPE) surgical implants.¹⁶⁷ E-beam radiation up to 100 kGy did not impact PIPAAM, but caused a continuous *M* decline for PETOX and a *M* increase above 20 kGy dose for PEG, along with increased polydispersities in each case, indicating degradation of PETOX and crosslinking of PEG. More pronounced effects were observed upon irradiation of polymers solutions in the presence of oxygen. Here, PEG and PETOX could not be redissolved for GPC measurements after γ radiation doses of more than 20 kGy or a β^- dose of more than 2 kGy. PIPAAM in solution remained soluble after every γ radiation dose (up to 100 kGy), but the T_{cp} values increased with higher dosages, with not fully turbid solutions observed after 50 kGy or more, presumably due to hydrolysis of the isopropyl amide group. Similar behavior was observed for β^- doses above 5 kGy. Other polymers, namely poly[*N*-(2-hydroxypropyl)methacrylamide] (PHPMA) and poly(*N*-vinyl-2-pyrrolidone) (PVP) were also comparatively more stable as PEG and PETOX polymers, assumedly due to their less reactive aliphatic backbones (Figure 16).¹⁶⁰ In conclusion, thermoresponsive polymers with aliphatic backbones, including PIPAAM, seem more suitable for applications requiring long-term storage or utilization as compared to polymers with heteroatoms in the backbone, such as PEG or POX.

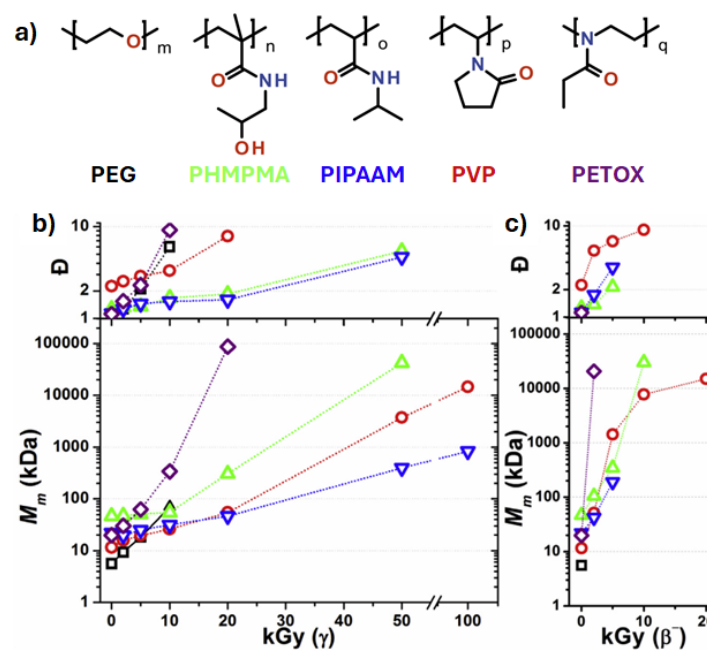


Figure 16. Color coded polymer structures with highlighted heteroatoms, which were probe via gamma and e-beam radiation in bulk and solution (a) and the mass-averaged molecular weight (M_m) and polydispersity (D) values of the polymers determined *via* GPC after gamma (b) and e-beam (c) irradiation of 1 w% polymer water solutions. Missing values indicate that the polymer could not be redissolved, and points are connected to guide the eye. All parts adapted from Sedlacek *et al.*, 2017,¹⁶⁰ with permission from Elsevier.

2. Objectives

PGE-based brush coatings provide a versatile thermoresponsive platform for cell sheet fabrication, which can be used to culture and harvest different cell types without further polymer modification. Furthermore, a selective self-assembly of PGE brushes on a variety of polymeric substrates is attainable through tailored benzophenone anchors. The control over the comonomer ratio and the chain length through living polymerization and an accessible range of grafting densities through optimized adsorption procedures render PGE brush coatings a well-suited candidate for studies of temperature dependent phase transition. The described control of intrinsic molecular properties can help to elucidate structure-property relationships and guide designs for applicable brush coatings. For applied and convenient cell culture products, sterilization and long-term storage stability are further essential features. Here, PGE polyethers might suffer from limited oxidation stability, similar to structurally related PEG brush and hydrogel systems, which can limit the materials' potential for market translation. Therefore, goals of the following work were the development of a similarly performing polymer coating for cell sheet fabrication as the introduced PGE brush system, with enhanced stability, and temperature dependent in-depth characterization studies of these polymer systems to elucidate useful structure-property relationships and the suitability for cell culture applications.

To achieve this goal, polymers with structural resemblance to PGE elements and appropriate amphiphilicity balance ought to be derived via rational molecular design. Controlled polymerization techniques should help to obtain well-defined PGE and PGE-alternative polymer structures. Successfully obtained new polymers ought to be characterized for their thermoresponsive properties in solution to verify the possible suitability for biomedical applications. Here, transition regions with a distinct dehydration below the physiological conditions (37 °C) and a sharp phase transition with little dependence on intrinsic parameters, such as molecular weight and polymer concentration, and extrinsic parameters, e. g. the typical presence of proteins and ions are expected to lead to a suitable thermoresponsive platform.

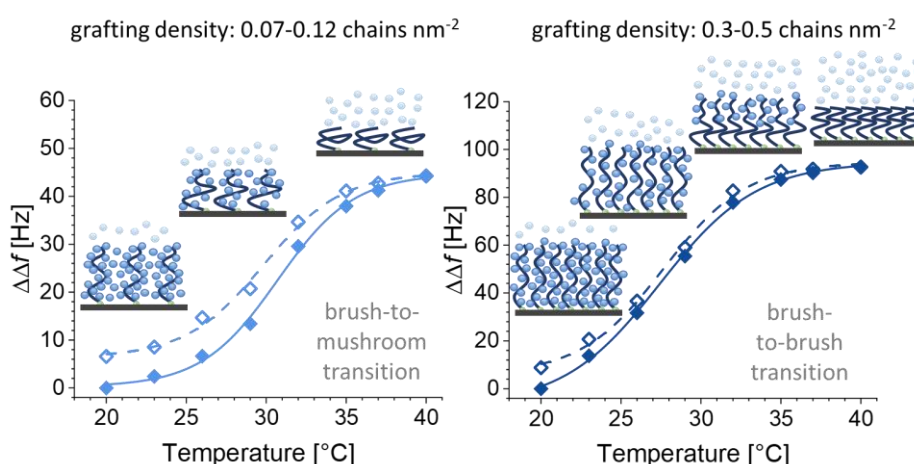
Strategies for surface immobilization of analyzed polymers will be derived from the successfully employed self-assembly procedures *via* benzophenone or sulfur-based anchor blocks, depending on the surface type. Continuous evaluation of surface properties will supply necessary insights for procedure adjustments. Optimized adsorption procedures are expected to allow the control of the surface parameters and yield well-defined brush structures. Cell culture experiments will provide information about coating biocompatibility and designing temperature dependent experiments for the brush surfaces will elucidate the potential for cell harvesting and the phase transition properties of the obtained brush structures. Furthermore, sterilization and stability comparison between established PGE and new brush systems should elucidate the benefit of the alternative monomer design for enhanced stability.

3. Publications and Manuscripts

3.1. Grafting Density-Dependent Phase Transition Mechanism of Thermoresponsive Poly(glycidyl ether) Brushes: A Comprehensive QCM-D Study

Schweigerdt, A.; Heinen, S.; Stöbener, D. D.; Weinhart, M. Grafting Density-Dependent Phase Transition Mechanism of Thermoresponsive Poly(glycidyl ether) Brushes: A Comprehensive QCM-D Study. *Langmuir* **2021**, *37* (23), 7087-7096.

DOI: <https://doi.org/10.1021/acs.langmuir.1c00695>



Thermoresponsive PGE polymers based on glycidyl methyl ether (GME) and ethyl glycidyl ether (EGE) monomers with a 1:1 ratio were synthesized with two different molecular weights (10 and 22 kDa) and functionalized with a thiol end group. Previously established grafting protocols allowed the preparation of brush coatings on gold coated QCM-D chips with varying grafting density and chain length, thus resulting in different grafting regimes and coating thicknesses. T_{cp} values in solution between 26 and 31 °C guided the design of temperature dependent quasi-static transition studies of PGE brushes on the surface between 20 and 40 °C, which were performed via QCM-D measurements. The experiments revealed broad transition regimes and highly comparable phase transition temperatures of distinct brush systems to corresponding concentration-dependent polymer solution values. Furthermore, distinct transition behaviors of PGE brushes with coating dehydration and brush collapse were identified, depending on the grafting density but not on the molecular weight.

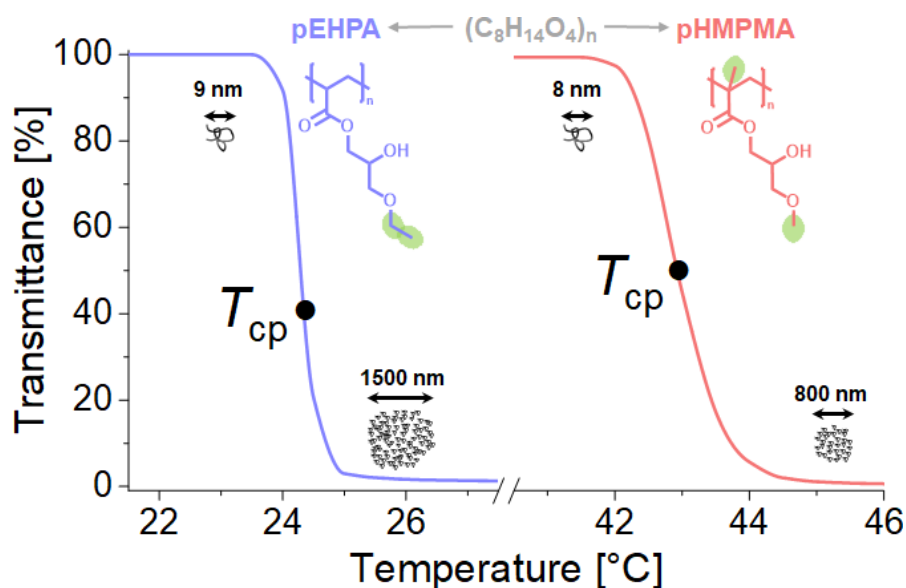
Polymer synthesis and characterization: Dr. S. Heinen. Thermoresponsive characterization in solution: Dr. S. Heinen, A. Schweigerdt. Brush layer immobilization and temperature dependent QCM-D measurements: Dr. S. Heinen, A. Schweigerdt. Research concept: Dr. S. Heinen, Dr. M. Weinhart. Project supervision: Dr. M. Weinhart, Dr. D.D. Stöbener. Manuscript preparation: A. Schweigerdt. Manuscript review: Dr. M. Weinhart, Dr. D.D. Stöbener.

3.2. Impact of Amphiphilicity Balance in Hydroxy-Functional, Isomeric, Thermoresponsive Poly(meth)acrylates

Schweigerdt, A.; Stöbener, D. D.; Schäfer, A.; Kara, S.; Weinhart, M. Impact of Amphiphilicity Balance in Hydroxy-Functional, Isomeric, Thermoresponsive Poly(meth)acrylates. *Macromolecules* **2023**, *56* (21), 8602-8613.

DOI: <https://doi.org/10.1021/acs.macromol.3c01251>

This publication is licensed under **CC-BY 4.0**. <https://creativecommons.org/licenses/by/4.0/>



Regioisomer-pure 3-ethoxy-2-hydroxypropylacrylate (EHPA) and 2-hydroxy-3-methoxypropylmethacrylate (HMPMA) monomers, derived through rational molecular design, were isolated and characterized. Corresponding PEHPA and PHMPMA polymers with molecular weights of 10 and 25 kDa and $\bar{D} \leq 1.17$ were obtained *via* an optimized RAFT polymerization. Temperature dependent phase transition of the polymer solutions was characterized by turbidimetry, DLS, NMR and fluorescence measurements. For the latter, a proof-of-concept functionalization method was established to immobilize the fluorescent Cy5-dye in the polymer chains. The dependence on molecular weight and ion influence of PBS solutions was evaluated and the results combined to deduce the phase transition mechanism for each polymer, thus estimating their suitability for cell culture applications.

Monomer synthesis: A. Schweigerdt, I. Fallaha (BSc thesis under supervision). Homopolymer synthesis and characterization: A. Schweigerdt, O. Staudhammer. Fluorescent modification of the polymer: A. Schweigerdt. Turbidimetry, DLS and fluorescence analysis: A. Schweigerdt. Temperature dependent NMR spectroscopy & analysis: A. Schäfer, A. Schweigerdt. Research concept: Dr. D.D. Stöbener, Dr. M. Weinhart, Dr. S. Kara, A. Schweigerdt. Project supervision: Dr. D.D. Stöbener, Dr. M. Weinhart. Manuscript preparation: A. Schweigerdt. Manuscript review: Dr. D.D. Stöbener, Dr. M. Weinhart.

Impact of Amphiphilicity Balance in Hydroxy-Functional, Isomeric, Thermoresponsive Poly(meth)acrylates

Alexander Schweigerdt, Daniel D. Stöbener, Andreas Schäfer, Selin Kara, and Marie Weinhart*



Cite This: *Macromolecules* 2023, 56, 8602–8613



Read Online

ACCESS |



Metrics & More

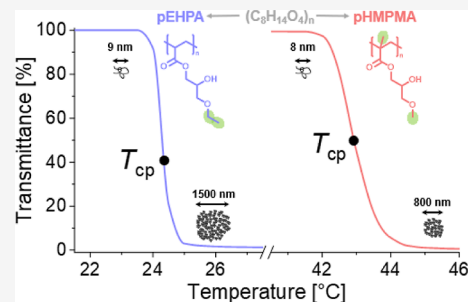


Article Recommendations



Supporting Information

ABSTRACT: Aqueous polymer solutions exhibiting a lower critical solution temperature (LCST) in the physiological range are widely used in biomedical applications. Of particular interest are polymers that contain additional reactive groups for further conjugation of drugs, dyes, or enzymes. For specific applications, detailed knowledge and understanding of the phase transition behavior (*e.g.*, phase separation, transition range, and dehydration on the micro- and macroscopic level) and its dependence on various intrinsic (molecular weight and polymer functionalization) and extrinsic (polymer concentration and salt presence) factors are critical. In this context, we present a comprehensive study of the thermoresponsive properties of two unprecedented glycerol ether-based poly(meth)acrylates with β -hydroxy-functional side chains, namely, the structurally isomeric poly(3-ethoxy-2-hydroxypropyl)acrylate (**pEHPA**) and poly(2-hydroxy-3-methoxypropyl methacrylate) (**pHMPMA**). The distinct amphiphilic balance of **pEHPA** with a higher side chain hydrophobicity resulted in lower cloud point temperatures (22–33 °C), while shifting hydrophobicity to the backbone in **pHMPMA** led to increased cloud point temperatures (37–67 °C), accompanied by higher sensitivity of the phase transition to intrinsic and extrinsic factors. Turbidimetry, dynamic light scattering, and NMR measurements revealed that the hydration of β -hydroxy side chains primarily governs the transition behavior, resulting in distinct phase separation mechanisms between the two polymer types. Based on this knowledge, the rational design of hydroxy groups presenting poly(meth)acrylates with adjustable hydration becomes feasible. Cyanine5 (Cy5)-labeling of the hydroxy groups and temperature-dependent fluorescence analysis demonstrated the potential of these polymers as postfunctionalizable thermoresponsive polymer platforms, *e.g.*, for bioseparation.



INTRODUCTION

Polymers that display thermoresponsive behavior in aqueous solutions are extensively researched for medical and biological applications.^{1–3} Of particular interest are polymers with a lower critical solution temperature (LCST) since they usually exhibit a sharp and readily reversible phase transition when passing the so-called cloud point temperature (T_{cp}). Above the T_{cp} , favorable hydrogen bonding and polar interactions between water molecules and the polymer chains can no longer compensate for the entropic loss caused by an ordered hydration shell. Exceeding the T_{cp} thus leads to a thermodynamically driven dehydration and coincidental aggregation of the polymer chains, resulting in macroscopic phase separation.⁴ Depending on the nature of the polymer, the aqueous mixture can undergo a liquid–solid phase separation (LSPS) or liquid–liquid phase separation (LLPS). The former LSPS is often observed for polymers such as poly(*N*-isopropylacrylamide) (**pNIPAM**), which undergo an abrupt coil-to-globule transition, resulting in the formation of dispersed or phase-segregated solid polymer precipitates. In contrast, dispersed liquid droplets, which consist of water-rich polymer coacervates, are formed during LLPS.^{5,6}

In general, the LCST behavior originates from the ratio and spatial distribution of hydrophobic and hydrophilic elements in

the polymer structure, which can be tailored by copolymerization or through the structure of monomers in homopolymers.^{1,7,8} Particularly, the temperature-dependent change in hydration and the value of the T_{cp} are primarily determined by the number and availability of hydrophilic groups that can partake in hydrogen bonding as well as by the stability of the water cage formed around hydrophobic groups.⁹ For example, the increasing T_{cp} of the structural isomers poly(*N*-*n*-propylacrylamide) (**pNNPAM**, $T_{cp} \sim 20$ °C), poly(*N*-isopropylacrylamide) (**pNIPAM**, $T_{cp} \sim 32$ °C), and poly(*N,N*-ethylmethyl acrylamide) (**pNEMAM**, $T_{cp} \sim 70$ °C) (Scheme 1a) reflects the increasing water cage stability around the *N*-substituents in the polymer side chains.^{10–12} Notably, a relocation of the amide units from the side groups to the polymer backbone, such as in isomeric polyoxazolines, yields a T_{cp} increase of roughly 4 °C for the isomer pairs poly(*n*-propyl

Received: June 26, 2023

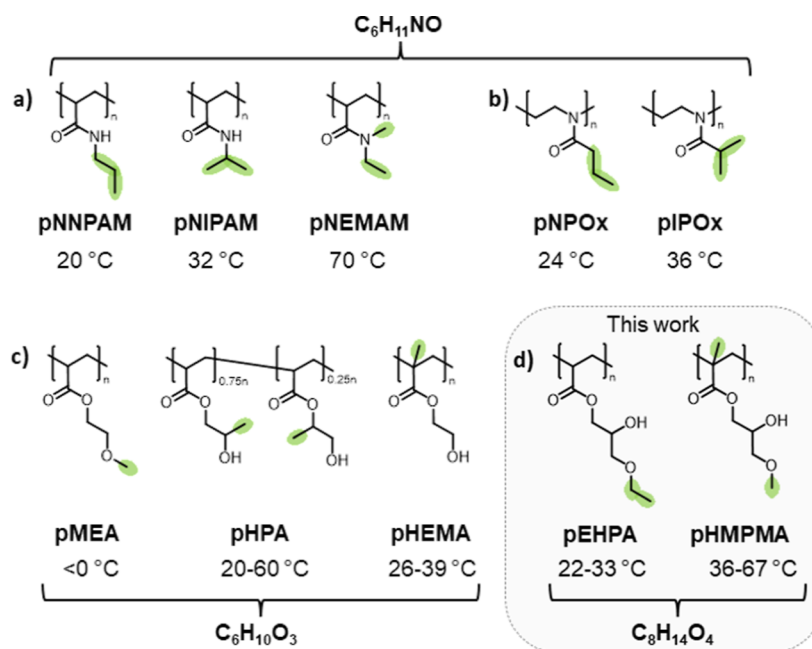
Revised: October 11, 2023

Accepted: October 18, 2023

Published: October 27, 2023



Scheme 1. Groups of Isomeric Thermoresponsive Polymers with Varying Amphiphilicity Balance with Corresponding T_{cp} Values Comprising (a) Poly(acrylamide)s,^{10–12} (b) Polyoxazolines,¹³ (c) Ethylene Glycol-Based Poly(meth)acrylates,^{22,23} and (d) Glycerol-Based Poly(meth)acrylates Presented in This Work^a



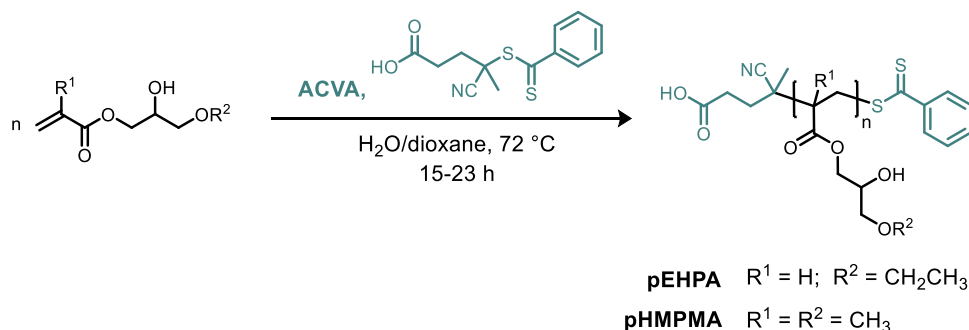
^aFor pHPA, the most available and researched copolymer structure is presented.^{24,25} Structural isomeric differences within the respective polymer groups are highlighted in green.

oxazoline) (pNPOx, $T_{cp} \sim 24$ °C)/pNPPAM and poly(isopropyl oxazoline) (pIPOx, $T_{cp} \sim 36$ °C)/pNIPAM (Scheme 1b).¹³ Besides the amphiphilic balance, the polymer end groups, concentration, molecular weight, and dispersity can influence the phase transition.^{14,15} Controlled polymerization techniques are, therefore, commonly used to synthesize narrowly dispersed polymers with tunable molecular weights. Furthermore, a detailed understanding of the thermoresponsive behavior on the macroscopic, microscopic, and molecular levels is essential for advanced application design.¹⁶

Thermoresponsive polymers with reactive groups (e.g., hydroxy groups), which allow further functionalization with fluorescent dyes, enzymes, or drugs, extend the scope of possible applications. Naturally, the hydrophilicity of hydroxy groups also influences the thermoresponsive behavior. Poly(4-hydroxybutyl vinyl ether) (pHBVE), a thermoresponsive polyalcohol, does not follow the prevalent coil-to-globule transition when passing the T_{cp} at ~ 42 °C. Instead, a coacervate is formed through an LLPS, resulting in polymer-rich aqueous droplets and a polymer-depleted water phase.¹⁷ This behavior becomes dominant in polymers with an elevated content of hydroxy groups, as demonstrated in copolymers of NIPAM and 2-hydroxyisopropylacrylamide (HIPAM). A series of studies have shown that the coil-to-globule transition gradually changes to an LLPS transition with increasing HIPAM content, which was accompanied by an increase in T_{cp} values due to the more hydrophilic nature of the hydroxy-functional HIPAM comonomer.^{6,18} A recent study showed how functionalized p(NIPAM-co-HIPAM) could effectively be used for antigen enrichment for disease diagnostics.¹⁹ The significant influence of hydroxy groups can also be observed in poly(meth)acrylates with oligo(ethylene glycol) side chains (pOEGA and pOEGMA).^{15,20,21} The number of repeating ethylene oxide units and the end group of the monomer side

chain influence the T_{cp} drastically despite the structural isomerism. Prominent isomeric examples are poly(hydroxyethyl methacrylate) (pHEMA), which is only thermoresponsive below $M \sim 6$ kDa (T_{cp} : 26–39 °C), poly(methoxyethyl acrylate) (pMEA), which only swells in water, and poly(hydroxypropyl acrylate) (pHPA) with a branched side chain, which has exhibited significantly concentration- and molecular weight-dependent LCST behavior in various studies (T_{cp} : 20–60 °C) (Scheme 1c).^{22–25} Two or more ethylene oxide units significantly increase the hydrophilicity, resulting in either thermoresponsive or completely soluble polymers, depending on the side chain length, end group, and backbone composition.^{15,20}

In previous studies, thermoresponsive poly(glycidyl ether) (PGE) copolymers have been established and intensively studied by our group for applications in solution and on surfaces.^{16,26,27} Herein, we translate the thermoresponsive properties of glycerol-based polymers from a polyether backbone to an acrylate [poly(3-ethoxy-2-hydroxypropyl)-acrylate, pEHPA] and methacrylate poly(2-hydroxy-3-methoxypropyl methacrylate, pHMPMA) backbone (Scheme 1d), introducing ether groups and functionalizable hydroxy groups into the resulting isomeric polymers. A detailed investigation of the thermally induced phase transition in solution on the macro- and microscopic scale allowed us to elucidate the impact of the structural amphiphilicity balance and compare it to those of other known thermoresponsive polymers. As a proof of concept, the polymers' reactive hydroxy groups were used to attach a fluorescent probe, allowing us to further characterize their thermoresponsive behavior *via* fluorescence spectroscopy.

Scheme 2. Synthesis of Isomeric Thermo-responsive pEHPA and pHMPMA Homopolymers *via* RAFT Polymerization

EXPERIMENTAL SECTION

Materials, detailed synthetic procedures and characterization of the used polymers, gel permeation chromatography (GPC) methods, sample preparation for thermo-responsive analysis, and additional ultraviolet/visible (UV/vis) spectroscopy, dynamic light scattering (DLS), and NMR data are presented in the [Supporting Information](#).

Turbidimetry (UV/Vis) Measurements. Absorbance and transmittance measurements were recorded on a PerkinElmer Lambda 950 UV/vis spectrometer with a PTP 6 Peltier temperature programmer (PerkinElmer). Temperature-dependent measurements were performed at heating rates of $0.5\text{ }^\circ\text{C min}^{-1}$ while recording data points every $0.5\text{ }^\circ\text{C}$. The temperature-dependent transmittance of the aqueous polymer solution was measured for at least three cycles per sample. The measurement points were connected *via* the Akima-spline interpolation, and T_{cp} was defined as the temperature at the inflection point of the normalized transmittance versus temperature curve.

Fluorescence Measurements. Fluorescence emission was recorded on a Jasco FP-6500 spectrometer with a temperature control, as illustrated in [Figure S18](#). The sample cuvettes were equilibrated in a tempered water bath, and the fluorescence emission in the 660 to 700 nm range was measured with a speed of 100 nm s^{-1} . The temperature error range was $+0.5\text{ }^\circ\text{C}$ for measurements up to 37, $+1.0\text{ }^\circ\text{C}$ for measurements up to 49, and $+1.5\text{ }^\circ\text{C}$ for measurements up to 65 $^\circ\text{C}$.

DLS Measurements. Intensity-dependent size distributions were performed on a Malvern Zetasizer Ultra analyzer (Malvern Instruments) by using a He–Ne laser ($\lambda = 633\text{ nm}$) and scattering detection at 173° . Aqueous polymer solutions were filtered over $0.45\text{ }\mu\text{m}$ CA filters directly before the start and equilibrated for 120 s at the appropriate temperature before each measurement.

Temperature-Dependent NMR Measurements. ^1H and ^{13}C NMR spectra were recorded on a Bruker AVANCE 3 instrument operating at 700 MHz and on a JEOL ECZ instrument operating at 600 MHz. Deuterated water (D_2O) was filtered over a $0.45\text{ }\mu\text{m}$ CA filter, and samples were prepared at a concentration of 10 mg mL^{-1} .

RESULTS AND DISCUSSION

Polymer Synthesis and Characterization. HMPMA and EHPA monomers were prepared *via* the boron trifluoride-catalyzed epoxide ring opening of glycidyl acrylates and methacrylates in methanol or ethanol according to the literature, which yields primarily the regioisomer from an epoxide attack on the sterically less hindered position ([Scheme S1](#)).^{28–30} The regioisomers of HMPMA or EHPA were separated *via* column chromatography, and isomerically pure monomers were obtained in 60% yield.

In a study from 1980, the water contents of pEHPA and pHMPMA gels obtained *via* free radical polymerization were determined to be around 20 and 70 wt %, respectively, while the homopolymers were reported insoluble in water.³⁰ With the controlled radical polymerization techniques available

nowadays, we looked more closely into these systems and found both polymers, in fact, to be thermo-responsive in water and thus ideal candidates for a comprehensive structure–property correlation. Structurally well-defined homopolymers were synthesized *via* a controlled reversible addition fragmentation chain transfer (RAFT) polymerization with 4,4-azobis(4-cyanovaleric acid) (ACVA) as the radical initiator and 4-cyano-4-(phenylcarbonothioylthio)pentanoic acid as the chain transfer agent ([Scheme 2](#)).³¹ ^1H NMR spectra of the crude reaction mixtures after overnight reactions indicated at least 85% monomer conversion, thereby confirming the compatibility of the chosen RAFT system with the monomers. The structures of purified polymers were analyzed *via* ^1H and ^{13}C NMR spectroscopy ([Figures S1–S7](#)).

Molecular weights of the purified polymers were evaluated *via* GPC in tetrahydrofuran (THF) and dimethylformamide (DMF) and ^1H NMR spectroscopy. A list of the results from polymers with targeted molecular weights of 10 and 30 kDa is presented in [Table S1](#). For the 10 kDa polymers, GPC results in THF matched with the targeted molecular weights (pEHPA10 and pHMPMA10), while for the 30 kDa targeted polymer, molecular weights indicated to be lower at around 25 kDa (pEHPA25 and pHMPMA25). Polydispersities from 1.08 to 1.17 were achieved, thus verifying the controlled polymerization of both monomers.

Evaluation of the Thermo-responsive Behavior. The T_{cps} of the pEHPA and pHMPMA polymers were first characterized at varying concentrations in Milli-Q water and in phosphate buffered saline (PBS) solutions. After the measurements, the samples were reanalyzed *via* GPC in THF as an eluent to verify the polymer stability during the thermal turbidimetry experiments ([Figure S11](#)), particularly regarding the RAFT end group.^{32,33} An overview of the transmittance curves is given in [Figure 1](#).

Generally, all polymers exhibited reversible phase transitions in water with minimal hysteresis and full clouding with a final transmittance of less than 3% at temperatures above the T_{cp} . The presence of salts resulted in a marked reduction of the transmittance for 10 kDa polymer solutions at $\geq 5\text{ mg mL}^{-1}$ already before the main phase transition. A similar trend, but to a lesser degree, was also observed for pHMPMA25 solutions at 20 mg mL^{-1} . Polymer precipitation in PBS solutions after the cloud point also resulted in broad and shifted transitions during subsequent cooling cycles due to polymer depletion ([Figure S10](#)). Therefore, the T_{cp} values of the PBS solutions were calculated from heating cycles only. Concentration-dependent T_{cp} values in water and PBS are summarized in [Figure 2](#).

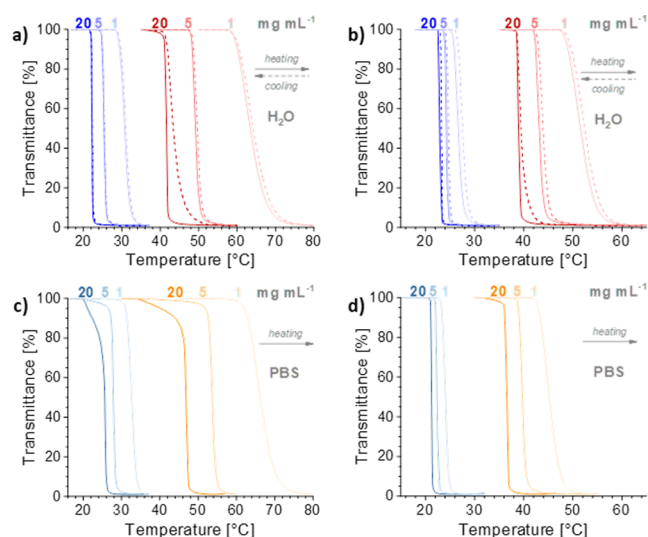


Figure 1. Representative normalized, concentration-dependent turbidimetry curves of pEHPA (blue, light blue) and pHMPMA (red, orange) in water ($n = 3$) and PBS ($n = 2$) for 10 kDa (a,c) and 25 kDa (b,d) polymers. Cooling cycles in PBS are listed in Figure S10.

The concentration- and molecular weight-dependent T_{cp} values for pEHPA polymers were located in the physiological range between 21.5 and 32.5 °C in both water and PBS. In contrast, the isomeric pHMPMA polymers exhibited their thermally induced phase transition in a broader interval exceeding the physiological range between 36.5 and 66.8 °C. The T_{cp} s of lower molecular weight polymers were more susceptible to concentration changes due to their lower local concentrations in solution. Overall, the sensitivity of the T_{cp} values to the screened parameters was generally more pronounced for the pHMPMA polymers. The screened concentrations revealed a T_{cp} range of up to 8 °C for pEHPA and up to 21 °C for pHMPMA. Increasing the molecular weight from 10 to 25 kDa under otherwise identical conditions resulted in a T_{cp} decrease of up to 8.5 °C for pEHPA and 21.8 °C for pHMPMA solutions. The presence of salts through PBS led to the precipitation of polymers in turbid solutions above the T_{cp} . This increased the T_{cp} values in subsequent measurement cycles due to retarded dissolution of the polymer-rich precipitate phase and caused lower polymer concentrations in the aqueous phase (see Figure S10). Similar precipitation effects in PBS were reported by Otulakowski *et al.* for pNIPAM, polyoxazolines, and pOEGMA-*co*-HEMA

polymers.³⁴ Interestingly, no general trend for the salt impact on the T_{cp} could be derived, as for the 10 kDa polymers a salting-in, and for the 25 kDa polymers, a salting-out effect was observed in PBS. According to the Hofmeister ion series, salting-in effects occur with “chaotropic” ions, while salting-out effects are caused through “kosmotropic” ions.^{35,36} Both effects, which scale with the ion and polymer concentrations, were observed for pNIPAM, pNPOx, pIPOx, and pOEGA copolymers with incorporated ribose side chains containing a significant percentage of hydroxyl groups. However, in literature reports, PBS or similarly concentrated NaCl solutions (0.1–0.2 M, PBS: 0.137 M) consistently showed a salting-out effect on the T_{cp} values.^{34,36–38} Conversely, low NaCl concentrations of ≤ 0.1 M induced a salting-in effect in the ribose functionalized pOEGA copolymers mentioned before.³⁸ Therefore, the observed molecular weight-dependent switch from salting-in to salting-out in PBS solutions in this work hints toward a specific ion interaction of hydroxy-functionalized polymers, as opposed to amide-based polymers for which no such NaCl-based salting-in effect has been reported so far.

Differential sensitivity toward parameter changes was also apparent from sharper phase transitions of pEHPA compared to pHMPMA solutions. The width of the phase transition can be determined *via* the temperature difference $\Delta T = (T_0 - T_{100})$ between temperature values T at 100 and 0% transmittance derived from linear fits of the sigmoidal turbidity curves (Figure S12 and Table S2). The phase transition widths of pHMPMA and pEHPA at 5 and 1 mg mL⁻¹ in water and PBS are listed in Table 1.

Generally, phase transitions were broader by a factor of 2–3 for pHMPMA compared to those for pEHPA. While at high concentrations of 5 mg mL⁻¹, there was hardly any impact of salts on the sharpness of the phase transition, at lower concentrations of 1 mg mL⁻¹, a marked sharpening through the presence of salts can be observed for both 25 kDa polymers but not for 10 kDa polymers. The molecular weight increase generally resulted in sharper transitions for all solutions. In summary, the thermal phase transition of pEHPA solutions appears sharp, while pHMPMA solutions exhibit a more continuous transition.

To gain further insights into the molecular aggregation of the polymer chains at the initial stages of the phase transition, we performed temperature-dependent DLS measurements of the polymer solutions at a concentration of 5 mg mL⁻¹. Measurements were performed after thermal equilibration for

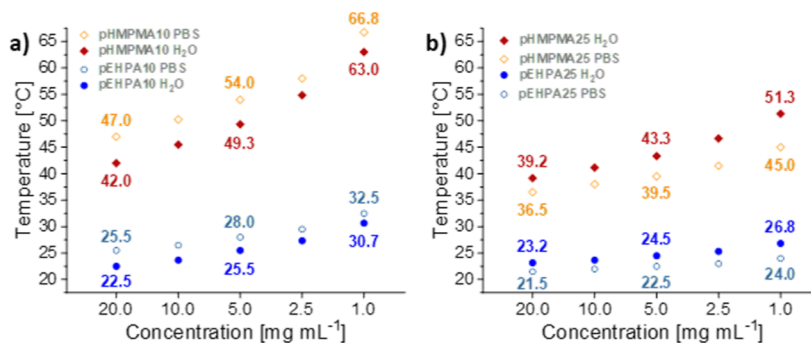


Figure 2. Concentration-dependent T_{cp} s of pHMPMA (diamonds) and pEHPA (circles) in H₂O ($n = 3$, full symbols) and PBS ($n = 2$, hollow symbols) at 10 kDa (a) and 25 kDa (b). Symbols and numbers indicate the mean value. Standard deviations for all measurements were within the experimental error (± 0.5 °C).

Table 1. Width of the Phase Transition ΔT in $^{\circ}\text{C}$ Derived from Heating Cycles of Turbidimetry Measurements at Polymer Concentrations of $c = 5$ and 1 mg mL^{-1} ^a

c [mg mL^{-1}] (solvent)	ΔT^{b} pHMPMA10	ΔT^{b} pEHPA10	ΔT^{b} pHMPMA25	ΔT^{b} pEHPA25
5 (H_2O)	2.6	1.3	2.0	0.6
5 (PBS)	2.7	1.4	1.8	0.7
1 (H_2O)	10.8	3.5	7.8	2.6
1 (PBS)	10.4	3.5	5.9	1.5

^aStandard deviations for all values were within the experimental error (± 0.5 $^{\circ}\text{C}$). ^bObtained from linear fits of the turbidity curves, as described in Figure S12 and Table S2.

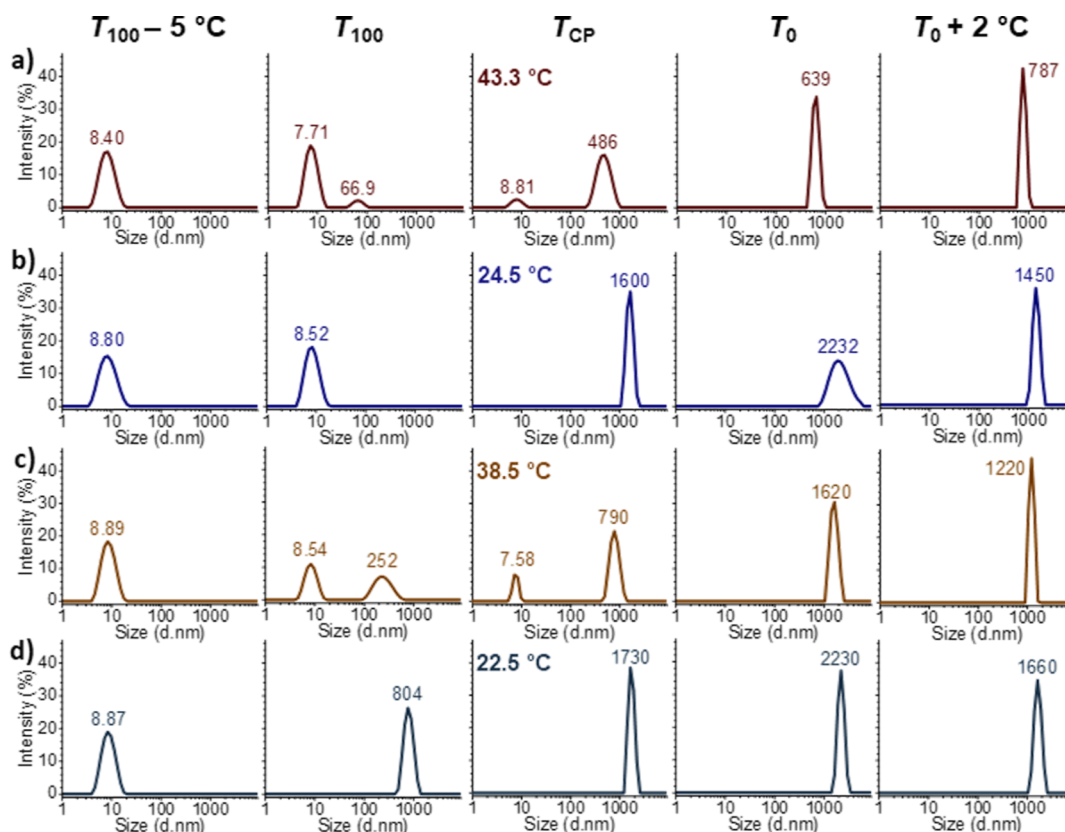


Figure 3. Temperature-dependent size distributions by intensity determined *via* DLS of pHMPMA25 (a,c) and pEHPA25 (b,d) at $c = 5 \text{ mg mL}^{-1}$ in water (a,b) and PBS (c,d), respectively.

120 s with freshly filtered solutions at defined temperatures around the thermal phase transition as derived from turbidimetry curves and defined by $T_{100} - 5$ $^{\circ}\text{C}$, T_{100} , T_{CP} , T_0 , and $T_0 + 2$ $^{\circ}\text{C}$ (Table S2). The acquired intensity-weighted size distributions in water and PBS are depicted in Figure 3 for 25 kDa and in Figure S13 for 10 kDa polymers.

Measured size distribution curves from polymer solutions of 25 kDa in the presence and absence of salts indicate hydrated chains below the cloud point at $T_{100} - 5$ $^{\circ}\text{C}$ with diameters of 8–9 nm. As expected, the 10 kDa chains are smaller with an average hydrated diameter of about 5 nm. Based on calculations of theoretical Flory radii in theta and good solvents, as well as the comparison to the calculated hydrodynamic radii of pNIPAM in water at 20 $^{\circ}\text{C}$, we assume the presence of fully solubilized individual chains (Table S3). With increasing temperature, the particle size increases due to progressing polymer chain dehydration and aggregation, which generally results in larger particles in PBS than in water solutions. Notably, thermally induced clouding does not necessarily occur with constantly increasing aggregate size

but rather involves dynamic stabilization between T_{CP} and $T_0 + 2$ $^{\circ}\text{C}$. DLS curves of pHMPMA25 at T_{100} revealed already starting aggregation with particles of 67 nm in water and 252 nm in PBS, respectively. At the macroscopically visible cloud point, 486 and 790 nm aggregate sizes in water and PBS coexist with minor amounts of residual individual chains. Above the cloud point at T_0 and $T_0 + 2$ $^{\circ}\text{C}$, individual pHMPMA25 chains are no longer observed, and the aggregates further increase to final sizes of 787 nm in water and 1220 nm in PBS. A qualitatively similar thermal aggregation behavior is observed for the pHMPMA10 solutions (Figure S13): aggregates of around 150 nm are already formed well below the cloud point at $T_{100} - 5$ $^{\circ}\text{C}$ with final aggregate sizes below 1000 nm at $T_{100} + 2$ $^{\circ}\text{C}$. In contrast to all other tested polymers, pEHPA25 formed no preaggregates in water prior to the macroscopic aggregation with around 1600 nm diameter at the cloud point, explaining the sharp transition width of 0.6 $^{\circ}\text{C}$ (Table 1). In the presence of salts, preaggregates of pEHPA10 and pEHPA25 of around 800 nm formed at T_{100} , which further increased to about

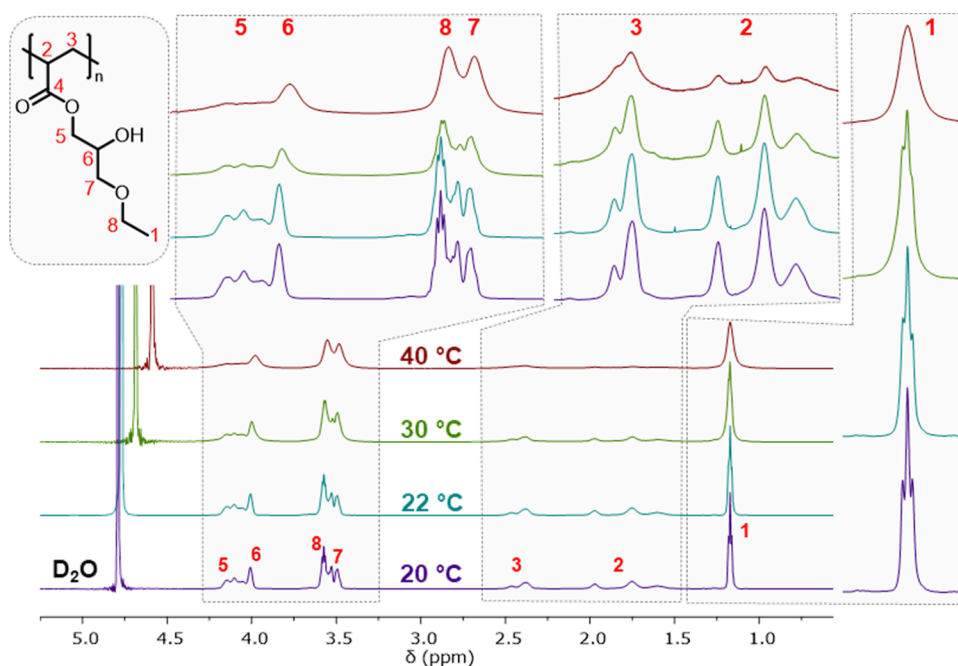


Figure 4. Temperature-dependent ^1H NMR spectra (D_2O , 700 MHz) of **pEHPA25** at a concentration of 10 mg mL^{-1} (T_{cp} : $23.7 \text{ }^\circ\text{C}$). The spectra were referenced to peak 1 at $20 \text{ }^\circ\text{C}$ (1.17 ppm). Peaks are assigned with numbers according to the illustrated chemical structure, and marked insets show enlarged regions for signals of interest.

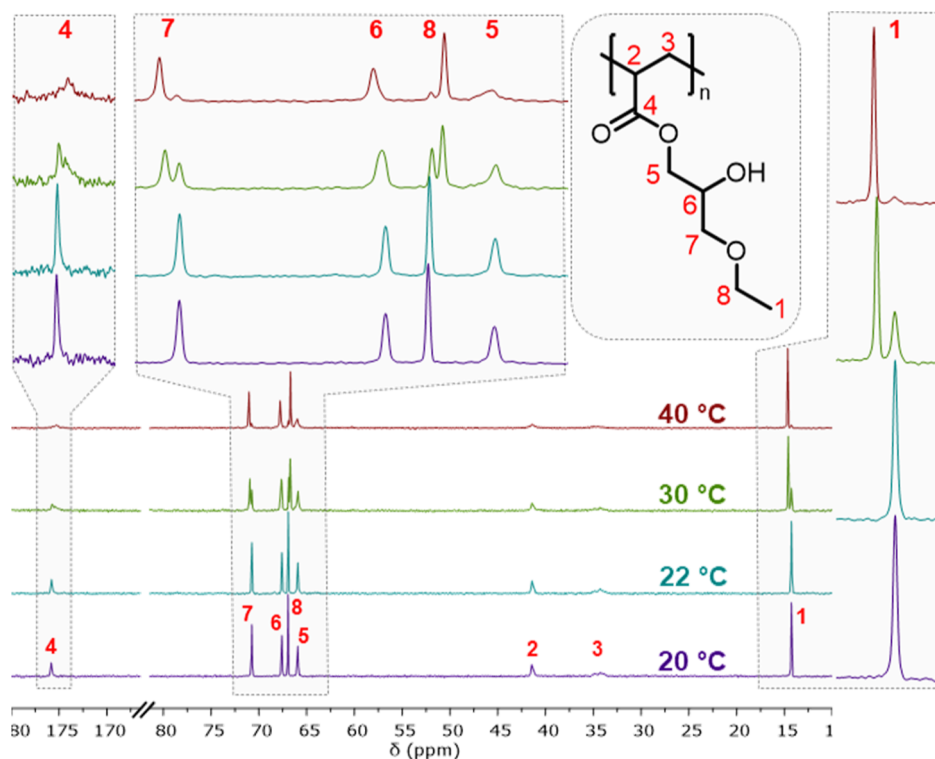


Figure 5. Temperature-dependent ^{13}C NMR spectra (D_2O , 176 MHz) of **pEHPA25** at a concentration of 10 mg mL^{-1} (T_{cp} : $23.7 \text{ }^\circ\text{C}$). The spectra were referenced to peak 1 at $20 \text{ }^\circ\text{C}$ (14.27 ppm). Signals are assigned with numbers according to the illustrated chemical structure, and marked insets show enlarged regions for signals of interest.

1600–1700 nm at T_{cp} (Figures 3 and S13). Cooling the polymer solutions back to the value of T_{100-5} usually resulted in similar size distributions, except for **pHMPMA25** solutions in PBS, which had a small percentage of remaining aggregates with a size of $\sim 480 \text{ nm}$ (data not shown). Overall, **pEHPA** solutions exhibit a more uniform aggregation behavior and less

tendency to preaggregation. In contrast, **pHMPMA** solutions are more susceptible to environmental changes (as is apparent from different final aggregate sizes) and tend to aggregate already below the macroscopic T_{cp} value. So far, these observations are well aligned with the results from turbidimetry measurements.

Table 2. Overview of Proton Peak Integrals of pEHPA25 (T_{cp} : 23.7 °C) as Obtained from Temperature-Dependent ^1H NMR (D_2O , 700 MHz) Spectra Measured at a Concentration of 10 mg mL $^{-1}$ ^a

assigned peak N ^o (δ [ppm])	5 + 6 (3.87–4.31)	8 + 7 (3.36–3.76)	3 (2.21–2.62)	2 (1.38–2.19)	1 (1.17)
integral at 20 °C	2.89	4.01	0.98	1.98	3.00
integral at 22 °C	2.84	4.04	0.97	1.89	3.00
integral at 30 °C	2.50	3.98	0.74	1.28	3.00
integral at 40 °C	2.27	3.83	0.70	0.93	3.00

^aAll peak integrals were referenced to the respective triplet of the methyl group (1) located at 1.17 ppm.

The hydration of certain chemical groups within a polymer chain can be accessed through structure analysis methods, such as infrared (IR) or NMR spectroscopy.^{26,32,39} Temperature-dependent NMR measurements are particularly useful since they can indicate hydration changes in the vicinity of the polymers' hydrogen and carbon atoms in the backbone and side chain regions through signal shifts, signal broadening, and change in integral values due to restricted chain movement, *e.g.*, in aggregates. Remarkably, none of those were observed in temperature-dependent ^1H and ^{13}C NMR spectra of pHMPMA25 solutions when passing the T_{cp} (41.2 °C) from 30 to 60 °C in D_2O at a concentration of 10 mg mL $^{-1}$ (Figures S14 and S15), also exhibiting almost identical ^1H integral values (Table S4). pEHPA25 ^1H and ^{13}C spectra are presented in Figures 4 and 5 with ^1H peak integrals listed in Table 2.

The temperature-dependent ^1H NMR spectra of pEHPA25 indicated distinct changes in the signal structure and integral values when passing T_{cp} (23.7 °C), as shown in Figure 4 and listed in Table 2. The well-resolved fine structure of the proton signals assigned to the ethoxy groups (1, 8) at 20 and 22 °C gradually converted into a single broad peak at 40 °C, indicating the ethoxy groups' increasingly reduced mobility. Interestingly, the corresponding integral of peak 8 decreased only around 5% when heating the system from 20 to 40 °C. However, it has to be noted that due to signal overlapping, the integrals of 8 + 7 can only be accessed cumulatively. Besides a signal broadening of all proton signals above 22 °C, a more substantial decrease of the residual side chain proton integrals 5 and 6 by ~20% (2.89 to 2.27) and the backbone proton integrals 2 and 3 by ~28% (0.98 to 0.70) and 50% (1.98 to 0.93), respectively, was observed. Therefore, the strongest dehydration appears on the pEHPA backbone and the side chain protons flanking the secondary carbon bearing the hydroxyl group.

Similar conclusions can be drawn from the temperature-dependent ^{13}C NMR spectra of the polymers. In agreement with proton spectra, the carbon signals of pHMPMA25 (Figure S15) hardly indicated any shifts or broadening. Therefore, we assume that the hydration state of single chains does not change significantly when increasing the temperature, even ~18 °C above the macroscopically detectable phase transition, and the aggregation is driven mainly through the hydrophobic backbone.⁴⁰ On the contrary, the thermal phase transition of pEHPA25 impacts all carbon signals, as shown in Figure 5. Most prominent appears the splitting of the carbon signals 7, 8, and 1 around the ether group in the side chain and the carbonyl carbon 4 above the T_{cp} . The split signals can be assigned to the respective carbons in the hydrated and dehydrated states.²⁶ Since the hydrated signal fraction is detected up to 40 °C, it can be assumed that pEHPA25 dehydration on the microscopic scale proceeds well above the macroscopically detectable cloud point at 23.7 °C. This observation agrees with the ^1H spectra in which the fine

structure of 7 and 8 can still be seen at 30 °C. The hydroxy group bearing secondary carbon 6 shifted to higher parts per million values at 30 and 40 °C, indicating progressing dehydration. The carbon signals 2, 3, and 5 broaden noticeably, consistent with the observed peak broadening and reduced integral values of the corresponding proton signals in Figure 4 and Table 2. In summary, we observed that pHMPMA chains remain similarly hydrated throughout the temperature ramp on the molecular scale. In contrast, pEHPA chains start dehydrating continuously after passing the macroscopic T_{cp} value up to 16 °C above the T_{cp} .

Overall, the microscopic phase transition of pHMPMA25 is similar to the one described for more hydrophilic thermoresponsive pOEGMA with T_{cp} values above 40 °C and to p(NIPAM-*co*-HIPAM) copolymers with a one-to-one monomer ratio.^{6,40} For such polymers with sufficiently hydrophilic side chains, distinct stably hydrated side chain signals are reported, even above the macroscopic cloud point at T_{cp} . Differently from pHMPMA25, the backbone protons of pOEGMA or p(NIPAM-*co*-HIPAM) typically broaden or even disappear during the phase transition, sometimes even below T_{cp} .^{6,40} The consistent, nonsplitting NMR peaks of pHMPMA side chain carbons can be attributed to a stable water shell due to its sterically well accessible hydroxy groups. The microscopic phase transition of pEHPA25 is comparable to that of pOEGMA polymers with less hydrophilic side chains and a T_{cp} ~ 26 °C, showing a thermally induced, pronounced broadening of the backbone protons, resulting in lower integral values with increasing temperature and a comparably less broadened side chain signal.⁴⁰ Furthermore, the apparent splitting of carbon signals of pEHPA25, indicating the presence of both hydrated and dehydrated structural elements around the ether moiety, is similarly observed with thermoresponsive PGE polymers. While peak splitting of pEHPA occurs after the macroscopic phase transition, it is detectable already below the T_{cp} for PGE.²⁶ This striking difference can be attributed to the presence of the hydroxy moiety in the side chain of pEHPA, which results in partial hydration, even in the aggregated state above the cloud point.

Proof-of-Concept Functionalization via Fluorescence Labeling. To demonstrate the functionalization potential of the hydroxy groups present in the side chain of the polymers, we used a straightforward two-step reaction sequence to convert a maximum of 0.5% of the available hydroxy groups to reactive carboxy groups with succinic anhydride and their subsequent carbodiimide-based amide coupling (Scheme S2 and Figures S8 and S9). An amine-functionalized fluorescent Cy5-dye was employed for amidation to easily prove successful functionalization due to the resulting concentration-dependent UV absorbance of the blue polymer conjugate measured in water (Figure S16). The phase transition of the labeled polymers pEHPA25-Cy5 and pHMPMA25-Cy5 was investigated using turbidimetry and fluorescence measurements

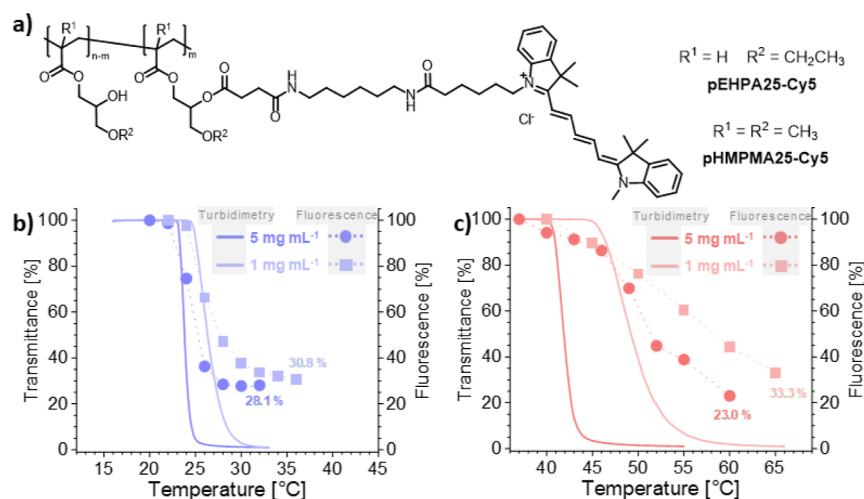


Figure 6. Chemical structure of fluorescent, Cy5-labeled thermoresponsive **pEHPA25-Cy5** and **pHMPMA25-Cy5** polymers (a). Concentration-dependent normalized turbidimetry (lines; $n = 4$) and fluorescence (circles, squares; $n = 1$) measurements of **pEHPA25-Cy5** (b) and **pHMPMA25-Cy5** (c) in H₂O at 5 and 1 mg mL⁻¹. The residual fluorescence (%) refers to the highest measured temperature, and symbols are connected to guide the eye.

(Figure 6). Corresponding cooling cycles and temperature-dependent fluorescence curves are presented in Figures S17 and S19, respectively. Maximum emission values were used to trace the thermally induced phase transition *via* the fluorescence signal of the conjugate between 660 and 700 nm.

The **pEHPA25-Cy5** solutions showed a reversible phase transition at 24.0 and 26.8 °C for the 5 and 1 mg mL⁻¹ solutions. The T_{cp} values matched well the T_{cp} values of the nonfunctionalized polymers (Figure 2). **pHMPMA25-Cy5** solutions exhibited a reversible phase transition at 42.3 and 49.0 °C for the 5 and 1 mg mL⁻¹ solutions, which is 1–2 °C below the T_{cp} of the respective nonfunctionalized polymer solutions (Figure 2), revealing the minor influence of the conjugated hydrophobic Cy5 dye.

The aggregation-induced fluorescence decline of each **pEHPA25-Cy5** solution during heating closely followed the respective sigmoidal-shaped transmittance curve. The decline continued slightly after the turbidimetry transition and resulted in ~30% residual fluorescence after the transition. In contrast, the temperature-dependent fluorescence change of the **pHMPMA25-Cy5** solutions deviated from the transition curve determined by turbidimetry. The fluorescence of the 5 mg mL⁻¹ solution steadily declined to 86% between 37 and 46 °C, passing the turbidimetrically determined T_{cp} at 42.3 °C along the way. From 46 to 60 °C, the decrease progressed rapidly to 23% in a mostly linear fashion. We assume a certain degree of preaggregation, also observed in DLS measurements for **pHMPMA** polymers, to be responsible for the initial moderate fluorescence decline. At approximately 4 °C after the turbidimetrically determined T_{cp} , the aggregates' size must increase significantly, causing a rapid emission decrease and, overall, a delayed broadened transition. Conversely, more dilute 1 mg mL⁻¹ **pHMPMA25-Cy5** solutions did not show a discrete transition. Instead, an almost linear fluorescence decline to 33% was observed from 40 to 65 °C, ranging from 9 °C below to 16 °C above the T_{cp} value at 49 °C. Notably, both dye conjugates exhibit a fully reversible phase transition behavior, as returning to the initial temperature led to fully restored fluorescence emission (data not shown).

Because **pEHPA** side chain dehydration contributes to the aggregation process, Cy5 moieties likely become embedded in

the aggregates, markedly reducing the optical transparency and the excitation and emission of Cy5 dyes after the phase transition. As detected by temperature-dependent NMR measurements, **pHMPMA** side chains do not dehydrate and thus cause aggregation. Hence, the macroscopically observed aggregation must be due to hydrophobic methacrylate backbone interactions. The Cy5 dye conjugated to **pHMPMA** is less likely to be embedded in aggregates due to the surrounding hydrated neighboring side chains. For this reason, we assume that the fluorescence decrease is mainly caused by aggregates, which scatter the light passing through the sample. Consequently, a temperature-driven increase in aggregated chains yields a linear emission decrease within the probed temperature range. This agrees well with the observed more rapid fluorescence decline after passing the T_{cp} due to a faster aggregate increase for higher concentrated 5 mg mL⁻¹ **pHMPMA** solutions.

Thermoresponsive polymers labeled with fluorescent dyes, which exhibit sigmoidal fluorescence decline profiles close to detected transmittance curves, such as **pEHPA25-Cy5**, can also be found in the literature. Usually, the sigmoidal fluorescence decline appears for polymers with higher molecular weights and polymer concentrations in solution. Fluorescent **pNIPAM** copolymer solutions with molecular weights between 22 and 27 kDa and 5 mg mL⁻¹ concentration exhibited a rapid fluorescence decline around the measured T_{cp} s of 30.5–32 °C, depending on M and the nature of the incorporated dye.⁴¹ Similarly, a 2.5 mg mL⁻¹ solution of fluorescent **pOEGMA** with $M = 29$ kDa and a T_{cp} of 18.3 °C showed a sigmoidal decrease in emission with a pronounced decline in the range between 11 and 21 °C.⁴² Low molecular weight polymers, on the other hand, typically exhibit a more linear fluorescence decline. The temperature-dependent fluorescence of **pNIPAM** copolymer solutions, each with a different dye type and molecular weights of ~6 and 11 kDa, declined linearly between 25 and 50 °C, even at high concentrations of 5 mg mL⁻¹.⁴³ Also, a fluorescent **pOEGA** copolymer ($M \sim 9$ kDa) solution at 0.1 mg mL⁻¹ with a T_{cp} of ~42 °C declined linearly in fluorescence between 35 and 50 °C.⁷ The first literature examples with higher molecular weights and polymer concentrations exhibiting sigmoidal

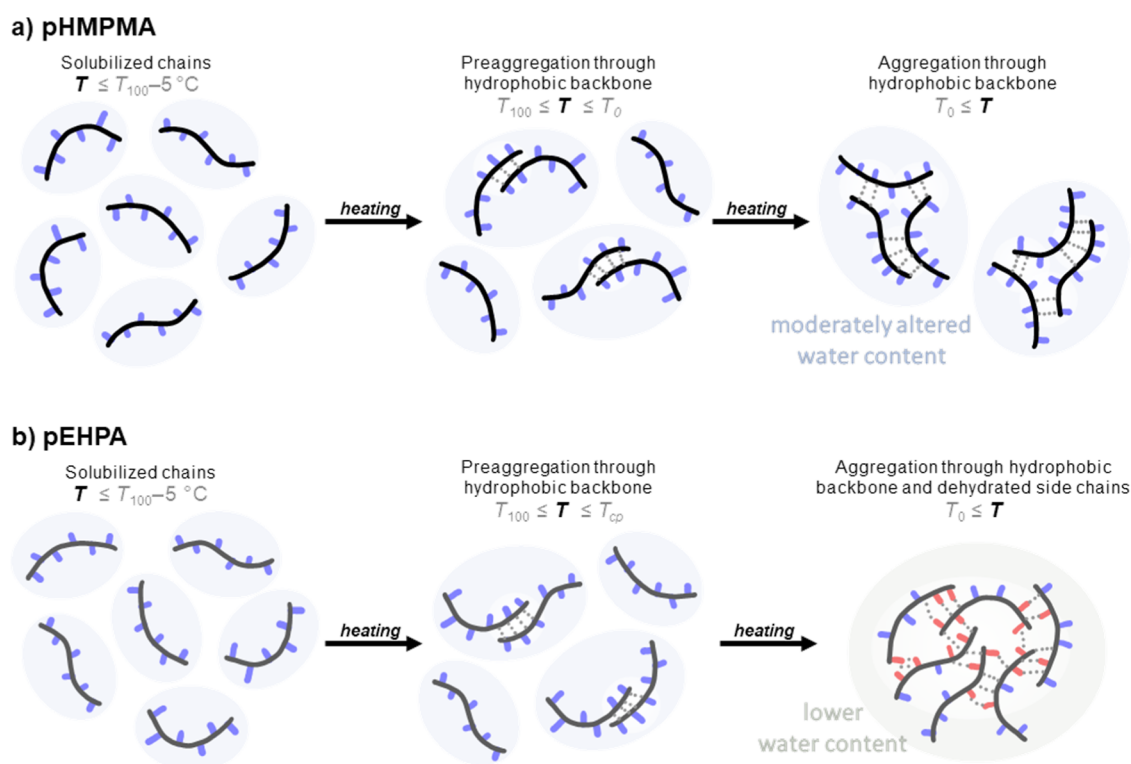


Figure 7. Schematic mechanistic phase transition of the **pHMPMA** (a) and **pEHPA** (b) chains in water.

fluorescence declines agree well with the detected sigmoidal fluorescence transitions of **pEHPA25-Cy5** and may be linked to their sharp phase transitions. Contrarily, following literature examples of low molecular weight polymers at low concentrations that typically result in broader transitions exhibit linear fluorescence declines with temperature and match our results for the fluorescence decline of **pHMPMA25-Cy5** in agreement with their broader phase transition.

Phase Transition Mechanism. The combined results provide a comprehensive picture (Figure 7) of how the shift in hydrophobicity from the side chain in **pEHPA** to the backbone in **pHMPMA** affects the molecular and microscopic phase transition behavior in addition to the macroscopically apparent difference in the T_{cp} values.

pHMPMA solutions were observed to be more sensitive to thermal and concomitant environmental changes, such as the presence of salts or the local polymer concentration, exhibiting broader transition regimes with smaller aggregates forming above the T_{cp} . Additionally, NMR analysis revealed no significant change in the hydration for any particular structural element of the polymer chain. Temperature-dependent fluorescence measurements of functionalized polymers indicated that the phase-transition-driven emission decline happens in an even wider range than turbidimetry measurements. Also, the typical sigmoidally shaped phase transition curve turns linear at low concentrations. Therefore, we conclude that the **pHMPMA** transition in water is driven mainly through the most hydrophobic polymer chain part—the methacrylate backbone. In contrast, terminal methoxy compared to ethoxy moieties on the side chains are not hydrophobic enough to induce marked dehydration of adjacent hydroxy groups. This results in continuously hydrated side chains over the measured temperature region, no driving force for the aggregation, and, finally, limited

aggregate size when compared to **pEHPA**, directly above the T_{cp} . Hence, the water content in the polymer phase remains rather constant, and the formation of a polymer-rich phase in PBS above the T_{cp} indicates an LLPS-like transition type. The pronounced molecular weight- and concentration-dependent thermoresponsiveness of **pHMPMA** is similarly reflected by structurally related **pHPA** polymers. The reported lower T_{cp} values of **pHPA** in the literature than those of **pHMPMA** agree with its shorter but more hydrophobic methyl group in the side chain compared to the methoxy group of **pHMPMA**.²⁵ Pronounced sensitivity to environmental changes, e.g., ion content, connected with the increasing aggregate size was also observed for LLPS type **p(NIPAM-co-HIPAM)** copolymers with a high content of hydroxy groups.^{6,18} Enhanced aggregate formation in PBS solutions can be explained through a strong competing effect of the ions for hydrating water, which can enable side chain dehydration, thus resulting in polymer aggregate precipitation.

pEHPA polymer solutions exhibit less sensitivity to the thermal phase transition toward the screened environmental parameters on the macroscopic level. Sharper transitions, even within a range of one degree, and the formation of larger aggregates already at the cloud point were observed. Preaggregates in water were smaller and occurred only close to the T_{cp} . On the microscopic scale, distinct dehydration of the backbone was observed *via* ^1H and ^{13}C NMR spectroscopy, leading to broader signals and reduced peak integrals. Furthermore, carbon signals near the hydroxy and ether groups indicated dehydration only above the macroscopic cloud point, either through peak shift or peak splitting. Fluorescence measurements confirmed a sharp transition, supporting the previous results. Therefore, a less pronounced driving force for **pEHPA** aggregation below the cloud point can be derived due to the less hydrophobic acrylate backbone

and a distinct side chain amphiphilicity compared to those of **pHMPMA**, which enforces partial side chain dehydration only above the T_{cp} , as indicated by NMR peak splitting. At and above T_{cp} , these structural factors add up to a higher driving force for **pEHPA** aggregation, resulting in larger aggregates directly at T_{cp} , as detected *via* DLS measurements and illustrated in Figure 7b. The increase in side chain hydrophobicity through the ethoxy group also explains the robust T_{cp} values in the screened concentration and molecular weight range in the presence and absence of salts. In general, the **pEHPA** transition can, therefore, be described as a coil-to-globule transition type with distinct dehydration and reduction of water content in the aggregates, similar to **PGE**, **pNIPAM**, and **p(NIPAM-co-HIPAM)** copolymers with a low **HIPAM** content.

CONCLUSIONS

Isomeric polyacrylates (**pEHPA**) and polymethacrylates (**pHMPMA**) bearing functional hydroxy groups in the side chain were synthesized, and their unprecedented LCST transition behavior was studied in detail. Turbidimetry and DLS measurements revealed a less parameter-dependent phase transition behavior in the 22 to 33 °C range for the **pEHPA** polymers with pronounced side-chain hydrophobicity. Conversely, **pHMPMA** polymers with more pronounced backbone hydrophobicity exhibited phase transitions between 37 and 67 °C and were more susceptible to the experimental conditions. These properties were linked to the transition behavior on the microscopic scale, as observed *via* NMR spectroscopy. **pEHPA** chains started dehydrating directly after the macroscopic cloud point, thus revealing a pronounced driving force for aggregation. **pHMPMA** chains showed no distinct dehydration behavior up to 18° above the T_{cp} . Therefore, we can conclude that for a distinct, thermally induced dehydratization of hydroxy groups in thermoresponsive polymers, it is necessary to add hydrophobic moieties in direct proximity, which also helps reduce the phase transition dependence on environmental influences. Finally, a straightforward polymer labeling with Cyanine5-dye showed the postfunctionalization potential for the presented thermoresponsive polymers. With the conjugate at hand, the temperature-dependent fluorescence decline was aligned with the deduced phase transition mechanism (Figure 7) and related to the transition behavior to literature known thermosensitive polymers, such as **pHPA** for **pHMPMA** and **pNIPAM** for **pEHPA**. With these functional polymers, whose thermoresponsive behavior in solution is fundamentally understood, next-level applied materials such as thermoresponsive microgels or surface-bound hydrogels can be rationally designed with optimized smart functions for, *e.g.*, flow biocatalysis.⁴⁴

ASSOCIATED CONTENT

Supporting Information

The Supporting Information is available free of charge at <https://pubs.acs.org/doi/10.1021/acs.macromol.3c01251>.

List of materials and methods, monomer synthesis and analytical data (NMR), polymer synthesis and analytical data (NMR and GPC), procedure for polymer Cy5 labeling and its analytical data (NMR and GPC), supporting turbidimetry, DLS, and NMR results of thermoresponsive analysis, calculation of T_{100} and T_0 values, calculation of hydrodynamic and Flory radii,

photographs of the temperature equilibration of fluorescent samples, and supporting fluorescence data (PDF)

AUTHOR INFORMATION

Corresponding Author

Marie Weinhart – Institute of Chemistry and Biochemistry, Freie Universitaet Berlin, Berlin 14195, Germany; Institute of Physical Chemistry and Electrochemistry, Leibniz Universitaet Hannover, Hannover 30167, Germany; orcid.org/0000-0002-5116-5054; Phone: +49 511-762 14938; Email: marie.weinhart@pci.uni-hannover.de, marie.weinhart@fu-berlin.de

Authors

Alexander Schweigerdt – Institute of Chemistry and Biochemistry, Freie Universitaet Berlin, Berlin 14195, Germany

Daniel D. Stöbener – Institute of Chemistry and Biochemistry, Freie Universitaet Berlin, Berlin 14195, Germany; Institute of Physical Chemistry and Electrochemistry, Leibniz Universitaet Hannover, Hannover 30167, Germany; orcid.org/0000-0003-1396-2607

Andreas Schäfer – Institute of Chemistry and Biochemistry, Freie Universitaet Berlin, Berlin 14195, Germany

Selin Kara – Institute of Technical Chemistry, Leibniz Universitaet Hannover, Hannover 30167, Germany

Complete contact information is available at:

<https://pubs.acs.org/10.1021/acs.macromol.3c01251>

Notes

The authors declare no competing financial interest.

ACKNOWLEDGMENTS

A.S. thanks I. Fallaha for providing batches of HMPMA and EHPA monomers and O. Staudhammer for synthesizing the **pEHPA10** polymer. The authors warmly thank the Federal Ministry of Education and Research (FKZ: 13N13523) (M.W. and A.S.) and the Core Facility BioSupraMol, supported by the German Research Foundation (DFG).

REFERENCES

- Matthes, R.; Frey, H. Polyethers Based on Short-Chain Alkyl Glycidyl Ethers: Thermoresponsive and Highly Biocompatible Materials. *Biomacromolecules* **2022**, *23* (6), 2219–2235.
- Sponchioni, M.; Capasso Palmiero, U.; Moscatelli, D. Thermoresponsive polymers: Applications of smart materials in drug delivery and tissue engineering. *Mater. Sci. Eng., C* **2019**, *102*, 589–605.
- Wei, M. L.; Gao, Y. F.; Li, X.; Serpe, M. J. Stimuli-responsive polymers and their applications. *Polym. Chem.* **2017**, *8* (1), 127–143.
- Zhang, Q.; Weber, C.; Schubert, U. S.; Hoogenboom, R. Thermoresponsive polymers with lower critical solution temperature: from fundamental aspects and measuring techniques to recommended turbidimetry conditions. *Mater. Horiz.* **2017**, *4* (2), 109–116.
- Aseyev, V.; Tenhu, H.; Winnik, F. M. Non-ionic Thermoresponsive Polymers in Water. *Self Organized Nanostructures of Amphiphilic Block Copolymers II*; Advances in Polymer Science, 2010; pp 29–89.
- Maeda, T.; Takenouchi, M.; Yamamoto, K.; Aoyagi, T. Analysis of the formation mechanism for thermoresponsive-type coacervate with functional copolymers consisting of N-isopropylacrylamide and 2-hydroxyisopropylacrylamide. *Biomacromolecules* **2006**, *7* (7), 2230–2236.

- (7) Vancoillie, G.; Van Guyse, J. F. R.; Voorhaar, L.; Maji, S.; Frank, D.; Holder, E.; Hoogenboom, R. Understanding the effect of monomer structure of oligoethylene glycol acrylate copolymers on their thermoresponsive behavior for the development of polymeric sensors. *Polym. Chem.* **2019**, *10* (42), 5778–5789.
- (8) Becherer, T.; Heinen, S.; Wei, Q.; Haag, R.; Weinhart, M. In-depth analysis of switchable glycerol based polymeric coatings for cell sheet engineering. *Acta Biomater.* **2015**, *25*, 43–55.
- (9) Zhao, C.; Ma, Z.; Zhu, X. X. Rational design of thermoresponsive polymers in aqueous solutions: A thermodynamics map. *Prog. Polym. Sci.* **2019**, *90*, 269–291.
- (10) Halperin, A.; Kröger, M.; Winnik, F. M. Poly(N-isopropylacrylamide) Phase Diagrams: Fifty Years of Research. *Angew. Chem., Int. Ed. Engl.* **2015**, *54* (51), 15342–15367.
- (11) Savoji, M. T.; Strandman, S.; Zhu, X. X. Block Random Copolymers of N-Alkyl-Substituted Acrylamides with Double Thermosensitivity. *Macromolecules* **2012**, *45* (4), 2001–2006.
- (12) Cao, Y.; Zhu, X. X.; Luo, J.; Liu, H. Effects of Substitution Groups on the RAFT Polymerization of N-Alkylacrylamides in the Preparation of Thermosensitive Block Copolymers. *Macromolecules* **2007**, *40* (18), 6481–6488.
- (13) Hoogenboom, R.; Thijs, H. M.; Jochems, M. J.; van Lankvelt, B. M.; Fijten, M. W.; Schubert, U. S. Tuning the LCST of poly(2-oxazoline)s by varying composition and molecular weight: alternatives to poly(N-isopropylacrylamide)? *Chem. Commun.* **2008**, 5758–5760.
- (14) He, T.; Wang, Y.; Xu, L.; Fu, X.; Narumi, A.; Sato, S.-i.; Shen, X.; Kakuchi, T. Poly[glycidyl oligo(oxyethylene)carbamate]s (PGn-EOmR' and R-PGn-EOmR'): controlled synthesis and effects of molecular parameters (n and m), side groups (R'), and end-groups (R) on thermoresponsive properties. *Polym. Chem.* **2021**, *12* (17), 2580–2591.
- (15) Weber, C.; Hoogenboom, R.; Schubert, U. S. Temperature responsive bio-compatible polymers based on poly(ethylene oxide) and poly(2-oxazoline)s. *Prog. Polym. Sci.* **2012**, *37* (5), 686–714.
- (16) Schweigerdt, A.; Heinen, S.; Stobener, D. D.; Weinhart, M. Grafting Density-Dependent Phase Transition Mechanism of Thermoresponsive Poly(glycidyl ether) Brushes: A Comprehensive QCM-D Study. *Langmuir* **2021**, *37* (23), 7087–7096.
- (17) Sugihara, S.; Hashimoto, K.; Matsumoto, Y.; Kanaoka, S.; Aoshima, S. Thermosensitive polyalcohols: Synthesis via living cationic polymerization of vinyl ethers with a silyloxy group. *J. Polym. Sci., Part A: Polym. Chem.* **2003**, *41* (21), 3300–3312.
- (18) Maeda, T.; Kanda, T.; Yonekura, Y.; Yamamoto, K.; Aoyagi, T. Hydroxylated poly(N-isopropylacrylamide) as functional thermoresponsive materials. *Biomacromolecules* **2006**, *7* (2), 545–549.
- (19) Hironaka, K.; Yoshihara, E.; Nabil, A.; Lai, J. J.; Kikuchi, A.; Ebara, M. Conjugation of antibody with temperature-responsive polymer via in situ click reaction to enable biomarker enrichment for increased diagnostic sensitivity. *Biomater. Sci.* **2021**, *9* (14), 4870–4879.
- (20) Vancoillie, G.; Frank, D.; Hoogenboom, R. Thermoresponsive poly(oligo ethylene glycol acrylates). *Prog. Polym. Sci.* **2014**, *39* (6), 1074–1095.
- (21) Hu, Z.; Cai, T.; Chi, C. Thermoresponsive oligo(ethylene glycol)-methacrylate- based polymers and microgels. *Soft Matter* **2010**, *6* (10), 2115.
- (22) Weaver, J. V. M.; Bannister, I.; Robinson, K. L.; Bories-Azeau, X.; Armes, S. P.; Smallridge, M.; McKenna, P. Stimulus-Responsive Water-Soluble Polymers Based on 2-Hydroxyethyl Methacrylate. *Macromolecules* **2004**, *37* (7), 2395–2403.
- (23) Ikemoto, Y.; Harada, Y.; Tanaka, M.; Nishimura, S. N.; Murakami, D.; Kurahashi, N.; Moriwaki, T.; Yamazoe, K.; Washizu, H.; Ishii, Y.; et al. Infrared Spectra and Hydrogen-Bond Configurations of Water Molecules at the Interface of Water-Insoluble Polymers under Humidified Conditions. *J. Phys. Chem. B* **2022**, *126* (22), 4143–4151.
- (24) Eggenhuisen, T. M.; Becer, C. R.; Fijten, M. W. M.; Eckardt, R.; Hoogenboom, R.; Schubert, U. S. Libraries of Statistical Hydroxypropyl Acrylate Containing Copolymers with LCST Properties Prepared by NMP. *Macromolecules* **2008**, *41* (14), 5132–5140.
- (25) Vo, C.-D.; Rosselgong, J.; Armes, S. P.; Tirelli, N. Stimulus-responsive polymers based on 2-hydroxypropyl acrylate prepared by RAFT polymerization. *J. Polym. Sci., Part A: Polym. Chem.* **2010**, *48* (9), 2032–2043.
- (26) Heinen, S.; Rackow, S.; Schäfer, A.; Weinhart, M. A Perfect Match: Fast and Truly Random Copolymerization of Glycidyl Ether Monomers to Thermoresponsive Copolymers. *Macromolecules* **2017**, *50* (1), 44–53.
- (27) Stobener, D. D.; Hoppensack, A.; Scholz, J.; Weinhart, M. Endothelial, smooth muscle and fibroblast cell sheet fabrication from self-assembled thermoresponsive poly(glycidyl ether) brushes. *Soft Matter* **2018**, *14* (41), 8333–8343.
- (28) Olszewski-Ortar, A.; Gros, P.; Fort, Y. Selective ring-opening of ω -epoxyalkyl (meth)acrylates. An efficient access to bifunctional monomers. *Tetrahedron Lett.* **1997**, *38* (50), 8699–8702.
- (29) Tauscher, S.; Angermann, J.; Catel, Y.; Moszner, N. Evaluation of alternative monomers to HEMA for dental applications. *Dent. Mater.* **2017**, *33* (7), 857–865.
- (30) Lu, C.; Chen, N.; Gu, Z. W.; Feng, X. Synthesis and polymerization of γ -alkoxy- β -hydroxypropyl acrylates. *J. Polym. Sci., Polym. Chem. Ed.* **1980**, *18* (12), 3403–3411.
- (31) Zamfir, M.; Rodriguez-Emmenegger, C.; Bauer, S.; Barner, L.; Rosenhahn, A.; Barner-Kowollik, C. Controlled growth of protein resistant PHEMA brushes via S-RAFT polymerization. *J. Mater. Chem. B* **2013**, *1* (44), 6027.
- (32) Plamper, F. A.; Steinschulte, A. A.; Hofmann, C. H.; Drude, N.; Mergel, O.; Herbert, C.; Erberich, M.; Schulte, B.; Winter, R.; Richtering, W. Toward Copolymers with Ideal Thermosensitivity: Solution Properties of Linear, Well-Defined Polymers of N-Isopropyl Acrylamide and N,N-Diethyl Acrylamide. *Macromolecules* **2012**, *45* (19), 8021–8026.
- (33) Thomas, D. B.; Convertine, A. J.; Hester, R. D.; Lowe, A. B.; McCormick, C. L. Hydrolytic Susceptibility of Dithioester Chain Transfer Agents and Implications in Aqueous RAFT Polymerizations. *Macromolecules* **2004**, *37* (5), 1735–1741.
- (34) Otulakowski, L.; Kaspro, M.; Strzelecka, A.; Dworak, A.; Trzebicka, B. Thermal Behaviour of Common Thermoresponsive Polymers in Phosphate Buffer and in Its Salt Solutions. *Polymers* **2020**, *13* (1), 90.
- (35) Jungwirth, P.; Cremer, P. S. Beyond Hofmeister. *Nat. Chem.* **2014**, *6* (4), 261–263.
- (36) Bloksma, M. M.; Bakker, D. J.; Weber, C.; Hoogenboom, R.; Schubert, U. S. The Effect of Hofmeister Salts on the LCST Transition of Poly(2-oxazoline)s with Varying Hydrophilicity. *Macromol. Rapid Commun.* **2010**, *31* (8), 724–728.
- (37) Zhang, Y.; Furyk, S.; Bergbreiter, D. E.; Cremer, P. S. Specific ion effects on the water solubility of macromolecules: PNIPAM and the Hofmeister series. *J. Am. Chem. Soc.* **2005**, *127* (41), 14505–14510.
- (38) Meng, X.; Li, D.; Zhang, A.; Zhang, Q. Probing the glycopolymer-ion interaction via specific ion effects. *Polym. Chem.* **2020**, *11* (41), 6681–6687.
- (39) Konefal, R.; Cernoch, P.; Konefal, M.; Spevacek, J. Temperature Behavior of Aqueous Solutions of Poly(2-oxazoline) Homopolymer and Block Copolymers Investigated by NMR Spectroscopy and Dynamic Light Scattering. *Polymers* **2020**, *12* (9), 1879.
- (40) Han, S.; Hagiwara, M.; Ishizone, T. Synthesis of Thermally Sensitive Water-Soluble Polymethacrylates by Living Anionic Polymerizations of Oligo(ethylene glycol) Methyl Ether Methacrylates. *Macromolecules* **2003**, *36* (22), 8312–8319.
- (41) Yamada, A.; Hiruta, Y.; Wang, J.; Ayano, E.; Kanazawa, H. Design of Environmentally Responsive Fluorescent Polymer Probes for Cellular Imaging. *Biomacromolecules* **2015**, *16* (8), 2356–2362.
- (42) Pietsch, C.; Vollrath, A.; Hoogenboom, R.; Schubert, U. S. A fluorescent thermometer based on a pyrene-labeled thermoresponsive polymer. *Sensors* **2010**, *10* (9), 7979–7990.

(43) Ding, Z.; Wang, C.; Feng, G.; Zhang, X. Thermo-Responsive Fluorescent Polymers with Diverse LCSTs for Ratiometric Temperature Sensing through FRET. *Polymers* **2018**, *10* (3), 283.

(44) Gkantzou, E.; Weinhart, M.; Kara, S. 3D printing for flow biocatalysis. *RSC Sustainability* **2023**, *1* (7), 1672–1685.

Supporting Information

Impact of Amphiphilicity Balance in Hydroxy-Functional, Isomeric, Thermoresponsive Poly(meth)acrylates

Alexander Schweigerdt¹, Daniel D. Stöbener^{1,2}, Andreas Schäfer¹, Selin Kara³, Marie Weinhart^{1,2}*

¹ Institute of Chemistry and Biochemistry, Freie Universitaet Berlin, Takustr. 3, 14195 Berlin, Germany

² Institute of Physical Chemistry and Electrochemistry, Leibniz Universitaet Hannover, Callinstr. 3A, 30167 Hannover, Germany

³ Institute of Technical Chemistry, Leibniz Universitaet Hannover, Callinstr. 3-9, 30167 Hannover, Germany

* Corresponding author: email marie.weinhart@pci.uni-hannover.de and marie.weinhart@fu-berlin.de, phone: +49 511-762 14938

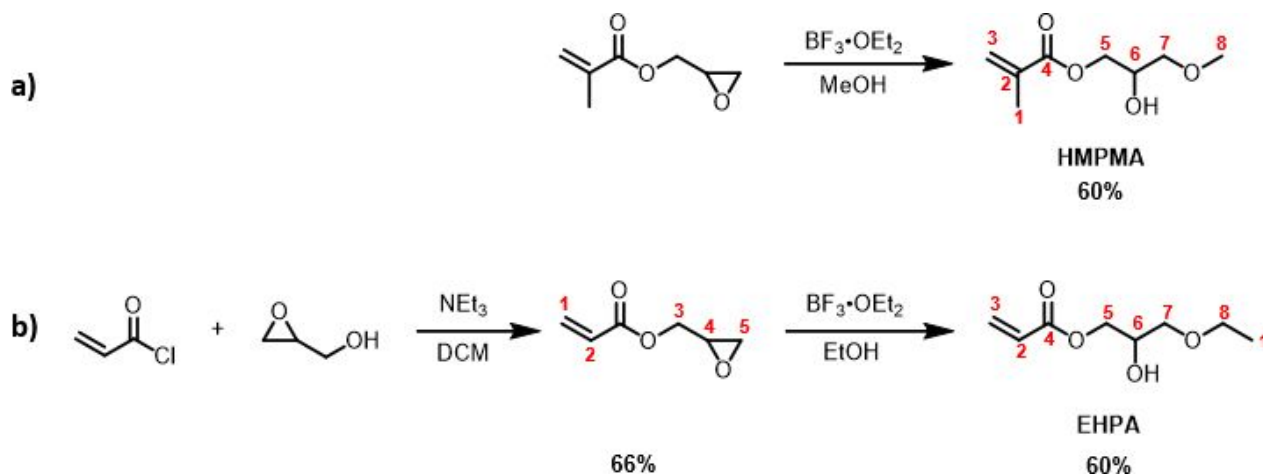
Materials. All materials and chemicals were used as received unless stated otherwise. Acryloyl chloride, 1-ethyl-3-(3-dimethylaminopropyl)carbodiimide hydrochloride (EDC HCl), and deuterated chloroform (CDCl_3) were purchased from ABCR (Karlsruhe, German). Glycidol, boron trifluoride etherate ($\text{BF}_3 \cdot \text{OEt}_2$, 46% solution in diethyl ether), azobis(4-cyanovaleric acid) (ACVA), and 4-cyano-4-(phenylcarbonothioylthio)pentanoic acid (RAFT Agent) were purchased from Sigma Aldrich (Steinheim, Germany). Triethylamine (NEt_3) was purchased from Sigma Aldrich or TCI GmbH (Eschborn, Germany). Glycidyl methacrylate and succinic anhydride (SA) were purchased from TCI GmbH. 4-Dimethylaminopyridine (DMAP) was purchased from Carbolution chemicals (St. Ingbert, Germany). *N*-Hydroxysuccinimide (NHS) was purchased from Alfa Aesar (Kandel, Germany). Cyanin-5-ammonium chloride (Cy5-NH₃Cl) was purchased from Lumiprobe (Hannover, Germany). Dichloromethane (DCM), methanol, acetonitrile, Al_2O_3 , and NaHCO_3 were purchased from Fisher Chemical (Loughborough, UK). Ethanol and ethyl acetate (EA) were purchased from Merck (Darmstadt, Germany). Cyclohexane (CH), Na_2SO_4 , deuterated methanol-d₄ (MeOD), and deuterated water (D_2O) were purchased from Carl Roth (Karlsruhe, Germany). 1,4-Dioxane and MgSO_4 were purchased from Grüssing (Filsburg, Germany). Deionized water with a minimum resistivity of 18.0 M Ω cm was used (Millipore™). Dulbecco's phosphate-buffered saline (PBS) was purchased from Thermofisher (Henningsdorf, Germany) and filtered over a 0.45 μm cellulose acetate (CA) filter directly before use. Pre-wetted regenerated cellulose dialysis tubes (molecular weight cut-off: 1 or 3.5 kDa, Spectra/Por® 6) from Spectrumlabs were used for dialysis.

Methods. Column chromatography was performed on a Teledyne Isco CombiFlash Rf+ (USA) using RediSep NP80 columns and HPLC-grade cyclohexane and ethyl acetate. Polymer dialysis

was performed with respective MWCO in methanol (1.8 L) for 48-72 hours, and the solvent was exchanged at least three times. Gel permeation chromatography (GPC) in THF as eluent was conducted on an Agilent 1100 Series instrument with concentrations of 3.5 mg mL⁻¹ and a flow rate of 1 mL min⁻¹ at 25 °C. Three PLgel 5 µm mix-C columns with the dimensions 7.5 × 300 mm from Agilent (Waldbronn, Germany) were used in line with a refractive index detector and polystyrene (PS) standards from PSS (Mainz, Germany) were used for calibration. Gel permeation chromatography (GPC) in DMF (10 mM LiBr) as eluent was conducted on a PSS Polymer Standard Service GmbH system with concentrations of 1.5 mg mL⁻¹ and a flow rate of 1 mL min⁻¹ at 50 °C. PSS SDV linear M 5 µm column (300 mm) was used in line with a refractive index detector, and poly(methyl methacrylate) (PMMA) standards from PSS (Mainz, Germany) were used for calibration. NMR spectra were processed with the software MestreNova 10.0.2, referenced to the solvent peak of the deuterated solvent unless stated otherwise, and the chemical shifts δ were reported in ppm.

Monomer synthesis

The synthesis of utilized monomers 2-hydroxy-3-methoxypropylmethacrylate (**HMPMA**) and 3-ethoxy-2-hydroxypropylacrylate (**EHPA**) was performed based on literature procedures.¹⁻³ The synthetic pathways are shown in Scheme S1.



Scheme S1. General synthesis route for the **HMPMA** (a) and **EHPA** (b) monomer with isolated yields of the pure constitutional isomers after silica column chromatography.

Synthesis of HMPMA

Glycidyl methacrylate (2.08 g, 14.6 mmol, 1 eq) was dissolved in methanol (11.5 mL, 282.5 mmol, 19 eq) and the mixture was cooled to 0 °C. $\text{BF}_3 \cdot \text{OEt}_2$ (0.8 mL, 6.31 mmol, 0.43 eq) was added dropwise over 10 min. The mixture was stirred for 1 h at -30 °C and then continued at rt until no starting material could be detected via TLC (4.5 h). Afterwards, the reaction mixture was filtered over an Al_2O_3 plug, washed with DCM (3 x 20 mL) and concentrated under reduced pressure. Purification via flash chromatography (CH:EA 7/3 v:v) yielded HMPMA (60%) as a colorless liquid.

$^1\text{H-NMR}$ (600 MHz, CDCl_3 δ): 6.13 (m_c, 1H, *trans-H*); 5.59 (m_c, 1H, *cis-H*); 4.22 (m_c, 2H, $-\text{COOCH}_2$); 4.05 (m_c, 1H, $-\text{CHOH}$), 3.46 (m_c, 2H, $-\text{CH}_2\text{OCH}_3$), 3.40 (s, 3H, $-\text{CH}_2\text{OCH}_3$), 2.56 (s, 1H, $-\text{CHOH}$), 1.95 (t, 3H, CH_2CCH_3) ppm.

$^{13}\text{C-NMR}$ (151 MHz; CDCl_3 δ): 167.58 (COO), 136.11 (CH_2CCOO), 126.19 (CH_2CHCOO), 73.57 ($-\text{CH}_2\text{OCH}_3$), 68.95 (CHOH), 65.88 ($-\text{COOCH}_2$), 59.40 (CH_2OCH_3), 18.45 (CH_2CCH_3) ppm.

Synthesis of glycidyl acrylate (GA)

Glycidol (11.16 g, 150.7 mmol, 1 eq) and triethylamine (25.0 mL, 180 mmol, 1.2 eq) were dissolved in DCM (156 mL) and cooled down to 0 °C. Acryloyl chloride (13.5 mL, 165 mmol, 1.1 eq) was dissolved in DCM (10 mL) and added dropwise to the reaction mixture over 60 min. The mixture was stirred for 16 h at rt. The precipitating solid was filtered off and the reaction mixture was washed with water (400 mL). The water phase was extracted with DCM (3 x 100 mL) and the combined organic layers were dried over MgSO_4 . The solvent was removed under reduced pressure and the raw product was purified by vacuum distillation (p : $1 \cdot 10^{-3}$ mbar, T_{bp} : 23 °C). GA (66%) was obtained as a colorless liquid.

$^1\text{H-NMR}$ (600 MHz, CDCl_3 δ): 6.45 (dd, 1H, *cis-H*); 6.16 (dd, 1H, CH_2CHCOO); 5.86 (dd, 1H, *trans-H*); 4.49 (dd, 1H, $-\text{COOCH}_2$); 4.01 (dd, 1H, $-\text{COOCH}_2$); 3.25 (m_c, 1H, $-\text{COOCH}_2\text{CHOCH}_2$), 2.86 (t, 1H, $-\text{COOCH}_2\text{CHOCH}_2$), 2.67 (dd, 1H, $-\text{COOCH}_2\text{CHOCH}_2$) ppm.

Synthesis of EHPA

Glycidyl acrylate (2.0 g, 15.6 mmol, 1 eq) was dissolved in ethanol (11 mL, 188.6 mmol, 12 eq) and cooled to 0 °C. $\text{BF}_3 \cdot \text{OEt}_2$ (0.9 mL, 7.02 mmol, 0.45 eq) was added dropwise over 10 min to the reaction mixture. The mixture was stirred 1 h at -30 °C and then continued at rt for 16 h. Afterwards, the reaction mixture was filtered over an Al_2O_3 plug, washed with DCM (3 x 20 mL)

and concentrated under reduced pressure. Purification via flash chromatography (CH:EA 7/3 v:v) yielded EHPA (60%) as a colorless liquid.

$^1\text{H-NMR}$ (500 MHz, CDCl_3 , δ): 6.44 (dd, 1H, *cis-H*); 6.16 (dd, 1 H, CH_2CHCOO); 5.86 (dd, 1H, *trans-H*); 4.24 (m_c , 2H, $-\text{COOCH}_2$); 4.04 (m_c , 1H, $-\text{CHOH}$), 3.59-3.42 (m, 4H, $-\text{CH}_2\text{OCH}_2\text{CH}_3$), 2.55 (d, 1H, $-\text{CHOH}$), 1.21 (t, 3H, $-\text{CH}_2\text{CH}_3$) ppm.

$^{13}\text{C-NMR}$ (151 MHz; CDCl_3 δ): 166.36 (COO), 131.48 (CH_2CHCOO), 128.17 (CH_2CHCOO), 71.30 ($\text{CH}_2\text{OCH}_2\text{CH}_3$), 68.96 (CHOH), 67.10 ($-\text{CH}_2\text{OCH}_2\text{CH}_3$), 65.84 ($-\text{COOCH}_2$), 15.20 ($-\text{CH}_2\text{CH}_3$) ppm.

Polymer synthesis

The general synthesis route is presented in Scheme 1. The resulting polymer structures are shown in Figure S1. Peak assignments were performed using the monomer spectra and ^1H ^{13}C HMQC spectra.

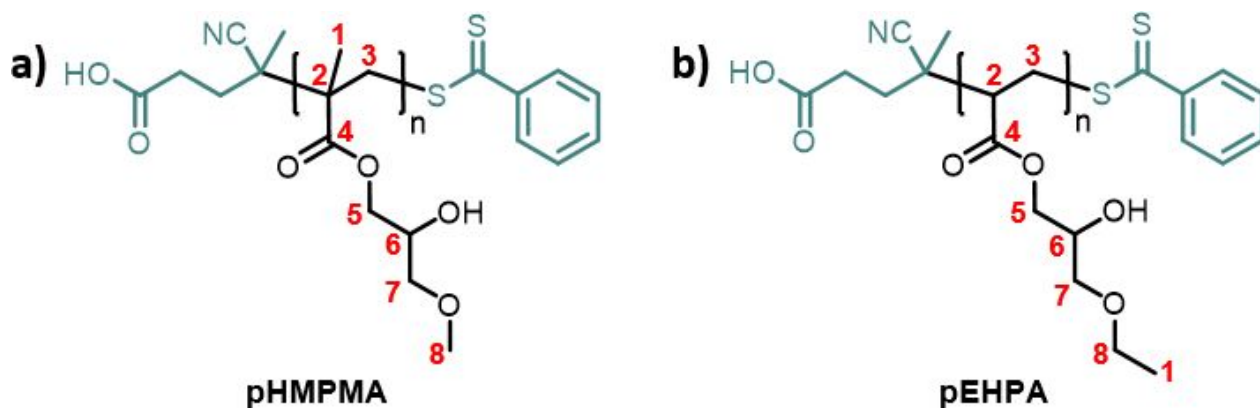


Figure S1. Structures of the resulting **pHPMA** (a) and **pEHPA** (b) polymers. Numbers were assigned following Figure S5 and Figure 4.

General procedure for pHPMA and pEHPA25 synthesis. The monomer was dissolved in 1,4-dioxane/water mixture (1/1 v:v) and cooled down to 0 °C. The radical initiator ACVA and the

RAFT agent were dissolved in 1,4-dioxane/water mixture (1/1 v:v) and added to the monomer solution. The combined solutions were degassed for 15 min with argon and the reaction mixture was stirred overnight in a preheated oil bath at 72 °C. The polymerization was stopped by air exposure at 0 °C. The solvent was removed under reduced pressure and the raw polymer dialyzed against methanol. The purified polymer was concentrated under reduced pressure.

pHMPMA10: HMPMA (2.00 g, 11.5 mmol, 58 eq), ACVA (10.0 mg, 0.037 mmol, 0.19 eq), RAFT agent (55.4 mg, 0.199 mmol, 1.0 eq), 1,4-dioxane/water (11 mL). Reaction time: 19.5 h. Dialysis MWCO: 1 kDa. The polymer (86%) was obtained as a light pink solid.

¹H-NMR (600 MHz, MeOD, δ): 7.91, 7.60, 7.43 (RAFT end-group); 4.15-3.65 (m, 3H, 5-*H*₂, 6-*H*); 3.65-3.44 (m, 2H, 7-*H*₂); 3.44-3.33 (m, 3H, 8-*H*₃); 2.47 (ACVA group); 2.20-1.50 (m, 2H, 3-*H*₂); 1.42-0.66 (m, 3H, 1-*H*₃) ppm.

Molecular weights determined by NMR: $M_n = 13.9$ kDa. GPC(THF): $M_n = 10700$ Da, $D = 1.10$. GPC(DMF): $M_n = 18500$ Da, $D = 1.28$.

pHMPMA25: HMPMA (2.41 g, 13.8 mmol, 173 eq), ACVA (4.1 mg, 0.015 mmol, 0.19 eq), RAFT agent (22.4 mg, 0.080 mmol, 1.0 eq), 1,4-dioxane/water (10 mL). Reaction time: 23 h. Dialysis MWCO: 3.5 kDa. The polymer (75%) was obtained as a light pink solid.

¹H-NMR (500 MHz, MeOD, δ): 7.91, 7.60, 7.43 (RAFT end-group); 4.24-3.79 (m, 3H, 5-*H*₂, 6-*H*); 3.64-3.45 (m, 2H, 7-*H*₂); 3.45-3.34 (br. s, 3H, 8-*H*₃); 2.48 (ACVA group); 2.32-1.43 (m, 2H, 3-*H*₂); 1.41-0.60 (m, 3H, 1-*H*₃) ppm.

¹³C-NMR (151 MHz; MeOD δ): 179.60-177.63 (4-*C*), 129.64, 129.58, 129.21, 127.61 (RAFT end-group), 75.15-74.62 (7-*C*) 69.15, 69.06, 68.94 (5-*C*), 67.46 (6-*C*), 59.61 (8-*C*), 55.93-52.73 (3-*C*), 46.93, 46.35, 46.01 (2-*C*), 22.12, 19.73, 18.00-17.33 (1-*C*) ppm.

Molecular weights determined by NMR: $M_n = 37.9$ kDa. GPC(THF): $M_n = 25300$ Da, $D = 1.10$.

GPC(DMF): $M_n = 46500$ Da, $D = 1.34$.

pEHPA25: EHPA (2.20 g, 12.6 mmol, 173 eq), ACVA (4.1 mg, 0.015 mmol, 0.20 eq), RAFT agent (20.4 mg, 0.073 mmol, 1.0 eq), 1,4-dioxane/water (6 + 1.4 mL). Reaction time: 15 h. Dialysis MWCO: 3.5 kDa. The polymer (81%) was obtained as a red wax.

$^1\text{H-NMR}$ (500 MHz, MeOD, δ): 8.01, 7.63, 7.46 (RAFT end-group); 4.31-4.01 (m, 2H, 5- H_2); 4.01-3.90 (br. s, 1H, 6- H); 3.56 (q, 2H, 8- H_2); 3.52-3.40 (m, 2H, 7- H_2); 2.69 (ACVA group); 2.63-2.26 (m, 1H, 2- H); 2.24-1.42 (m, 2H, 3- H_2); 1.21 (t, 3H, 1- H_3) ppm.

$^{13}\text{C-NMR}$ (151 MHz; MeOD δ): 176.40-175.90 (4- C), 129.70, 128.05 (RAFT end-group), 72.79 (7- C), 69.49, 69.44 (6- C), 67.89 (8- C), 67.31 (5- C), 42.83 (2- C), 37.31-35.09 (3- C), 15.58 (1- C) ppm.

Molecular weights determined by NMR: $M_n = 38.8$ kDa. GPC (THF): $M_n = 25200$ Da, $D = 1.17$.

GPC (DMF): $M_n = 38700$ Da, $D = 1.50$.

Procedure for pEHPA10. EHPA (1.50 g, 8.61 mmol, 58 eq), ACVA (8.3 mg, 0.03 mmol, 0.20 eq), RAFT agent (41.0 mg, 0.150 mmol, 1.0 eq), were dissolved in 1,4-dioxane/water mixture (5.74 ml, 1/1 v:v) and cooled down to 0 °C. The mixture was degassed for 15 min with argon and then stirred in a preheated oil bath at 72 °C for 16 h. The polymerization was stopped by air exposure at 0 °C. The solvent was removed under reduced pressure and the raw polymer dialyzed against methanol. Purified product was concentrated under reduced pressure. The polymer (75%) was obtained as a red wax.

Supporting Information

$^1\text{H-NMR}$ (500 MHz, MeOD, δ): 8.01, 7.62, 7.46 (RAFT end-group); 4.30-4.01 (m, 2H, 5- H_2); 4.01-3.89 (br. s, 1H, 6- H); 3.56 (q, 2H, 8- H_2); 3.53-3.38 (m, 2H, 7- H_2); 2.69 (ACVA group); 2.61-2.23 (m, 1H, 2- H); 2.23-1.44 (m, 2H, 3- H_2); 1.21 (t, 3H, 1- H_3) ppm.

Molecular weights determined by NMR: $M_n = 11.1$ kDa. GPC (THF): $M_n = 9700$ Da, $D = 1.08$.

GPC(DMF): $M_n = 13300$ Da, $D = 1.29$.

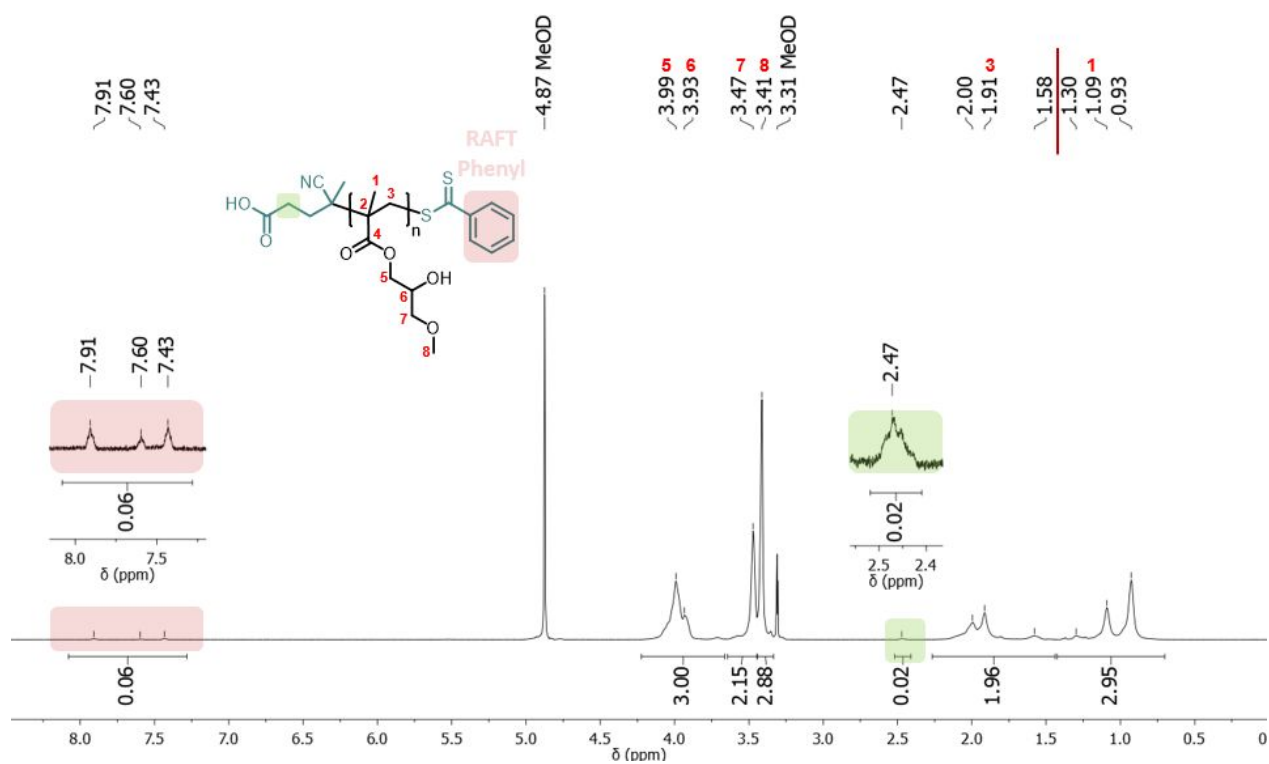


Figure S2. ¹H NMR spectrum of pHPMA10 in MeOD with peak assignment.

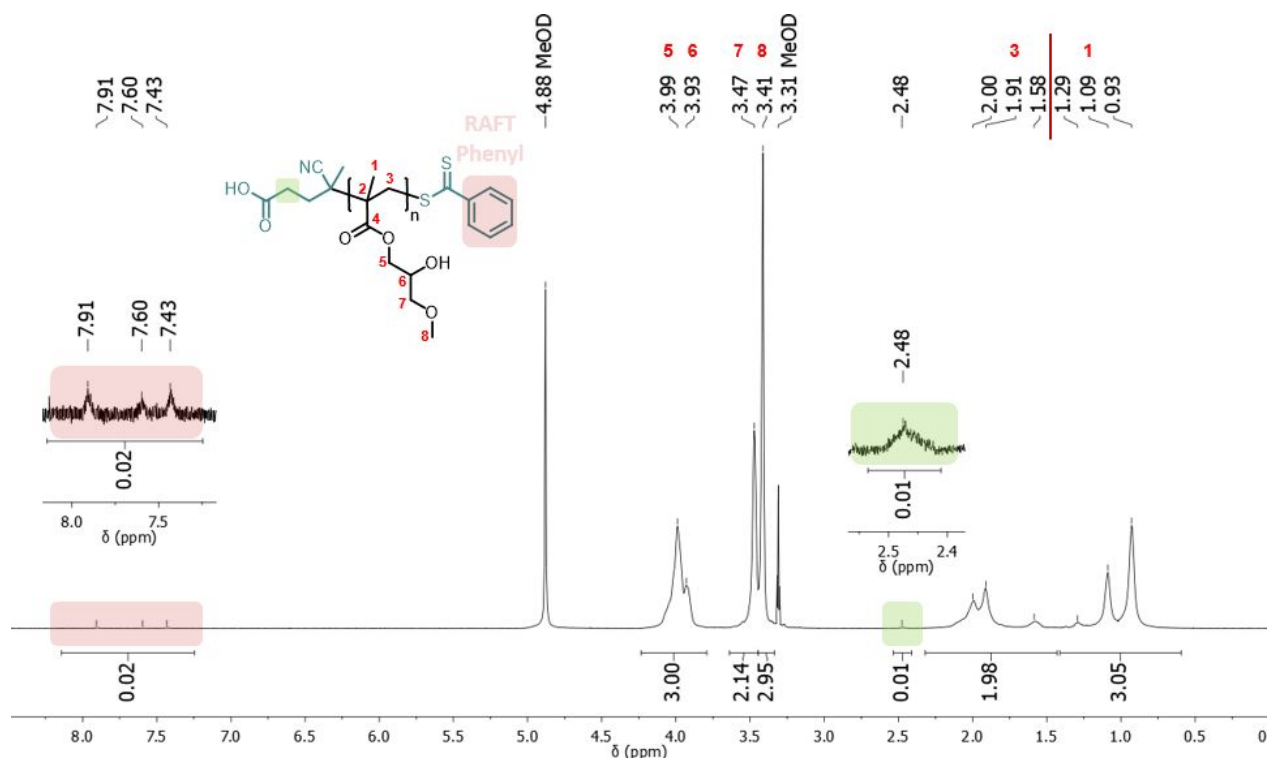
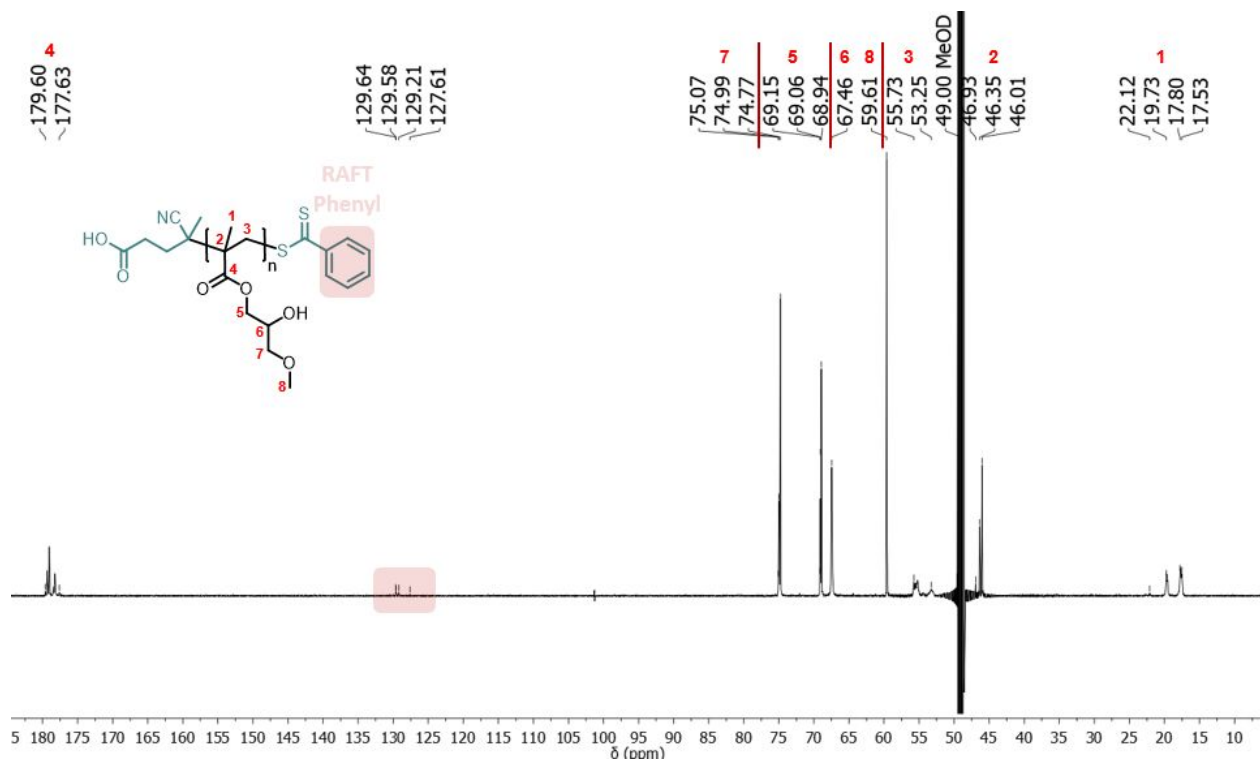
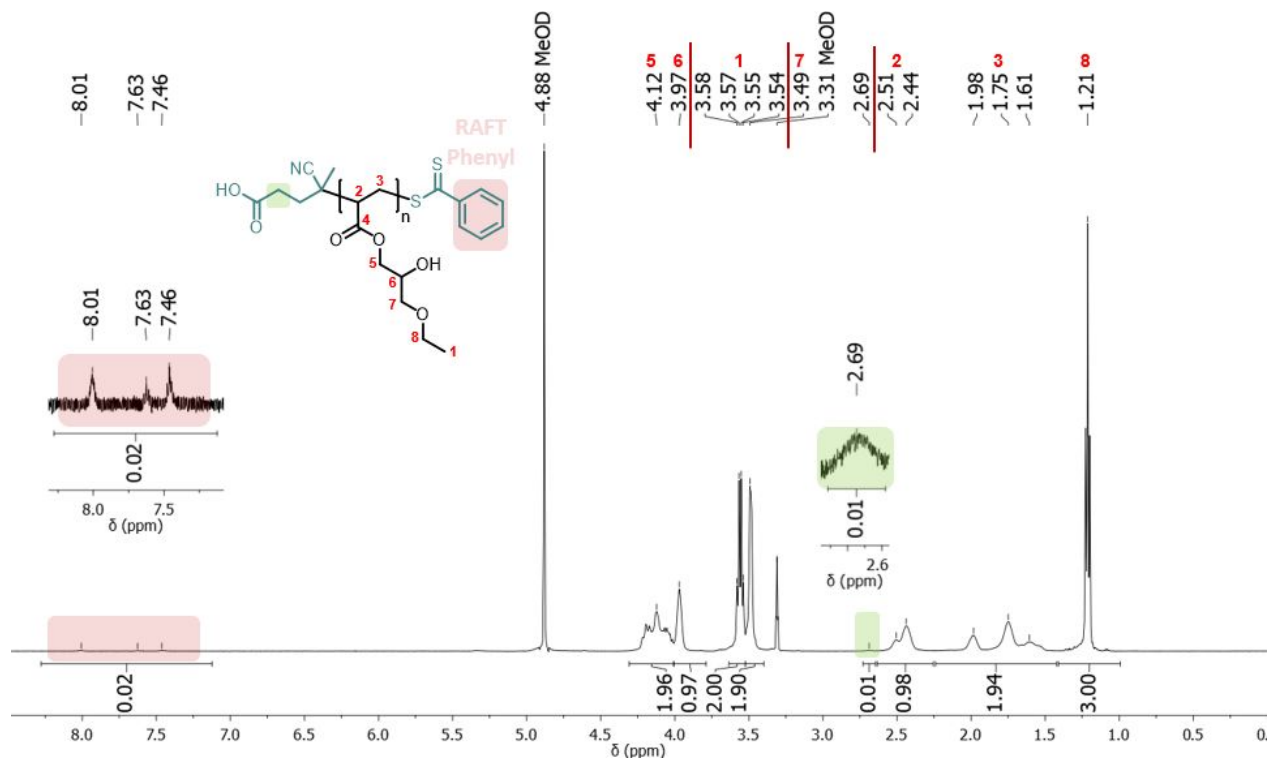
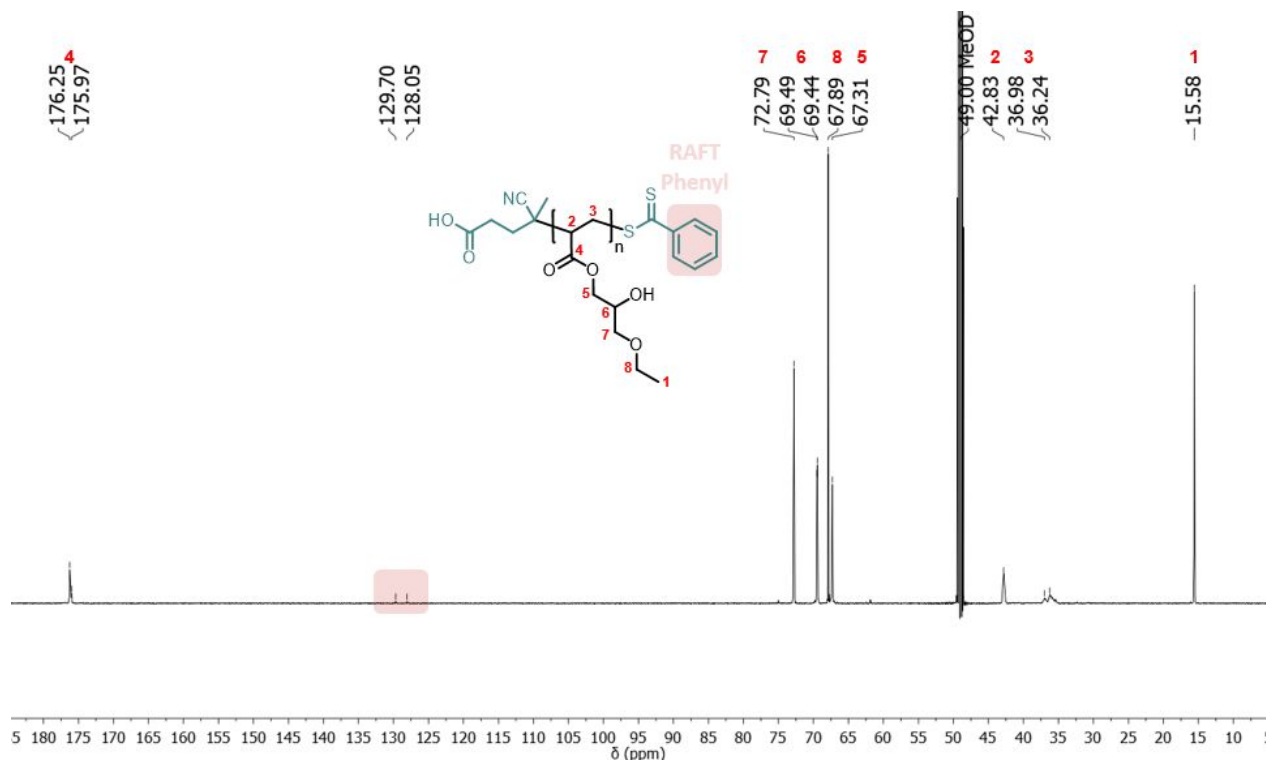
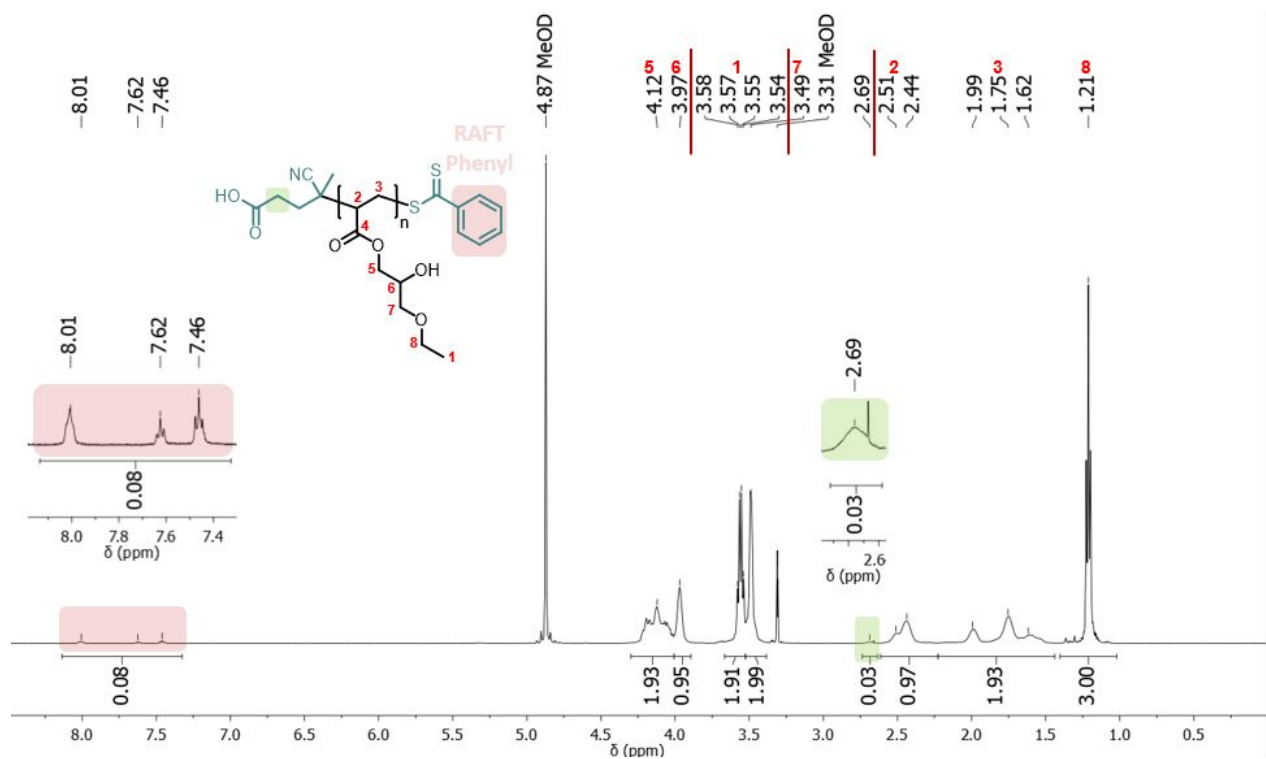


Figure S3. ¹H NMR spectrum of pHPMA25 in MeOD with peak assignment.

Figure S4. ¹³C NMR spectrum of pHPMA25 in MeOD with peak assignment.Figure S5. ¹H NMR spectrum of pEHPA25 in MeOD with peak assignment.

Figure S6. ¹³C NMR spectrum of pEHPA25 in MeOD with peak assignment.Figure S7. ¹H NMR spectrum of pEHPA10 in MeOD with peak assignment.

Molecular weight analysis

Molecular weights of the purified polymers were evaluated via ^1H NMR spectroscopy and GPC in THF and DMF using polystyrene (PS) and polymethylmethacrylate (PMMA) standards, respectively. A comparative list of the results from polymers with targeted molecular weights of 10 and 30 kDa, including dispersities and isolated yields is presented in Table S1.

Table S1. Overview of the polymers synthesized via RAFT polymerization.

Polymer	M_n [kDa] ^a	D^a	M_n [kDa] ^c	D^c	M_n [kDa] ^b	Yield [%] ^d
pEHPA10	9.7	1.08	13.3	1.29	11.1	76
pEHPA25	25.2	1.17	38.7	1.5	38.8	81
pHMPMA10	10.7	1.10	18.5	1.28	13.9	86
pHMPMA25	25.3	1.10	46.5	1.34	37.9	75

^adetermined via GPC in THF with PS standards, ^bdetermined via GPC in DMF with PMMA standards, ^cdetermined from ^1H NMR end group analysis ^disolated yield after purification via dialysis.

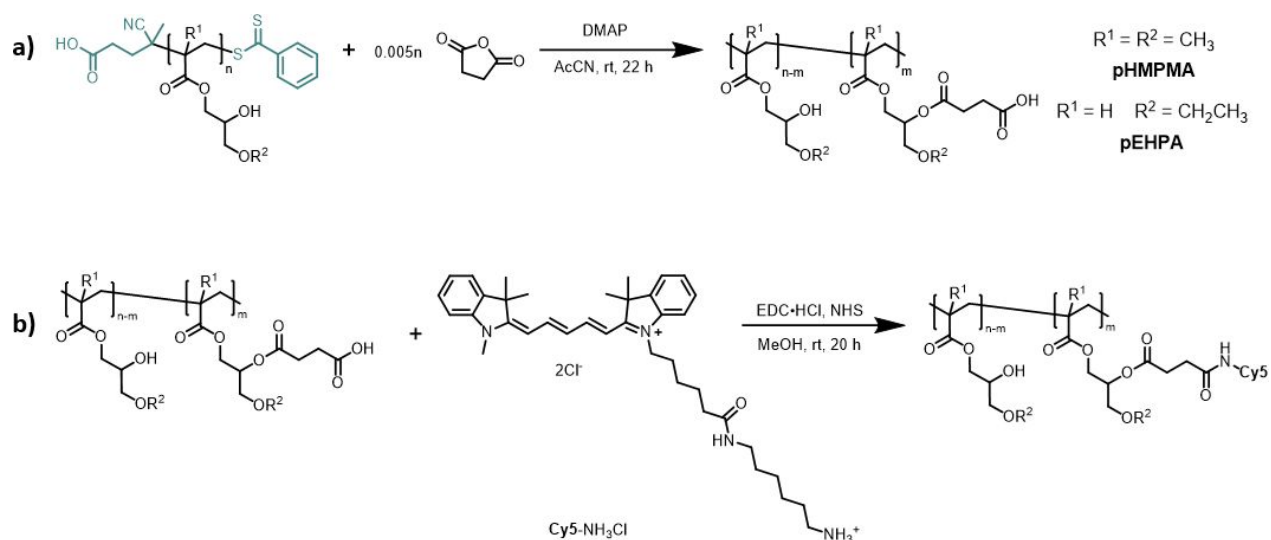
For the 10 kDa polymers, GPC results in THF match well with the targeted molecular weights. For polymers with a target of 30 kDa, GPC traces revealed a lower molecular weight of around 25 kDa. Narrow polydispersities indicated the success of the controlled polymerization.

Molecular weight determination from the ^1H NMR spectra was achieved by comparing the integral values of the terminating RAFT phenyl moiety to the integral value of the backbone protons. An increase of 14% for **pEHPA10** and 30% for **pHMPMA10** was observed when compared to GPC results in THF, and an increase of ~50% was observed for the higher molecular weight polymers.

However, an overestimation of molecular weights determined from ^1H NMR is not unusual. The small number of protons resulting in low-intensity signals, restricted movement of the end groups in the coil resulting in longer proton relaxation times and therefore, non-quantitative signals, and dead chains lacking the RAFT end group can add up to rather large errors for polymers with molecular weights ≥ 10 kDa.⁴⁻⁶ In DMF, the molecular weights appeared to be overestimated by 37-53% for **pEHPA** and 73-84% for **pHMPMA** with broader PDIs which might indicate better solvation of the polymers in DMF compared to PMMA standards. Weaver *et al.* reported an overestimation of the molecular weight of pHEMA by at least 200% when measured in DMF and analyzed with PMMA standards.⁷ Hence it seems reasonable that the more hydrophilic **pHMPMA** is generally more overestimated in DMF compared to the **pEHPA**. Since the hydrogen bonding ability of THF is less pronounced, the difference in the solvodynamic radius between PS and **pHMPMA** or **pEHPA** is expected to be smaller. Thus, GPC results in THF were chosen to label the polymers.

Cy5 labeling

The labeling of **pHMPMA25** and **pEHPA25** with the fluorescent Cy5 dye was conducted in two steps. First, the succinic anhydride amount equaling 0.05% of the side chain hydroxy groups (based on M_n by GPC in THF) was used to generate reactive carboxy groups in the side chains. Second, the amino-functional Cy5 dye was coupled via amidation by an EDC NHS coupling protocol. The general synthetic route is shown in Scheme S2.



Scheme S2. a) Polymer (25 kDa) functionalization with succinic anhydride to yield side chains with reactive carboxy groups. b) EDC-NHS coupling of the fluorescent Cy5-NH₃Cl dye to the carboxy-functionalized polymers.

Functionalization with succinic anhydride. The respective hydroxy-functional polymer (420 mg, 0.017 mmol, 1 eq) was dissolved in acetonitrile (1.5 mL). Stock solutions of SA (0.049 M, 0.24 mL, 0.71 eq) and DMAP (0.041 M, 0.3 mL, 0.71 eq) in acetonitrile were added and the reaction was stirred at rt for 22 h. The polymer solution was dialyzed against methanol (MWCO 3.5 kDa) and concentrated under reduced pressure.

pHMPMA25-SA: light pink solid. Yield: 99 %. ¹H NMR peak assignment was performed according to the numbering provided in Figure S1a.

¹H-NMR (500 MHz, MeOD, δ): 7.91, 7.60, 7.43 (RAFT end-group); 4.25-3.80 (m, 3H, 5-*H*₂, 6-*H*); 3.67-3.45 (m, 2H, 7-*H*₂); 3.45-3.34 (br. s, 3H, 8-*H*₃); 2.67 (SA group); 2.48 (ACVA group); 2.35-1.47 (m, 2H, 3-*H*₂); 1.41-0.69 (m, 3H, 1-*H*₃) ppm.

pEHPA25-SA: light pink wax. Yield: 99 %. ¹H NMR signals were identified according to Figure S1b.

¹H-NMR (500 MHz, MeOD, δ): 8.01, 7.63, 7.46 (RAFT end-group); 4.37-4.01 (m, 2H, 5-*H*₂); 4.01-3.89 (br. s, 1H, 6-*H*); 3.73-3.52 (m, 2H, 8-*H*₂); 3.52-3.40 (m, 2H, 7-*H*₂); 2.73-2.60 (SA group, ACVA group); 2.60-2.27 (m, 1H, 2-*H*) 2.23-1.44 (m, 2H, 3-*H*₂) 1.21 (t, 3H, 1-*H*₃) ppm.

Conjugation with Cy5. The respective SA-functionalized polymer (250 mg, 0.01 mmol, 1 eq) was dissolved in methanol (0.8 mL), a stock solution of NHS in methanol (0.073 M, 0.01 mL, 0.73 eq) was added, and the reaction mixture stirred for 2 min. After adding a stock solution of EDC HCl in methanol (0.073 M, 0.1 mL, 0.73 eq) the reaction mixture was stirred for 3 h at rt. Finally, a stock solution of the Cy5 dye in methanol (0.003 M, 0.59 mL, 0.18 eq) was added and the reaction mixture stirred for 17 h at rt. The polymer solution was dialyzed against methanol (MWCO 3.5 kDa) and concentrated under reduced pressure.

pHMPMA25-Cy5: blue wax. Yield: 91 %. ¹H NMR signals are identified according to Figure S1a.

¹H-NMR (500 MHz, MeOD, δ): 8.24, 7.71, 7.63, 7.51, 7.28, 6.63, 6.30 (Cy5 π -system); 4.26-3.78 (m, 3H, 5-*H*₂, 6-*H*); 3.76-3.45 (m, 2H, 7-*H*₂); 3.45-3.34 (br. s, 3H, 8-*H*₃); 2.76-2.60 (SA group, Cy5 group); 2.43 (ACVA group); 2.25-1.50 (m, 2H, 3-*H*₂); 1.42-0.66 (m, 3H, 1-*H*₃) ppm.

GPC(THF): $M_n = 24600$ Da, $D = 1.15$.

pEHPA25-Cy5: blue wax. Yield: 92 %. ¹H NMR signals are identified according to Figure S1b.

¹H-NMR (700 MHz, MeOD, δ): 8.24, 7.51, 7.28, 6.63, 6.30 (Cy5 π -system); 8.00, 7.62, 7.46 (RAFT end-group) 4.33-4.02 (m, 2H, 5-*H*₂); 4.01-3.90 (br. s, 1H, 6-*H*); 3.74-3.53 (m, 2H, 8-*H*₂); 3.52-3.42 (m, 2H, 7-*H*₂); 2.73-2.60 (SA group, Cy5 group, ACVA group); 2.60-2.25 (m, 1H, 2-*H*) 2.23-1.40 (m, 2H, 3-*H*₂); 1.21 (t, 3H, 1-*H*₃) ppm.

GPC(THF): $M_n = 24700$ Da, $D = 1.20$.

The labeling was verified by the change of polymer color (light pink to blue). Furthermore, the signals of the incorporated succinic acid (methyl groups) and Cy5 (π -system) were detected in the ^1H proton spectra. The spectra comparison along with peak assignment is shown in Figures S8 and S9 for pEHPA25-Cy5 and pHMPMA25-Cy5 respectively.

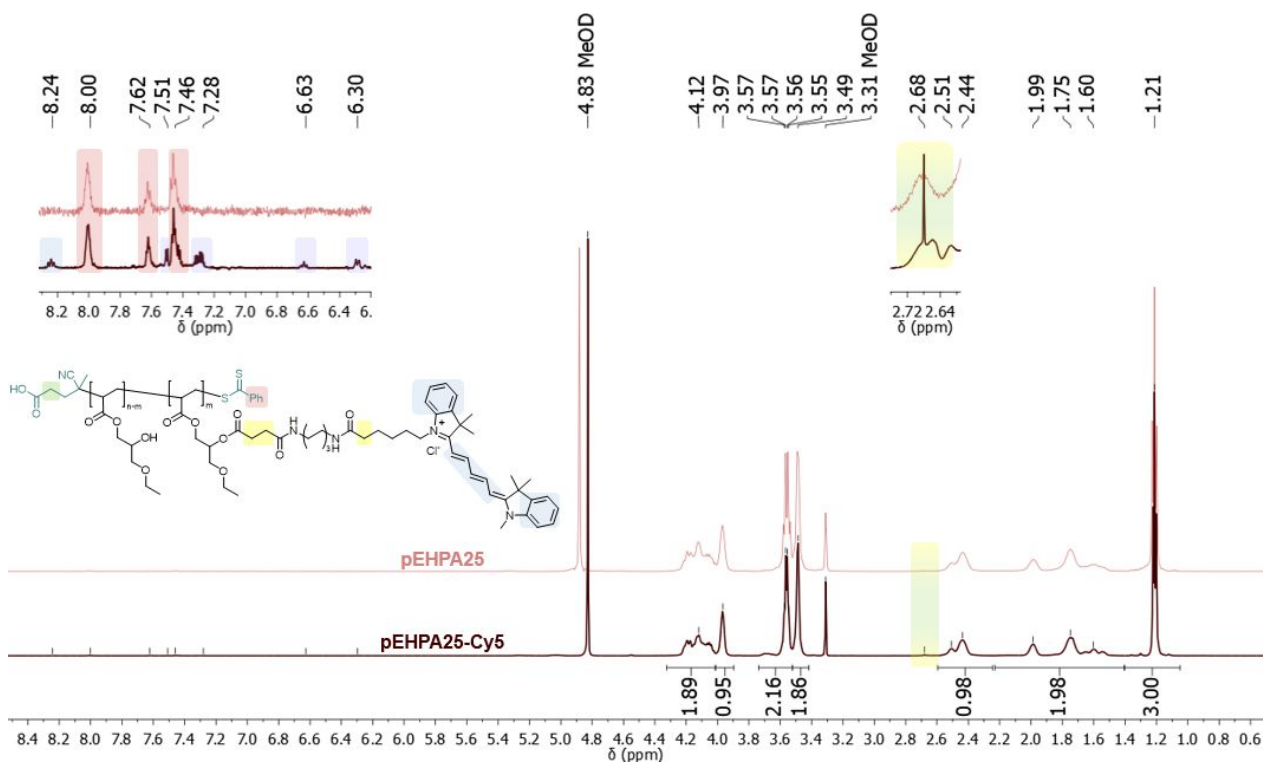


Figure S8. ^1H NMR spectra comparison of pEHPA25 and pEHPA25-Cy5 in MeOD with peak assignment.

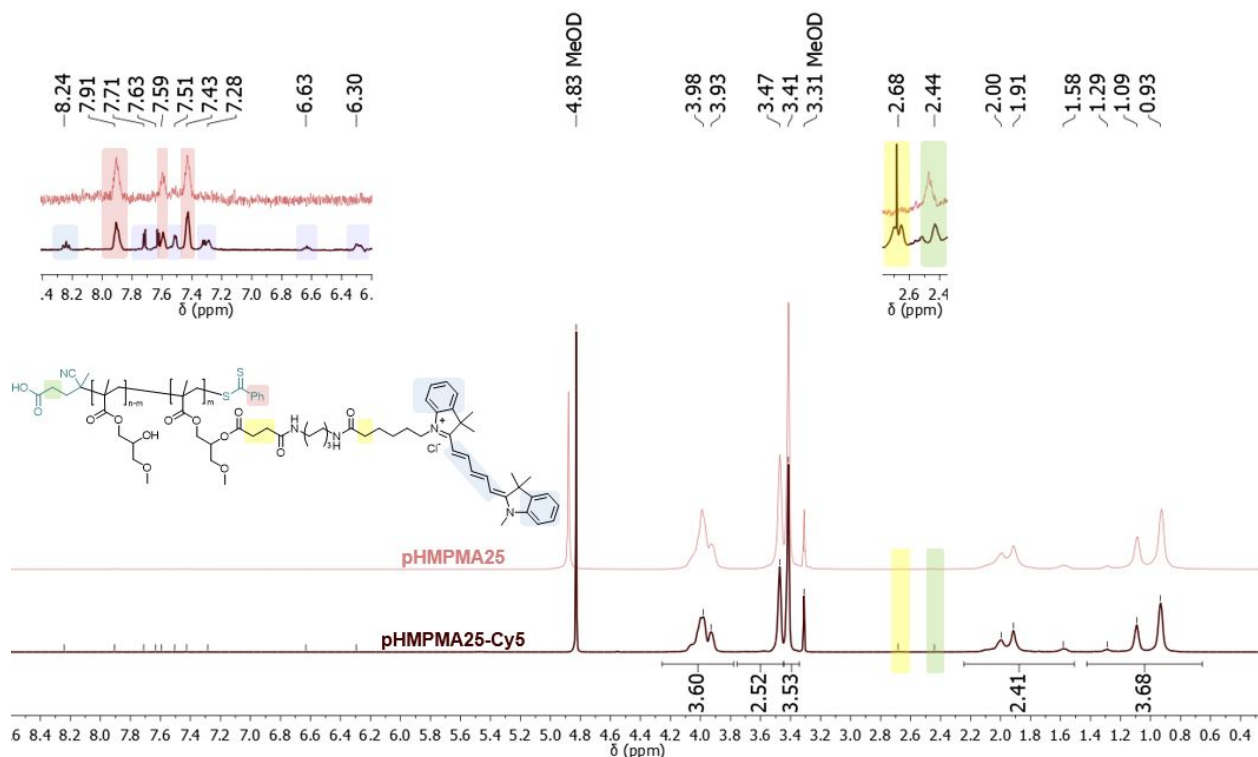


Figure S9. ^1H NMR spectra comparison of **pHMPMA25** and **pHMPMA25-Cy5** in MeOD with peak assignment.

Sample preparation for the analysis of the thermoresponsive behavior

Turbidimetry. The polymer samples were dissolved in water and lyophilized to remove traces of methanol. A 20 mg mL^{-1} stock solution in the respective solvent (water or PBS) was prepared and 2 mL dilutions with 10, 5, 2.5, and 1 mg mL^{-1} were prepared for analysis. Temperature-dependent turbidity curves were measured as described in the experimental section by detecting the transmittance at 600 nm. The non-normalized heating and cooling runs in PBS for all probed polymers and concentrations are shown in Figure S10. The combined polymer solutions of one sample were lyophilized after the analysis and the recovered polymers were analyzed via GPC in THF to detect chemical alteration or degradation (Figure S11).^{8,9}

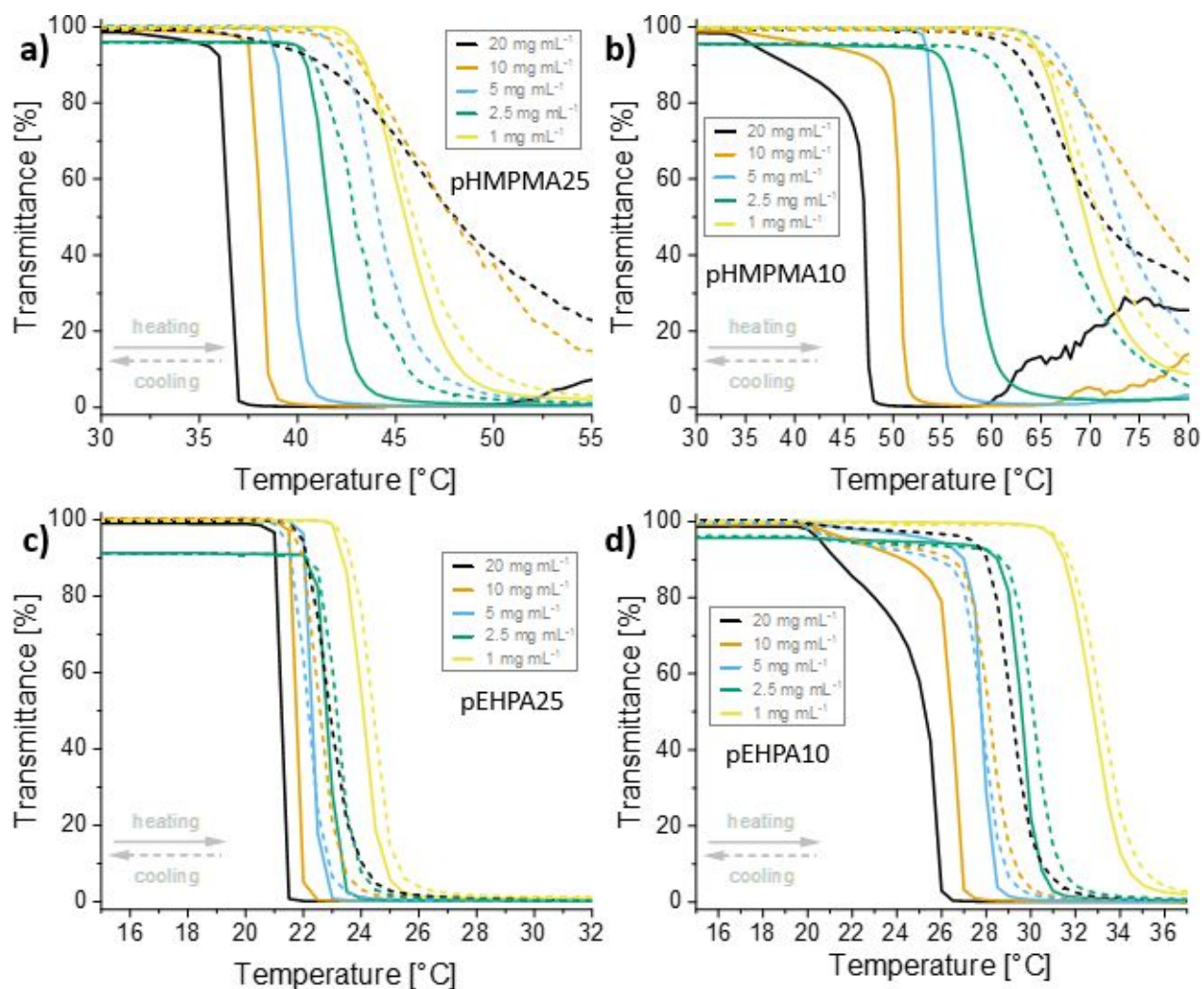


Figure S10. Overview of non-normalized turbidimetry heating (straight) and cooling (dashed) cycles in PBS for **pHMPMA** (a, b) and **pEHPA** (c, d) of 25 and 10 kDa, respectively. A full heating-cooling cycle over the measured temperature range is shown.

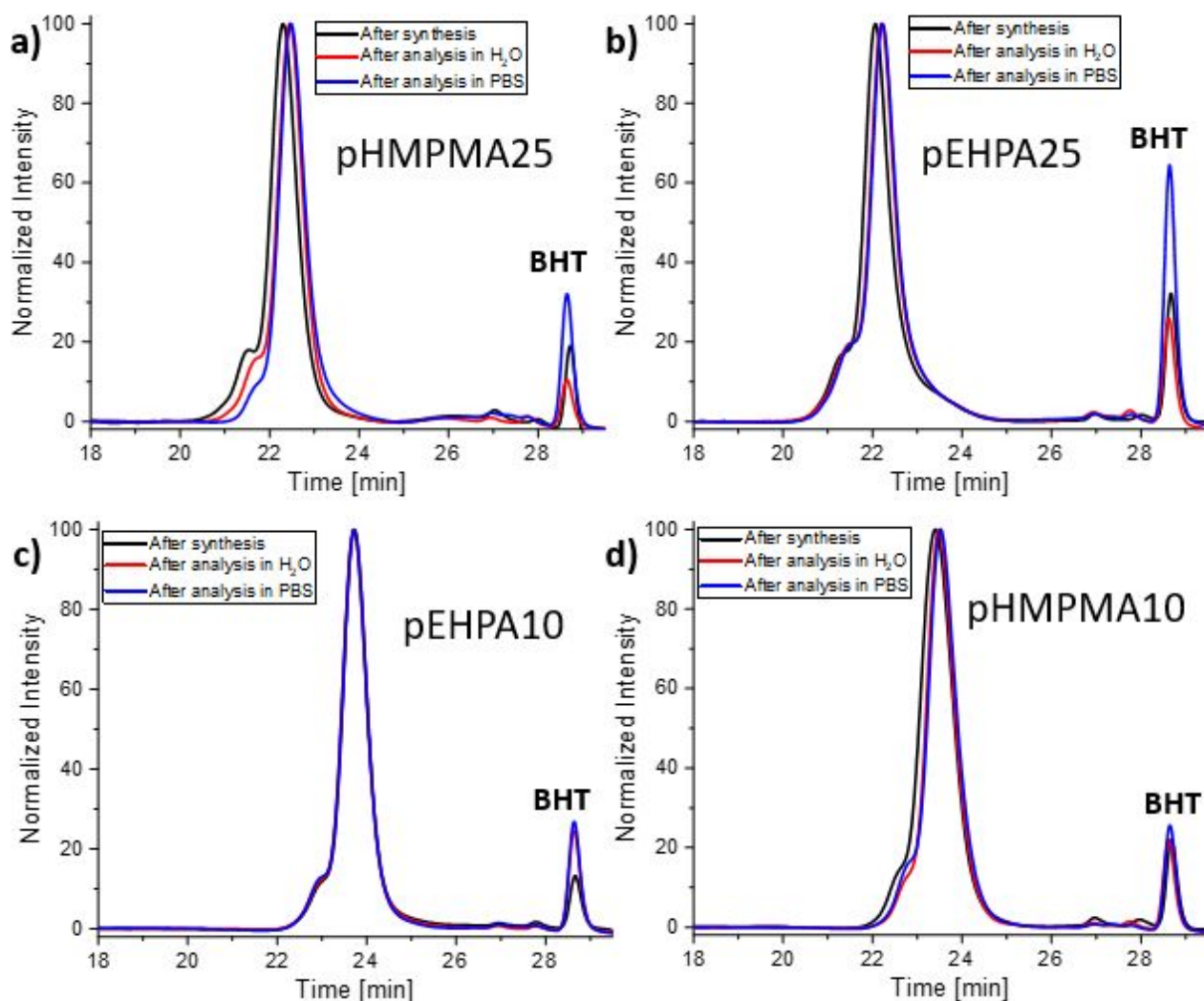


Figure S11. Overview of GPC traces of (a) **pHMPMA25**, (b) **pEHPA25**, (c) **pEHPA10** and (d) **pHMPMA10** obtained in THF at room temperature and referenced to butylated hydroxytoluene (**BHT**). The measurements were performed directly after synthesis and isolation (black), after turbidimetry and DLS analysis, either in water (red) or in PBS (blue).

Calculation of the phase transition width ΔT

The phase transition borders were calculated by applying a linear fit on the transition region of the normalized turbidimetry curves. The temperature values for 0 and 100% transmittance (T_0 and T_{100} , respectively) were then used to calculate the apparent phase transition width $\Delta T = T_0 - T_{100}$. An

example graph for the calculation using the **pHMPMA10** 5 mg mL⁻¹ sample in H₂O and the resulting values are presented in Figure S12 and Table S2.

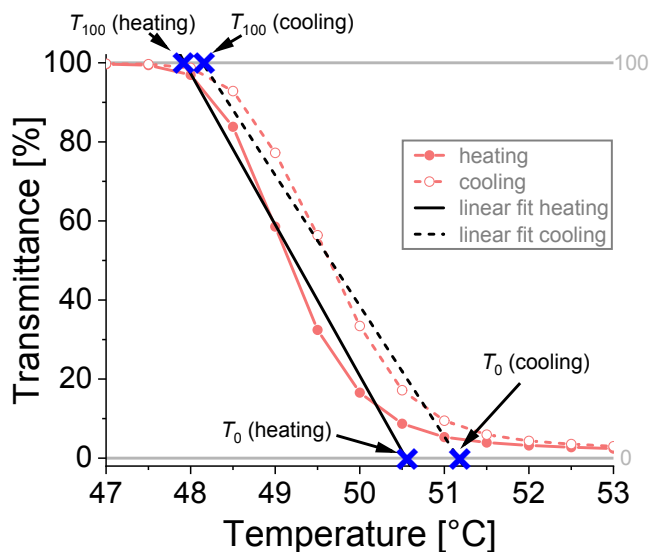


Figure S12. Turbidimetric curves of **pHMPMA10** in H₂O at a concentration of 5 mg mL⁻¹ (red) and the corresponding linear fits of the phase transition region (black). Blue crosses mark the position of derived T_{100} and T_0 values.

Table S2. Results of the linear fit of the **pHMPMA10** transmittance curves in H₂O are depicted in Figure S12.

	Heating cycle	Cooling cycle
Derived linear fit*	$y = -38x + 1932$	$y = -33x + 1690$
R^2	0.976	0.979
T_{100} [°C]	47.9	48.1
T_0 [°C]	50.5	51.2
$\Delta T = T_0 - T_{100}$ [°C]	2.6	3.1

* y = transmittance, x = temperature

DLS sample preparation and intensity distribution of the 10 kDa polymers

The prepared samples for turbidimetry measurements were also used for DLS measurements. Before the measurement, each sample was filtered through a 0.45 μm CA filter to break up loose polymer aggregates. The samples were then placed in the measurement chamber and equilibrated for 120 s at each temperature prior to the measurement. The size distributions by intensity for the 10 kDa polymers are shown in Figure S13.

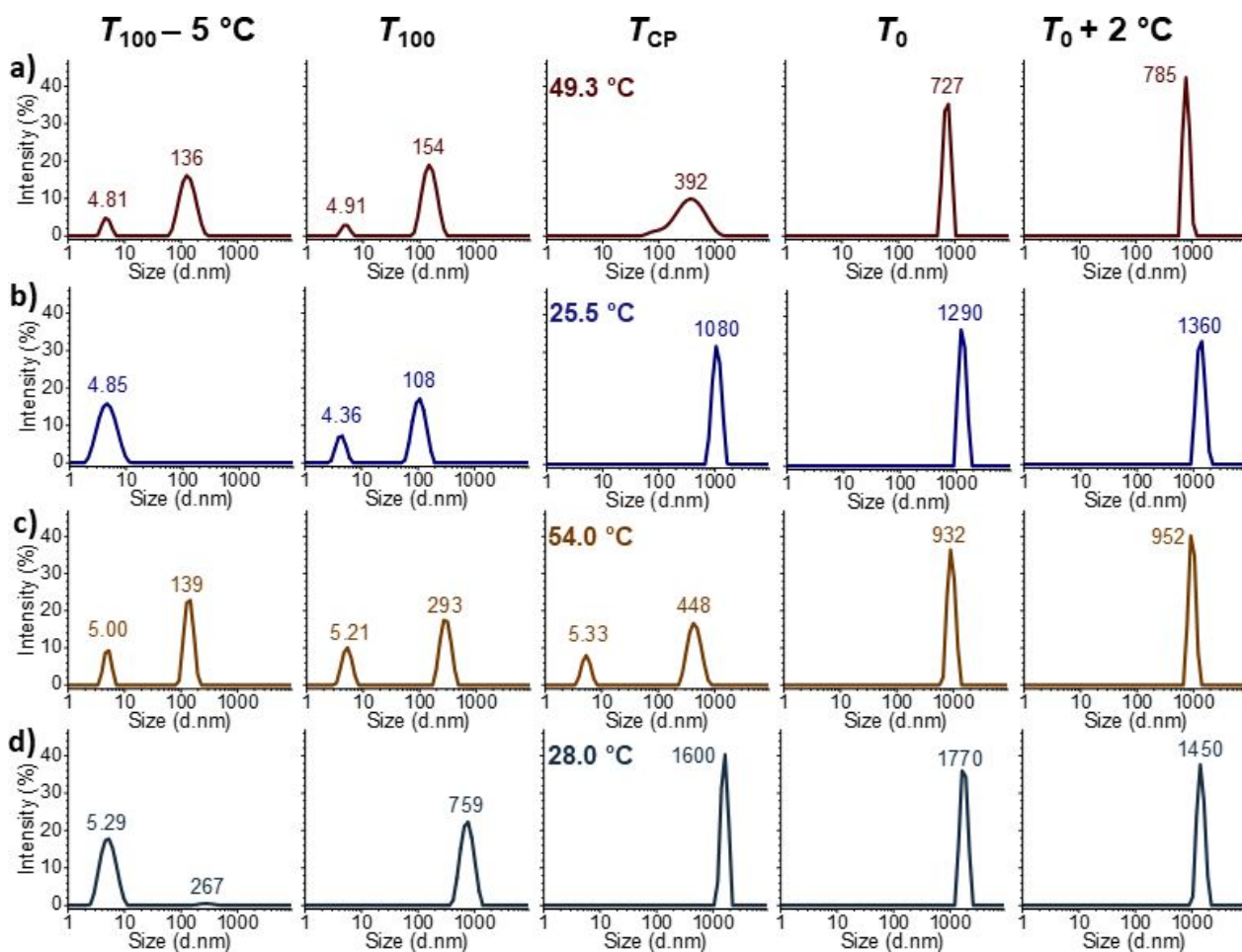


Figure S13. Temperature-dependent size distributions by intensity determined via DLS of **pHPMA10** (a, c) and **pEHPA10** (b, d) at $c = 5\text{ mg mL}^{-1}$ in water (a, b) and PBS (c, d), respectively.

Comparison of hydrodynamic radii to theoretical and literature values

In order to estimate whether the polymers in this work are dissolved as single chains in water well below the cloud point temperature ($T_{100} - 5$ °C), we used the measured hydrodynamic radii by DLS data ($R_{h, \text{exp}} = d/2$ with the measured hydrodynamic diameter d) and compared it to their theoretical Flory radii (R_f) and R_h of poly(*N*-isopropyl acrylamide) (**pNIPAM**) in water at 20 °C derived from light scattering data.¹⁰ The Flory radii of our polymers were calculated in a theta ($R_{f, \text{theta}} = N^{1/2}a$) and good ($R_{f, \text{good}} = N^{3/5}a$) solvent with N as the number of repeating units in the polymer chain and a as the segment chain length.¹¹ The number of repeating units N was calculated as the ratio of the molecular weight M_n to the monomer molecular weight M_0 (174.2 g/mol) and the segment length was estimated to be $a = 0.25$ nm, which is a typical value for vinyl-based polymers such as (**pNIPAM**)¹⁰. Furthermore, we calculated the hydrodynamic radii using the power law equation derived from experimental **pNIPAM** light scattering and viscometry data in water at 20 °C ($R_{h, \text{pNIPAM}} = 0.016M_w^{0.54}$).¹⁰ The results are presented in Table S3.

Table S3. Comparison of experimentally-derived hydrodynamic radii to the theoretically-derived polymer radii according to the Flory theory and hydrodynamic radii based on pNIPAM measurements.

Polymer	N	$R_{h, \text{exp}}$ [nm]	$R_{f, \text{theta}}$ [nm]	$R_{f, \text{good}}$ [nm]	$R_{h, \text{pNIPAM}}$ [nm]
pEHPA10	61.4	2.43	1.86	2.77	2.36
pEHPA25	145.2	4.40	3.01	4.94	4.14
pHMPMA10	55.1	2.41	1.96	2.96	2.51
pHMPMA25	144.7	4.20	3.01	4.96	4.01

Since the experimental radii consistently locate between the calculated Flory values for theta and good solvent and are within 4-6% of the experimentally derived $R_{h, \text{pNIPAM}}$ values, we assume that the hydrodynamic radii derived from our measurements can be attributed to fully solubilized single chains.

Temperature-dependent pHMPMA25 NMR measurements.

The NMR spectra were acquired as described in the experimental section. The ^1H and ^{13}C spectra of **pHMPMA25** in the temperature range of 30-60 °C are shown in Figures S14 and S15. Additionally, the integral values from the ^1H spectra are shown in Table S4.

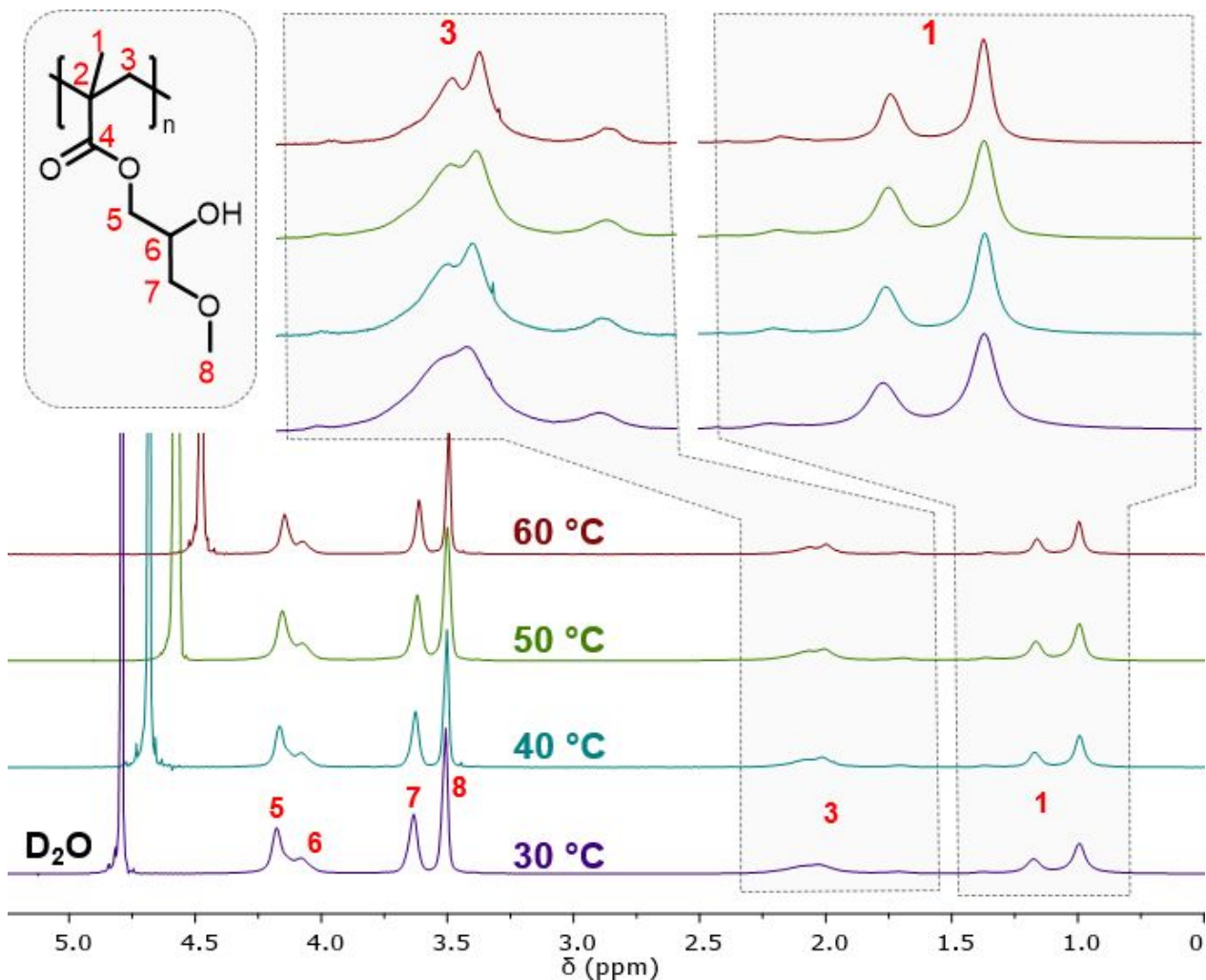


Figure S14. Temperature-dependent ^1H NMR spectra (D_2O , 600 MHz) of **pHMPMA25** at a concentration of 10 mg mL^{-1} (T_{cp} : $41.2 \text{ }^\circ\text{C}$). The spectra were referenced to the methyl group (**1**, right peak) at $30 \text{ }^\circ\text{C}$ at 0.99 ppm . Peaks were assigned with numbers according to the illustrated chemical structure, and marked insets show zoomed-in regions for signals of interest.

Table S4. Overview of proton peak integrals of **pHMPMA25** (T_{cp} : $41.2 \text{ }^\circ\text{C}$) as obtained from temperature-dependent ^1H NMR (D_2O , 600 MHz) spectra measured at a concentration of 10 mg mL^{-1} . All peak integrals were referenced to the respective backbone protons of peaks (**5+6**) between $3.91\text{-}4.35 \text{ ppm}$.

Assigned peak N°	5+6	7	8	3	1
(δ [ppm])	(3.91-4.35)	(3.58-3.79)	(3.41-3.58)	(1.57-2.51)	(0.66-1.52)
Integral at $30 \text{ }^\circ\text{C}$	3.00	2.07	3.14	1.73	2.92
Integral at $40 \text{ }^\circ\text{C}$	3.00	2.01	3.03	1.79	2.82
Integral at $50 \text{ }^\circ\text{C}$	3.00	2.29	3.20	1.87	2.97
Integral at $60 \text{ }^\circ\text{C}$	3.00	2.15	3.21	1.80	2.92

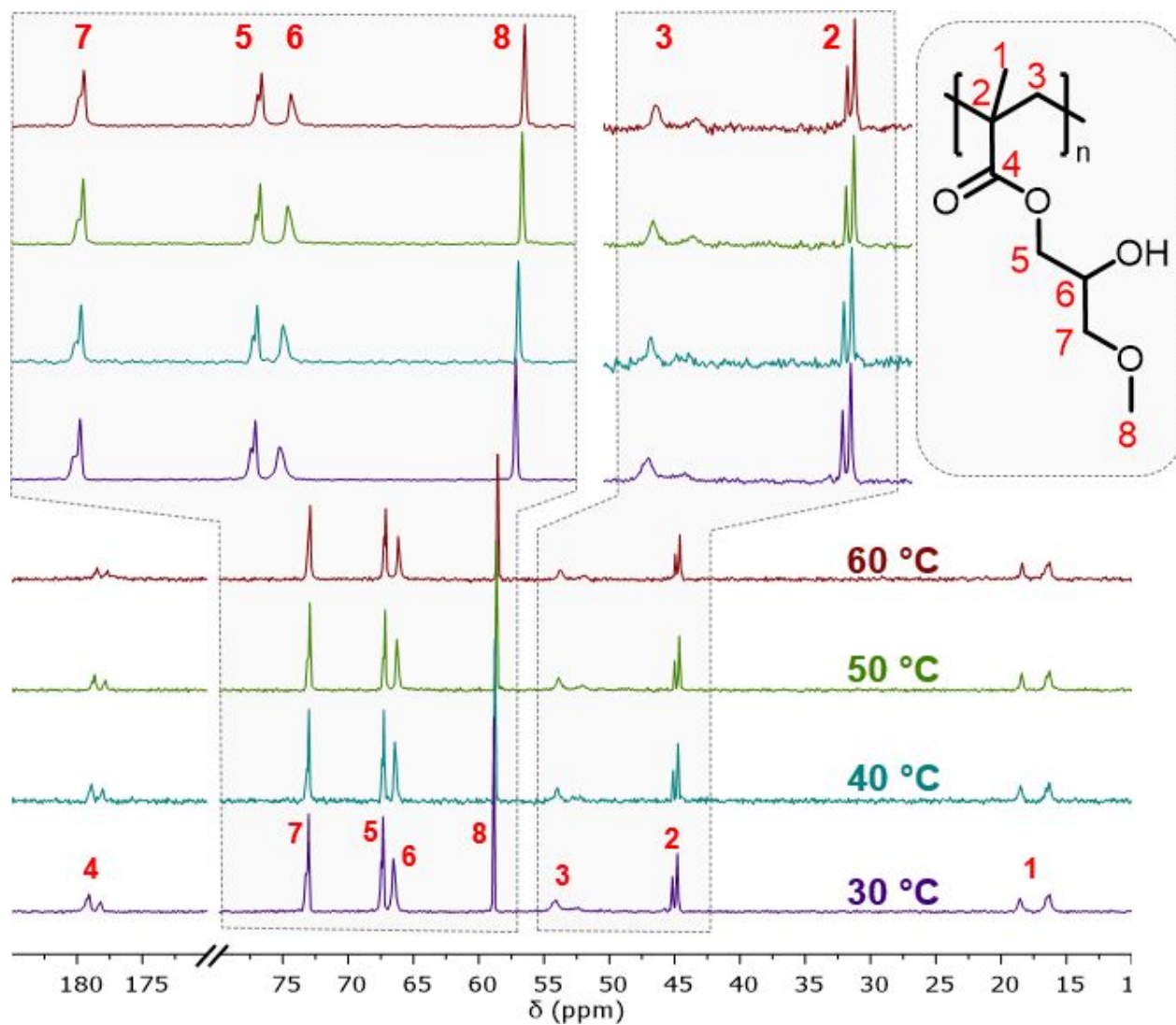


Figure S15. Temperature-dependent ^{13}C NMR spectra (D_2O , 151 MHz) of **pHMPMA25** at a concentration of 10 mg mL^{-1} (T_{cp} : $41.2 \text{ }^\circ\text{C}$). The spectra were referenced to the methyl group (**1**, right peak) at $30 \text{ }^\circ\text{C}$ (16.29 ppm). Peaks were assigned with numbers according to the illustrated chemical structure, and color-marked insets show zoomed-in regions for signals of interest.

UV/Vis and fluorescence spectroscopy data of Cy5-functionalized polymers.

The **pEHPA25-Cy5** and **pHMPMA25-Cy5** polymers were first analyzed over the region of 400 to 700 nm to verify the labeling and find the appropriate wavelength for the turbidimetry

measurements with sufficiently low absorbance. After the analysis of the absorbance spectra in Figure S16, a wavelength of 500 nm was chosen for turbidimetry (Figure S17).

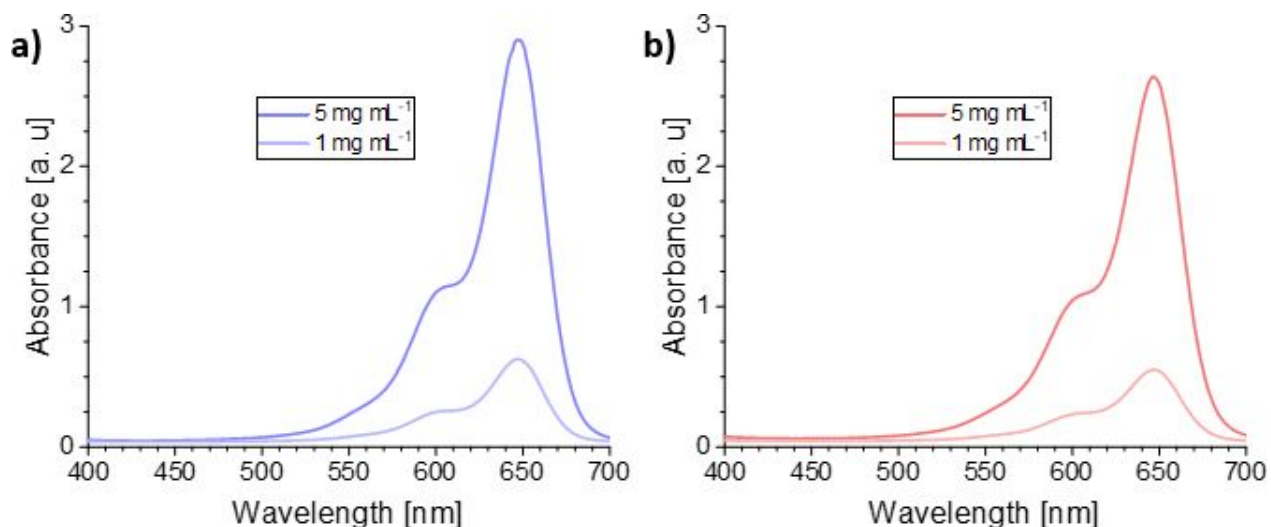


Figure S16. UV/Vis-absorption spectra of **pEHPA25-Cy5** (a) and **pHMPMA25-Cy5** (b) at concentrations of 5 and 1 mg mL⁻¹ in H₂O at 20 °C.

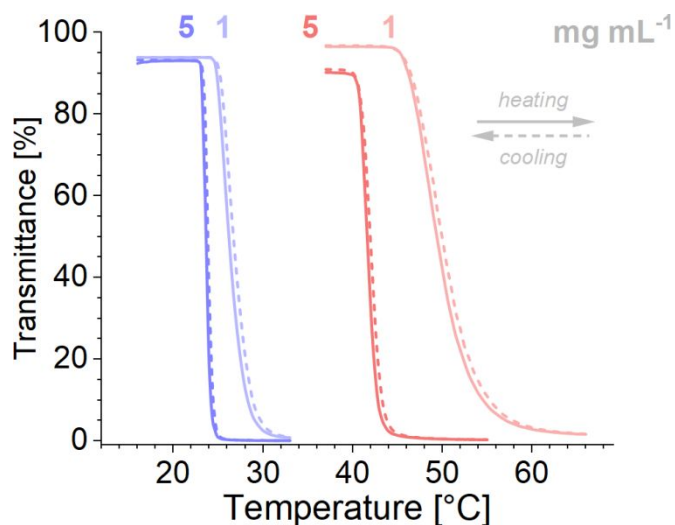


Figure S17. Overview of non-normalized turbidimetry heating (straight) and cooling (dashed) cycles in water for **pEHPA25-Cy5** (blue) and **pHMPMA25-Cy5** (red) 5 and 1 mg mL⁻¹ samples, respectively. A full heating-cooling cycle over the measured temperature range is shown.

As described in the experimental part of the main manuscript, the fluorescence measurements were recorded on a Jasco FP-6500 spectrometer and equilibrated in a water bath prior to the measurements. Close-up pictures of the fluorescent solution during the measurement process are presented in Figure S18.

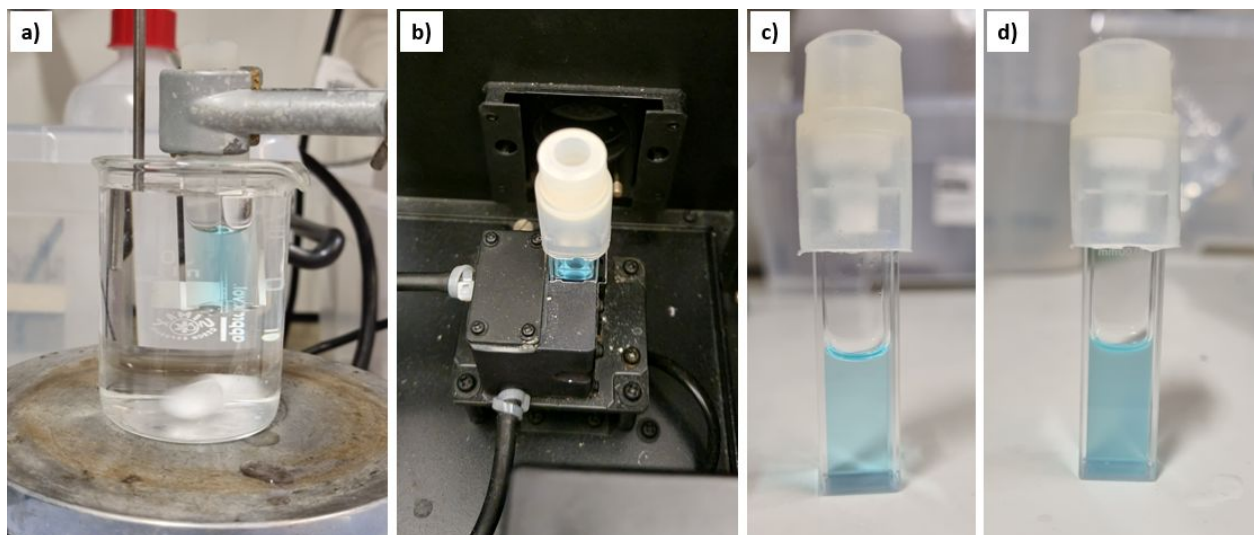


Figure S18. Representative photograph of the fluorescent **pEHPA25-Cy5** solution (1 mg/mL) a) in a tempered water bath equilibrating the fluorescent sample, b) in the tempered sample holder of the fluorescence spectrometer, c) directly after equilibration at 22 °C (first measurement point), and d) directly after equilibration at 36 °C (last measurement point).

The raw fluorescence emission spectra in the region between 660 and 700 nm are shown in Figure S19. The emission maximum of the first spectrum was set as 100 %, and the maxima of the following spectra at each temperature were used to calculate the relative fluorescence decline shown in Figure 7b and c. The temperature steps were chosen accordingly to the considered measurement range.

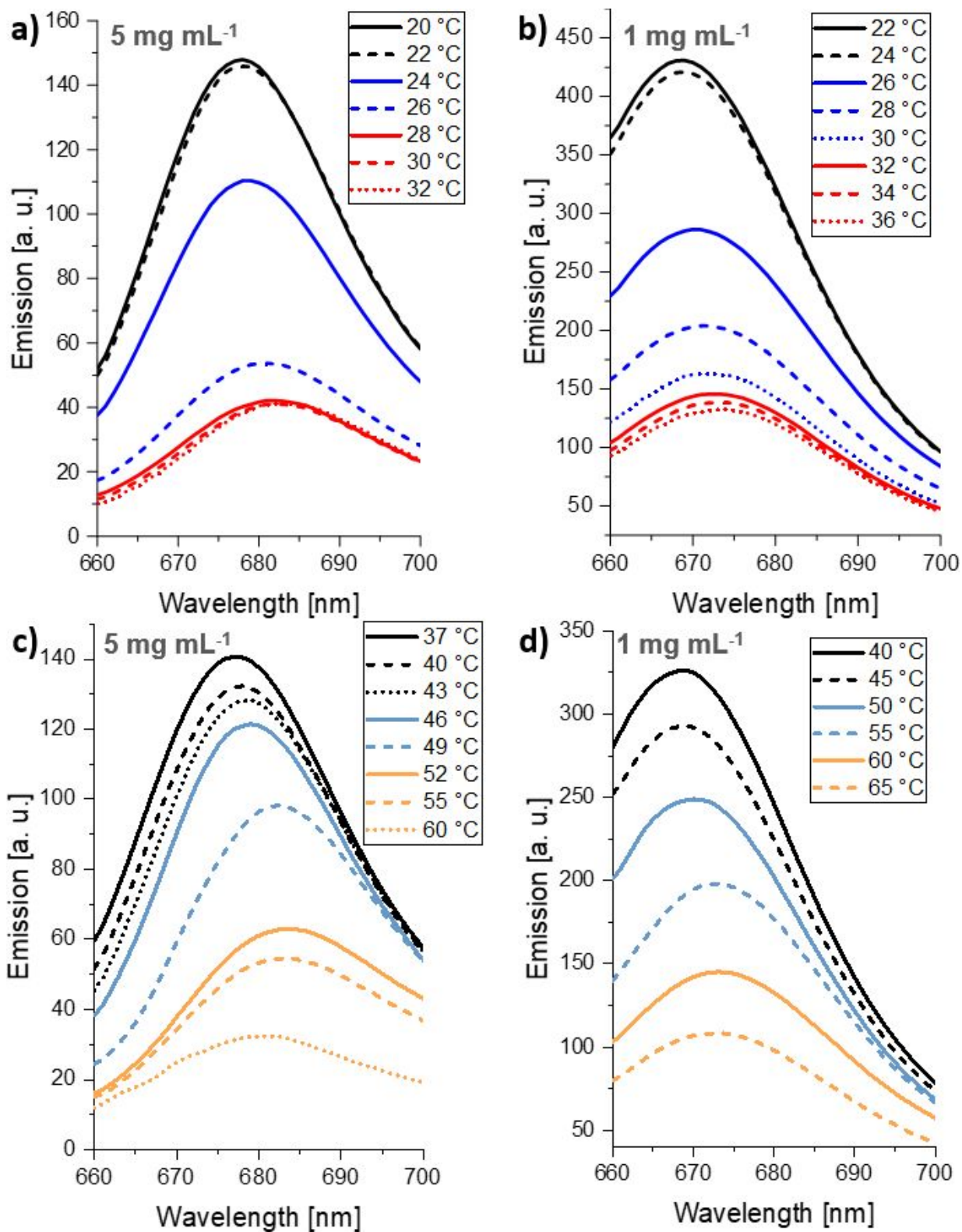


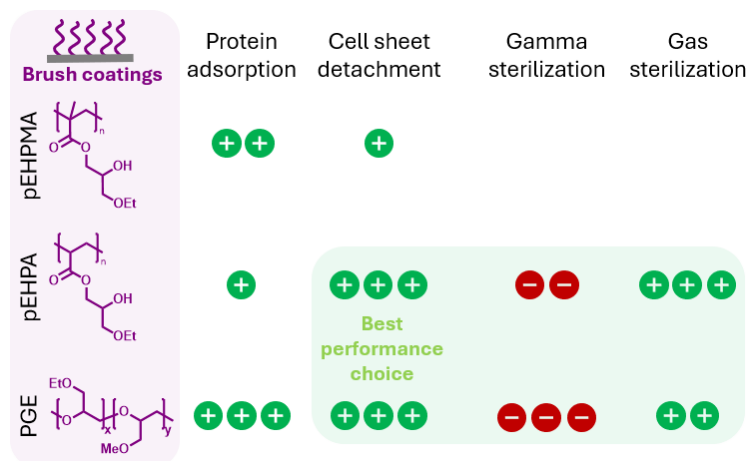
Figure S19. Temperature-dependent fluorescence emission spectra of **pEHPA25-Cy5** (a, b) and **pHMPMA25-Cy5** (c, d) at 5 and 1 mg mL⁻¹ in H₂O.

References.

- (1) Tauscher, S.; Angermann, J.; Catel, Y.; Moszner, N. Evaluation of alternative monomers to HEMA for dental applications. *Dent Mater* **2017**, *33* (7), 857-865.
- (2) Olszewski-Ortar, A.; Gros, P.; Fort, Y. Selective ring-opening of ω -epoxyalkyl (meth)acrylates. An efficient access to bifunctional monomers. *Tetrahedron Lett* **1997**, *38* (50), 8699-8702.
- (3) Vanbiervliet, E.; Fouquay, S.; Michaud, G.; Simon, F.; Carpentier, J.-F.; Guillaume, S. M. From Epoxide to Cyclodithiocarbonate Telechelic Polycyclooctene through Chain-Transfer Ring-Opening Metathesis Polymerization (ROMP): Precursors to Non-Isocyanate Polyurethanes (NIPUs). *Macromolecules* **2016**, *50* (1), 69-82.
- (4) Pach, M.; Zehm, D.; Lange, M.; Dambowsky, I.; Weiss, J.; Laschewsky, A. Universal polymer analysis by ^1H NMR using complementary trimethylsilyl end groups. *J Am Chem Soc* **2010**, *132* (25), 8757-8765.
- (5) Chen, D. X.; Gao, L. F.; Li, X. H.; Tu, Y. F. Precise molecular weight determination and structure characterization of end-functionalized polymers: An NMR approach via combination of one-dimensional and two-dimensional techniques. *Chin J Polym Sci* **2017**, *35* (5), 681-692.
- (6) Chen, S.; Chen, D.; Lu, M.; Zhang, X.; Li, H.; Zhang, X.; Yang, X.; Li, X.; Tu, Y.; Li, C. Y. Incorporating Pendent Fullerenes with High Refractive Index Backbones: A Conjunction Effect Method for High Refractive Index Polymers. *Macromolecules* **2015**, *48* (23), 8480-8488.
- (7) Weaver, J. V. M.; Bannister, I.; Robinson, K. L.; Bories-Azeau, X.; Armes, S. P.; Smallridge, M.; McKenna, P. Stimulus-Responsive Water-Soluble Polymers Based on 2-Hydroxyethyl Methacrylate. *Macromolecules* **2004**, *37* (7), 2395-2403.
- (8) Thomas, D. B.; Convertine, A. J.; Hester, R. D.; Lowe, A. B.; McCormick, C. L. Hydrolytic Susceptibility of Dithioester Chain Transfer Agents and Implications in Aqueous RAFT Polymerizations. *Macromolecules* **2004**, *37* (5), 1735-1741.
- (9) Plamper, F. A.; Steinschulte, A. A.; Hofmann, C. H.; Drude, N.; Mergel, O.; Herbert, C.; Erberich, M.; Schulte, B.; Winter, R.; Richtering, W. Toward Copolymers with Ideal Thermosensitivity: Solution Properties of Linear, Well-Defined Polymers of N-Isopropyl Acrylamide and N,N-Diethyl Acrylamide. *Macromolecules* **2012**, *45* (19), 8021-8026.
- (10) Kubota, K.; Fujishige, S.; Ando, I. Solution Properties of Poly(N-isopropylacrylamide) in Water. *Polym J* **1990**, *22* (1), 15-20.
- (11) Israelachvili, J. N. *Intermolecular and Surface Forces*; Elsevier Science, 2011.

3.3. Thermoresponsive brush coatings for cell sheet engineering with low protein adsorption below and above the polymers' phase transition temperature

Schweigerdt, A.; Stöbener, D. D.; Scholz, J.; Schäfer, A.; Weinhart, M. Thermoresponsive brush coatings for cell sheet engineering with low protein adsorption below and above the polymers' phase transition temperature. *ACS Biomater Sci Eng* **2024**, *submitted*.



Thermoresponsive PEHPA and poly(3-ethoxy-2-hydroxypropyl methacrylate) (PEHPMA) polymers were modified with a short block comprising benzophenone acrylate or methacrylate, respectively. A benzophenone-based self-assembly and immobilization procedure for both copolymers with molecular weights of 22-24 kDa was established and the resulting brush coatings were characterized *via* ellipsometry, contact angle and QCM-D measurements for protein adsorption. Both brush coatings allowed adhesion, proliferation and detachment of HDF cell sheets, despite low protein adsorption above cloud point temperatures. PEHPA-based brush coatings were further sterilized along with established PGE coatings on PS and TCPS surfaces via gamma radiation and FO gas in a storage time window of 14 – 18 d. Gamma irradiation emerged as a too harsh procedure, resulting in coating depletion and loss of functionality to various degrees. FO sterilization was suitable for all evaluated coating types and PEHPA-based coatings demonstrated better storage stability, compared to PGE coatings, showing the benefit of the aliphatic backbone.

Monomer synthesis: A. Schweigerdt, O. Staudhammer, L. Lehmann, F. Junge (various research stays under supervision). Polymer synthesis: A. Schweigerdt, O. Staudhammer. Turbidimetry & DLS analysis: A. Schweigerdt. Temperature dependent NMR spectroscopy & analysis: A. Schäfer, A. Schweigerdt. Coating fabrication concept and surface characterization: A. Schweigerdt. Cell culture experiments: A. Schweigerdt, J. Scholz. Live dead staining experiments: J. Scholz, Dr. S. Wedepohl. Research concept: Dr. D.D. Stöbener, Dr. M. Weinhart, A. Schweigerdt. Project supervision: Dr. M. Weinhart. Manuscript preparation: A. Schweigerdt, Dr. M. Weinhart.

Thermoresponsive brush coatings for cell sheet engineering with low protein adsorption below and above the polymers' phase transition temperature

Alexander Schweigerdt¹, Daniel D. Stöbener^{1,2}, Johanna Scholz¹, Andreas Schäfer¹, Marie Weinhart^{1,2}*

¹ Institute of Chemistry and Biochemistry, Freie Universitaet Berlin, Takustr. 3, 14195 Berlin, Germany

² Institute of Physical Chemistry and Electrochemistry, Leibniz Universitaet Hannover, Callinstr. 3A, 30167 Hannover, Germany

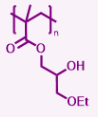
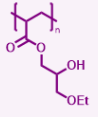
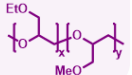
* Corresponding author: email marie.weinhart@pci.uni-hannover.de and marie.weinhart@fu-berlin.de, phone: +49 511-762 14938

ABSTRACT

Thermoresponsive polymer coatings on cell culture substrates enable non-invasive cell detachment and cell sheet fabrication for biomedical applications. Optimized coatings should support controlled culture and detachment of various cell types and allow chemical modifications, e.g., to introduce specific growth factors for enhanced gene expression. Furthermore, the sterilization and storage stability of the coatings must be assessed for translational attempts. Poly(glycidyl ether) (**PGE**) brush coatings with short alkoxy side chains provide a versatile platform for cell culture and detachment, but their polyether backbones are susceptible to oxidation and degradation. Thus, we rationally designed potential alternatives with thermoresponsive glycerol-based block copolymers comprising a stable polyacrylate or polymethacrylate backbone and an oligomeric benzophenone (BP)-based anchor. The resulting poly(ethoxy hydroxypropyl acrylate-*b*-benzophenone acrylate) (**pEHPA-*b*-BP**) and poly(ethoxy hydroxypropyl methacrylate-*b*-benzophenone methacrylate) (**pEHPMA-*b*-BP**) block copolymers preserve the short alkoxy-terminated side chains of the **PGE** derived structure on a stable, but hydrophobic aliphatic backbone. The amphiphilicity balance is maintained through incorporated hydroxyl groups, which simultaneously can be used for chemical modification. The polymers were tailored into brush coatings on polystyrene surfaces *via* directed adsorption using the BP oligomer anchor. The resulting coatings with thickness values up to ~3 nm supported efficient adhesion and proliferation of human fibroblasts despite minimal protein adsorption. The conditions for cell sheet fabrication on **pEHPA-*b*-BP** were gentler and more reliable than on **pEHPMA-*b*-BP**, which required additional cooling. Hence, the stability of **pEHPA-*b*-BP** and **PGE** coatings was evaluated post gamma and formaldehyde (FO) gas sterilization. Gamma sterilization partially degraded **PGE** coatings and hindered cell detachment on **pEHPA-*b*-BP**. In contrast, FO sterilization only slowed detachment on **PGE** coatings and had no adverse effects on **pEHPA-*b*-BP**, maintaining their efficient performance in cell sheet fabrication.

Keywords: functional coatings, antifouling, cell sheet fabrication, sterilization.

For Table of Contents only

Brush coatings	Protein adsorption	Cell sheet detachment	Gamma sterilization	Gas sterilization
<p>pEHPMA</p> 	++	+		
<p>pEHPA</p> 	+	+++ Best performance choice +++		
<p>PGE</p> 	+++	+++	---	++

INTRODUCTION

Polymer coatings with a lower critical solution temperature (LCST) behavior enable gentle, enzyme-free cell harvesting *in vitro*. These coatings promote cell adhesion and proliferation above the polymers' LCST at physiological conditions (37 °C) and become cell-repellent below their LCST, allowing controlled cell detachment without damaging cells or the extracellular matrix (ECM).^{1,2}

The properties of LCST-type polymers can be tailored through monomer selection to direct the location of their phase transitions in aqueous solution to the physiological temperature range³⁻⁵ and fine-tune their amphiphilic balance through copolymerization.^{6,7} Functional polymer coatings, exhibiting a phase transition on the surface of cell culture materials, can be designed with brush, bottlebrush, or hydrogel architecture.⁸⁻¹¹ At physiological conditions, these coatings should be in a dehydrated, collapsed state to promote serum protein adsorption, which mediates cell adhesion of anchorage-dependent cells.^{12, 13} Non-specific serum protein adsorption on artificial surfaces occurs spontaneously and requires minimal exposure to enable cell-surface interactions.^{13, 14} For instance, *Horbett et al.* demonstrated that fibroblasts spread similarly on substrates exposed to serum for either 10 seconds or 90 minutes.¹⁵ Adsorbed fibronectin (Fn) and vitronectin from serum-containing medium mediate cell adhesion *via* integrin-binding RGD sequences, provided they remain structurally intact.¹⁶ Upon RGD-binding of anchorage-dependent cells, adhesion and proliferation processes, such as cytoskeleton reorganization and production of ECM proteins, are initiated.^{17, 18}

For efficient thermally induced cell detachment, the thermoresponsive coating or at least its outermost layer¹⁹ must transition into a rehydrated state upon cooling. Concomitantly, interactions between the cell-derived ECM and the culture substrate become unfavorable, leading to ECM-substrate separation.^{13, 19} For practical convenience, detachment at room temperature (20-25 °C) is preferred, although successful detachment procedures at temperatures below 20 °C were also developed.^{20, 21} Thermoresponsive polymer coatings generally exhibit broader phase transitions compared to their aqueous polymer solutions due to restricted chain movement after surface tethering.^{19, 22, 23} Additionally, phase transition temperatures can be influenced through the coating-substrate or polymer-salt and polymer-protein interactions.^{11, 24, 25}

Consequently, inhomogeneous layer (de)hydration and hampered phase transitions must be considered when optimizing the coating performance for cell sheet fabrication. For example, poly(*N*-isopropyl acrylamide) (**pNIPAM**, LCST ~32 °C) hydrogel and poly(oligo ethylene glycol methacrylate) (**pOEGMA**) (LCST ~28-34 °C) brush coatings can lack cell adhesive properties above their phase transition temperature^{9, 26-28} and poly(glycidyl ether) (**PGE**) brushes (LCST ~20-30 °C) may not reliably mediate controlled cell sheet detachment at distinct grafting densities.¹¹

The performance of thermoresponsive coatings can be further optimized by incorporating functional units. For instance, copolymers of 2-carboxy isopropyl acrylamide with **NIPAM** were functionalized with heparin using the carboxyl group, which enabled the binding of epidermal growth factors for enhanced expression of hepatocyte-specific genes in primary hepatocytes.²⁹ Therefore, polymers with accessible reactive groups, e.g., hydroxyl, carboxyl, or amine groups, are desirable.^{30, 31} However, most established thermoresponsive polymers, such as **pNIPAM**, **pOEGMA**, or poly(oxazoline)s (**POX**) lack reactive groups and require copolymerization, which may impact their LCST behavior.³² Additionally, stability during sterilization is crucial for technology translation into biomedical laboratories and potential product development. While **pNIPAM** surfaces are compatible with gas sterilization, frequently used ionizing radiation increases the LCST or induces crosslinking in **pNIPAM** or **POX** polymers, thus potentially limiting their phase transition and application in the physiological range.^{33, 34}

In previous work, we established thermoresponsive poly(glycidyl ether) (**PGE**) coatings optimized for cell sheet fabrication.³⁵ Their alkoxy side groups induce LCST behavior, allowing thermal control over cell adhesion, though lacking post-functionalization options.^{35, 36} Limitations in the shelf-life and sterilization stability of structurally similar poly(ethylene glycol) (**PEG**) coatings further raise concerns about the stability of thermoresponsive **PGE** brushes under storage or radiation sterilization conditions.³⁷⁻³⁹ Therefore, we applied molecular design principles to conceptualize, synthesize, and characterize poly(γ -alkoxy- β -hydroxy-(meth)acrylate) polymers, incorporating stable aliphatic backbones and hydroxyl groups for post-functionalization while preserving **PGE**-like short alkoxy side chains.³ The resulting poly(hydroxy

methoxypropyl methacrylate) (**pHMPMA**), however, exhibited cloud point temperatures (T_{cp}) mainly above the physiological range (37-51 °C). Furthermore, no distinct microscopic dehydration was detected, which is an important prerequisite for cell culture applications.³ In contrast, poly(ethoxy hydroxypropyl acrylate) (**pEHPA**) homopolymers exhibited T_{cp} values of 22-27 °C and distinct chain dehydration above the T_{cp} , thus showing potential for a functional cell sheet fabrication coating.³ To develop functional brush coatings via block copolymer self-assembly on PS substrates in this work, we prepared thermoresponsive block copolymers with a poly(meth)acrylate backbone comprising ethoxy hydroxypropyl side chains, avoiding methoxy side chains, which have been shown to introduce unfavorable thermoresponsive properties³ to the polymer (Figure 1).

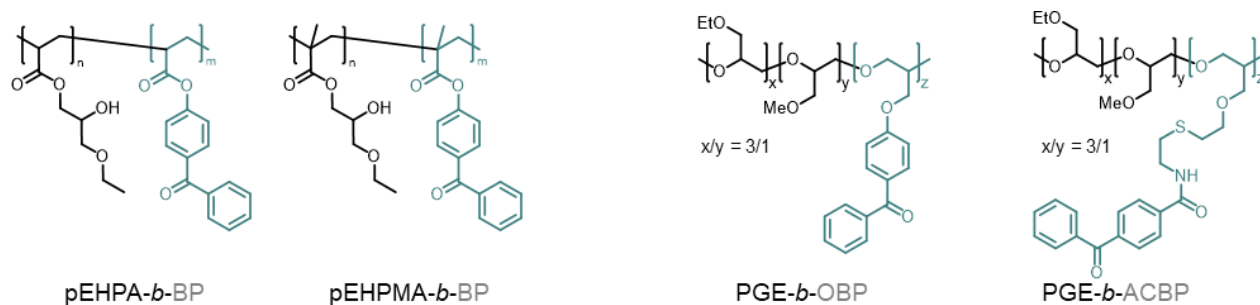


Figure 1. Chemical structures of the glycerol-based thermoresponsive copolymers **pEHPA-*b*-BP** and **pEHPMA-*b*-BP**, which were used to functionally coat PS surfaces in this work (left) as well as **PGE-*b*-OBP** and **PGE-*b*-ACBP** which were used for comparison as established (TC)PS coating systems (right).

Both thermoresponsive poly(ethoxy hydroxypropyl acrylate-*b*-benzophenone acrylate) (**pEHPA-*b*-BP**) and poly(ethoxyhydroxypropyl methacrylate-*b*-benzophenone methacrylate) (**pEHPMA-*b*-BP**) were designed with a short benzophenone (BP)-comprising block for efficient self-assembly and covalent surface attachment. The performance of the resulting brush coatings was evaluated in cell culture. Cell sheet fabrication on these surfaces was investigated before and after formaldehyde (FO) gas and gamma sterilization and compared to established **PGE-*b*-OBP** and **PGE-*b*-ACBP** brush coatings on PS and TCPS (Figure 1).¹¹ **pEHP[M]A**-based functional coatings showed efficient cell adhesion despite striking

differences in protein adsorption, compared to **PGE**, and the aliphatic backbone further enhanced post-sterilization performance.

EXPERIMENTAL SECTION

Materials, synthetic pathways and procedures, as well as the characterization of the used monomers (Scheme S1) and polymers (Scheme S2), including gel permeation chromatography (GPC) methods, sample preparation for thermoresponsive analysis, additional UV-Vis, dynamic light scattering (DLS), and nuclear magnetic resonance (NMR) spectroscopy data are presented in the electronic Supporting Information (SI). Procedures for the preparation of PS-coated surfaces on silicon wafers or quartz crystal microbalance (QCM-D) chips are also provided in the SI.

Turbidimetry (UV-Vis) measurements. Absorbance and transmittance measurements were recorded on a PerkinElmer Lambda 950 UV-Vis spectrometer with a PTP 6 Peltier temperature programmer (PerkinElmer). Temperature-dependent measurements were performed at heating rates of $0.5\text{ }^{\circ}\text{C min}^{-1}$ while recording data points every $0.5\text{ }^{\circ}\text{C}$. The temperature-dependent transmittance of the aqueous polymer solution was measured for two cycles per sample. The measurement points were connected via the Akima-spline interpolation, and the cloud point temperature T_{cp} was defined as the temperature at the inflection point of the normalized transmittance versus temperature curve.

Temperature-dependent NMR measurements. ^1H and ^{13}C NMR spectra were recorded on a JEOL ECZ operating at 600 and 150 MHz, respectively. Deuterated water (D_2O) was filtered over a $0.45\text{ }\mu\text{m}$ syringe filter (cellulose acetate), and samples were prepared at a concentration of 10 mg mL^{-1} .

Preparation of polymer solutions and fabrication of brush coatings. Milli-Q water and absolute ethanol were used for all polymer solutions. The preparation of thermoresponsive **PGE** brush coatings was described in detail previously.^{11, 40} Briefly, (TC)PS model substrates, placed in PS petri dishes, or plain (TC)PS petri dish surfaces were incubated in **PGE**-block copolymer solution (2 mL , $250\text{ }\mu\text{g mL}^{-1}$) for 60 min. A **PGE-*b*-OBP** solution in 54/46 water/ethanol (v:v) or a **PGE-*b*-ACBP** solution in 52/48 water/ethanol (v:v) was used for the self-assembly process on PS and TCPS substrates, respectively. After

incubation, the polymer solution was discarded, the coatings briefly washed with water, dried under a nitrogen stream, and irradiated under UV light (UV KUB, LED, $\lambda = 365$ nm) for 160 s to covalently attach the adsorbed polymer brushes to the substrate.

pEHP[M]A-*b*-BP polymer solutions in 55/45 water/ethanol (v:v) were prepared at a concentration of 250 or 62.5 $\mu\text{g mL}^{-1}$. Before the adsorption step, the polymer solutions (2.5 mL per substrate) gauged in a syringe were equilibrated at 35 °C for 20 min together with the dry model PS substrates or PS petri dishes. Afterward, the polymer solutions were filtered (0.22 μm cellulose acetate syringe filter) onto substrates, and the incubation procedure proceeded for 60 min at 35 °C. After incubation, the polymer solutions were discarded, and the brush coatings were briefly washed with water at room temperature (RT), dried under a nitrogen stream, and irradiated under UV light (UV KUB, LED, $\lambda = 365$ nm) for 16 min to covalently attach the adsorbed brushes to the substrate.

After irradiation, all brush-coated surfaces were immersed in ethanol for at least 16 h to remove non-covalently attached chains from the surface and dried under a stream of nitrogen before characterization and usage in further experiments.

Brush coating analysis. Coating thickness in the dry state was analyzed through spectroscopic ellipsometry measurements and evaluated *via* a Cauchy fit. A fixed refractive index $R_f = 1.45$ was used for **PGE** brush coatings,⁴⁰ while for **pEHP[M]A** brush coatings, an $R_f = 1.51$ was approximated due to the structural resemblance to poly(hydroxyethyl methacrylate) (**pHEMA**).^{41,42} Water contact angles (CA) were measured at ambient conditions (20 °C) via the sessile drop method (2 μL) applying the Laplace-Young model.

Quartz crystal microbalance with dissipation (QCM-D) measurements for quantification of protein adsorption. Protein adsorption from standard Dulbecco's modified eagle medium (DMEM) supplemented with 10% fetal bovine serum (FBS) (v:v) on **pEHP[M]A** brushes and TCPS controls was measured at 20 and 37 °C under a constant flow of 0.1 mL min^{-1} . After thermal surface equilibration under phosphate buffered saline (PBS) flow, the medium was changed to serum protein-containing DMEM medium for 20 minutes and flushed again with PBS until the signal remained constant (5 min). The frequency differences

Δf of the third overtone before and after protein exposure to the surface were converted to areal mass coverage using the Sauerbrey equation and the fundamental QCM-D chip frequency of 4.95 MHz to access the adsorbed areal protein mass. Representative frequency curves are shown in Figure S10.

Cell culture conditions. Detailed cell culture conditions are described in the SI. For adhesion studies on **pEHP[M]A** coatings, human dermal fibroblasts (HDF) were seeded with a density of 43×10^5 cells cm^{-2} , and phase contrast images were taken after 1, 4, 24, 48, and 72 h. For cell detachment studies on **PGE** coatings, HDF were seeded with a density of 160×10^5 cells cm^{-2} , and phase images were taken after 24 h, as established previously.¹⁹ For cell detachment studies on **pEHP[M]A** coatings, HDFs were seeded with a density of 104×10^5 cells cm^{-2} and phase images were taken after 24 and 48 h for **pEHPA-*b*-BP** and additionally after 72 h for **pEHPMA-*b*-BP**.

Cell detachment. Thermal detachment of cell sheets on **pEHPA-*b*-BP**, **PGE-*b*-OBP**, and **PGE-*b*-ACBP** coatings was triggered as follows: after reaching confluency, the cell culture medium was exchanged against PBS at RT for 10 minutes. Afterwards, the PBS was exchanged for warm PBS (37 °C), and the dishes were placed in the cell culture incubator for 10 minutes. Finally, cell sheet detachment was observed under ambient conditions.

Thermal detachment on **pEHPMA-*b*-BP** coatings was triggered as follows: after reaching confluency, the cell culture medium was exchanged against 4 °C PBS with incubation for 10 minutes at 4 °C. Then, the PBS was exchanged for warm PBS (37 °C), and the dishes were placed in the cell culture incubator for 10 minutes. Finally, cell sheet detachment was observed under ambient conditions.

Sterilization of substrates. Surface disinfection or sterilization of **PGE** and **pEHP[M]A** brush coatings were performed via aq. EtOH (70 v-%) treatment, FO gas sterilization, and gamma radiation. Disinfection was performed by fully immersing the coated dishes in aq. EtOH for 10 minutes, followed by a two-fold PBS wash afterward. Gas sterilization was performed with a Euro Formomat 5 device from MMM Group (München, Germany) using water-based 3% formaldehyde gas at 200 mbar and 60 °C for 6 h, according to the DIN EN 14180. Gamma sterilization was performed by BBF Sterilisationservice GmbH (Kernen,

Germany). Cobalt-60 was used as a source for gamma radiation, and a total dose of 45 kGy \pm 10% was applied to the substrates, according to the DIN EN ISO 11137-1.

Data evaluation. Raw data processing and evaluation were performed with OriginPro and Microsoft Excel. Statistical comparison was performed using the Mann-Whitney-U test for two independent sample sets (ns, $p > 0.1$; *, $p < 0.1$; **, $p < 0.05$).

RESULTS AND DISCUSSION

Polymer synthesis and characterization. The synthesis of **pEHPA** and **pEHPMA** homopolymers was performed according to previously established conditions for the controlled reversible addition-fragmentation transfer (RAFT) polymerization of **pEHPA**.³ Due to the poor solubility of the corresponding **pEHPMA** polymer in water, the polymerization of EHPMA was performed in dimethylformamide instead of water/1,4-dioxane mixture (Scheme S2a). The RAFT polymerization system allowed a convenient chain extension using benzophenone (BP) acrylate or methacrylate as comonomers (Scheme S1b,c and S2b,c) with overall isolated copolymer yields above 80%. The block copolymers **pEHPA-*b*-BP** and **pEHPMA-*b*-BP** comprise a short functional surface anchoring block with 2-4 BP units. Efficient attachment of the BP monomers to the homopolymer chains was indicated through the systematic increase of the whole distribution curve in the UV detector signal of the GPC elugrams (Figure S1). The structural characteristics of the synthesized polymers are listed in Table 1.

Table 1. Number average molecular weight M_n , dispersity \mathcal{D} , number of BP units per anchor block, and isolated yield of the synthesized polymers after dialysis.

Polymer	M_n [kDa] ^a	\mathcal{D} ^a	BP units ^b	Yield [%] ^c
pEHPA	22.6	1.15	-	69
pEHPMA	21.7	1.16	-	89
pEHPA-<i>b</i>-BP	24.1	1.25	3.9	87

pEHPMA-*b*-BP

22.1

1.18

2.4

88

^aDerived from GPC measurements in THF calibrated with PMMA standards^bCalculated from ¹H NMR measurements^cMonomer to polymer yield ratio

The narrow dispersities ≤ 1.25 of the homo- and copolymers with molecular weights around 23 kDa indicate controlled polymerization conditions, essential for block copolymer synthesis close to the targeted value of 30 kDa. The BP-based anchor block enables directed physical adsorption of the block copolymers from selective solvents to hydrophobic surfaces such as PS *via* hydrophobic and π - π interactions. Furthermore, BP units promote covalent attachment of the assembled polymer chains to the PS surface via C-H insertion upon UV exposure,^{40, 43} offering a convenient material-efficient and geometry-independent surface modification strategy.

Evaluation of thermoresponsive behavior. The transition range of aqueous **pEHPA** solutions with a concentration between 20 and 5 mg mL⁻¹ is located between 22 and 27 °C, comprising sharp phase transitions and a distinct dehydration behavior of the hydroxy groups as determined previously.³ Concentration-dependent turbidity measurements of analogous aqueous **pEHPMA** solutions (Figure S2) also indicate a sharp and reversible phase transition behavior. However, the more hydrophobic methacrylate backbone reduced the phase transition regime of the aqueous **pEHPMA** solutions to 8 - 11 °C with only a minor impact of salts on the T_{cp} (Table 2). Additional DLS measurements revealed solvated **pEHPMA** chains of ~7 nm size at 8 °C, which increased to around 4800 nm in PBS and 630 nm in water upon thermally induced aggregation at RT (Figure S4). To further ensure that the hydrophobic BP block in **pEHPA-*b*-BP** and **pEHPMA-*b*-BP** is not adversely impacting the copolymers' transition behavior, concentration-dependent turbidity studies were performed in PBS (Figure 2).

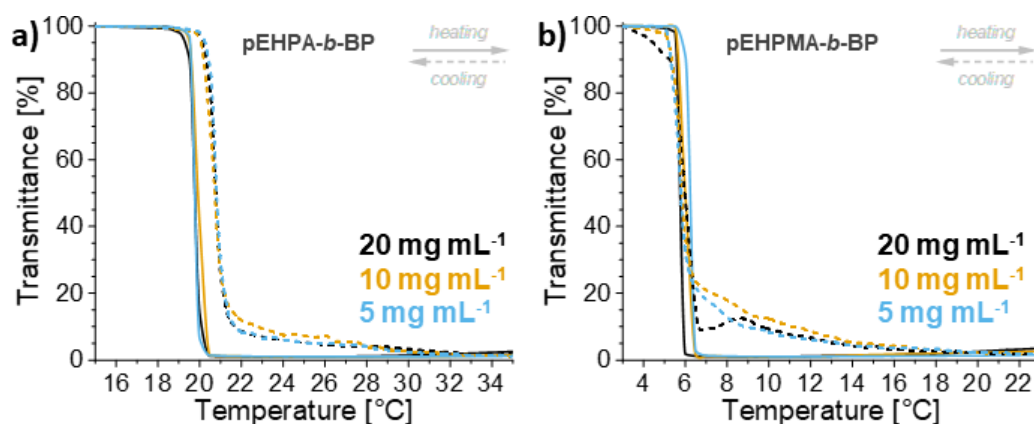


Figure 2. Representative concentration-dependent turbidimetry curves of **pEHPA-*b*-BP** (a) and **pEHPMA-*b*-BP** (b) in PBS after normalization from heating and cooling cycles ($n = 2$ per cycle).

Both block copolymers exhibit concentration-independent, sharp, and reversible transitions in PBS over the scanned temperature and concentration range. A minor increase in transmittance during cooling cycles can be attributed to irreversible polymer precipitation due to a salting-out effect, which slightly decreases the polymer concentration.^{3, 24} While the presence of salts hardly altered the phase transition behavior of **pEHPA-*b*-BP** solutions, a significant impact was observed for **pEHPMA-*b*-BP** when comparing turbidity curves in water (Figure S3) and PBS (Figure 2). In water, two sigmoidal transition regions were detected between 7-8 °C and 10-14 °C, corresponding to a polymer aggregate size of 37 and 67 nm (Figure S5), respectively. In the presence of ions, the two transition regimes unified to a single cloud point at approximately 6 °C. The first cloud point in water can be attributed to the phase transition of the **pEHPMA** block, since the T_{cp} values are located between the ones of **pEHPMA** in H₂O (9-10 °C) and **pEHPMA-*b*-BP** in PBS (~6 °C). The hydrophobic **BP**-based block then stabilizes the aggregates for temperatures up to ~14 °C in agreement with DLS data (Figure S5), before the transition continues, resulting in larger aggregates. An overview of the average T_{cp} values of the aqueous polymer solutions, including T_{cp} values of pEHPA solutions,³ is presented in Table 2.

Table 2. Concentration-dependent cloud point temperatures T_{cp} stated as average values \pm standard deviation (SD) from heating and cooling cycles of thermoresponsive homo- and copolymers in PBS and water (n = 4). The minimal SD was aligned with the experimental error (± 0.5 °C).

Polymer	T_{cp} (20 mg mL ⁻¹) [°C]	T_{cp} (10 mg mL ⁻¹) [°C]	T_{cp} (5 mg mL ⁻¹) [°C]
pEHPA (H ₂ O) ^a	23.2 \pm 0.5	23.7 \pm 0.5	24.5 \pm 0.5
pEHPA (PBS) ^a	21.5 \pm 0.5	22.0 \pm 0.5	22.5 \pm 0.5
pEHPA-<i>b</i>-BP (H ₂ O)	22.3 \pm 0.5	22.5 \pm 0.5	23.3 \pm 0.5
pEHPA-<i>b</i>-BP (PBS)	20.3 \pm 0.6	20.3 \pm 0.5	20.3 \pm 0.6
pEHPMA (H ₂ O)	9.0 \pm 0.5	9.8 \pm 0.5	10.3 \pm 0.5
pEHPMA (PBS)	8.4 \pm 0.6	8.8 \pm 0.6	8.8 \pm 0.5
pEHPMA-<i>b</i>-BP (H ₂ O) ^b	7 \pm 0.5	7.5 \pm 0.5	7.6 \pm 0.5
pEHPMA-<i>b</i>-BP (H ₂ O) ^c	10.5 \pm 0.8	13.9 \pm 1.9	14.3 \pm 1.3
pEHPMA-<i>b</i>-BP (PBS)	5.8 \pm 0.5	6 \pm 0.5	5.9 \pm 0.5

^a literature data obtained from *Schweigerdt et al.*³

^b value refers to the first of the two observed T_{cp} 's

^c value refers to the second of the two observed T_{cp} 's.

The T_{cp} values of the block copolymers decrease by \sim 2-3 °C compared to respective homopolymers due to the hydrophobic benzophenone block.³ Only a minimal concentration dependence of the T_{cp} values was observed, spanning \sim 1 °C between 5 and 20 mg mL⁻¹, except for the bimodal transition of **pEHPMA-*b*-BP** in water. As expected, the presence of ions in PBS and the hydrophobic BP block caused a minor T_{cp} decrease.^{3, 40}

In general, the phase transition range of **pEHPA-*b*-BP** is comparable to the one of functional **PGE** coatings at approximately 20 °C and thus well-suited for cell culture applications.¹¹ **pEHPMA**-based polymers with a lower phase transition range might still be suitable for cell culture, based on literature examples of successful cell detachment at temperatures as low as 4 °C.^{20, 21} Furthermore, **pEHPMA-*b*-BP** solutions in PBS showed a slight transmittance increase already at \sim 20 °C upon cooling, which might be enough to

impact cell behavior, when used as a coating. To investigate the hydration changes of **pEHPMA** on a microscopic scale, temperature-dependent ^1H and ^{13}C NMR spectra were recorded in D_2O at 10 mg mL^{-1} (Figure S6 and Figure 3).

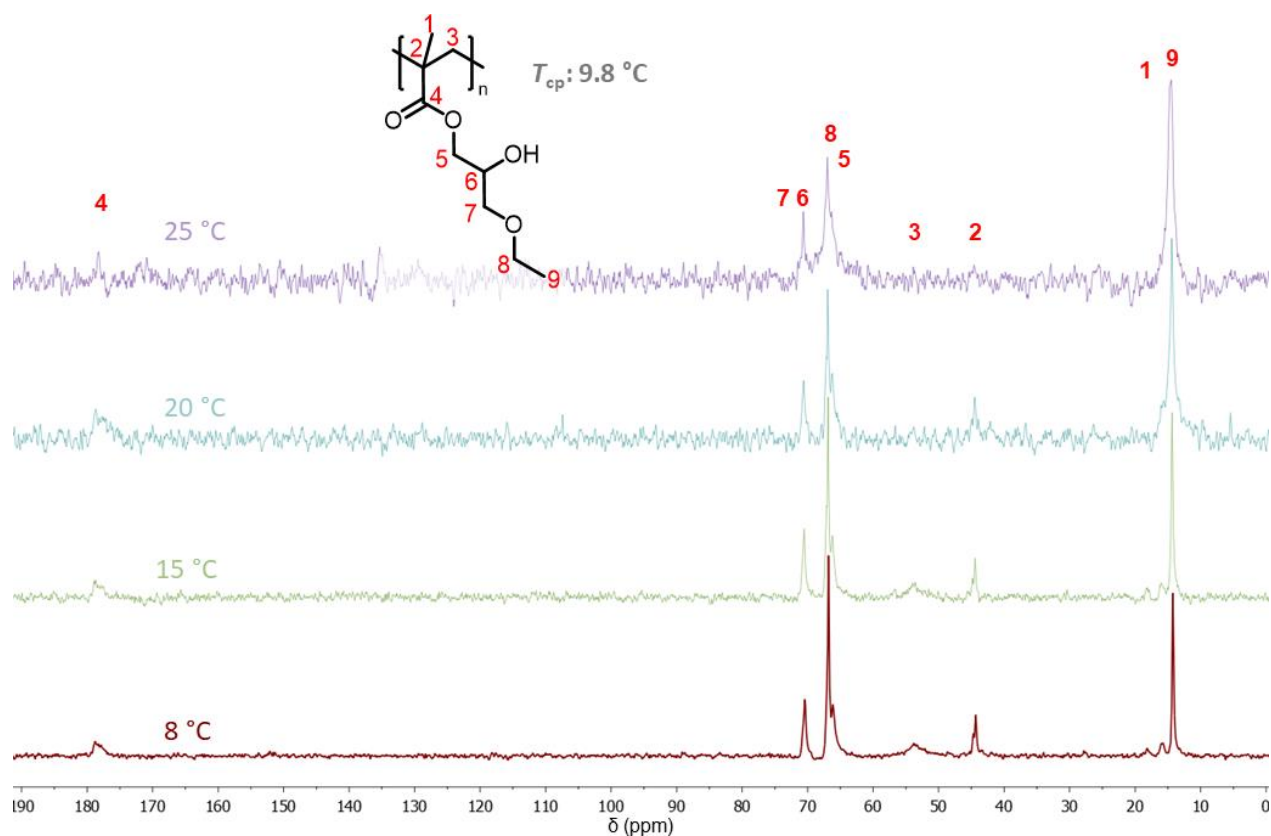


Figure 3. Temperature-dependent ^{13}C NMR spectra (D_2O , 150 MHz) of **pEHPMA** at a concentration of 10 mg mL^{-1} ($T_{\text{cp}}: 9.8\text{ }^\circ\text{C}$) acquired after thermal equilibration in a heating cycle. The spectra were referenced to peak **9** at $8\text{ }^\circ\text{C}$. Peaks were assigned with numbers according to the illustrated chemical structure.

The ^{13}C spectra of the **pEHPMA** solution with a T_{cp} of $\sim 10\text{ }^\circ\text{C}$ indicate only minimal chain dehydration on the microscopic scale between 8 and $15\text{ }^\circ\text{C}$, according to minor spectral changes. The transition becomes more pronounced at temperatures of $20\text{ }^\circ\text{C}$ and above. For instance, signals **8** and **9** of the outermost carbons of the side chain show marked signal broadening due to reduced mobility upon dehydration and increasing hydrophobic-hydrophobic interactions, particularly between 15 and $20\text{ }^\circ\text{C}$. Furthermore, the declining signal intensity is accompanied by an increasing signal-to-noise ratio, rendering backbone carbon signals **1+3** and

2+4 undetectable at 20 and 25 °C, respectively. In contrast, the side chain carbon signals **6**, **8** and **9** remain detectable, while signals of **5** and **7** are difficult to differentiate due to similar chemical shifts to signals **6** and **8**. In support of a major loss in chain mobility between 15 and 20 °C, the ¹H NMR spectra of **pEHPMA** solution (Figure S6) also show a marked decrease in the intensity of all detected signals accompanied with a gradual signal broadening over the whole temperature range, indicating uniform polymer segment dehydration and a continuous phase transition.^{44,45}

The observed temperature-dependent dehydration pattern on the microscopic scale across all structural elements is typical for a coil-to-globule transition, as similarly observed with **pNIPAM** or **POX** polymers. However, in contrast to **pNIPAM** and **POX** solutions, which show drastic changes over a 2-3 °C range above their respective macroscopically determined T_{cp} values, the microscopic transition process in **pEHPMA** solutions is more continuous.^{46,47} Similar to **pEHPA** polymers, the microscopic dehydration of **pEHPMA** becomes visible in the NMR spectra at temperatures above the T_{cp} and proceeds continuously.³ However, the dehydration of **pEHPMA** is more pronounced compared to **pEHPA**, as evidenced by the disappearing signals attributed to the backbone carbons and broadened signals of the side chain carbons. Given that the microscopic transition extends up to 25 °C, **pEHPMA**-based coatings might well be suitable for cell sheet detachment at RT. Prior studies indicated that an initiated transition is sufficient for cell sheet detachment through rehydration of the outermost 'fuzzy hair' layer.¹⁹ The degree of polymer dehydration upon the thermal phase transition decreases in aqueous **pEHPMA**, **pEHPA**, and virtually non-dehydrating poly(hydroxymethoxy methacrylate) (**pHMPMA**)³ solutions with the polymer hydrophilicity. The decreasing dehydration is accompanied with a transformation from a coil-to-globule to a liquid-liquid phase separation type. A similar transformation is observed with **NIPAM** copolymers with increasing 2-hydroxyisopropylacrylamide content which exhibit raised T_{cp} values and reduced dehydration during the phase transition, correlating with the hydroxyl group content.⁴⁸

Fabrication and characterization of brush coatings. Directed adsorption of **pEHPA-*b*-BP** and **pEHPMA-*b*-BP** onto PS surfaces was achieved from dilute water-ethanol mixtures (250 and 62.5 µg mL⁻¹

¹) as a selective solvent, based on a previous report.^{19, 40} The block copolymer self-assembly parameters were kept identical for both polymers to ensure comparability, as detailed in the experimental section. A sufficient UV-light (360 nm) exposure ensured covalent attachment of the adsorbed polymer brushes on the substrate via C,H-insertion.⁴⁹ Adsorption at 35 °C was established, since preliminary results of **pHMPMA-*b*-BP** immobilization from utilized 62.5 µg mL⁻¹ mixtures revealed thicknesses of 1.1 – 1.8 nm after adsorption at RT and 1.6 – 2.4 nm after adsorption at 35 °C, including consecutive immobilization and extraction steps (data not shown). To assist the surface adsorption of singularized copolymer chains, their tendency for aggregation (Figure S5) was disturbed by filtering the block copolymer solutions through 0.22 µm syringe filters at 35 °C directly before the self-assembly process. The resulting surface characteristics of the covalently grafted coatings are shown in Figure 4.

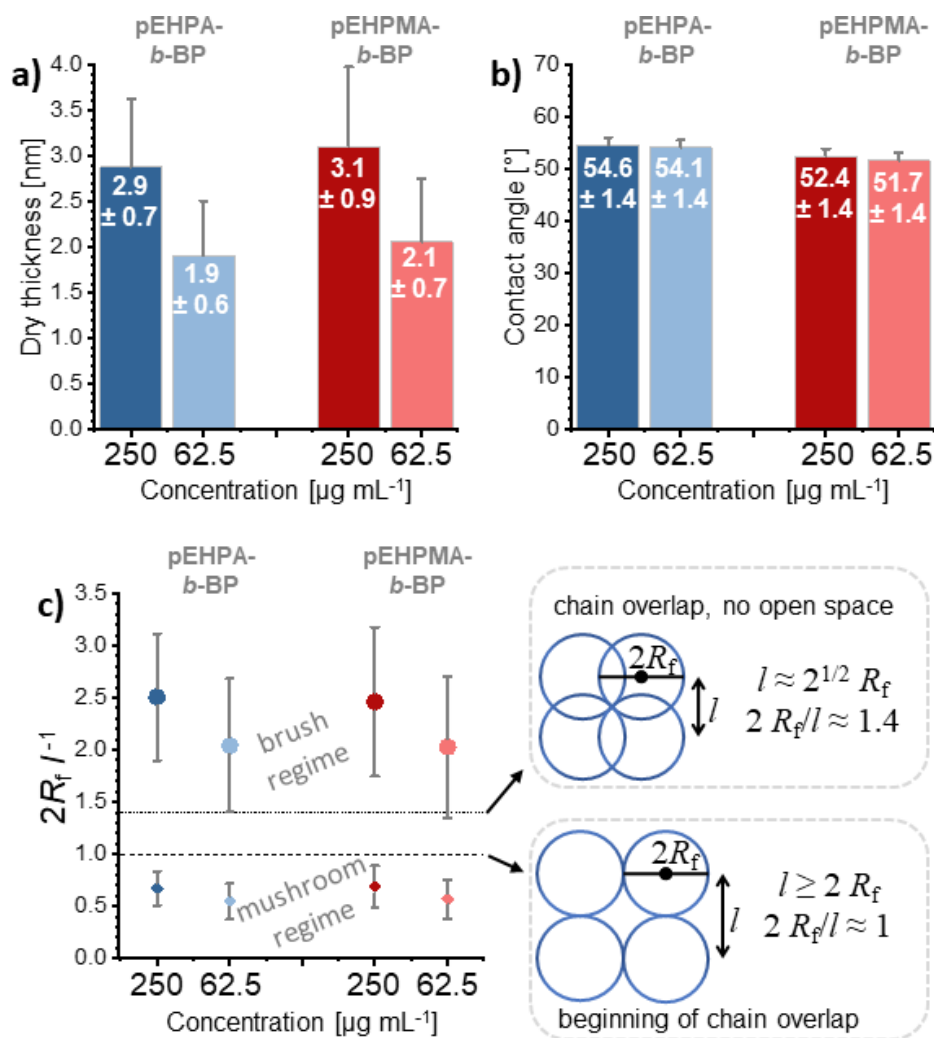


Figure 4. Surface characteristics of **pEHPA-*b*-BP** and **pEHPMA-*b*-BP** brush coatings on PS substrates prepared by adsorption, covalent UV-immobilization, and extraction in ethanol. Concentration-dependent dry layer thicknesses (a), water contact angles (b), and theoretical degree of polymer chain overlap of the grafted polymers in a good (dots) and bad (diamonds) solvent (c). Mean values with SD are plotted. ($n \geq 4$)

For both block copolymers, comparable coating thicknesses of ~ 3 and ~ 2 nm at concentrations of 250 and $62.5 \mu\text{g mL}^{-1}$ were obtained, respectively. The directed adsorption of the copolymers *via* their benzophenone block was demonstrated by the significant ($p < 0.05$) differences in dry layer thickness to their respective **pEHPA** and **pEHPMA** homopolymer coatings after adsorption and irradiation but before extraction. The complete thickness loss of the homopolymer layers after extraction (Figure S7a) was detected *via* ellipsometry with slightly reduced CA values of 85 - 87° ($p < 0.05$) compared to pristine PS ($\sim 90^\circ$) (Figure

S7b). In contrast, immobilized brush coatings from block copolymer adsorption exhibited reduced contact angle values of 52-55°. In the literature, **pNIPAM** coatings with contact angle values from 38 to 72° have been reported to successfully promote cell adhesion and thermally triggered detachment.⁵⁰ In addition, **PGE** and **pNIPAM** surface coatings with thicknesses of ~3 nm are suitable for cell sheet fabrication.^{9, 35} According to these roughly predictive surface parameters, the produced **pEHPA** and **pEHPMA** would qualify as thermoresponsive substrates for cell culture applications.

To estimate whether the PS substrate is fully covered by the coating during cell culture (37 °C) and detachment (RT) conditions, we calculated the degree of chain overlap ($2R_f l^{-1}$) of the surface tethered polymer chains from the ratio of their Flory radius (R_f) to the respective chain anchor distance (l) (Table S2). The hydrodynamic radius under cell culture conditions above the polymer's T_{cp} was estimated with a Flory radius in a bad solvent, while at detachment temperatures below the T_{cp} , the Flory radius in a good solvent was used. These polymer theory-based calculations revealed that the hydrated coatings at temperatures below the polymer's T_{cp} are in the brush regime and transition into a mushroom regime upon dehydration at temperatures above the T_{cp} (Figure 4c). Hence, this thermally induced phase transition may expose the basal PS substrate, interfering with proteins and cells. Since our homopolymers non-specifically interact with the PS surface (Figure S3), full surface coverage by the tethered polymer chains can still be assumed even in a theoretical mushroom configuration under cell culture conditions.

Cell sheet fabrication and protein adsorption. The general suitability of **pEHPA-*b*-BP** and **pEHPMA-*b*-BP** coated PS dishes for cell culture was first assessed *via* HDF adhesion and proliferation studies on these substrates and compared to TCPS controls. Therefore, **pEHP(M)A-*b*-BP** coated dishes were sterilized *via* aq. EtOH (70 v-%) disinfection, as described in the experimental part. Afterward, fibroblasts were seeded at a density of 43×10^5 cells cm^{-2} and were cultured in DMEM supplemented with 10% FBS at 37 °C. Cell morphology was monitored time-dependently after 1, 4, 24, 48, and 72 h *via* phase contrast microscopy (Figure 5, Figure S8), demonstrating uniform adhesion on all coatings according to the shape change and spreading of fibroblasts on the surface.

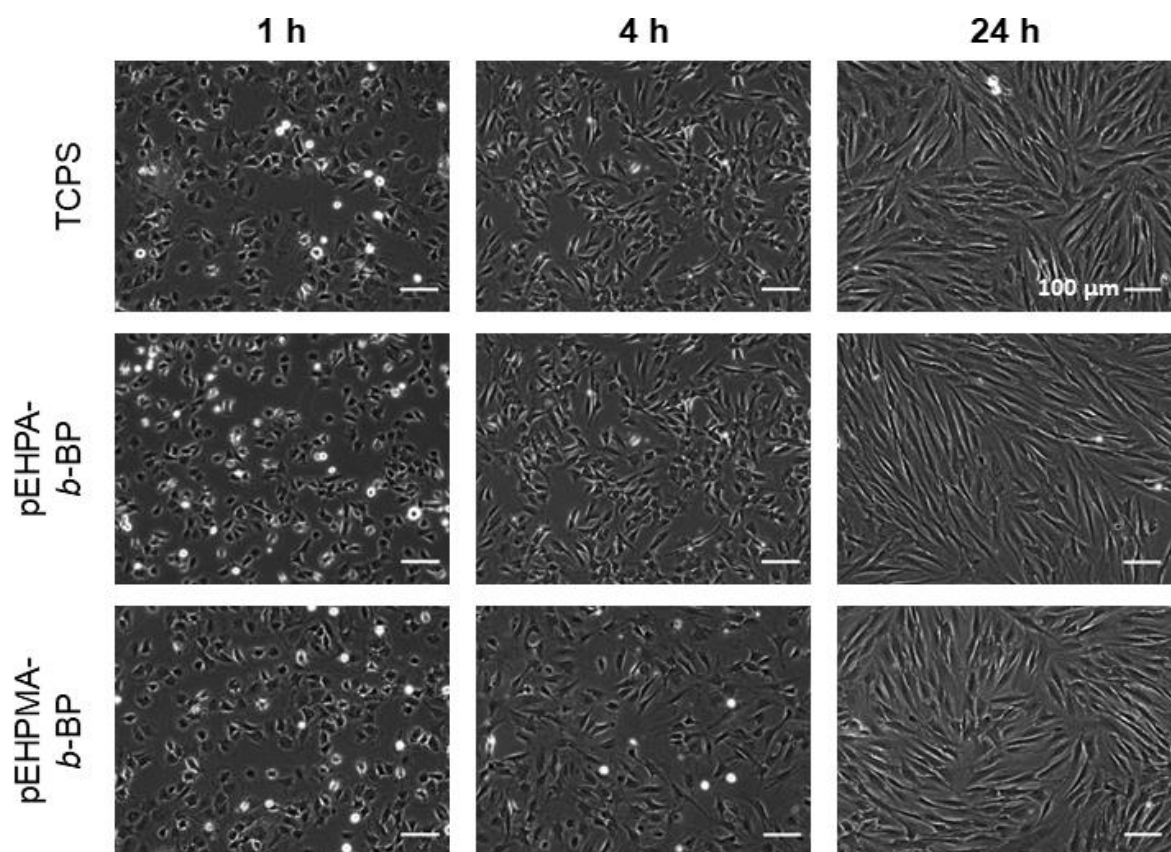


Figure 5. Representative phase contrast images of human dermal fibroblasts on **TCPS** (top), **pEHPA-*b*-BP** (middle), and **pEHPMA-*b*-BP** (bottom) coatings 1, 4, and 24 h after seeding at a density of 43×10^5 cells cm^{-2} ($n = 3$).

Within the first hour, slightly faster cell attachment was observed on TCPS, where 80-90% of the seeded cells were already attached compared to 60-70% on brush coatings. After four hours, ~95% of the cells were attached on all surfaces, and after 24 hours, no visible differences in the growing monolayers were observable on the culture substrates. HDF confluency of 100% was reached after 48 h on TCPS and, at the latest, after 72 h on **pEHPA-*b*-BP** and **pEHPMA-*b*-BP** brush coatings.

Since cell attachment to the culture substrates is closely linked to protein adsorption, we further screened the initial protein adsorption from DMEM cell culture medium supplemented with 10% FBS medium on the substrates *via* temperature-dependent QCM-D measurements.^{13, 14} Representative frequency curves at

37 °C are shown and the calculated areal masses are presented in Figure 6. Additional frequency curves at 20 °C are shown in Figure S10.

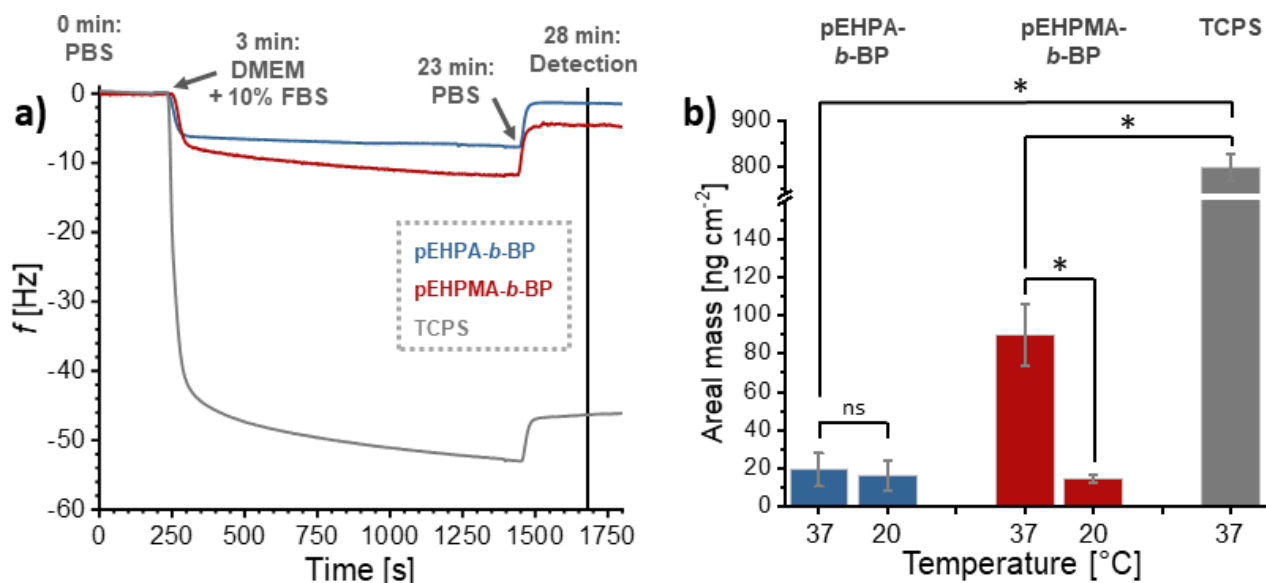


Figure 6. Quantitative protein adsorption from DMEM cell culture medium supplemented with 10% FBS on **pEHPA-*b*-BP** and **pEHPMA-*b*-BP** brush coatings and TCPS controls *via* QCM-D measurements. a) Representative frequency curves of the protein adsorption at 37 °C. b) Areal mass of adsorbed proteins was derived from the frequency changes Δf *via* the Sauerbrey equation at the measurement start and finish after protein exposure for 20 min and PBS flush for 5 min. Bars indicate mean values along with standard deviation ($n = 3$).

For QCM-D measurements, the polymer brushes were prepared on PS-coated QCM-D silicone substrates. Their dry layer thicknesses and contact angles (Figure S9) were comparable to the corresponding coatings on PS-coated silicon wafers. Surprisingly, for **pEHPA-*b*-BP**, no significant difference in adsorbed mass was observed between 37 and 20 °C, with values of 19 ± 9 and 16 ± 8 ng cm⁻², respectively. In contrast, **pEHPMA-*b*-BP** brush coatings showed a significant ($p < 0.1$) difference, with 90 ± 16 ng cm⁻² at 37 °C and 14 ± 2 ng cm⁻² at 20 °C. However, all these areal masses are an order of magnitude lower than those observed on TCPS (797 ± 29 and ~ 780 ng cm⁻²) at 37 and 20 °C^{11, 19}. Low protein adsorption below the polymers' T_{cp} is characteristic of thermoresponsive coatings that facilitate thermally induced cell detachment.^{11, 28} In

contrast, efficient cell adhesion under cell culture conditions typically requires higher amounts of adsorbed proteins. Thus, the low amounts of adsorbed proteins on the fully synthetic **pEHPA-*b*-BP** and **pEHPMA-*b*-BP** brushes at 37 °C appear contradictory to the observed cell adhesion and proliferation on these substrates (Figure 5), as cell adhesion is generally a protein-mediated process.

Aligning with this theory, thermoresponsive **PGE** coatings adsorb protein areal masses between 400-700 ng cm⁻² from FBS-containing cell culture media at 37 °C.^{11, 19} The distinct adsorption values vary with the **PGE** copolymer composition and substrate type. Fn, one of FBS's main cell adhesive proteins, has been the focus of several single-protein adsorption studies. These studies demonstrate reduced areal masses of adsorbed Fn compared to the adsorbed protein masses from multi-protein mixtures like FBS. For instance, thermoresponsive **pNIPAM** hydrogel coatings (~16 nm) adsorb only ~150 ng cm⁻² Fn at 37 °C, with no Fn adsorption detected at 20 °C.²⁸ Similarly, poly(*n*-propyl oxazoline) (**PnPrOX**) bottlebrushes (~270 nm) adsorb an areal mass of 90 ng cm⁻² Fn at 37 °C, enabling cell adhesion and proliferation on Fn pre-treated substrates.^{12, 51}

Besides the adsorbed amount, the activity of Fn in presenting functional RGD units is crucial for recognition by anchorage-dependent cells. Protein-resistant, non-responsive **pHEMA** brushes,⁵² which comprise a methacrylic backbone and β -hydroxy side chains similar to **pEHPA** and **pEHPMA**, adsorb only ~4-6 ng cm⁻² Fn on 3-20 nm thick coatings from FCS-containing cell culture medium.⁵³ Interestingly, the RGD activity decreased abruptly between coatings of 3 and 6 nm thickness, reducing the spreading and increasing the migration of cultured vascular smooth muscle cells. The high RGD activity on 3 nm thick brushes was explained through the limited penetration depth of adsorbed Fn on a thin brush, resulting in unmasked RGD domains.⁵³ A similarly active Fn layer adsorbed from FBS-containing medium at 37 °C could explain the observed cell adhesion on thin **pEHP(M)A-*b*-BP** coatings despite the comparably low areal mass of adsorbed proteins.

Additional thermally triggered cell detachment experiments were performed with confluent cell monolayers produced from an initial HDF seeding density of $104 \times 10^5 \text{ cm}^{-2}$. Representative phase contrast images after 24, 48, and 72 h, along with macroscopic photographs of detached sheets, are shown in Figure 7.

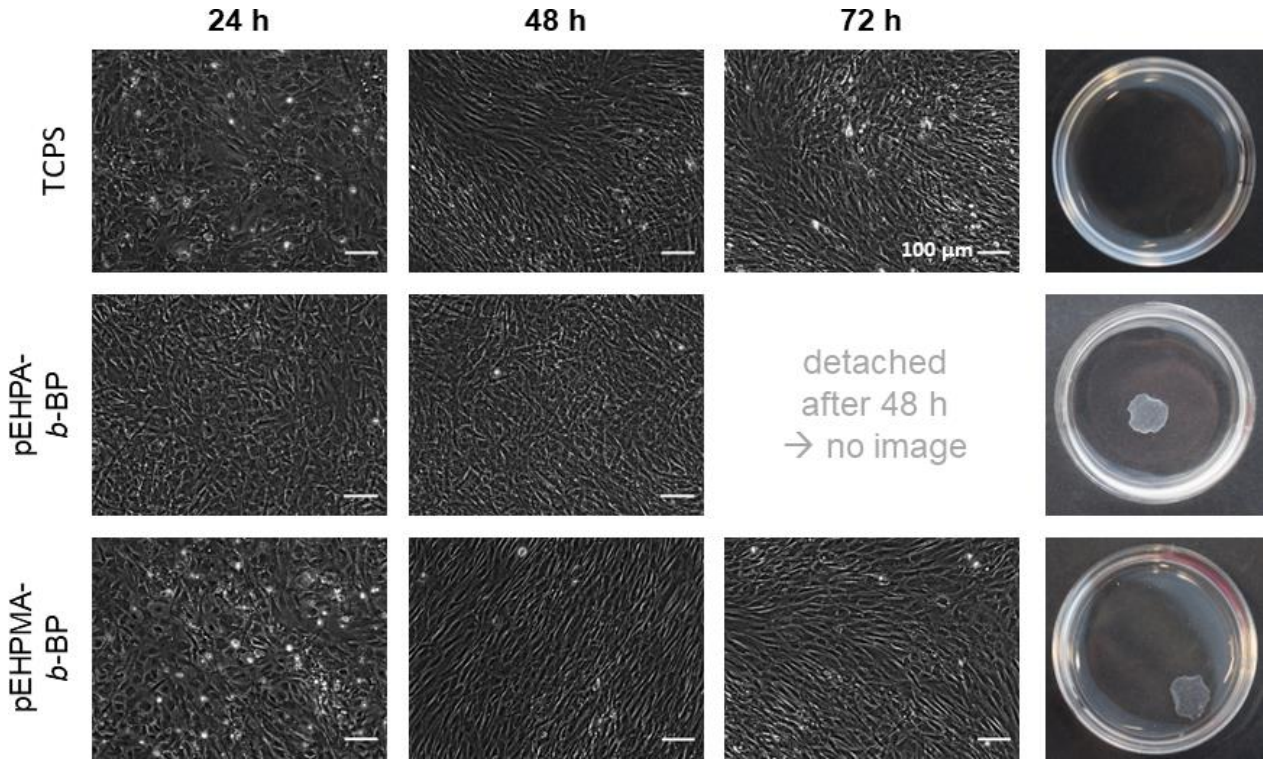


Figure 7. Representative phase contrast images of human dermal fibroblasts on **TCPS** (top), **pEHPA-*b*-BP** (middle), and **pEHPMA-*b*-BP** (bottom) coatings 24, 48, and 72 h after seeding at a density of $104 \times 10^5 \text{ cells cm}^{-2}$ and photographs of the resulting cell sheets after the thermally triggered detachment procedure (t_{max} (**pEHPA-*b*-BP**) = 60 min, t_{max} (**pEHPMA-*b*-BP**) = 120 min). Cells on TCPS controls did not detach under the same conditions (n = 4).

HDFs on TCPS and **pEHPA-*b*-BP** surfaces reached confluency after 48 h, and the detachment procedure reproducibly yielded fully detached cell sheets within one hour. In some cases, initiated detachment was already observed after the first exchange of warm medium to PBS at RT, with complete detachment after a 10-minute incubation at 37 °C. To ensure the viability of the thermally detached cells from **pEHPA-*b*-BP** coatings, cell sheets were trypsinized, stained with propidium iodide, and counted *via* flow cytometry

alongside controls cultured on TCPS and harvested by conventional trypsinization (Figure S11). No significant difference in the percentage of dead cells was observed within the standard deviation (**pEHPA-*b*-BP**: $1.7 \pm 0.2\%$, **TCPS**: $1.5 \pm 0.1\%$, $n = 3$), demonstrating the general cell compatibility of the newly developed **pEHPA-*b*-BP** coatings.

In contrast, thermally triggered cell detachment from **pEHPMA-*b*-BP** surfaces was less efficient. Confluency was achieved only after 72 h, and reliable initiation of the detachment process required incubation at 4 °C. Additionally, cells did not always detach as a complete sheet, sometimes resulting in sheets with holes or fragmentation. Comparatively, **pEHPA-*b*-BP** coatings performed more reliably without sheet disruption and were thus selected for subsequent sterilization studies with on-par performing **PGE** brush coatings.¹¹

Sterilization of brush-coated surfaces by FO gas and gamma radiation. Sterile ready-to-use culture ware is essential in routine cell culture and for biomedical products, ensuring product safety and performance reliability. Non-invasive gas and radiation procedures enable industrially normed sterilization of substrates directly in their final packaging, making them ideal for upscaling and translation efforts. However, the oxidative and radical fragmentation mechanisms that neutralize biological entities and pathogens can also adversely affect the functional materials by chemical fragmentation or crosslinking, as observed with **PEG**, **pNIPAM**, and **POX**.^{34, 37, 54}

To assess the stability of the functional thermoresponsive surfaces developed in our previous and current work, we evaluated their surface properties and performance in cell sheet fabrication after sterilization. Therefore, **PGE-*b*-OBP** brushes on PS, **PGE-*b*-ACBP** brushes on TCPS, and **pEHPA-*b*-BP** brushes on PS were prepared on silicon wafers and evaluated after sterilization by treatment with FO gas or gamma radiation normed to DIN standards. The sterilized model substrates were extracted for 16 h in ethanol to remove any degraded surface components and assess the coating stability. To consider the impact of storage time, the non-sterilized brush coatings' dry layer thickness and CA values were evaluated after storage at ambient conditions for 14-18 d, resembling the average time between sample preparation and analysis after

sterilization treatment. An overview of these substrate parameters before and after sterilization, including extraction, is shown in Figure 8. Corresponding results for the sole impact of storage time are shown in Figure S12.

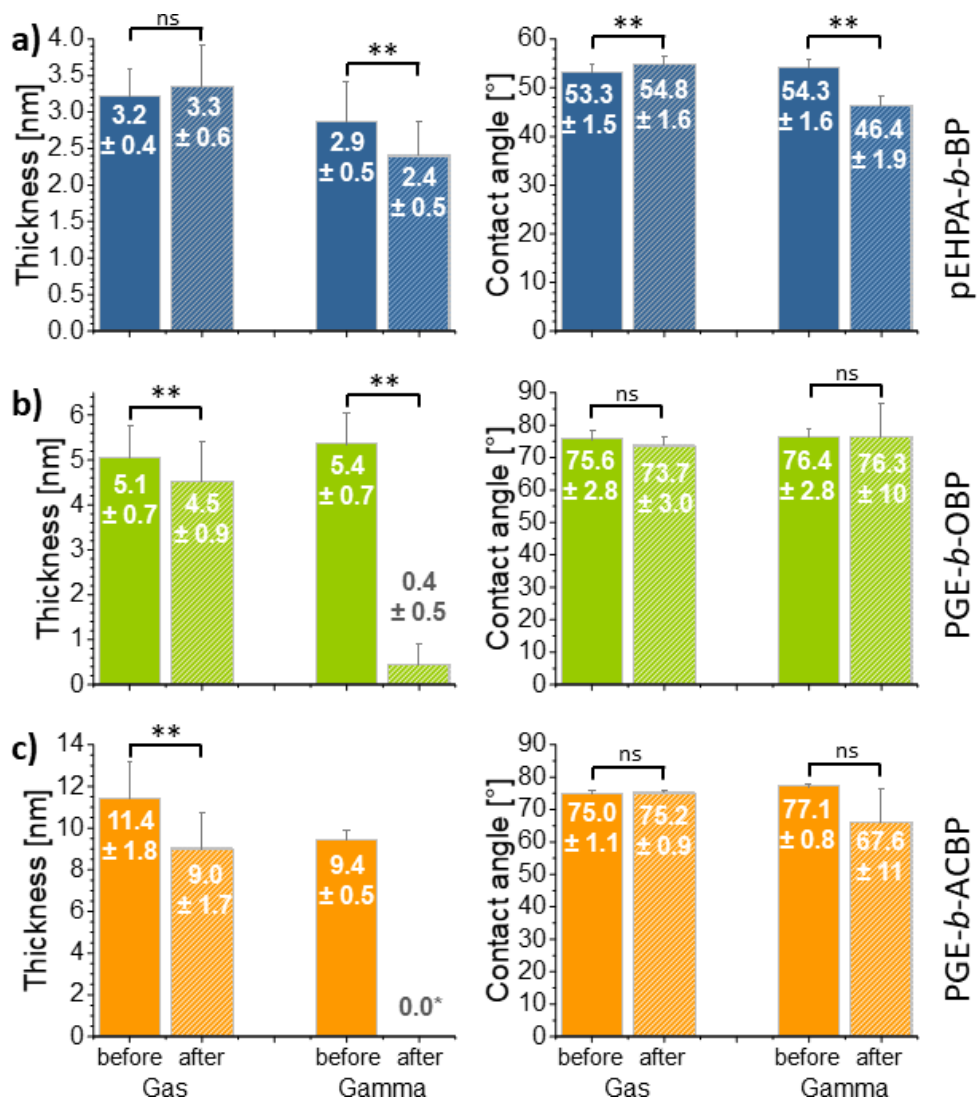


Figure 8. Dry layer thicknesses and water contact angles before and after sterilization by FO gas and gamma treatment with subsequent extraction of the **pEHPA-*b*-BP** (a), **PGE-*b*-OBP** (b), and **PGE-*b*-ACBP** (c) brush-coated substrates. Number values and bars indicate mean values with standard deviation ($n \geq 3$). *All

measured values were below the basal TCPS layer, resulting in negative thickness values indicative of oxidative degradation of not only the brush coating but also the basal substrate.

The **pEHPA-*b*-BP** brushes were preserved on the PS-coated silicon wafers after FO and gamma sterilization, as shown in Figure 8a. While thickness values did not change significantly after FO sterilization, a slight increase in contact angle ($p < 0.05$) from ~ 53 to $\sim 55^\circ$ indicates a possible surface reaction with the FO gas or coating reorientation during the procedure. The latter seems more likely, since no significant difference was found between CA values of FO-treated surfaces, CA values of untreated **pEHPA-*b*-BP** brushes in Figure 4b, and only 14-18 d stored **pEHPA-*b*-BP** samples (Figure S12). In contrast, gamma sterilization significantly decreased the dry layer thickness of the brush from 2.9 to 2.4 nm and the CA value from 54.3° to 46.4° , suggesting possible oxidation and/or partial degradation or crosslinking of the coatings. Gamma or e-beam radiation in the presence of ambient oxygen have been shown to oxidize hydroxyl groups, cleave ester bonds and induce crosslinking reactions, which in turn can increase surface hydrophilicity, limit chain movement and reduce the layer thickness.^{34, 39}

Similar effects but to a larger extent were observed for the **PGE** brush systems, drastically degrading the polyether coating by gamma sterilization. After radiative gamma treatment and surface extraction, the **PGE-*b*-OBP** brush thickness was reduced to ~ 0.4 nm. Furthermore, the CA values varied more drastically from $76.4 \pm 2.8^\circ$ before to $76.3 \pm 10^\circ$ after the treatment, with individual measurements ranging from 86° to 60° . In contrast, FO treatment resulted in a minor decline of the dry thickness from 5.1 to 4.5 nm, which might simply be attributed to an effect of storage time (Figure S12b), indicating no distinct impact of FO sterilization. Furthermore, non-significant CA changes from $\sim 75.5^\circ$ to 73.7° were observed.

The **PGE-*b*-ACBP** brush thickness declined from 9.5 to 5.3 nm under ambient storage conditions, which we attribute to a drying effect of the polymer layer during long-term dry storage. The FO gas sterilized surfaces showed a similar decline from 11.4 nm before to 9.0 nm after the treatment, with no significant alterations of the CA regardless of the gas treatment (Figure 8c) or ambient storage for 14-18 d (Figure S12c). As expected, also the **PGE-*b*-ACBP** coating on TCPS substrates was drastically degraded by gamma

sterilization, resulting in even negative thickness values indicative of additional degradation of the basal TCPS layer. Accordingly, the CA value declined from $77.1 \pm 0.8^\circ$ to $66.5 \pm 10^\circ$, suggesting a non-uniform surface state. Control experiments on uncoated PS substrates revealed that gamma sterilization also significantly impacts the pristine PS surface by lowering CA values from 89.5° to 74.7° (Figure S13). FO sterilization only had a minimal impact on PS surfaces, with a resulting contact angle of 87.7° , as shown in Figure S13.

To further evaluate the impact of the sterilization treatment on the functionality of the thermoresponsive coatings in cell culture, the brush-coated cell culture dishes were employed in cell sheet detachment experiments under previously established cell culture conditions. Based on the results shown in Figure 8, we excluded gamma sterilized **PGE** surfaces. Representative phase contrast images of HDFs cultured on the sterilized brush coatings with TCPS controls are in Figure 9 along with macroscopic photographs of the dishes after exposure to detachment conditions.

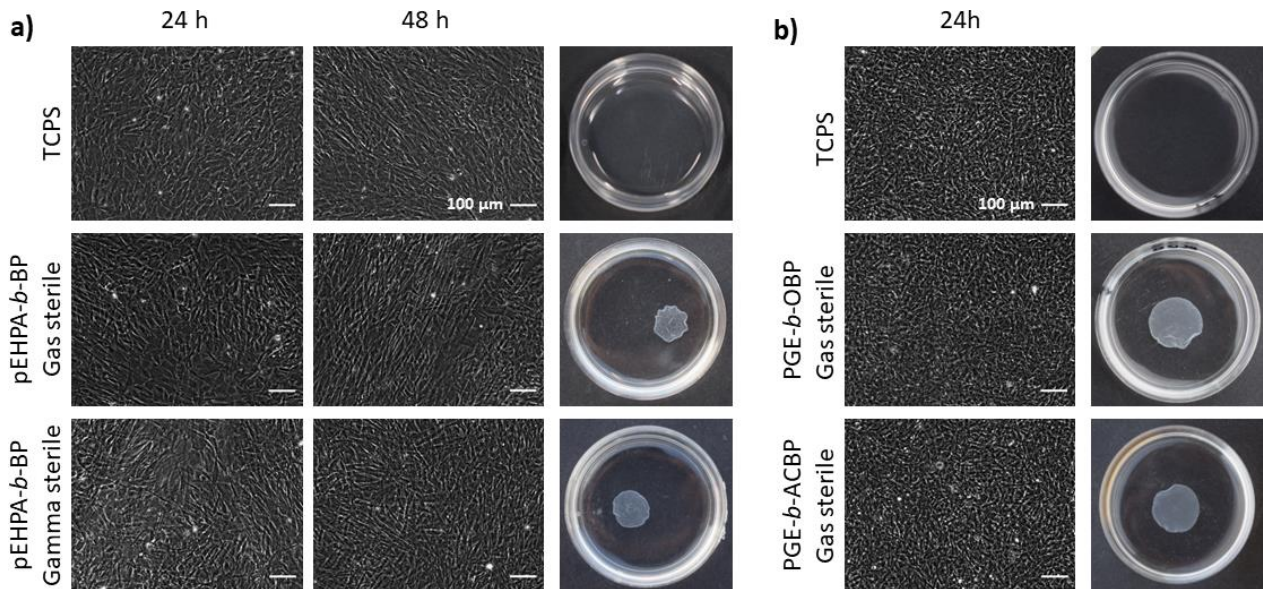


Figure 9. Representative time-dependent phase contrast images of HDFs cultures on sterilized substrates and photographs of resulting cell sheets after thermally triggered detachment from thermoresponsive coatings ($n \geq 3$). (a) TCPS controls (top, no detachment) and **pEHPA-*b*-BP** brush-coated PS substrates after

FO (middle, $t_{\max} = 90$ min) and gamma (bottom, $t_{\max} = 16$ h) sterilization with a seeding density of 104×10^5 cells cm^{-2} . (b) TCPS controls (top, no detachment) and FO-sterilized **PGE-*b*-OBP** (middle, $t_{\max} = 180$ min) and **PGE-*b*-ACBP** (bottom, $t_{\max} = 180$ min) brush-coated substrates with a seeding density of 160×10^5 cells cm^{-2} .

HDFs adhered and proliferated comparably on sterilized and aq. EtOH (70 v-%) disinfected coatings, confirming the cell attachment-supporting nature of all coatings. Moreover, also the thermally triggered detachment of HDF cell sheets after FO sterilization was successful on all tested **PGE** and **pEHPA-*b*-BP** coated substrates employing the established detachment conditions. Thus, we can conclude that the normed FO gas treatment for effective sterilization is compatible with the developed functional brush coatings ($n = 3$). However, sheet detachment on **PGE** coatings was slowed, with timeframes reaching up to 180 min, compared to ~ 60 min for freshly prepared and disinfected (70% aq. EtOH) coatings.¹¹ Detachment times on **pEHPA-*b*-BP** coatings ranged from 20 to 90 min, slightly exceeding the maximal timeframe of 60 min determined with disinfected brush surfaces. These results on the functional performance of the coatings align with the observed surface changes of **PGE** and **pEHPA-*b*-BP** coatings after storage and/or FO treatment. More pronounced loss in dry layer thickness through storage or FO treatment of **PGE** brushes, even if only caused by drying effects, correlates with impaired functionality in thermally triggered cell sheet detachment but not in cell adhesion and proliferation.

Gamma sterilization significantly impaired the functionality of the **pEHPA-*b*-BP** coatings as indicated by the markedly altered surface properties. While there was no noticeable impact on the cell adhesion and culture, the established detachment protocol, exchanging the warm medium with PBS at RT, did not induce cell detachment ($n = 3$). Therefore, we adopted the procedure established for **pEHPMA-*b*-BP** coatings, which helped to induce the detachment, but required up to ~ 16 h, thus exceeding a useful application timeframe due to possible cell apoptosis after 4 or more hours.⁵⁵ Additionally, in ~ 50 % of the experiments ($n = 7$) the cell sheets did not fully detach, indicating a true loss of functionality on gamma sterilized **pEHPA-*b*-BP** surfaces.

Overall, the obtained results demonstrate the benefit of the newly developed thermoresponsive coatings with an aliphatic backbone in terms of coating stability and functional performance in cell culture. While gas-sterilized **PGE** brushes exhibited prolonged cell sheet detachment times after 14-18 d of dry storage, detachment times of gas-sterilized **pEHPA-*b*-BP** surfaces remained almost unaffected, with minimal changes in surface properties. These findings align with reports on ethylene oxide gas-sterilized **PEG** hydrogels and surfaces, which retain the morphological properties or coating thickness but can exhibit slightly altered crosslinking density.^{37, 39} Ultimately, oxidation through ambient oxygen can limit the air storage stability of **PEG** in bulk to less than a month.^{38, 56} The stability of **pEHPA-*b*-BP** coatings appears comparable to **pNIPAM** coatings, which can also be gas sterilized without adverse effects on structure and properties.³³

Gamma irradiation significantly damaged all evaluated surface coatings. Similarly, previous reports indicate strong morphological changes and an increase in free radicals and crosslinking in radiation treated **PEG** hydrogels.^{37, 57} Free radicals can lead to chain scission and degradation, explaining the observed drastic loss in thickness. Gamma radiation of **pNIPAM** solutions with a comparable dosage (50 kGy) resulted in an increased LCST and hampered transition, along with increased molecular weight and polydispersity due to crosslinking reactions.³⁴ Furthermore, controlled oxidation of hydroxyl groups to carbonyl groups in **pHEMA** brush systems leads to a bio-adhesive system, which cannot be excluded for **pEHPA-*b*-BP** brushes.⁵⁸ Additionally, also the underlying PS substrate can get oxidized, as indicated in Figure S13, decreasing the overall thickness and rendering **pEHPA-*b*-BP** brush systems partially non-responsive, which causes the loss of functionality. Nevertheless, gas sterilization remains an attractive option for a scalable and effective sterilization process when aiming at transfer of such functional coatings from research to market.

CONCLUSIONS

Thermoresponsive brush coatings with adjustable dry layer thicknesses values up to ~3 nm, based on **pEHPA-*b*-BP** and **pEHPMA-*b*-BP** polymers, were successfully immobilized on PS surfaces for cell sheet

fabrication. Despite unusually low protein adsorption at 37 °C (~20-90 ng cm⁻²), both coatings demonstrated cell adhesive properties, likely due to a thin but active layer of fibronectin, as observed on structurally similar **pHEMA** coatings.⁵³ **pEHPA-*b*-BP** coatings, with a T_{cp} of 20.3 °C, reliably detached fibroblast sheets after cooling to RT. In contrast, **pEHPMA-*b*-BP** coatings, with a T_{cp} of 6 °C, required cooling to 4 °C, occasionally resulting in perforated or disrupted cell sheets. The stability of **pEHPA-*b*-BP** and previously established **PGE** coatings on PS and TCPS toward sterilization and short-term storage (up to 18 d) was further evaluated. Gamma sterilization with a dose of ~45 kGy was found to be too harsh, completely degrading **PGE** and adversely affecting **pEHPA-*b*-BP** coatings, as evidenced by decreasing thickness and CA values, along with significantly hampered cell sheet detachment. In contrast, gas sterilization had no significant impact on **pEHPA-*b*-BP** coatings, although detachment times slightly increased in some cases. The stability of **pEHPA-*b*-BP** coatings during storage and after gas sterilization highlights the advantage of an aliphatic backbone system since these coatings maintained their functionality better than **PGE** coatings. Future work will explore the compatibility of these coatings with different cell types. Experiments towards an understanding of the underlying mechanisms of minimal protein adsorption, which impressively mediate cell adhesion, are in progress.

Supporting information

Materials and methods, monomer and polymer synthesis and characterization, additional temperature dependent turbidimetry and DLS data of utilized polymers, temperature dependent ¹H NMR spectra of pEHPMA in D₂O, additional thickness and CA values of **pEHPA** and **pEHPMA** adsorption experiments, calculation of chain overlap parameters, additional cell culture images and live dead staining data, properties of prepared QCM-D chip surfaces, thickness and CA values for storage-only surfaces and CA evaluation of sterilized PS surfaces.

Acknowledgments

AS would like to thank L. Lehmann and F. Junge for the synthesis of the BPA and BPMA monomers, O. Staudhammer for the synthesis of the pEHPA and pEHPA-*b*-BP polymers, A. Hartmann for measuring

replicates, P. Tang for the processing of the gas sterilization samples and S. Wedepohl for performing the live dead staining experiments. The authors warmly thank the Federal Ministry of Education and Research (FKZ: 13N13523) (MW, AS) and the Core Facility BioSupraMol, supported by the German Research Foundation (DFG).

References.

- (1) Canavan, H. E.; Cheng, X.; Graham, D. J.; Ratner, B. D.; Castner, D. G. Cell sheet detachment affects the extracellular matrix: a surface science study comparing thermal liftoff, enzymatic, and mechanical methods. *J Biomed Mater Res A* **2005**, *75* (1), 1-13. DOI: 10.1002/jbm.a.30297.
- (2) Huang, H. L.; Hsing, H. W.; Lai, T. C.; Chen, Y. W.; Lee, T. R.; Chan, H. T.; Lyu, P. C.; Wu, C. L.; Lu, Y. C.; Lin, S. T.; et al. Trypsin-induced proteome alteration during cell subculture in mammalian cells. *J Biomed Sci* **2010**, *17* (1), 36. DOI: 10.1186/1423-0127-17-36.
- (3) Schweigerdt, A.; Stöbener, D. D.; Schäfer, A.; Kara, S.; Weinhart, M. Impact of Amphiphilicity Balance in Hydroxy-Functional, Isomeric, Thermoresponsive Poly(meth)acrylates. *Macromolecules* **2023**, *56* (21), 8602-8613. DOI: 10.1021/acs.macromol.3c01251.
- (4) Zhao, C. Z.; Ma, Z. Y.; Zhu, X. X. Rational design of thermoresponsive polymers in aqueous solutions: A thermodynamics map. *Prog Polym Sci* **2019**, *90*, 269-291. DOI: 10.1016/j.progpolymsci.2019.01.001.
- (5) Işık, D.; Quaas, E.; Klinger, D. Thermo- and oxidation-sensitive poly(meth)acrylates based on alkyl sulfoxides: dual-responsive homopolymers from one functional group. *Polym Chem-Uk* **2020**, *11* (48), 7662-7676. DOI: 10.1039/d0py01321h.
- (6) Becherer, T.; Heinen, S.; Wei, Q.; Haag, R.; Weinhart, M. In-depth analysis of switchable glycerol based polymeric coatings for cell sheet engineering. *Acta Biomater* **2015**, *25*, 43-55. DOI: 10.1016/j.actbio.2015.06.036.
- (7) Vancoillie, G.; Van Guyse, J. F. R.; Voorhaar, L.; Maji, S.; Frank, D.; Holder, E.; Hoogenboom, R. Understanding the effect of monomer structure of oligoethylene glycol acrylate copolymers on their thermoresponsive behavior for the development of polymeric sensors. *Polym Chem-Uk* **2019**, *10* (42), 5778-5789. DOI: 10.1039/c9py01326a.
- (8) Stobener, D. D.; Scholz, J.; Schedler, U.; Weinhart, M. Switchable Oligo(glycidyl ether) Acrylate Bottlebrushes "Grafted-from" Polystyrene Surfaces: A Versatile Strategy toward Functional Cell Culture Substrates. *Biomacromolecules* **2018**, *19* (11), 4207-4218. DOI: 10.1021/acs.biomac.8b00933.
- (9) Fukumori, K.; Akiyama, Y.; Kumashiro, Y.; Kobayashi, J.; Yamato, M.; Sakai, K.; Okano, T. Characterization of ultra-thin temperature-responsive polymer layer and its polymer thickness dependency on cell attachment/detachment properties. *Macromol Biosci* **2010**, *10* (10), 1117-1129. DOI: 10.1002/mabi.201000043 From NLM Medline.
- (10) Healy, D.; Nash, M. E.; Gorelov, A.; Thompson, K.; Dockery, P.; Beloshapkin, S.; Rochev, Y. Fabrication and Application of Photocrosslinked, Nanometer-Scale, Physically Adsorbed Films for Tissue Culture Regeneration. *Macromol Biosci* **2017**, *17* (2). DOI: 10.1002/mabi.201600175 From NLM Medline.
- (11) Stobener, D. D.; Weinhart, M. On the foundation of thermal "Switching": The culture substrate governs the phase transition mechanism of thermoresponsive brushes and their performance in cell sheet fabrication. *Acta Biomater* **2021**, *136*, 243-253. DOI: 10.1016/j.actbio.2021.09.012 From NLM Medline.
- (12) Zhang, N.; Pompe, T.; Amin, I.; Luxenhofer, R.; Werner, C.; Jordan, R. Tailored poly(2-oxazoline) polymer brushes to control protein adsorption and cell adhesion. *Macromol Biosci* **2012**, *12* (7), 926-936. DOI: 10.1002/mabi.201200026 From NLM Medline.
- (13) Cole, M. A.; Voelcker, N. H.; Thissen, H.; Griesser, H. J. Stimuli-responsive interfaces and systems for the control of protein-surface and cell-surface interactions. *Biomaterials* **2009**, *30* (9), 1827-1850. DOI: 10.1016/j.biomaterials.2008.12.026 From NLM Medline.
- (14) Wilson, C. J.; Clegg, R. E.; Leavesley, D. I.; Percy, M. J. Mediation of biomaterial-cell interactions by adsorbed proteins: a review. *Tissue Eng* **2005**, *11* (1-2), 1-18. DOI: 10.1089/ten.2005.11.1 From NLM Medline.
- (15) Horbett, T. A.; Schway, M. B. Correlations between mouse 3T3 cell spreading and serum fibronectin adsorption on glass and hydroxyethylmethacrylate-ethylmethacrylate copolymers. *J Biomed Mater Res* **1988**, *22* (9), 763-793. DOI: 10.1002/jbm.820220903 From NLM Medline.

- (16) Arima, Y.; Iwata, H. Preferential adsorption of cell adhesive proteins from complex media on self-assembled monolayers and its effect on subsequent cell adhesion. *Acta Biomater* **2015**, *26*, 72-81. DOI: 10.1016/j.actbio.2015.08.033 From NLM Medline.
- (17) Garcia, A. J.; Boettiger, D. Integrin-fibronectin interactions at the cell-material interface: initial integrin binding and signaling. *Biomaterials* **1999**, *20* (23-24), 2427-2433. DOI: 10.1016/s0142-9612(99)00170-2 From NLM Medline.
- (18) Garcia, A. J.; Huber, F.; Boettiger, D. Force required to break alpha5beta1 integrin-fibronectin bonds in intact adherent cells is sensitive to integrin activation state. *J Biol Chem* **1998**, *273* (18), 10988-10993. DOI: 10.1074/jbc.273.18.10988 From NLM Medline.
- (19) Stobener, D. D.; Weinhart, M. "Fuzzy hair" promotes cell sheet detachment from thermoresponsive brushes already above their volume phase transition temperature. *Biomater Adv* **2022**, *141*, 213101. DOI: 10.1016/j.bioadv.2022.213101 From NLM Publisher.
- (20) Dworak, A.; Utrata-Wesolek, A.; Szweda, D.; Kowalczyk, A.; Trzebicka, B.; Aniol, J.; Sieron, A. L.; Klama-Baryla, A.; Kawecki, M. Poly[tri(ethylene glycol) ethyl ether methacrylate]-coated surfaces for controlled fibroblasts culturing. *ACS Appl Mater Interfaces* **2013**, *5* (6), 2197-2207. DOI: 10.1021/am3031882.
- (21) Nash, M. E.; Carroll, W. M.; Foley, P. J.; Maguire, G.; Connell, C. O.; Gorelov, A. V.; Beloshapkin, S.; Rochev, Y. A. Ultra-thin spin coated crosslinkable hydrogels for use in cell sheet recovery—synthesis, characterisation to application. *Soft Matter* **2012**, *8* (14). DOI: 10.1039/c2sm06466a.
- (22) Laloyaux, X.; Mathy, B.; Nysten, B.; Jonas, A. M. Surface and bulk collapse transitions of thermoresponsive polymer brushes. *Langmuir* **2010**, *26* (2), 838-847. DOI: 10.1021/la902285t.
- (23) Adam, S.; Koenig, M.; Rodenhausen, K. B.; Eichhorn, K.-J.; Oertel, U.; Schubert, M.; Stamm, M.; Uhlmann, P. Quartz crystal microbalance with coupled spectroscopic ellipsometry-study of temperature-responsive polymer brush systems. *Appl Surf Sci* **2017**, *421*, 843-851. DOI: 10.1016/j.apsusc.2017.02.078.
- (24) Otulakowski, L.; Kaspro, M.; Strzelecka, A.; Dworak, A.; Trzebicka, B. Thermal Behaviour of Common Thermoresponsive Polymers in Phosphate Buffer and in Its Salt Solutions. *Polymers (Basel)* **2020**, *13* (1). DOI: 10.3390/polym13010090 From NLM PubMed-not-MEDLINE.
- (25) Zhang, Y.; Furyk, S.; Bergbreiter, D. E.; Cremer, P. S. Specific ion effects on the water solubility of macromolecules: PNIPAM and the Hofmeister series. *J Am Chem Soc* **2005**, *127* (41), 14505-14510. DOI: 10.1021/ja0546424 From NLM Medline.
- (26) Anderson, C. R.; Gambinossi, F.; DiLillo, K. M.; Laschewsky, A.; Wischerhoff, E.; Ferri, J. K.; Sefcik, L. S. Tuning reversible cell adhesion to methacrylate-based thermoresponsive polymers: Effects of composition on substrate hydrophobicity and cellular responses. *J Biomed Mater Res A* **2017**, *105* (9), 2416-2428. DOI: 10.1002/jbm.a.36100.
- (27) Sefcik, L. S.; Kaminski, A.; Ling, K.; Laschewsky, A.; Lutz, J.-F.; Wischerhoff, E. Effects of PEG-Based Thermoresponsive Polymer Brushes on Fibroblast Spreading and Gene Expression. *Cel Mol Bioeng* **2013**, *6* (3), 287-298. DOI: 10.1007/s12195-013-0286-7.
- (28) Akiyama, Y.; Kikuchi, A.; Yamato, M.; Okano, T. Ultrathin poly(N-isopropylacrylamide) grafted layer on polystyrene surfaces for cell adhesion/detachment control. *Langmuir* **2004**, *20* (13), 5506-5511. DOI: 10.1021/la036139f From NLM Medline.
- (29) Arisaka, Y.; Kobayashi, J.; Ohashi, K.; Tatsumi, K.; Kim, K.; Akiyama, Y.; Yamato, M.; Okano, T. A heparin-modified thermoresponsive surface with heparin-binding epidermal growth factor-like growth factor for maintaining hepatic functions in vitro and harvesting hepatocyte sheets. *Regen Ther* **2016**, *3*, 97-106. DOI: 10.1016/j.reth.2016.03.003 From NLM PubMed-not-MEDLINE.
- (30) Ebara, M.; Yamato, M.; Aoyagi, T.; Kikuchi, A.; Sakai, K.; Okano, T. Immobilization of cell-adhesive peptides to temperature-responsive surfaces facilitates both serum-free cell adhesion and noninvasive cell harvest. *Tissue Eng* **2004**, *10* (7-8), 1125-1135. DOI: 10.1089/ten.2004.10.1125 From NLM Medline.
- (31) Desseaux, S.; Klok, H. A. Temperature-controlled masking/unmasking of cell-adhesive cues with poly(ethylene glycol) methacrylate based brushes. *Biomacromolecules* **2014**, *15* (10), 3859-3865. DOI: 10.1021/bm501233h.
- (32) Chen, G.; Hoffman, A. S. Graft copolymers that exhibit temperature-induced phase transitions over a wide range of pH. *Nature* **1995**, *373* (6509), 49-52. DOI: 10.1038/373049a0 From NLM Medline.
- (33) Kikuchi, A.; Okuhara, M.; Karikusa, F.; Sakurai, Y.; Okano, T. Two-dimensional manipulation of confluent cultured vascular endothelial cells using temperature-responsive poly(N-isopropylacrylamide)-grafted surfaces. *J Biomater Sci Polym Ed* **1998**, *9* (12), 1331-1348. DOI: 10.1163/156856298x00424 From NLM Medline.
- (34) Sedlacek, O.; Kucka, J.; Monnery, B. D.; Slouf, M.; Vetric, M.; Hoogenboom, R.; Hruby, M. The effect of ionizing radiation on biocompatible polymers: From sterilization to radiolysis and hydrogel formation. *Polym Degrad Stab* **2017**, *137*, 1-10. DOI: 10.1016/j.polymdgradstab.2017.01.005.

- (35) Stobener, D. D.; Hoppensack, A.; Scholz, J.; Weinhart, M. Endothelial, smooth muscle and fibroblast cell sheet fabrication from self-assembled thermoresponsive poly(glycidyl ether) brushes. *Soft Matter* **2018**, *14* (41), 8333-8343. DOI: 10.1039/c8sm01099d.
- (36) Aoki, S.; Koide, A.; Imabayashi, S.-i.; Watanabe, M. Novel Thermosensitive Polyethers Prepared by Anionic Ring-Opening Polymerization of Glycidyl Ether Derivatives. *Chem Lett* **2002**, *31* (11), 1128-1129. DOI: 10.1246/cl.2002.1128.
- (37) Kanjickal, D.; Lopina, S.; Evancho-Chapman, M. M.; Schmidt, S.; Donovan, D. Effects of sterilization on poly(ethylene glycol) hydrogels. *J Biomed Mater Res A* **2008**, *87* (3), 608-617. DOI: 10.1002/jbm.a.31811.
- (38) Han, S.; Kim, C.; Kwon, D. Thermal/oxidative degradation and stabilization of polyethylene glycol. *Polymer* **1997**, *38* (2), 317-323. DOI: 10.1016/s0032-3861(97)88175-x.
- (39) Iqbal, Z.; Moses, W.; Kim, S.; Kim, E. J.; Fissell, W. H.; Roy, S. Sterilization effects on ultrathin film polymer coatings for silicon-based implantable medical devices. *J Biomed Mater Res B Appl Biomater* **2018**, *106* (6), 2327-2336. DOI: 10.1002/jbm.b.34039.
- (40) Stobener, D. D.; Weinhart, M. Thermoresponsive Poly(glycidyl ether) Brush Coatings on Various Tissue Culture Substrates-How Block Copolymer Design and Substrate Material Govern Self-Assembly and Phase Transition. *Polymers (Basel)* **2020**, *12* (9). DOI: 10.3390/polym12091899.
- (41) Brandrup, J.; Immergut, E. H.; Grulke, E. A.; Abe, A.; Bloch, D. R. *Polymer handbook*; Wiley New York, 1999.
- (42) Xu, X.; Goponenko, A. V.; Asher, S. A. Polymerized PolyHEMA photonic crystals: pH and ethanol sensor materials. *J Am Chem Soc* **2008**, *130* (10), 3113-3119. DOI: 10.1021/ja077979+ From NLM Medline.
- (43) Dorman, G.; Nakamura, H.; Pulsipher, A.; Prestwich, G. D. The Life of Pi Star: Exploring the Exciting and Forbidden Worlds of the Benzophenone Photophore. *Chem Rev* **2016**, *116* (24), 15284-15398. DOI: 10.1021/acs.chemrev.6b00342.
- (44) Han, S.; Hagiwara, M.; Ishizone, T. Synthesis of Thermally Sensitive Water-Soluble Polymethacrylates by Living Anionic Polymerizations of Oligo(ethylene glycol) Methyl Ether Methacrylates. *Macromolecules* **2003**, *36* (22), 8312-8319. DOI: 10.1021/ma0347971.
- (45) Deshmukh, M. V.; Vaidya, A. A.; Kulkarni, M. G.; Rajamohanam, P. R.; Ganapathy, S. LCST in poly(N-isopropylacrylamide) copolymers: high resolution proton NMR investigations. *Polymer* **2000**, *41* (22), 7951-7960. DOI: 10.1016/s0032-3861(00)00174-9.
- (46) Zeng, F.; Tong, Z.; Feng, H. N.m.r. investigation of phase separation in poly(N-isopropyl acrylamide)/water solutions. *Polymer* **1997**, *38* (22), 5539-5544. DOI: 10.1016/s0032-3861(97)00118-3.
- (47) Konefal, R.; Cernoch, P.; Konefal, M.; Spevacek, J. Temperature Behavior of Aqueous Solutions of Poly(2-oxazoline) Homopolymer and Block Copolymers Investigated by NMR Spectroscopy and Dynamic Light Scattering. *Polymers (Basel)* **2020**, *12* (9). DOI: 10.3390/polym12091879 From NLM PubMed-not-MEDLINE.
- (48) Maeda, T.; Takenouchi, M.; Yamamoto, K.; Aoyagi, T. Analysis of the formation mechanism for thermoresponsive-type coacervate with functional copolymers consisting of N-isopropylacrylamide and 2-hydroxyisopropylacrylamide. *Biomacromolecules* **2006**, *7* (7), 2230-2236. DOI: 10.1021/bm060261m From NLM Medline.
- (49) Stöbener, D. D.; Uckert, M.; Cuellar-Camacho, J. L.; Hoppensack, A.; Weinhart, M. Ultrathin Poly(glycidyl ether) Coatings on Polystyrene for Temperature-Triggered Human Dermal Fibroblast Sheet Fabrication. *ACS Biomaterials Science & Engineering* **2017**, *3* (9), 2155-2165. DOI: 10.1021/acsbiomaterials.7b00270.
- (50) Nash, M. E.; Healy, D.; Carroll, W. M.; Elvira, C.; Rochev, Y. A. Cell and cell sheet recovery from pNIPAm coatings; motivation and history to present day approaches. *J Mater Chem* **2012**, *22* (37). DOI: 10.1039/c2jm31748f.
- (51) Hoogenboom, R.; Thijs, H. M.; Jochems, M. J.; van Lankvelt, B. M.; Fijten, M. W.; Schubert, U. S. Tuning the LCST of poly(2-oxazoline)s by varying composition and molecular weight: alternatives to poly(N-isopropylacrylamide)? *Chem Commun (Camb)* **2008**, (44), 5758-5760. DOI: 10.1039/b813140f From NLM Medline.
- (52) Yoshikawa, C.; Goto, A.; Tsujii, Y.; Fukuda, T.; Kimura, T.; Yamamoto, K.; Kishida, A. Protein Repellency of Well-Defined, Concentrated Poly(2-hydroxyethyl methacrylate) Brushes by the Size-Exclusion Effect. *Macromolecules* **2006**, *39* (6), 2284-2290. DOI: 10.1021/ma0520242.
- (53) Deng, J.; Ren, T.; Zhu, J.; Mao, Z.; Gao, C. Adsorption of plasma proteins and fibronectin on poly(hydroxyethyl methacrylate) brushes of different thickness and their relationship with adhesion and migration of vascular smooth muscle cells. *Regen Biomater* **2014**, *1* (1), 17-25. DOI: 10.1093/rb/rbu008 From NLM PubMed-not-MEDLINE.
- (54) Ghosh, D.; Peterson, B. W.; de Waal, C.; de Vries, J.; Kaper, H.; Zu, G.; Witjes, M.; van Rijn, P. Effects of sterilization on nanogel-based universal coatings: An essential step for clinical translation. *Mater Des* **2024**, *238*. DOI: 10.1016/j.matdes.2024.112689.

- (55) Kulkarni, G. V.; McCulloch, C. A. Serum deprivation induces apoptotic cell death in a subset of Balb/c 3T3 fibroblasts. *J Cell Sci* **1994**, *107* (Pt 5), 1169-1179. DOI: 10.1242/jcs.107.5.1169 From NLM Medline.
- (56) Bortel, E.; Hodorowicz, S.; Lamot, R. Relation between crystallinity degree and stability in solid state of high molecular weight poly(ethylene oxide)s. *Makromol Chem* **2003**, *180* (10), 2491-2498. DOI: 10.1002/macp.1979.021801023.
- (57) Galante, R.; Pinto, T. J. A.; Colaco, R.; Serro, A. P. Sterilization of hydrogels for biomedical applications: A review. *J Biomed Mater Res B Appl Biomater* **2018**, *106* (6), 2472-2492. DOI: 10.1002/jbm.b.34048 From NLM Medline.
- (58) Wang, J.; Karami, P.; Ataman, N. C.; Pioletti, D. P.; Steele, T. W. J.; Klok, H. A. Light-Activated, Bioadhesive, Poly(2-hydroxyethyl methacrylate) Brush Coatings. *Biomacromolecules* **2020**, *21* (1), 240-249. DOI: 10.1021/acs.biomac.9b01196.

Supporting Information for the following manuscript

Thermoresponsive brush coatings for cell sheet engineering with low protein adsorption below and above the polymers' phase transition temperature

Alexander Schweigerdt¹, Daniel D. Stöbener^{1,2}, Johanna Scholz¹, Andreas Schäfer¹, Marie Weinhart^{1,2}*

¹ Institute of Chemistry and Biochemistry, Freie Universitaet Berlin, Takustr. 3, 14195 Berlin, Germany

² Institute of Physical Chemistry and Electrochemistry, Leibniz Universitaet Hannover, Callinstr. 3A, 30167 Hannover, Germany

* Corresponding author: email marie.weinhart@pci.uni-hannover.de and marie.weinhart@fu-berlin.de, phone: +49 511-762 14938

Content

1. Materials and Methods	4
1.1. Materials	4
1.1.1. Materials for cell culture	5
1.2. Methods	5
1.2.1. Preparation of model substrates	6
1.2.2. Cell Isolation and Culture	7
2. Monomer synthesis.....	7
2.1. Synthesis of EHPMA.....	8
2.2. Synthesis of BPA.....	9
2.3. Synthesis of BPMA	9
3. Polymer synthesis	10
3.1. Synthesis of pEHPMA	11
3.2. Synthesis of pEHPMA-<i>b</i>-BP.....	13
3.3. Synthesis of pEHPA-<i>b</i>-BP	14
3.4. Calculation of the benzophenone repeating units from the ¹H NMR spectra	15
4. Sample preparation and analysis of the thermoresponsive behavior.....	16
4.1. Turbidimetry	16
4.2. DLS measurements and intensity distribution of polymer samples	18
4.3. Temperature-dependent pEHPMA ¹H NMR measurements	19
5. Comparison of homo- and block copolymer adsorption on PS	21

5.1. Estimation of the chain overlap parameters based on polymer theory	22
6. Additional cell adhesion images	23
7. Surface parameters of brush-coated QCM-D chips.....	24
8. Viability of thermally detached cells	26
9. Storage stability of coated substrates	26
10. Impact of gamma and FO treatment on CAs of pristine PS substrates.....	27
11. References	28

1. Materials and Methods

1.1. Materials

All materials and chemicals were used as received unless stated otherwise. Acryloyl chloride, methacryloyl chloride and deuterated chloroform (CDCl_3) were purchased from ABCR (Karlsruhe, Germany). Glycidol, boron trifluoride etherate ($\text{BF}_3 \cdot \text{OEt}_2$, 46% solution in diethyl ether), azobis(4-cyanovaleric acid) (ACVA), dimethyl formamide (DMF) and 4-cyano-4-(phenylcarbonothioylthio)pentanoic acid (radical addition fragmentation transfer (RAFT) agent) were purchased from Sigma Aldrich (Steinheim, Germany). Triethylamine (NEt_3) was purchased from Sigma Aldrich or TCI GmbH (Eschborn, Germany). Glycidyl methacrylate and 4-hydroxybenzophenone were purchased from TCI GmbH. 4-Dimethylaminopyridine (DMAP) was purchased from Carbolution chemicals (St. Ingbert, Germany). Dichloromethane (DCM), diethyl ether, methanol, acetonitrile, Al_2O_3 , and NaHCO_3 were purchased from Fisher Chemical (Loughborough, UK). Ethanol and ethyl acetate (EA) were purchased from Merck (Darmstadt, Germany). Cyclohexane (CH), Na_2SO_4 , deuterated methanol- d_4 (MeOD), and deuterated water (D_2O) were purchased from Carl Roth (Karlsruhe, Germany). 1,4-Dioxane and MgSO_4 were purchased from Grüssing (Filsburg, Germany).

Deionized water with a minimum resistivity of $18.0 \text{ M}\Omega \text{ cm}$ was used (MilliporeTM). Dulbecco's phosphate-buffered saline (PBS) was purchased from Thermofisher (Henningsdorf, Germany). Pre-wetted regenerated cellulose dialysis tubes (molecular weight cut-off: 3.5 kDa, Spectra/Por[®] 6) from Spectrumlabs were used for dialysis. Silicon wafers were supplied by Silchem GmbH (Freiberg, Germany). QCM-D QSXT 303 chips with silicon surface were purchased from Biolin Scientific (Gothenburg, Sweden).

1.1.1. Materials for cell culture

Falcon® PS culture dishes (35 mm diameter) were purchased from Th. Geyer GmbH & Co. KG (Berlin, Germany) and Corning® tissue culture PS (TCPS, 35 mm diameter) were supplied by VWR International (Leuven, Belgium). Dulbecco's modified Eagle medium (DMEM) was purchased from Thermo Fisher Scientific (Darmstadt, Germany). Propidium iodide (PI) was supplied by Sigma Aldrich (Steinheim, Germany). Fetal bovine serum (FBS, #S0115) was purchased from Biochrom GmbH (Berlin, Germany). All other expendable materials for cell culture were purchased from Sarstedt (Nümbrecht, Germany).

1.2. Methods

Column chromatography was performed on a Teledyne Isco CombiFlash Rf+ (USA) using RediSep NP80 columns and HPLC-grade cyclohexane and ethyl acetate. Polymer dialysis was performed against methanol (1.8 L) for 48-72 hours, and the solvent was exchanged at least three times. Gel permeation chromatography (GPC) in tetrahydrofuran (THF) as eluent was conducted on an Agilent 1100 Series instrument with concentrations of 3.5 mg mL⁻¹ and a flow rate of 1 mL min⁻¹ at 25 °C. Three PLgel 5 µm mix-C columns with the dimensions 7.5 × 300 mm from Agilent (Waldbronn, Germany) were used in line with a refractive index detector and polystyrene (PS) standards from PSS (Mainz, Germany) were used for calibration. Intensity-dependent size distributions were measured on a Malvern Zetasizer Ultra analyzer (Malvern Instruments) using a He-Ne laser ($\lambda = 633$ nm) and scattering detection at 173°. Aqueous polymer solutions were equilibrated for 120 s at the corresponding temperature before each measurement. Nuclear magnetic resonance (NMR) spectra were processed with the MestreNova 10.0.2 software, referenced to the solvent peak of the deuterated solvent unless stated otherwise, and the chemical

shifts δ were reported in ppm. Spin-coating was performed using a WS-650-23 spin-coater from Laurell Technologies Corporation (North Wales, PA, USA). Photoimmobilization of brush coatings was performed with ultraviolet (UV)-light using a UV-KUB 2 from KLOÉ (Montpellier, France) with a wavelength of 365 nm and a radiant exposure of 4.0 J cm⁻². Spectroscopic ellipsometry (SE) was performed on a SENpro ellipsometer and evaluated with SpectraRay 3 (Version 5.3.2.1853) software from SENTECH instruments GmbH (Berlin, Germany). Static water contact angles (CA) were measured with an OCA contact angle system from DataPhysics Instruments GmbH (Filderstadt, Germany) and fitted with the software package SCA202 (version 3.12.11). QCM-D measurements were performed on Q-Sense E1 system from LOT QuantumDesign (Wertheim, Germany) with a standard flow module and a Reglo Digital peristaltic pump from Ismatec (Wertheim, Germany). QSoft401 software (version 2.5.22) was used for data acquisition and QTools 3 software (version 3.1.25) from Biolin Scientific AB 2000-2014 (Stockholm, Sweden) was used for data analysis. Microscopic images were taken on a Zeiss Observer Z1 from Carl Zeiss Microscopy GmbH (Jena, Germany) and evaluated with the software Zen 2 Version 2.0.0.0 from Carl Zeiss Microscopy GmbH (Jena, Germany). Macroscopic photographs were taken with a Nikon D3100 from Nikon GmbH (Düsseldorf, Germany). Flow cytometry was performed on Attune NxT cytometer from Thermo Fisher.

1.2.1. Preparation of model substrates

PS model substrates were prepared by spin coating silicon wafers (11 × 11 mm) or QCM-D chips using a 1-2% (w/w) solution of PS (35 μL) in toluene at 3000 rpm for 60 s, resulting in PS thickness values of 30-80 nm. PS solutions were prepared using PS ($M_n = 132$ kDa, $\mathcal{D} = 1.9$) from Falcon® culture dishes supplied by Th. Geyer GmbH & Co. KG (Berlin, Germany). Tissue culture polystyrene (TCPS) substrates were fabricated by irradiation of PS coated silicon wafers in a

Beltron UV chamber (Hg lamp, 850 W) from Beltron GmbH (Rödermark/Urberach, Germany) at a distance of 24 cm ($\sim 10 \text{ mW cm}^{-2}$) for 150 s. The oxidized samples were extracted in ethanol for 1 d, subsequently washed with Milli-Q water and directly used for coating experiments within 1–2 d.

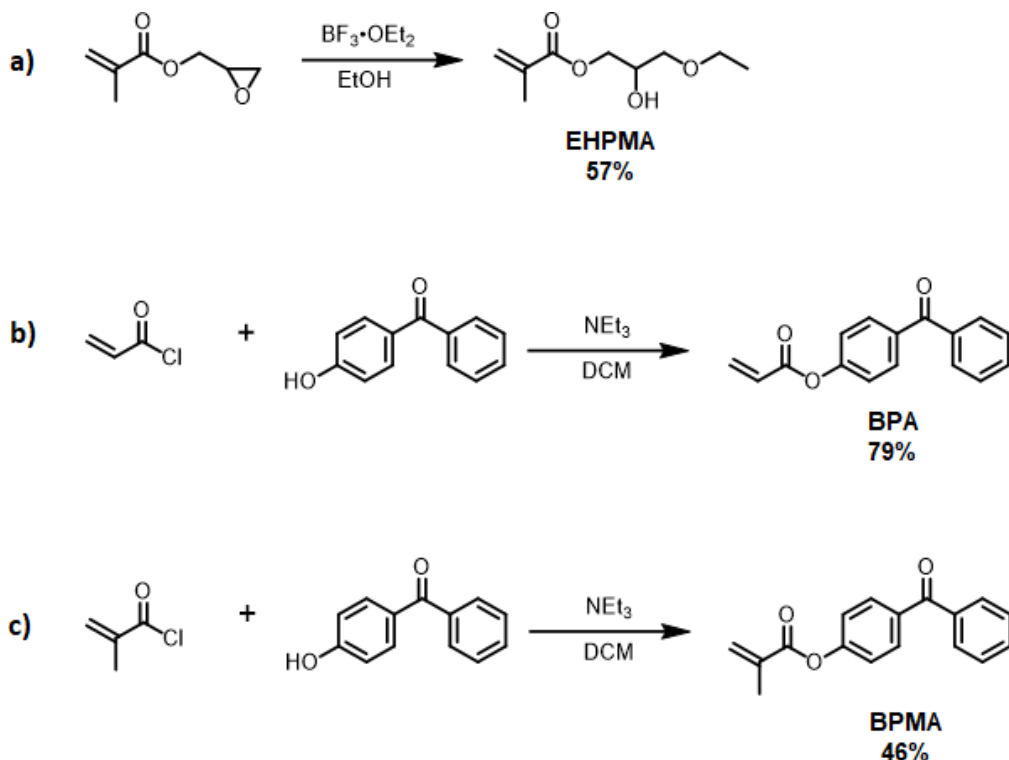
1.2.2. Cell Isolation and Culture

Cell isolation and culture was performed analogously to previously established protocols.¹ Human dermal fibroblasts (HDF) were isolated from human foreskin biopsies after ethical approval and informed parental consent. Connective tissue was mechanically removed, and remaining skin tissue was dissected into approximately $1 \times 10 \text{ mm}$ stripes. They were incubated in dispase II (2 U mL^{-1} in PBS) for 16 h at $4 \text{ }^\circ\text{C}$. Epidermis and dermis were mechanically separated, followed by mincing of the dermis. Minced tissue was digested with collagenase NB4 (0.5 U mL^{-1} in PBS with Ca^{2+} and Mg^{2+}) for 45 min at $37 \text{ }^\circ\text{C}$. After centrifugation ($200 \times g$, 5 min), the pellet was washed with culture medium consisting of DMEM supplemented with 10% FBS, 100 U mL^{-1} penicillin, and $100 \text{ } \mu\text{g mL}^{-1}$ streptomycin. The tissue fragments were resuspended in 2 mL of medium and seeded into a 75 cm^2 tissue culture flask. Additional 6 mL medium was added to the outgrowing cells after 24 h. Cells were cultured in a humidified atmosphere at $37 \text{ }^\circ\text{C}$ and 5% CO_2 and used in passages 3 to 8.

2. Monomer synthesis

The synthesis of 2-hydroxy-3-ethoxypropylacrylate (**EHPA**) was performed according to previous report.² The synthesis of further monomers 2-hydroxy-3-ethoxypropylmethacrylate (**EHPMA**), benzophenone acrylate (**BPA**), and benzophenone methacrylate (**BPMA**) was performed based on

literature procedures.^{2, 3} The reaction pathways for **EHPMA**, **BPA**, and **BPMA** are shown in Scheme S1.



Scheme S1. General synthesis route for the **EHPMA** (a), **BPA** (b), and **BPMA** (c) monomers with isolated yields after purification.

2.1. Synthesis of EHPMA

$\text{BF}_3 \cdot \text{OEt}_2$ (0.18 mL, 1.41 mmol, 0.1 eq) was dissolved in ethanol (18.5 mL, 317 mmol, 22 eq) and the mixture was heated to 50 °C. Glycidyl methacrylate (1.95 ml, 14.3 mmol, 1 eq) was added dropwise over 10 min. The mixture was stirred until no starting material could be detected via thin-layer chromatography (1.5 h). The reaction mixture was cooled down to 0 °C and 20 mL of THF was added. The reaction mixture was filtered over an Al_2O_3 plug, washed with 1/1 v:v THF/EtOH mixture (4×20 mL), and concentrated under reduced pressure. Purification via flash chromatography (CH:EA 7/3 v:v) yielded EHPMA (57%) as a colorless liquid.

$^1\text{H-NMR}$ (500 MHz, CDCl_3 δ): 6.14 (m, 1H, *trans-H*); 5.59 (m, 1H, *cis-H*); 4.22 (m, 2H, $-\text{COOCH}_2$); 4.05 (m, 1H, $-\text{CHOH}$); 3.60-3.41 (m, 4H, $-\text{CH}_2\text{OCH}_2\text{CH}_3$); 2.57 (d, 1H, $-\text{CHOH}$); 1.95 (m, 3H, CH_2CCH_3); 1.21 (t, 3H, $-\text{CH}_2\text{CH}_3$) ppm.

2.2. Synthesis of BPA

4-Hydroxybenzophenone (5.0 g, 25.2 mmol, 1 eq) and NEt_3 (4.19 mL, 30.2 mmol, 1.2 eq) were dissolved in DCM (25 mL) and cooled down to 0 °C in a tinfoil protected flask. Acryloyl chloride (2.73 mL, 30.2 mmol, 1.2 eq) was dissolved in DCM (5 mL) and added dropwise to the reaction mixture over 30 min. The mixture was stirred for 16 h at rt. The precipitating solid was filtered off and washed with DCM (3 \times 20 mL). The crude reaction mixture was washed with 0.1 M HCL (50 mL), saturated Na_2CO_3 (50 mL), and saturated brine (50 mL). The combined organic layers were dried over Na_2SO_4 . The solvent was removed under reduced pressure, and the raw product was purified by column chromatography (DCM:EA 4/1 v:v) and dried in high vacuum. BPA (79%) was obtained as a white solid.

$^1\text{H-NMR}$ (500 MHz, CDCl_3 δ): 7.88 (m, 2H, *Ar-H*); 7.81 (m, 2H, *Ar-H*); 7.60 (m, 1H, *Ar-H*); 7.49 (m, 2H, *Ar-H*); 7.27 (m, 2H, *Ar-H*); 6.65 (dd, 1H, *cis-H*); 6.35 (dd, 1H, CH_2CHCOO); 6.07 (d, 1H, *trans-H*) ppm.

2.3. Synthesis of BPMA

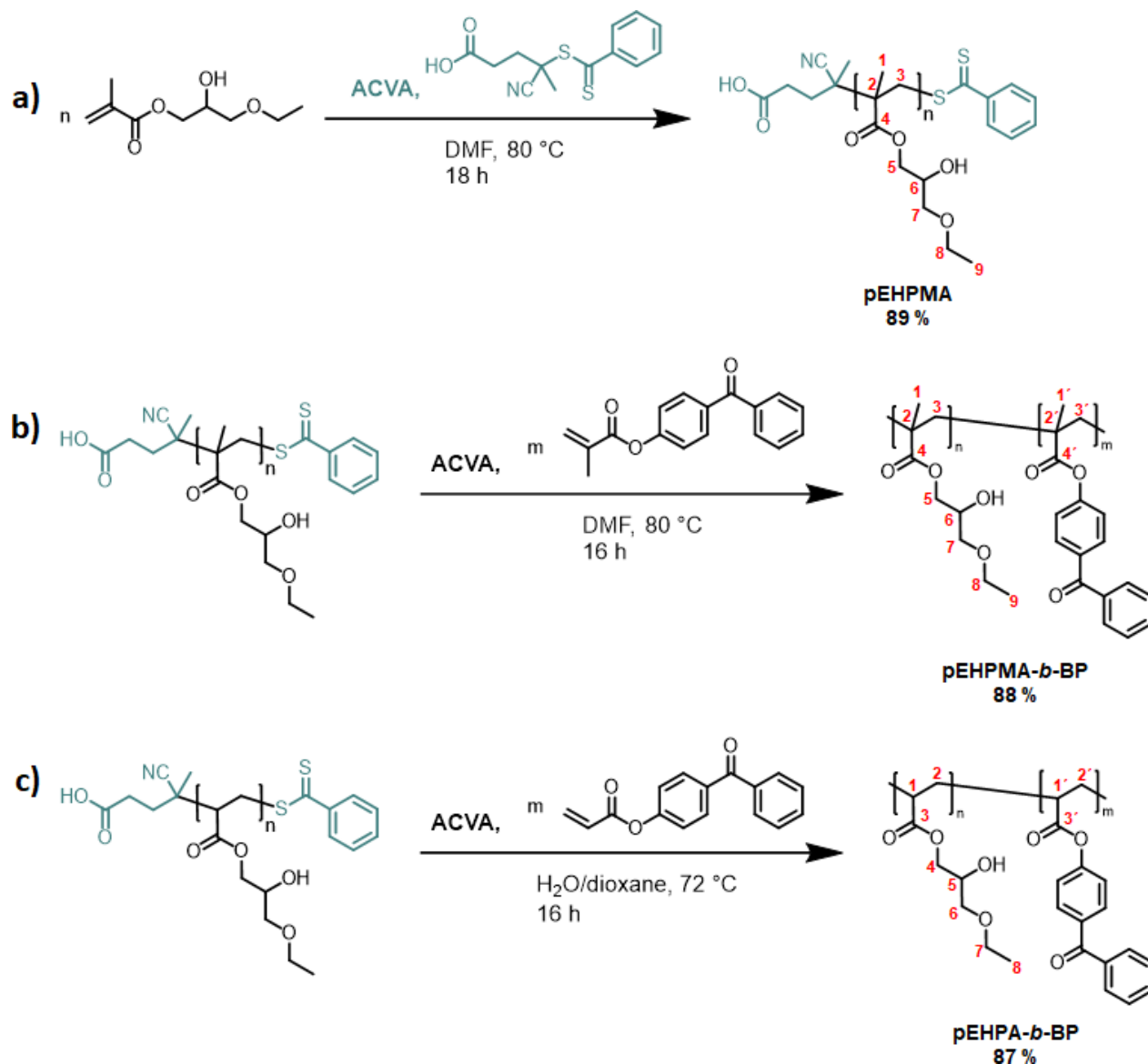
4-Hydroxybenzophenone (5.64 g, 28.5 mmol, 1.1 eq) and NEt_3 (3.9 mL, 27 mmol, 1 eq) was dissolved in DCM (25 mL) and cooled down to 0 °C in a tinfoil protected flask. Methacryloyl chloride (4.2 mL, 43 mmol, 1.6 eq) was dissolved in DCM (5 mL) and added dropwise to the reaction mixture over 20 min. The mixture was stirred for 20 h at rt. The crude reaction mixture was washed with saturated NaHCO_3 (150 mL), water (2 \times 100 mL), and saturated brine (100 mL). The combined organic layers were dried over Na_2SO_4 . The solvent was removed under reduced

pressure and the raw product was purified by double recrystallization from pentane/hexane (6/4 v:v). BPMA (46%) was obtained as a white solid.

$^1\text{H-NMR}$ (400 MHz, CDCl_3 δ): 7.90-7.85 (m, 2H, Ar-*H*); 7.82-7.78 (m, 2H, Ar-*H*); 7.60 (m_c, 1H, Ar-*H*); 7.49 (m_c, 2H, Ar-*H*); 7.26 (m_c, 2H, Ar-*H*); 6.39 (m_c, 1H, cis-*H*); 5.81 (m_c, 1H, trans-*H*); 2.09 (m_c, 3H, CH_2CCH_3) ppm.

3. Polymer synthesis

The synthesis of **PGE-*b*-OBP**, **PGE-*b*-ACBP** and **pEHPA** was reported in previous works.^{2,4} The general synthesis route of **pEHPMA**, **pEHPMA-*b*-BP** and **pEHPA-*b*-BP** is presented in Scheme S2. Peak assignments were based on previous work.



Scheme S2. Polymerization routes for **pEHPMA** (a), **pEHPMA-*b*-BP** (b), and **pEHPA-*b*-BP** (c) polymers.

3.1. Synthesis of pEHPMA

EHPMA (3.22 g, 17.1 mmol, 160 eq), radical initiator ACVA (4.3 mg, 0.015 mmol, 0.14 eq) and the RAFT agent (29.7 mg, 0.11 mmol, 1.0 eq) were dissolved in DMF (6.9 mL) at 0 °C. The solution was degassed for 20 min with argon and the reaction mixture was stirred overnight in a preheated oil bath at 80 °C. The polymerization was stopped by air exposure at 0 °C. The polymer

was precipitated from diethyl ether and dried overnight under high vacuum. pEHPMA (89 %) was obtained as a pink solid, which was used directly for the preparation of pEHPMA-*b*-BP. A small fraction was further dialyzed against methanol for the polymer analysis (NMR, GPC, turbidimetry).

¹H-NMR (600 MHz, MeOD, δ): 7.91, 7.59, 7.43 (RAFT Ar end-group); 4.23-3.78 (m, 3H, 4-*H*₂, 5-*H*); 3.76-3.41 (m, 4H, 7-*H*₂, 8-*H*₂); 2.46 (ACVA group); 2.36-1.44 (m, 2H, 3-*H*₂); 1.43-0.73 (m, 6H, 1-*H*₃, 9-*H*₃) ppm.

¹³C-NMR (151 MHz; MeOD δ): 179.70- 178.10, 178.29 (4-*C*), 73.1-72.50 (7-*C*) 69.40-68.98 (5-*C*), 67.93 (8-*C*), 67.61 (6-*C*), 55.99-54.84 (3-*C*), 46.40, 46.05 (2-*C*), 19.77, 17.74 (1-*C*), 15.64 (9-*C*) ppm.

Molecular weights determined by NMR: $M_n = 23.2$ kDa. GPC(THF): $M_n = 21700$ Da, $D = 1.16$.

The best results for block copolymers can be obtained, as long as the majority of the transfer agents at the end of the chains is still active. Therefore, the block copolymerization of **pEHPA** with **BPA** was proceeded directly after the polymerization in one-pot sequential manner, as described below. However, since **pEHPMA** is a solid polymer (contrary to the viscous **pEHPA**) and therefore can be prepurified via precipitation, this step was performed, before adding the benzophenone methacrylate block.

For the determination of equivalents for the block copolymerization of **pEHPMA-*b*-BP** the yield percentage of **pEHPMA** was used to determine the reacted monomer amount in the polymer for the equivalent calculation: $160 \times 0.89 = 142$ eq. The theoretical amount of substance was calculated by dividing the used polymer mass (1.80 g) through the molecular weight of the used **EHPMA** monomer (188.2 g/mol)

3.2. Synthesis of pEHPMA-*b*-BP

pEHPMA (1.80 g, 9.6 mmol, 142 eq), and BPMA (126.0 mg, 0.47 mmol, 7 eq) were dissolved in DMF (3.84 ml) and cooled down to 0 °C. ACVA (3.0 mg, 0.011 mmol, 0.16 eq) was added and the mixture was degassed for 25 min with argon and then stirred in a preheated oil bath overnight at 80 °C. The polymerization was stopped by air exposure at 0 °C. The raw polymer was dialyzed against methanol and dried under high vacuum. pEHPMA-*b*-BP (88%) was obtained as a pink solid.

¹H-NMR (700 MHz, MeOD, δ): 8.18-6.75 (Ar-*H*, BP); 4.28-3.80 (m, 3H, 4-*H*₂, 5-*H*); 3.78-3.38 (m, 4H, 7-*H*₂, 8-*H*₂); 2.46 (ACVA group); 2.26-1.45 (m, 2H, 3-*H*₂, 3'-*H*₂); 1.42-0.69 (m, 6H, 1-*H*₃, 9-*H*₃, 1'-*H*₃) ppm.

¹³C-NMR (176 MHz; MeOD δ): 179.76- 177.49 (4-*C*, 4'-*C*), 138.55, 136.43, 133.90, 132.71, 130.96, 129.63, 122.71 (Ar-*C*, BP) 73.1-72.50 (7-*C*) 69.50-68.90 (5-*C*), 67.92 (8-*C*), 67.61 (6-*C*), 56.19-52.75 (3-*C*, 3'-*C*), 47.00 46.41, 46.06 (2-*C*, 2'-*C*), 22.09, 19.72, 17.83 (1-*C*, 1'-*C*), 15.64 (9-*C*) ppm.

Molecular weights determined by NMR: $M_n = 22.6$ kDa. GPC (THF): $M_n = 22100$ Da, $\bar{D} = 1.18$.

Since **pEHPA** polymers are obtained in a form of a viscous wax, rather than a solid, a purification via precipitation was not feasible. Therefore, the synthesis of **pEHPA-*b*-BP** was performed as a sequenced one-pot polymerization after verifying an appropriate conversion (95 %). Amounts of the radical starter and BPA were calculated based on the remaining mixture volume and initial monomer concentration in the reaction mixture.

3.3. Synthesis of pEHPA-*b*-BP

EHPA (3.00 g, 17.22 mmol, 172 eq), radical initiator ACVA (5.6 mg, 0.2 mmol, 0.2 eq) and the RAFT agent (27.8 mg, 0.10 mmol, 1.0 eq) were dissolved in 1,4-dioxane/water mixture (10.1 mL, 1/1 v:v) at 0 °C. The mixture was degassed for 30 min with argon and then stirred in a preheated oil bath overnight at 72 °C. The reaction was paused through cooling the reaction down to 0 °C under argon atmosphere. Reaction sample (2.7 mL, equivalent to ~800 mg polymer) for NMR and GPC analysis was withdrawn. BPA (0.11 g, 0.44 mmol, 5.9 eq) and ACVA (4.1 mg, 0.015 mmol, 0.2 eq) were dissolved in 1,4-dioxane/water mixture (0.46 ml, 1/1 v:v) and added to the polymer mixture. The mixture was degassed for 30 min with argon at 0 °C and then stirred in a preheated oil bath overnight at 72 °C. The polymerization was stopped by air exposure at 0 °C. The raw polymers were dialyzed against methanol and dried under high vacuum. pEHPA (69%) and pEHPA-*b*-BP (88%) were obtained as a red wax.

pEHPA:

¹H-NMR (500 MHz, MeOD, δ): 8.01, 7.63, 7.46 (RAFT end-group); 4.31-4.01 (m, 2H, 4-*H*₂); 4.01-3.90 (br. s, 1H, 5-*H*); 3.56 (q, 2H, 7-*H*₂); 3.52-3.40 (m, 2H, 6-*H*₂); 2.69 (ACVA group); 2.62-2.22 (m, 1H, 1-*H*); 2.22-1.42 (m, 2H, 2-*H*₂); 1.21 (t, 3H, 8-*H*₃) ppm.

Molecular weights determined by NMR: $M_n = 24.6$ kDa. GPC (THF): $M_n = 22600$ Da, $D = 1.15$.

pEHPA-*b*-BP:

¹H-NMR (700 MHz, MeOD, δ): 8.07-7.13 (Ar-*H*, BP); 4.28-4.01 (m, 2H, 4-*H*₂); 4.01-3.90 (br. s, 1H, 5-*H*); 3.56 (q, 2H, 7-*H*₂); 3.52-3.42 (m, 2H, 6-*H*₂); 2.69 (ACVA group); 2.64-2.27 (m, 1H, 1-*H*, 1'-*H*); 2.25-1.41 (m, 2H, 2-*H*₂, 2'-*H*₂); 1.21 (t, 3H, 8-*H*₃) ppm.

^{13}C -NMR (176 MHz; MeOD δ): 176.48- 175.92 (3-C, 3'-C), 138.72, 136.50, 133.85, 132.73, 130.97, 129.60, 128.03, 123.15 (Ar-C, RAFT end-group, BP), 72.80 (6-C), 69.51, 69.46 (5-C), 67.90 (7-C), 67.34 (4-C), 43.15-42.61 (1-C, 1'-C), 37.31-35.18 (2-C, 2'-C), 15.60 (8-C) ppm.

Molecular weights determined by NMR: $M_n = 26.9$ kDa. GPC (THF): $M_n = 24100$ Da, $D = 1.25$.

3.4. Calculation of the benzophenone repeating units from the ^1H NMR spectra

The calculation of the benzophenone (meth)acrylate repeating units in the respective **pEHPA-*b*-BP** and **pEHPMA-*b*-BP** polymers was performed as follows: in the corresponding ^1H NMR spectra the methylene group located directly to the carboxyl group in the ACVA-based structure unit at 2.69 (**pEHPA**) and 2.46 (**pEHPMA**) was integrated and set to two. The integral value of the aromatic region on polymers without BP block (representing the aromatic RAFT moiety) was then subtracted from the value of the benzophenone integral value. The difference was then divided through the number of aromatic protons in the monomer (9) to yield the corresponding average BP units. The consistent presence of the BP block in the monomer was verified through UV-detected elugrams of polymers without and with BP block, as shown in Figure S1. While the RI signal stayed in the same detection range, the UV signal increased ~10-fold over the whole polymer detection range.

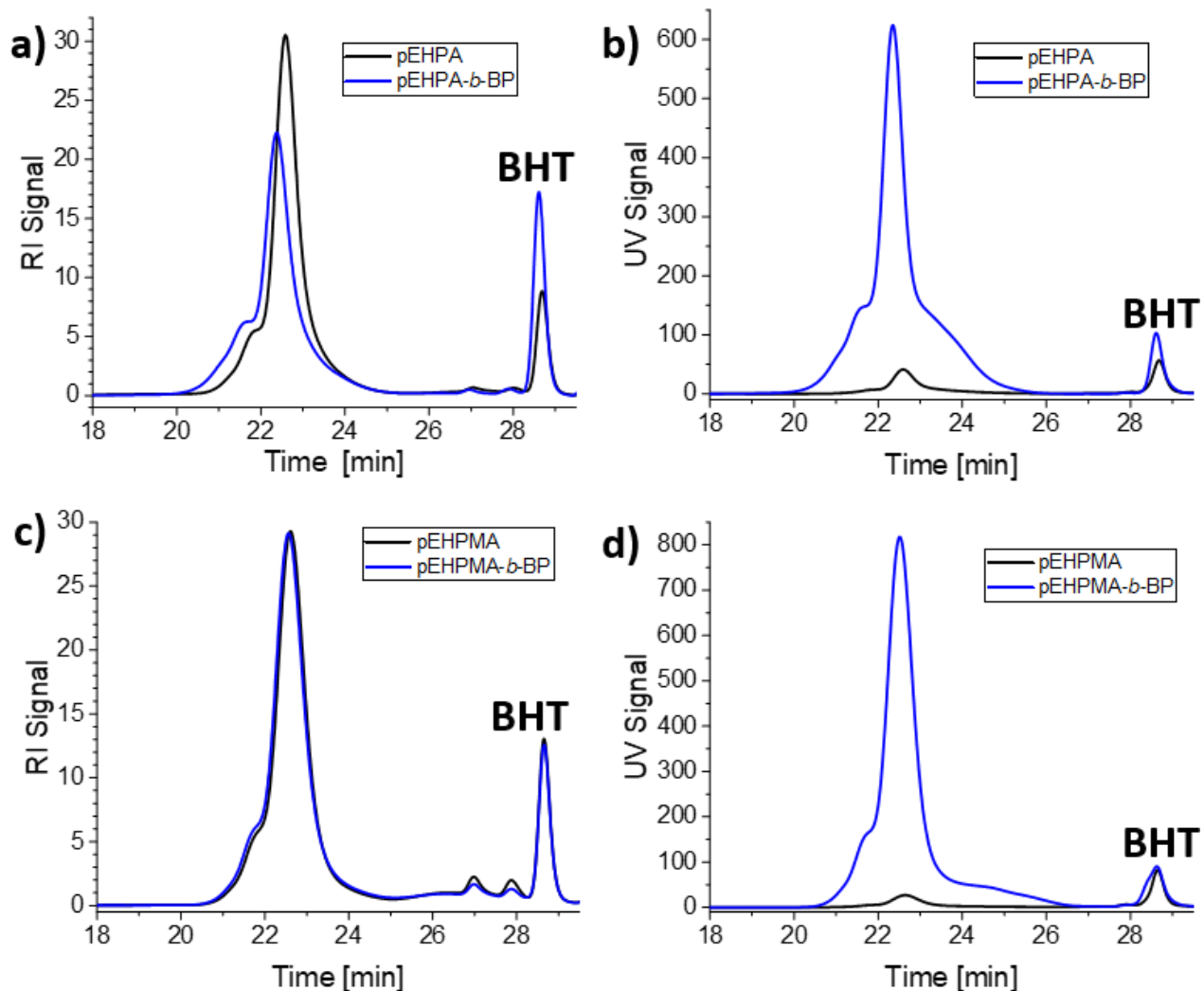


Figure S1. Overview of GPC traces of **pEHPA** and **pEHPA-*b*-BP** detected via RI (a) and UV (b) and **pEHPMA** and **pEHPMA-*b*-BP** detected via RI (c) and UV (d). The measurements were performed at room temperature with THF as eluent and butylated hydroxytoluene (**BHT**) as reference.

4. Sample preparation and analysis of the thermoresponsive behavior

4.1. Turbidimetry

The polymer samples were dissolved in water and lyophilized to remove traces of methanol. A 20 mg mL⁻¹ stock solution in the respective solvent (water or PBS) was prepared and 2 mL dilutions with 10 and 5 mg mL⁻¹ were prepared for analysis. Temperature-dependent turbidity curves were

measured as described in the experimental section of the main article by detecting the transmittance at 600 nm. The normalized turbidimetry curves of the **pEHPMA** homopolymer in water and PBS are presented in Figure S2. Analogous turbidimetry curves of **pEHPA-*b*-BP** and **pEHPMA-*b*-BP** block copolymers in water are presented in Figure S3.

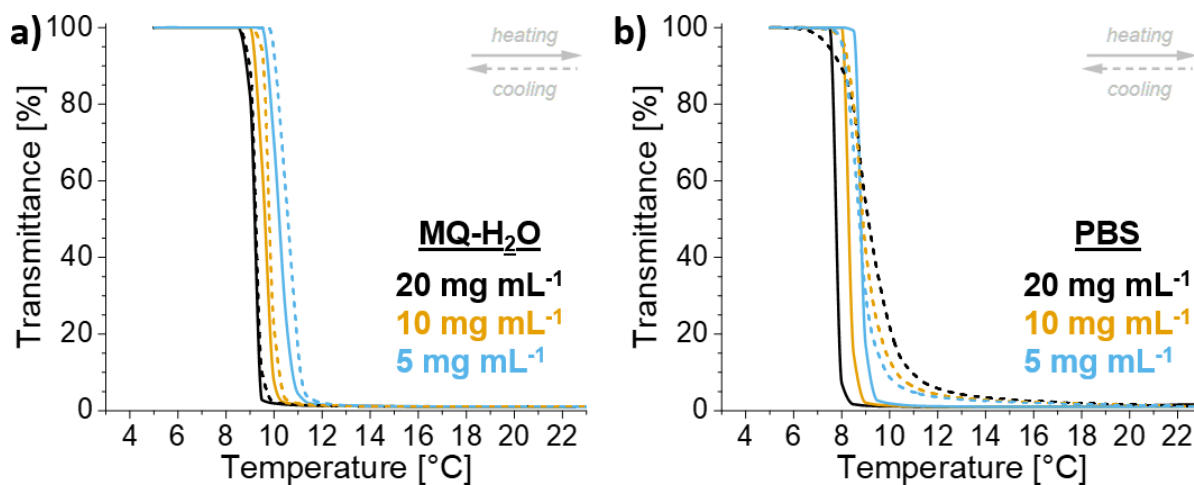


Figure S2. Representative concentration-dependent turbidimetry curves of **pEHPMA** in MQ-H₂O (a) and PBS (b) after normalization in heating and cooling cycles ($n = 2$ per cycle).

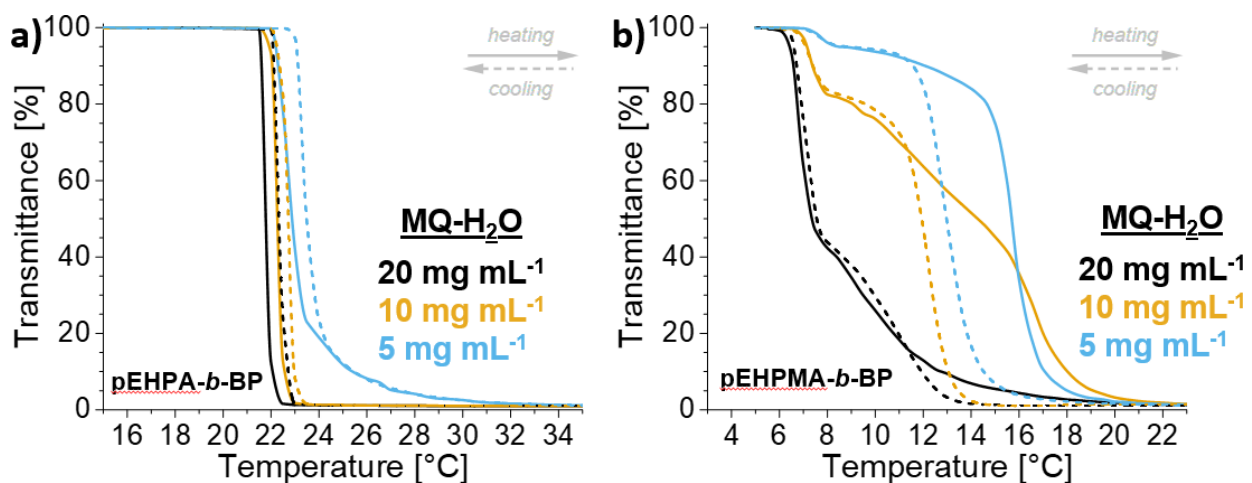


Figure S3. Representative concentration-dependent turbidimetry curves of **pEHPA-*b*-BP** (a) and **pEHPMA-*b*-BP** (b) in MQ-H₂O after normalization in heating and cooling cycles ($n = 2$ per cycle).

4.2. DLS measurements and intensity distribution of polymer samples

The prepared samples for turbidimetry measurements were additionally investigated by DLS. The obtained size distribution curves by intensity in aqueous solutions are shown in Figure S4 for **pEHPMA** and in Figure S5 for **pEHPA-*b*-BP** and **pEHPMA-*b*-BP**.

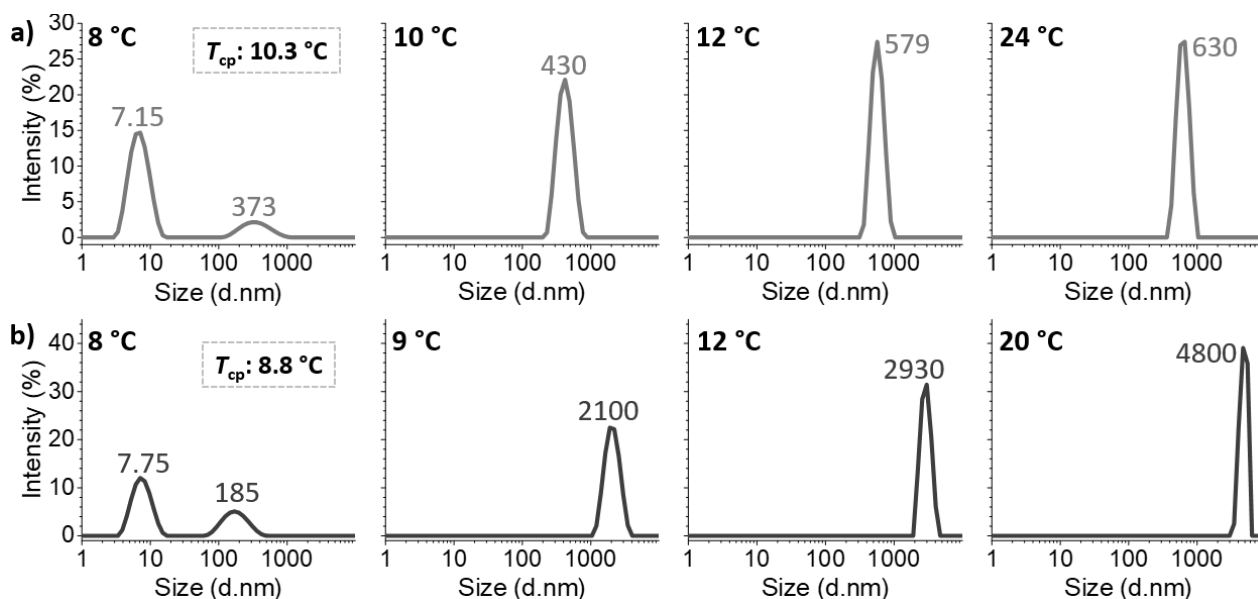


Figure S4. Temperature-dependent size distributions obtained from DLS measurements of **pEHPMA** in MilliQ-H₂O (a) and PBS (b).

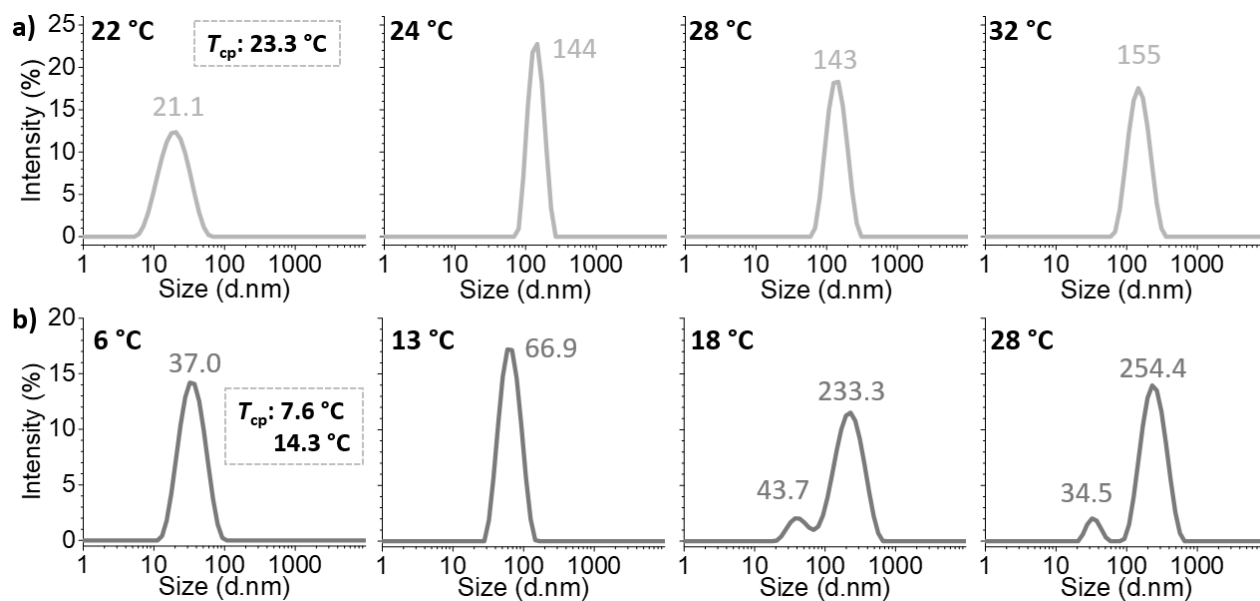


Figure S5. Temperature-dependent size distributions obtained from DLS measurements of **pEHPA-*b*-BP** (a) and **pEHPMA-*b*-BP** (b) in MilliQ-H₂O.

4.3. Temperature-dependent pEHPMA ¹H NMR measurements

The NMR spectra were acquired as described in the experimental section of the main manuscript.

The ¹H spectra of **pEHPMA** in D₂O in the temperature range of 8-25 °C are shown in Figure S6.

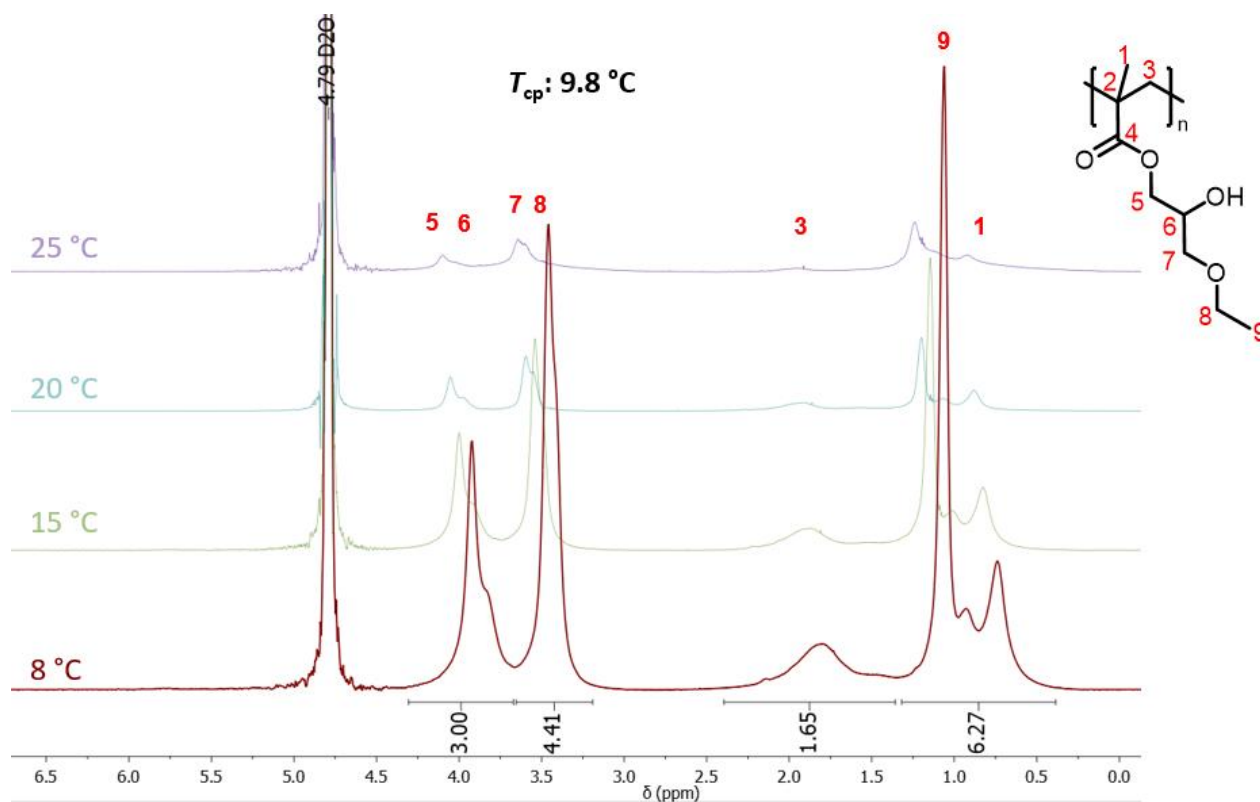


Figure S6. Temperature-dependent ^1H NMR spectra (D_2O , 600 MHz) of **pEHPMA** at a concentration of 10 mg mL^{-1} (T_{cp} : $9.8 \text{ }^\circ\text{C}$). The spectra were referenced to the solvent peak of D_2O at $8 \text{ }^\circ\text{C}$ at 4.79 ppm. Peaks were assigned with numbers according to the illustrated chemical structure.

The ^1H NMR spectra of **pEHPMA** solution in Figure S6 show a slight temperature-dependent shift of the chemical shifts of the polymer signals. More importantly, a uniform transition can be observed through the gradual broadening of the proton signals from the methacrylic backbone as well as the γ -ethoxy- β -hydroxy-side chain. This hints towards a dehydration and aggregation of the polymer chains, which causes a significant mobility loss, resulting in the increased signal broadening along with declining signal intensity.^{5,6}

5. Comparison of homo- and block copolymer adsorption on PS

To estimate the directed adsorption potential of **pEHPA-*b*-BP** and **pEHPMA-*b*-BP**, comparative dry layer thickness measurements were performed after block- and homopolymer adsorption ($c = 250 \mu\text{g mL}^{-1}$) under established conditions, and UV-irradiation (Figure S7a). Furthermore, the resulting contact angles after the extraction of the irradiated **pEHPA** and **pEHPMA** substrates were compared to pristine PS surfaces since no layer thickness was detected after the extraction of **pEHPA** and **pEHPMA** surfaces (Figure S7b).

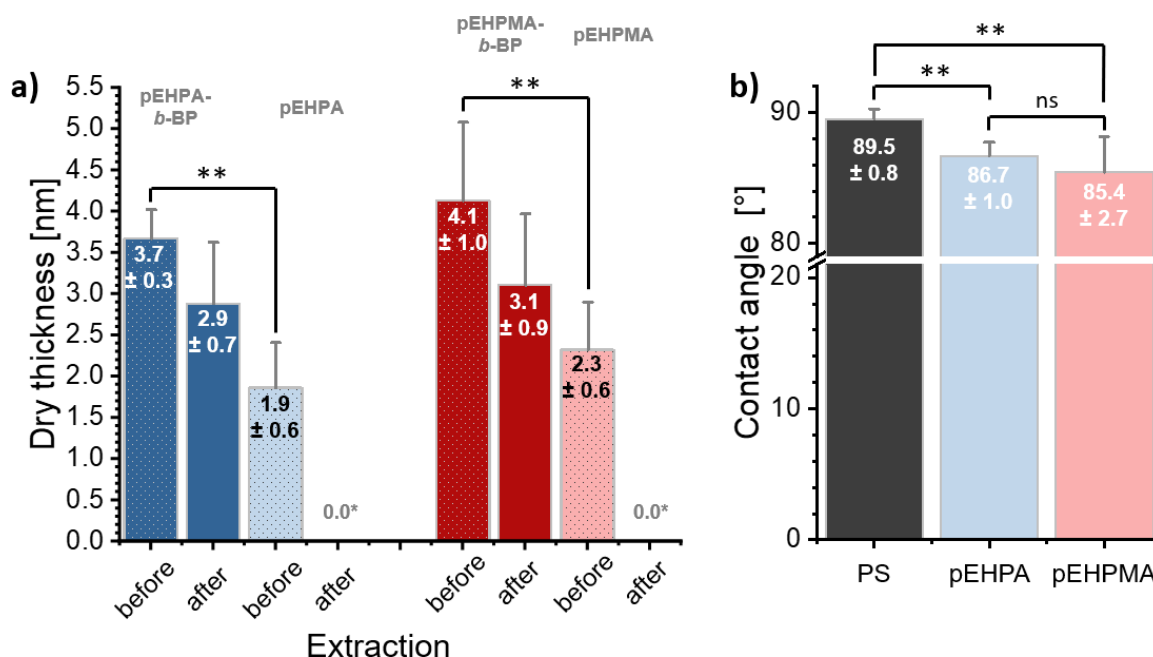


Figure S7. Comparison of surface characteristics of block copolymer and homopolymer grafted PS surfaces. (a) Comparative dry layer thickness of adsorbed ($c = 250 \mu\text{g mL}^{-1}$) and UV irradiated **pEHPA-*b*-BP** and **pEHPA** as well as **pEHPMA-*b*-BP** and **pEHPMA** coatings before and after extraction. (b) Comparative water contact angles of native PS substrates and extracted PS substrates after **pEHPA** or **pEHPMA** homopolymer adsorption ($n \geq 3$). *Measured values were below the detection limit of the spectroscopic ellipsometer.

5.1. Estimation of the chain overlap parameters based on polymer theory

In order to estimate the configuration of the surface tethered polymer chains in aqueous solution above and below their cloud point temperature T_{cp} , we calculated the theoretical degree of chain overlap. Therefore, the ratio of the Flory radius R_f of the polymer chains in a good ($R_{f, \text{good}}$) and bad solvent ($R_{f, \text{bad}}$), representing the conditions below and above the cloud point in water, and the anchor distance (l) of the chains on the surface was calculated. In previous work, we showed that the estimation of water as a good solvent is valid by comparing hydrodynamic radii of **pEHPA** in water derived from DLS data below T_{cp} to the theoretical Flory radii in a good solvent.^{2, 7} Furthermore, we assume water as a bad solvent above the T_{cp} due to chain aggregation observed in turbidimetry and DLS measurements. Flory radii were calculated in a good ($R_{f, \text{good}} = N^{3/5}a$) and bad ($R_{f, \text{bad}} = N^{1/3}a$) solvent with N as the number of repeating units in the polymer chain and a as the segment chain length.⁸ The number of repeating units N was calculated as the ratio of the polymer's molecular weight M_n to the respective monomer weight of **EHPA** (174.2 g/mol) or **EHPMA** (188.2 g/mol). The segment length was estimated to $a = 0.25$ nm as a typical value for vinyl-based polymers such as **pNIPAM**.⁹ The respective anchor distance l was calculated using the dry thickness values (h) and approximating the density of **pEHPA** and **pEHPMA** to the density of **pNIPAM** ($\rho_{\text{pNIPAM}} = 1.2 \text{ g cm}^{-3}$).^{10, 11} Furthermore, a model with homogeneous distribution of circular chains on a square surface area was assumed, which is frequently used in surface science.^{12, 13} This allows to calculate the anchor distance l with the chain grafting density (GD) from the layer thickness h , the polymer density ρ , the Avogadro number N_A , and the molecular weight M_n of the polymer as follows:

$$l = \sqrt{\frac{4}{\pi} \frac{1}{\text{GD}}} \quad \text{with grafting density (GD):} \quad \text{GD} = \frac{h \cdot \rho_{\text{polymer}} \cdot N_A}{M_n}$$

The parameters for estimating the grafting density $2R_f l^{-1}$ of the surface tethered chains in the extracted polymer layers in a good and a bad solvent are shown in Table S2. The standard deviations of the chain overlap values were calculated based on the standard deviations of the layer thickness using Gaussian propagation of error.

Table S1. Polymer and coating parameters as described and defined in the text for the estimation of the degree of chain overlap of grafted polymers in a bad and a good solvent.

Polymer (concentration [$\mu\text{g mL}^{-1}$])	N	$R_{f, \text{good}}$ [nm]	$R_{f, \text{bad}}$ [nm]	h [nm]	GD [nm^{-3}]	l [nm]	$2R_{f, \text{good}} l^{-1}$	$2R_{f, \text{bad}} l^{-1}$
pEHPA-<i>b</i>-BP (250)	138.3	4.81	1.29	2.9 ± 0.7	0.086	3.84	2.51 ± 0.61	0.67 ± 0.16
pEHPA-<i>b</i>-BP (62.5)	138.3	4.81	1.29	1.9 ± 0.6	0.057	4.72	2.04 ± 0.64	0.55 ± 0.17
pEHPMA-<i>b</i>-BP (250)	117.4	4.36	1.22	3.1 ± 1.9	0.101	3.54	2.46 ± 0.71	0.69 ± 0.20
pEHPMA-<i>b</i>-BP (62.5)	117.4	4.36	1.22	2.1 ± 0.7	0.069	4.31	2.03 ± 0.68	0.57 ± 0.19

6. Additional cell adhesion images

The adhesion and proliferation of human dermal fibroblasts seeded on polymer brush coated substrates and TCPS controls at a density of 43×10^5 cells cm^{-2} was observed up to 72 h after seeding. Representative phase contrast images after 48 and 72 h are shown in Figure S8.

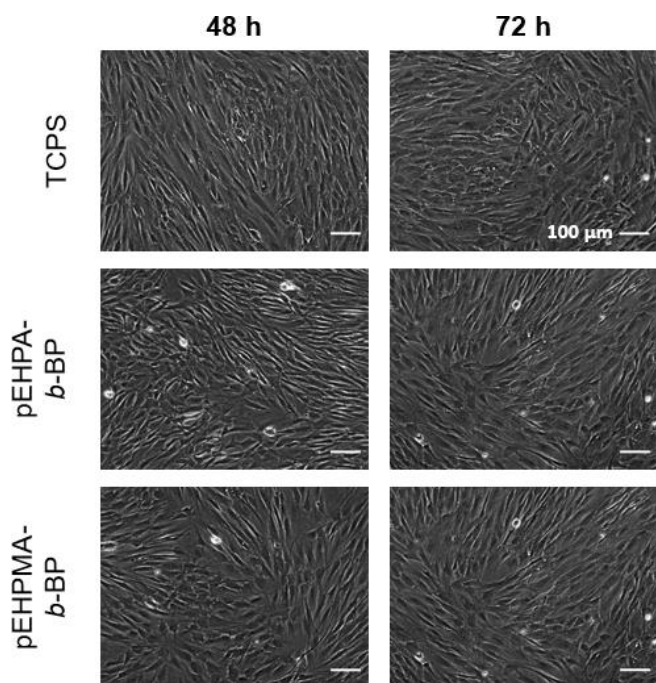


Figure S8. Representative phase contrast images of human dermal fibroblasts on **TCPS** (top), **pEHPA-*b*-BP** (middle), and **pEHPMA-*b*-BP** (bottom) coated PS substrates 48 and 72 h after seeding at a density of 43×10^5 cells cm^{-2} .

7. Surface parameters of brush-coated QCM-D chips

The average dry layer thickness of **pEHPA-*b*-BP** and **pEHPMA-*b*-BP** coatings on PS-coated QCM-D chips, used to quantify the areal mass of adsorbed proteins are shown in Figure S9a. Corresponding water contact angles on these brush coatings, along with the values of the used **TCPS** reference, are shown in Figure S9b. Representative real-time frequency curves of protein adsorption measurements conducted *via* QCM-D are shown in Figure S10.

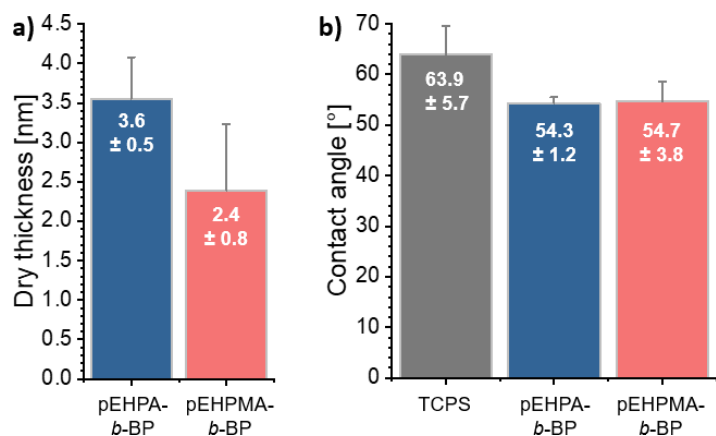


Figure S9. Dry layer thickness of **pEHPA-*b*-BP** and **pEHPMA-*b*-BP** brush coatings on PS-coated QCM-D chips (a) and their corresponding water contact angles, along with the values for TCPS controls (b) ($n \geq 3$).

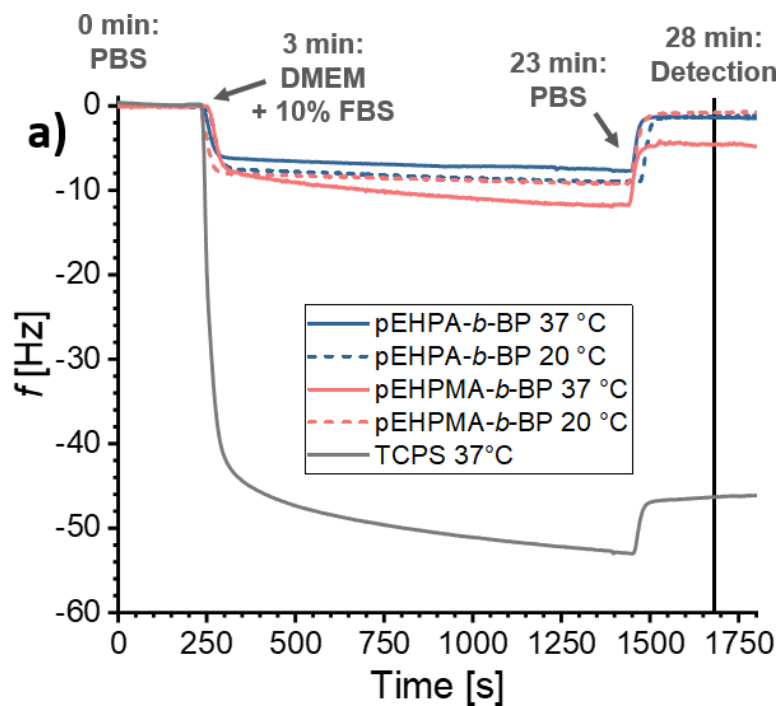


Figure S10. Representative frequency curves of the protein adsorption from DMEM cell culture medium supplemented with 10% FCS obtained from QCM-D measurements at 37 °C and 20 °C on brush coatings and a TCPS control at 37 °C.

8. Viability of thermally detached cells

To assess the viability of thermally detached confluent sheets from **pEHPA-*b*-BP** surfaces, the cells were trypsinized after detachment parallel to confluent cells cultured on TCPS substrates and harvested conventionally by trypsinization. Dead cells were stained with propidium iodide, and all cells were counted via flow cytometry. The counted values of all measurements on **pEHPA-*b*-BP** and TCPS ($n = 3$, respectively), along with the threshold for the dead cells, are shown in Figure S11. The average percentage of dead cells and standard deviation are embedded.

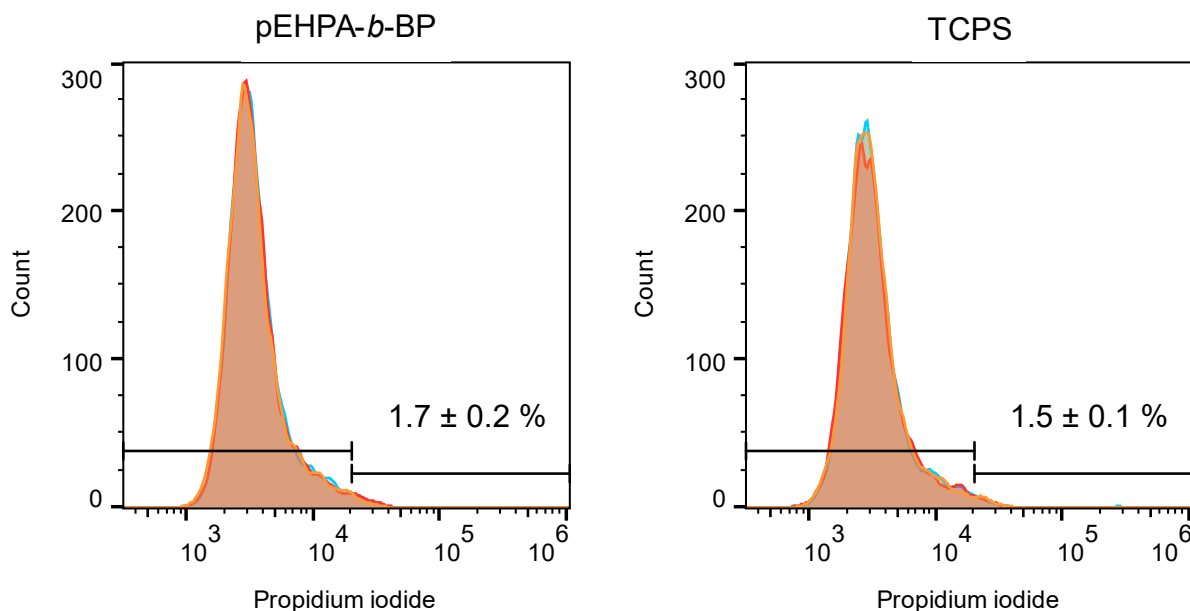


Figure S11. Flow cytometry counts of cells (red, orange, blue) thermally detached from **pEHPA-*b*-BP** (left) and trypsinized from TCPS (right). Number values indicate the mean percentage of dead cells along with the standard deviation ($n = 3$).

9. Storage stability of coated substrates

In order to distinguish between the impact of the sterilization treatment and the storage time between measurements of pristine and sterilized surfaces, pristine brush surfaces were stored under

ambient conditions until the sterilized samples were returned and analyzed (14-18 d). The non-sterilized samples were then treated identically (extraction in ethanol for 16 h) for comparison. The thickness and contact angle differences of **pEHPA-*b*-BP**, **PGE-*b*-OBP**, and **PGE-*b*-ACBP** coatings are summarized in Figure S12.

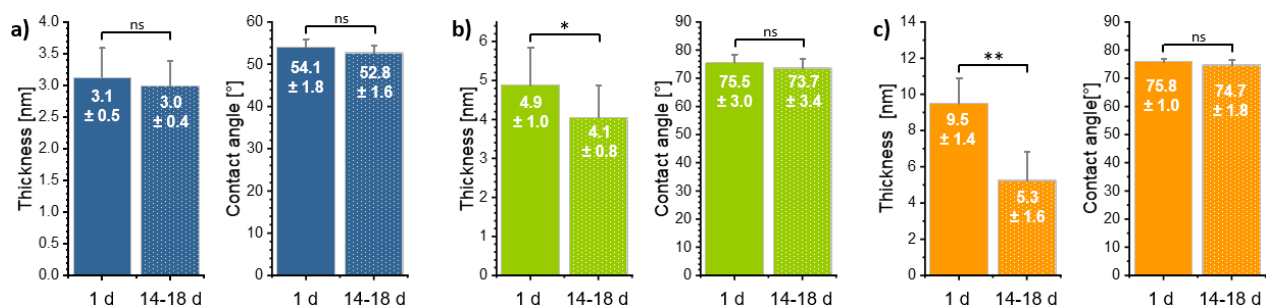


Figure S12. Thickness and contact angle values of **pEHPA-*b*-BP** (a), **PGE-*b*-OBP** (b), and **PGE-*b*-ACBP** (c) after coating preparation and extraction (1 d) and after 14-18 d of ambient storage and subsequent extraction ($n \geq 3$).

10. Impact of gamma and FO treatment on CAs of pristine PS substrates

In order to assess the impact of the used sterilization methods on pristine **PS** substrates, untreated **PS** was sterilized under identical conditions to the brush coatings and extracted in ethanol for 16 h after sterilization. The resulting CAs are shown in Figure S13.

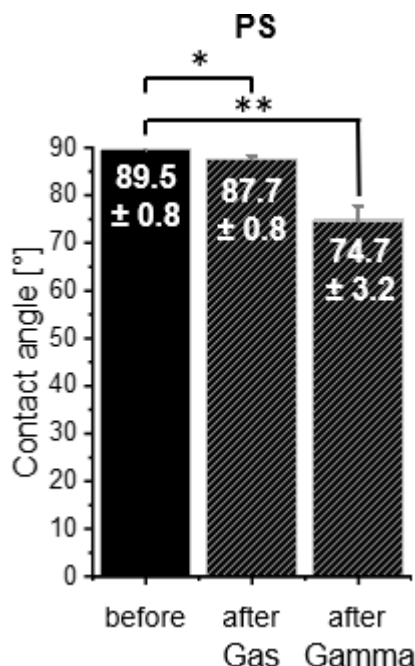


Figure S13. Contact angles of untreated and sterilized PS after ethanol extraction.

11. References

- (1) Stöbener, D. D.; Uckert, M.; Cuellar-Camacho, J. L.; Hoppensack, A.; Weinhart, M. Ultrathin Poly(glycidyl ether) Coatings on Polystyrene for Temperature-Triggered Human Dermal Fibroblast Sheet Fabrication. *ACS Biomaterials Science & Engineering* **2017**, *3* (9), 2155-2165. DOI: 10.1021/acsbomaterials.7b00270.
- (2) Schweigerdt, A.; Stöbener, D. D.; Schäfer, A.; Kara, S.; Weinhart, M. Impact of Amphiphilicity Balance in Hydroxy-Functional, Isomeric, Thermoresponsive Poly(meth)acrylates. *Macromolecules* **2023**, *56* (21), 8602-8613. DOI: 10.1021/acs.macromol.3c01251.
- (3) Kecici, Z.; Babaoglu, S.; Temel, G. Methacrylated benzophone as triple functional compound for the synthesis of partially crosslinked copolymers. *Progress in Organic Coatings* **2018**, *115*, 138-142. DOI: 10.1016/j.porgcoat.2017.11.015.
- (4) Stobener, D. D.; Weinhart, M. Thermoresponsive Poly(glycidyl ether) Brush Coatings on Various Tissue Culture Substrates-How Block Copolymer Design and Substrate Material Govern Self-Assembly and Phase Transition. *Polymers (Basel)* **2020**, *12* (9). DOI: 10.3390/polym12091899.
- (5) Han, S.; Hagiwara, M.; Ishizone, T. Synthesis of Thermally Sensitive Water-Soluble Polymethacrylates by Living Anionic Polymerizations of Oligo(ethylene glycol) Methyl Ether Methacrylates. *Macromolecules* **2003**, *36* (22), 8312-8319. DOI: 10.1021/ma0347971.
- (6) Deshmukh, M. V.; Vaidya, A. A.; Kulkarni, M. G.; Rajamohanam, P. R.; Ganapathy, S. LCST in poly(N-isopropylacrylamide) copolymers: high resolution proton NMR investigations. *Polymer* **2000**, *41* (22), 7951-7960. DOI: 10.1016/s0032-3861(00)00174-9.
- (7) Kubota, K.; Fujishige, S.; Ando, I. Solution Properties of Poly(N-isopropylacrylamide) in Water. *Polym J* **1990**, *22* (1), 15-20. DOI: 10.1295/polymj.22.15.
- (8) Israelachvili, J. N. *Intermolecular and Surface Forces*; Elsevier Science, 2011.
- (9) Ohta, H.; Ando, I.; Fujishige, S.; Kubota, K. A ¹³C PST/MAS NMR study of poly (N-isopropylacrylamide) in solution and in the gel phase. *Journal of Molecular Structure* **1991**, *245* (3-4), 391-397. DOI: 10.1016/0022-2860(91)87113-v.
- (10) Lele, A. K.; Hirve, M. M.; Badiger, M. V.; Mashelkar, R. A. Predictions of Bound Water Content in Poly(N-isopropylacrylamide) Gel†. *Macromolecules* **1997**, *30* (1), 157-159. DOI: 10.1021/ma950894l.
- (11) Ishida, N.; Biggs, S. Direct observation of the phase transition for a poly(N-isopropylacrylamide) layer grafted onto a solid surface by AFM and QCM-D. *Langmuir* **2007**, *23* (22), 11083-11088. DOI: 10.1021/la701461b.

- (12) Plunkett, K. N.; Zhu, X.; Moore, J. S.; Leckband, D. E. PNIPAM chain collapse depends on the molecular weight and grafting density. *Langmuir* **2006**, *22* (9), 4259-4266. DOI: 10.1021/la0531502.
- (13) Kim, M.; Schmitt, S.; Choi, J.; Krutty, J.; Gopalan, P. From Self-Assembled Monolayers to Coatings: Advances in the Synthesis and Nanobio Applications of Polymer Brushes. *Polymers* **2015**, *7* (7), 1346-1378. DOI: 10.3390/polym7071346.

4. Short summary

The combined parts of this thesis aimed to elucidate the transition mechanisms of thermoresponsive glycerol-based polymers and utilize these insights to establish a robust platform for the fabrication of thermally detached cell sheets. Conclusions from temperature-dependent studies of PGE and PGE-like alkoxy hydroxypropyl [meth]acrylate (AHP[M]A) polymers led to a PEHPA-based brush coating for cell sheet fabrication. A comparison of PGE and PEHPA brush coating properties and cell harvesting performance before and after sterilization highlighted the upside of the newly developed PEHPA polymer design.

The phase transition behavior of thin brush layers with transition temperatures below the physiological range was studied using 10 and 22 kDa PGE chains, which were immobilized on inert gold surfaces by precedingly introduced thiol anchor blocks. Optimized grafting procedures were adapted to obtain molecular control of brush properties with dry thicknesses of 1.6 – 10 nm and grafting densities of 0.07 – 0.5 chains nm⁻². Remarkably, similar transition temperatures in solution and on surface were detected between 26 and 31 °C and attributed to the non-interacting gold surface, which does not affect the reversible transition process. However, the phase transition concluded between 35 and 40 °C, which could hamper effective cell attachment due to remaining coating hydration and should be considered when designing cell-adhesive functional surfaces. Furthermore, the phase transition mechanism of surface-tethered PGE chains was found to be primarily dependent on the grafting density. Low GD regimes (0.07 – 0.12 chains nm⁻²) exhibited a brush-to-mushroom transition with parallel chain dehydration and collapse processes. In contrast, middle GD regimes (0.3 – 0.5 chains nm⁻²) displayed a brush-to-brush transition, with initially more distinct dehydration and a more pronounced brush collapse after water molecules were expelled.

In the following study, AHP[M]A monomers were derived through molecular design, to establish an alternative to PGE polymers. The design featured PGE-like short alkoxy side chains for similar functionality and hydroxy groups to balance the hydrophobic aliphatic backbone. Polymerization under optimized RAFT conditions yielded narrow dispersed 22-25 kDa polymers. Subsequent phase transition studies of 20 – 5 mg mL⁻¹ concentrated aqueous solutions of PHMPMA, PEHPA and PEHPMA revealed transition temperatures of 37 – 43 °C, 22 – 25 °C, and 8 – 10 °C, respectively. The increase in side-chain hydrophobicity from a methoxy to an ethoxy group resulted in less concentration- and molecular weight-dependent cloud point temperatures, particularly in the comparison of isomeric PHMPMA and PEHPA polymers, where a methyl group was “shifted” from the PHMPMA backbone to the end of the PEHPA side chain through molecular monomer design. Furthermore, NMR spectra of PHMPMA in deuterated water did not reveal any chain dehydration, indicating an LLPS transition type. In contrast, a distinct dehydration of all PEHP[M]A chain parts was observed in

Short summary

temperature-dependent NMR spectra after passing the cloud point temperature, indicating a pronounced CTG behavior which is an important precondition for cell harvesting coatings.

The conclusions from PGE brush studies revealed the concordance of transition temperatures of solutions and thin brush layers, as well as the possible impact of broad transition ranges. Keeping that in mind, PEHPA and PEHPMA polymers with CTG transition type and sufficiently low T_{cp} values in solution were chosen for the preparation of coatings for cell sheet fabrication on applicable hydrophobic PS surfaces. An immobilization strategy through self-assembly, directed by a short (2 – 4 repeating units) hydrophobic benzophenone (meth)acrylate block (BP), copolymerized to the homopolymer chains, was transferred from previous PGE reports. Layers of surface tethered 22 – 24 kDa PEHP[M]A-BP polymers with thicknesses up to ~3 nm were obtained after UV irradiation, which induced a covalent crosslinking reaction between BP and PS, followed by layer extraction. Protein adsorption on these brush surfaces was an order of magnitude lower compared to TCPS surfaces (20 – 90 ng cm⁻² and 800 ng cm⁻², respectively) under cell culture conditions (37 °C), which is typically linked with cell-repellent surfaces. Nevertheless, both polymer coatings enabled the adhesion, proliferation and detachment of human dermal fibroblasts. PEHPA-BP brushes reliably detached cell sheets after cooling to room temperature, whereas PEHPMA-BP surfaces required cooling to 4 °C and performed less reliably, sometimes resulting in sheet fragmentation. Consequently, DIN normed sterilization with formaldehyde gas or gamma radiation were performed with PEHPA-BP coatings and previously established PGE brush coatings on PS and TCPS substrates. Gamma sterilization with a dose of 45 kGy degraded PGE brush coatings and significantly altered the properties of PEHPA-BP brush coatings, rendering them unable to detach cell sheets post-sterilization. In contrast, FO gas treatment had no adverse effects on the brush coatings. However, after the timeframe of sterilization and transport processes (14 – 18 d), the thickness of PGE brush coatings, irrespective of FO sterilization, decreased significantly, possibly due to a drying effect of the brush layer. At the same time, no changes were detected for PEHPA-BP brushes. Consequently, detachment times on PGE brushes increased markedly from 60 to a maximum of 180 min. Only a slight increase was observed on PEHPA-BP brushes, from 60 to 90 min maximum time, showing the advantage of the new polymer design.

In conclusion, thermoresponsive PHMPMA, PEHPA and PEHPMA polymers were established through molecular design, inspired through PGE structures. The investigation of the phase transition in solution, combined with insights from phase transition studies of PGE brush layers, were used to select PEHPA and PEHPMA polymers for designing functional coatings for cell sheet fabrication. The CTG transition-type polymers supported cell proliferation and detachment and PEHPA-based coatings exhibited enhanced durability. These findings highlight the benefit of the aliphatic backbone, compared to polyether-based PGE coatings.

5. Kurzzusammenfassung

Die vereinten Abschnitte dieser Arbeit hatten zum Ziel, die Übergangsmechanismen von glycerinbasierten, thermoresponsiven Polymeren aufzuklären und diese Erkenntnisse zu nutzen, um eine robuste Plattform für die Herstellung thermisch ablösbarer Zellmonlagen zu etablieren. Erkenntnisse aus temperaturabhängigen Studien von PGE- und PGE-ähnlichen Alkoxyhydroxypropyl[meth]acrylat (AHP[M]A)-Polymeren führten zu einer PEHPA-basierten Bürstenbeschichtung für das Ablösen von Zellmonlagen. Ein Vergleich der PGE- und PEHPA-Bürstenbeschichtungen hinsichtlich ihrer Eigenschaften und der Zellablöseprozedur vor und nach der Sterilisation zeigte die positiven Auswirkungen des alternativen Polymerdesigns.

Das Phasenübergangsverhalten dünner Bürstenschichten mit Übergangstemperaturen unterhalb des physiologischen Bereichs wurde untersucht mithilfe von 10 und 22 kDa schweren PGE-Ketten, die auf inerten Goldoberflächen durch zuvor eingebaute Thiol-Ankerblöcke immobilisiert wurden. Optimierte Adsorptionsverfahren wurden übernommen, um Bürstenparameter auf molekular Ebene einzustellen und Trockenschichtdicken von 1,6 – 10 nm, sowie Kettendichten (KD) von 0,07 – 0,5 Ketten nm⁻² zu erhalten. Bemerkenswerterweise stimmten die Übergangstemperaturen im Bereich zwischen 26 und 31 °C jeweils in der Lösung und auf der Oberfläche überein. Dies wurde auf die nicht mit Polymeren wechselwirkende Goldoberfläche zurückgeführt, die den reversiblen Phasenübergangsprozess nicht beeinflusste. Der Phasenübergang endete jedoch zwischen 35 und 40 °C, was eine effektive Zellanhaftung aufgrund der verbleibenden Hydratation behindern könnte und bei der Entwicklung von funktionellen zelladhäsiven Oberflächen berücksichtigt werden sollte. Darüber hinaus wurde festgestellt, dass der Phasenübergangs-mechanismus der gebundenen PGE-Ketten wesentlich von der KD abhängt. Niedrige KD-Bereiche von 0,07 – 0,12 Ketten nm⁻² zeigten einen Bürste-Pilzhut-Übergang mit paralleler Dehydratisierung und Kollaps der Ketten. Im Gegensatz dazu zeigten mittlere KD-Bereiche von 0,3 – 0,5 Ketten nm⁻² einen Bürste-Bürste-Übergang mit einer prägnanten Dehydratisierung zu Beginn und folgend mehr sichtbaren Ketten-Kollaps, der durch die abwesenden Wassermoleküle ermöglicht wird.

In der folgenden Studie wurden AHP[M]A-Monomere durch molekulares Design abgeleitet, um eine Alternative zu PGE-Polymeren zu etablieren. Das Design enthielt PGE-ähnliche kurze Alkoxy-Seitenketten für eine ähnliche Funktionalität und Hydroxygruppen zum Ausgleich des hydrophoben aliphatischen Rückgrats. Die Polymerisation unter optimierten RAFT-Bedingungen ergab 22-25 kDa schwere Polymere mit enger Molekulargewichtsverteilung. Anschließende Phasenübergangsstudien von 20 – 5 mg mL⁻¹ konzentrierten wässrigen Lösungen von PHMPMA, PEHPA und PEHPMA ergaben Übergangsbereiche von jeweils 37 – 43 °C, 22 – 25 °C und 8 – 10 °C. Die Erhöhung der Hydrophobie in der Seitenkette von

Kurzzusammenfassung

einer Methoxy- zu einer Ethoxygruppe führte zu einer geringeren Abhängigkeit der Schaltunkte von Konzentration und Molekulargewicht, insbesondere beim Vergleich der isomeren PHMPMA- und PEHPA-Polymere, bei denen eine Methylgruppe vom PHMPMA-Rückgrat zum Ende der PEHPA-Seitenkette durch molekulares Monomerdesign "verschoben" wurde. Zudem zeigten die NMR-Spektren von PHMPMA in deuteriertem Wasser keine Dehydratisierung von Polymerketten, was auf einen sogenannten „LLPS“-Übergangstyp hindeutet. Im Gegensatz dazu wurde in temperaturabhängigen NMR-Spektren von PEHP[M]A Lösungen nach Überschreiten der Schalttemperatur eine deutliche Dehydratisierung aller Kettenteile beobachtet. Dies deutet auf ein Knäuel-Globuli (KG) hin, eine wichtige Voraussetzung für temperaturabhängige Beschichtungen für Zellablösevorgänge.

Die Erkenntnisse aus der Untersuchung der PGE-Bürsten ergaben die Übereinstimmung der Übergangstemperaturen in Lösung und auf der Oberfläche, sowie den möglichen Einfluss des breiten Übergangsbereichs. Dementsprechend wurden PEHPA- und PEHPMA-Polymere mit ausreichend tiefen Schaltwerten in Lösung und dem KG-Übergangstyp für die Entwicklung von Beschichtungen auf gängigen hydrophoben PS-Oberflächen für das Ablösen von Zellmonolagen ausgewählt. Eine Immobilisierungsstrategie basierend auf PGE-Bürstenschichten wurde übernommen, indem gezielte Adsorption durch einen zuvor eingeführten, kurzen (2-4 Einheiten), hydrophoben Benzophenon(meth)acrylat-Block (BP) gesteuert wurde. Schichten aus oberflächen-gebundenen 22 – 24 kDa schweren PEHPA-BP und PEHPMA-BP Polymeren mit Dicken von bis zu ~3 nm wurden nach der Vernetzung von BP mit PS durch UV-Bestrahlung und anschließender Oberflächenextraktion erhalten. Überraschenderweise war die Proteinadsorption auf diesen Bürstenoberflächen bei 37 °C um eine Größenordnung geringer als auf TCPS (20 – 90 ng cm⁻² und 800 ng cm⁻²), was im Allgemeinen eher bei zellabweisenden Oberflächen beobachtet wird. Dennoch gelangen sowohl die Kultivierung als auch das Ablösen von humanen dermalen Fibroblast-Monolagen, wobei sich die Zellen von PEHPA-BP-Oberflächen nach Abkühlung auf Raumtemperatur zuverlässig ablösten, während bei PEHPMA-BP-Oberflächen eine Abkühlung auf 4 °C erforderlich war und das Ablösen teils nicht in Monolagen erfolgte. Daher wurden PEHPA-BP-Beschichtungen und zuvor etablierte PGE-Bürstenbeschichtungen auf PS- und TCPS-Substraten einer DIN-genormten Sterilisation durch Formaldehydgas oder Gammabestrahlung unterzogen. Gammasterilisation mit einer 45 kGy Dosis führte dabei zur Degradation der PGE-Beschichtungen und modifizierte die PEHPA-BP Eigenschaften derart, dass nach der Sterilisation kein zuverlässiges Ablösen der Zellen gewährleistet war. FO-Gas hingegen zeigte keine Auswirkungen auf die Bürstenbeschichtungen. Allerdings nahm die Dicke der PGE-Bürstenbeschichtungen nach dem Zeitrahmen der Sterilisations- und Transportprozesse (14 - 18 d) unabhängig von der FO-Sterilisation ab, was mutmaßlich ein langfristiger Trocknungseffekt der Bürstenschicht ist. Gleichzeitig wurden bei PEHPA-BP-

Kurzzusammenfassung

Bürsten keine Veränderungen festgestellt. Die Ablöseszeiten auf PGE-Bürsten stiegen deutlich von 60 Minuten auf maximal 180 Minuten an. Bei PEHPA-BP-Bürsten wurde nur ein leichter Anstieg von 60 auf 90 Minuten beobachtet, was den Vorteil des neuen Polymerdesigns nahelegt.

Zusammenfassend, wurden thermoresponsive PHMPMA-, PEHPA- und PEHPMA-Polymere durch molekulares Design entwickelt, inspiriert durch PGE-Strukturen. Die detaillierte Studie des Phasenübergangs in Lösung, kombiniert mit Erkenntnissen aus Phasenübergangsstudien von PGE-Bürstenschichten, wurde genutzt, um PEHPA- und PEHPMA-Polymere für die Entwicklung funktioneller Beschichtungen zum Ablösen von Zellmonolagen zu identifizieren. Die Polymere mit dem KG-Übergangstyp unterstützten sowohl Zellwachstum als auch -ablöse. Beschichtungen auf PEHPA-Basis wiesen zudem eine erhöhte Haltbarkeit auf. Insgesamt unterstreichen diese Ergebnisse den Vorteil des aliphatischen Polymerrückgrats im Vergleich zu PGE-Beschichtungen auf Polyetherbasis.

6. Outlook

Despite possible limitations for long-term storage, PGE coatings remain an attractive option for biomedical coatings, due to their biocompatibility and special ability to activate dendritic cells.⁴² Efficient and non-destructive disinfection of these coatings can be achieved by treatment with 70% aqueous ethanol. Moreover, the suitability of the gas sterilization method was verified, and the coating stability could be enhanced through antioxidant additives, if necessary.^{45, 46} The straightforward self-assembly procedures could also be used for the on-demand fabrication of coatings. Furthermore, PGEs could be utilized for *in vivo* applications, e. g. as self-degrading coatings to assure biocompatibility and initiate wound healing and integration of implants after invasive medical procedures, without the need of long-term care, comparable to self-degrading surgical sutures.¹⁶⁸

The developed PEHPA coatings showed their potential for a durable cell culture platform. The next step for this coating would be the cultivation and detachment of different cell types to further evaluate their utility potential. The cell adhesion and detachment properties, despite generally low protein adsorption, are unique for a thermoresponsive coating in the literature so far and could be further elucidated. Experiments quantifying the adsorbed amount and activity of RGD containing proteins, such as fibronectin and vitronectin, similar to a study in literature on PHEMA brushes¹⁶⁹ could prove our current hypothesis of a thin but bioactive adsorbed layer of fibronectin on these coatings. Furthermore, possible links between brush thickness and cell adhesion, protein adsorption, and RGD activity could be evaluated.¹⁶⁹ A possible intrinsic affinity between the brush surface and cells could also be probed by blocking the integrin bonding domains in seeded cells¹⁵⁰ or utilization of serum-free cell culture e. g. with human corneal epithelial cells, which can effectively adapt to serum free conditions.¹⁷⁰

When the research and application potential is deemed attractive enough, further risk assessment studies could lead to lower radiation dosage (25 kGy) and still enable radiation sterilization, eventually under inert conditions. In addition, aging studies could be carried out for potential translation.¹⁵⁴ Methacrylate based coatings could be further optimized either through optimization of the brush fabrication procedure or through a copolymer of EHPMA and HMPMA, to optimize the phase transition temperature, while providing suitable dehydration. PHMPMA with the LLPS transition type and temperatures at the verge of human body could be utilized for bioseparation, similar to other LLPS polymers, especially when utilizing the functionalization possibility of the hydroxyl groups.⁵⁹

7. References

- (1) Sponchioni, M.; Capasso Palmiero, U.; Moscatelli, D. Thermo-responsive polymers: Applications of smart materials in drug delivery and tissue engineering. *Mater Sci Eng C Mater Biol Appl* **2019**, *102*, 589-605. DOI: 10.1016/j.msec.2019.04.069 From NLM Medline.
- (2) Bratek-Skicki, A. Towards a new class of stimuli-responsive polymer-based materials – Recent advances and challenges. *Applied Surface Science Advances* **2021**, *4*. DOI: 10.1016/j.apsadv.2021.100068.
- (3) Hu, L.; Zhang, Q.; Li, X.; Serpe, M. J. Stimuli-responsive polymers for sensing and actuation. *Materials Horizons* **2019**, *6* (9), 1774-1793. DOI: 10.1039/c9mh00490d.
- (4) Kim, Y. J.; Matsunaga, Y. T. Thermo-responsive polymers and their application as smart biomaterials. *J Mater Chem B* **2017**, *5* (23), 4307-4321. DOI: 10.1039/c7tb00157f.
- (5) Doberenz, F.; Zeng, K.; Willems, C.; Zhang, K.; Groth, T. Thermoresponsive polymers and their biomedical application in tissue engineering - a review. *J Mater Chem B* **2020**, *8* (4), 607-628. DOI: 10.1039/c9tb02052g From NLM Medline.
- (6) Conrad, J. C.; Robertson, M. L. Towards mimicking biological function with responsive surface-grafted polymer brushes. *Current Opinion in Solid State and Materials Science* **2019**, *23* (1), 1-12. DOI: 10.1016/j.cossms.2018.09.004.
- (7) Aseyev, V.; Tenhu, H.; Winnik, F. M. Non-ionic Thermoresponsive Polymers in Water. In *Self Organized Nanostructures of Amphiphilic Block Copolymers II*, Advances in Polymer Science, 2010; pp 29-89.
- (8) Halperin, A.; Kröger, M.; Winnik, F. M. Poly(N-isopropylacrylamide) Phase Diagrams: Fifty Years of Research. *Angew Chem Int Ed Engl* **2015**, *54* (51), 15342-15367. DOI: <https://doi.org/10.1002/anie.201506663>.
- (9) Nagase, K.; Yamato, M.; Kanazawa, H.; Okano, T. Poly(N-isopropylacrylamide)-based thermoresponsive surfaces provide new types of biomedical applications. *Biomaterials* **2018**, *153*, 27-48. DOI: 10.1016/j.biomaterials.2017.10.026.
- (10) Canavan, H. E.; Cheng, X.; Graham, D. J.; Ratner, B. D.; Castner, D. G. Cell sheet detachment affects the extracellular matrix: a surface science study comparing thermal liftoff, enzymatic, and mechanical methods. *J Biomed Mater Res A* **2005**, *75* (1), 1-13. DOI: 10.1002/jbm.a.30297.
- (11) Kobayashi, J.; Kikuchi, A.; Aoyagi, T.; Okano, T. Cell sheet tissue engineering: Cell sheet preparation, harvesting/manipulation, and transplantation. *J Biomed Mater Res A* **2019**, *107* (5), 955-967. DOI: 10.1002/jbm.a.36627 From NLM Medline.
- (12) Ghasemi-Mobarakeh, L.; Kolahreez, D.; Ramakrishna, S.; Williams, D. Key terminology in biomaterials and biocompatibility. *Current Opinion in Biomedical Engineering* **2019**, *10*, 45-50. DOI: 10.1016/j.cobme.2019.02.004.
- (13) Utrata-Wesolek, A.; Oleszko-Torbus, N.; Bochenek, M.; Kosowski, D.; Kowalczyk, A.; Trzebiecka, B.; Dworak, A. Thermoresponsive polymer surfaces and their application in tissue engineering. *Polimery* **2018**, *63* (05), 327-338. DOI: 10.14314/polimery.2018.5.1.
- (14) Heskins, M.; Guillet, J. E. Solution Properties of Poly(N-isopropylacrylamide). *J Macromol Sci A* **1968**, *2* (8), 1441-1455. DOI: 10.1080/10601326808051910.
- (15) Yamada, N.; Okano, T.; Sakai, H.; Karikusa, F.; Sawasaki, Y.; Sakurai, Y. Thermo-responsive polymeric surfaces; control of attachment and detachment of cultured cells. *Die Makromolekulare Chemie, Rapid Communications* **1990**, *11* (11), 571-576. DOI: 10.1002/marc.1990.030111109.
- (16) Jana, S.; Hoogenboom, R. Poly(2-oxazoline)s: a comprehensive overview of polymer structures and their physical properties—an update. *Polymer International* **2022**, *71* (8), 935-949. DOI: 10.1002/pi.6426.
- (17) Zhang, N.; Pompe, T.; Amin, I.; Luxenhofer, R.; Werner, C.; Jordan, R. Tailored poly(2-oxazoline) polymer brushes to control protein adsorption and cell adhesion. *Macromol Biosci* **2012**, *12* (7), 926-936. DOI: 10.1002/mabi.201200026 From NLM Medline.
- (18) Badi, N. Non-linear PEG-based thermoresponsive polymer systems. *Progress in Polymer Science* **2017**, *66*, 54-79. DOI: 10.1016/j.progpolymsci.2016.12.006.
- (19) Vancoillie, G.; Van Guyse, J. F. R.; Voorhaar, L.; Maji, S.; Frank, D.; Holder, E.; Hoogenboom, R. Understanding the effect of monomer structure of oligoethylene glycol acrylate copolymers on their thermoresponsive behavior for the development of polymeric sensors. *Polym Chem-Uk* **2019**, *10* (42), 5778-5789. DOI: 10.1039/c9py01326a.
- (20) Russo, E.; Villa, C. Ploxadmer Hydrogels for Biomedical Applications. *Pharmaceutics* **2019**, *11* (12). DOI: 10.3390/pharmaceutics11120671 From NLM PubMed-not-MEDLINE.
- (21) Matthes, R.; Frey, H. Polyethers Based on Short-Chain Alkyl Glycidyl Ethers: Thermoresponsive and Highly Biocompatible Materials. *Biomacromolecules* **2022**, *23* (6), 2219-2235. DOI: 10.1021/acs.biomac.2c00223 From NLM Medline.

References

- (22) Stobener, D. D.; Hoppensack, A.; Scholz, J.; Weinhart, M. Endothelial, smooth muscle and fibroblast cell sheet fabrication from self-assembled thermoresponsive poly(glycidyl ether) brushes. *Soft Matter* **2018**, *14* (41), 8333-8343. DOI: 10.1039/c8sm01099d.
- (23) Oleszko, N.; Walach, W.; Utrata-Wesolek, A.; Kowalczyk, A.; Trzebicka, B.; Klama-Baryla, A.; Hoff-Lenczewska, D.; Kawecki, M.; Lesiak, M.; Sieron, A. L.; et al. Controlling the Crystallinity of Thermoresponsive Poly(2-oxazoline)-Based Nanolayers to Cell Adhesion and Detachment. *Biomacromolecules* **2015**, *16* (9), 2805-2813. DOI: 10.1021/acs.biomac.5b00745 From NLM Medline.
- (24) Dworak, A.; Utrata-Wesolek, A.; Szweda, D.; Kowalczyk, A.; Trzebicka, B.; Aniol, J.; Sieron, A. L.; Klama-Baryla, A.; Kawecki, M. Poly[tri(ethylene glycol) ethyl ether methacrylate]-coated surfaces for controlled fibroblasts culturing. *ACS Appl Mater Interfaces* **2013**, *5* (6), 2197-2207. DOI: 10.1021/am3031882.
- (25) Mizutani, A.; Kikuchi, A.; Yamato, M.; Kanazawa, H.; Okano, T. Preparation of thermoresponsive polymer brush surfaces and their interaction with cells. *Biomaterials* **2008**, *29* (13), 2073-2081. DOI: 10.1016/j.biomaterials.2008.01.004 From NLM Medline.
- (26) Fukumori, K.; Akiyama, Y.; Yamato, M.; Kobayashi, J.; Sakai, K.; Okano, T. Temperature-responsive glass coverslips with an ultrathin poly(N-isopropylacrylamide) layer. *Acta Biomater* **2009**, *5* (1), 470-476. DOI: 10.1016/j.actbio.2008.06.018 From NLM Medline.
- (27) Nagase, K.; Watanabe, M.; Kikuchi, A.; Yamato, M.; Okano, T. Thermo-responsive polymer brushes as intelligent biointerfaces: preparation via ATRP and characterization. *Macromol Biosci* **2011**, *11* (3), 400-409. DOI: 10.1002/mabi.201000312 From NLM Medline.
- (28) Akiyama, Y.; Kikuchi, A.; Yamato, M.; Okano, T. Ultrathin poly(N-isopropylacrylamide) grafted layer on polystyrene surfaces for cell adhesion/detachment control. *Langmuir* **2004**, *20* (13), 5506-5511. DOI: 10.1021/la036139f From NLM Medline.
- (29) Aoyagi, T.; Ebara, M.; Sakai, K.; Sakurai, Y.; Okano, T. Novel bifunctional polymer with reactivity and temperature sensitivity. *J Biomater Sci Polym Ed* **2000**, *11* (1), 101-110. DOI: 10.1163/156856200743526 From NLM Medline.
- (30) Ebara, M.; Yamato, M.; Aoyagi, T.; Kikuchi, A.; Sakai, K.; Okano, T. Temperature-responsive cell culture surfaces enable "on-off" affinity control between cell integrins and RGDS ligands. *Biomacromolecules* **2004**, *5* (2), 505-510. DOI: 10.1021/bm0343601 From NLM Medline.
- (31) Tsuda, Y.; Kikuchi, A.; Yamato, M.; Nakao, A.; Sakurai, Y.; Umezumi, M.; Okano, T. The use of patterned dual thermoresponsive surfaces for the collective recovery as co-cultured cell sheets. *Biomaterials* **2005**, *26* (14), 1885-1893. DOI: 10.1016/j.biomaterials.2004.06.005 From NLM Medline.
- (32) Akiyama, Y.; Kushida, A.; Yamato, M.; Kikuchi, A.; Okano, T. Surface characterization of poly(N-isopropylacrylamide) grafted tissue culture polystyrene by electron beam irradiation, using atomic force microscopy, and X-ray photoelectron spectroscopy. *J Nanosci Nanotechnol* **2007**, *7* (3), 796-802. DOI: 10.1166/jnn.2007.509 From NLM Medline.
- (33) Vrtacnik, P.; Kos, S.; Bustin, S. A.; Marc, J.; Ostanek, B. Influence of trypsinization and alternative procedures for cell preparation before RNA extraction on RNA integrity. *Anal Biochem* **2014**, *463*, 38-44. DOI: 10.1016/j.ab.2014.06.017 From NLM Medline.
- (34) Nash, M. E.; Healy, D.; Carroll, W. M.; Elvira, C.; Rochev, Y. A. Cell and cell sheet recovery from pNIPAm coatings; motivation and history to present day approaches. *J Mater Chem* **2012**, *22* (37). DOI: 10.1039/c2jm31748f.
- (35) Takahashi, H.; Matsuzaka, N.; Nakayama, M.; Kikuchi, A.; Yamato, M.; Okano, T. Terminally functionalized thermoresponsive polymer brushes for simultaneously promoting cell adhesion and cell sheet harvest. *Biomacromolecules* **2012**, *13* (1), 253-260. DOI: 10.1021/bm201545u From NLM Medline.
- (36) Fukumori, K.; Akiyama, Y.; Yamato, M.; Okano, T. A Facile Method for Preparing Temperature-Responsive Cell Culture Surfaces by Using a Thioxanthone Photoinitiator Immobilized on a Polystyrene Surface. *ChemNanoMat* **2016**, *2* (5), 454-460. DOI: 10.1002/cnma.201600056.
- (37) Morita, S.; Takasu, A. Adhesion control of human umbilical vein endothelial cells using clickable poly(2-oxazoline)-grafted biosynthesized extracellular matrix protein. *Polymer* **2018**, *136*, 194-204. DOI: 10.1016/j.polymer.2017.12.059.
- (38) Dworak, A.; Utrata-Wesolek, A.; Oleszko, N.; Walach, W.; Trzebicka, B.; Aniol, J.; Sieron, A. L.; Klama-Baryla, A.; Kawecki, M. Poly(2-substituted-2-oxazoline) surfaces for dermal fibroblasts adhesion and detachment. *J Mater Sci Mater Med* **2014**, *25* (4), 1149-1163. DOI: 10.1007/s10856-013-5135-7.
- (39) *Labware Chemical Resistance Table*. <https://tools.thermofisher.com/content/sfs/brochures/D20480.pdf> (accessed 2024-07-15).
- (40) Stobener, D. D.; Weinhart, M. On the foundation of thermal "Switching": The culture substrate governs the phase transition mechanism of thermoresponsive brushes and their performance in cell sheet fabrication. *Acta Biomater* **2021**, *136*, 243-253. DOI: 10.1016/j.actbio.2021.09.012 From NLM Medline.

References

- (41) Heinen, S.; Rackow, S.; Cuellar-Camacho, J. L.; Donskyi, I. S.; Unger, W. E. S.; Weinhart, M. Transfer of functional thermoresponsive poly(glycidyl ether) coatings for cell sheet fabrication from gold to glass surfaces. *J Mater Chem B* **2018**, *6* (10), 1489-1500. DOI: 10.1039/c7tb03263c From NLM PubMed-not-MEDLINE.
- (42) Stobener, D. D.; Cosimi, A.; Weinhart, M.; Peiser, M. Efficient material-induced activation of monocyte-derived dendritic cells releasing surface molecules, matrix metalloproteinases, and growth factors needed for regenerative tissue remodeling. *Mater Today Bio* **2023**, *23*, 100869. DOI: 10.1016/j.mtbio.2023.100869 From NLM PubMed-not-MEDLINE.
- (43) Heinen, S.; Weinhart, M. Poly(glycidyl ether)-Based Monolayers on Gold Surfaces: Control of Grafting Density and Chain Conformation by Grafting Procedure, Surface Anchor, and Molecular Weight. *Langmuir* **2017**, *33* (9), 2076-2086. DOI: 10.1021/acs.langmuir.6b03927.
- (44) Stobener, D. D.; Weinhart, M. Thermoresponsive Poly(glycidyl ether) Brush Coatings on Various Tissue Culture Substrates-How Block Copolymer Design and Substrate Material Govern Self-Assembly and Phase Transition. *Polymers (Basel)* **2020**, *12* (9). DOI: 10.3390/polym12091899.
- (45) Han, S.; Kim, C.; Kwon, D. Thermal/oxidative degradation and stabilization of polyethylene glycol. *Polymer* **1997**, *38* (2), 317-323. DOI: 10.1016/s0032-3861(97)88175-x.
- (46) Li, L.; Chen, S.; Jiang, S. Protein interactions with oligo(ethylene glycol) (OEG) self-assembled monolayers: OEG stability, surface packing density and protein adsorption. *J Biomater Sci Polym Ed* **2007**, *18* (11), 1415-1427. DOI: 10.1163/156856207782246795 From NLM Medline.
- (47) Kanjickal, D.; Lopina, S.; Evancho-Chapman, M. M.; Schmidt, S.; Donovan, D. Effects of sterilization on poly(ethylene glycol) hydrogels. *J Biomed Mater Res A* **2008**, *87* (3), 608-617. DOI: 10.1002/jbm.a.31811.
- (48) Abraham, M. H. Free energies, enthalpies, and entropies of solution of gaseous nonpolar nonelectrolytes in water and nonaqueous solvents. The hydrophobic effect. *Journal of the American Chemical Society* **2002**, *104* (8), 2085-2094. DOI: 10.1021/ja00372a001.
- (49) Silverstein, K. A. T.; Haymet, A. D. J.; Dill, K. A. A Simple Model of Water and the Hydrophobic Effect. *Journal of the American Chemical Society* **1998**, *120* (13), 3166-3175. DOI: 10.1021/ja973029k.
- (50) Zhao, C. Z.; Ma, Z. Y.; Zhu, X. X. Rational design of thermoresponsive polymers in aqueous solutions: A thermodynamics map. *Prog Polym Sci* **2019**, *90*, 269-291. DOI: 10.1016/j.progpolymsci.2019.01.001.
- (51) Zhang, Q.; Weber, C.; Schubert, U. S.; Hoogenboom, R. Thermoresponsive polymers with lower critical solution temperature: from fundamental aspects and measuring techniques to recommended turbidimetry conditions. *Mater Horiz* **2017**, *4* (2), 109-116. DOI: 10.1039/c7mh00016b.
- (52) Osváth, Z.; Iván, B. The Dependence of the Cloud Point, Clearing Point, and Hysteresis of Poly(N-isopropylacrylamide) on Experimental Conditions: The Need for Standardization of Thermoresponsive Transition Determinations. *Macromolecular Chemistry and Physics* **2017**, *218* (4). DOI: 10.1002/macp.201600470.
- (53) Maeda, T.; Takenouchi, M.; Yamamoto, K.; Aoyagi, T. Analysis of the formation mechanism for thermoresponsive-type coacervate with functional copolymers consisting of N-isopropylacrylamide and 2-hydroxyisopropylacrylamide. *Biomacromolecules* **2006**, *7* (7), 2230-2236. DOI: 10.1021/bm060261m From NLM Medline.
- (54) Maeda, T.; Kanda, T.; Yonekura, Y.; Yamamoto, K.; Aoyagi, T. Hydroxylated poly(N-isopropylacrylamide) as functional thermoresponsive materials. *Biomacromolecules* **2006**, *7* (2), 545-549. DOI: 10.1021/bm050829b From NLM Medline.
- (55) Heinen, S.; Rackow, S.; Schäfer, A.; Weinhart, M. A Perfect Match: Fast and Truly Random Copolymerization of Glycidyl Ether Monomers to Thermoresponsive Copolymers. *Macromolecules* **2016**, *50* (1), 44-53. DOI: 10.1021/acs.macromol.6b01904.
- (56) Konefal, R.; Cernoch, P.; Konefal, M.; Spevacek, J. Temperature Behavior of Aqueous Solutions of Poly(2-oxazoline) Homopolymer and Block Copolymers Investigated by NMR Spectroscopy and Dynamic Light Scattering. *Polymers (Basel)* **2020**, *12* (9). DOI: 10.3390/polym12091879 From NLM PubMed-not-MEDLINE.
- (57) Sugihara, S.; Hashimoto, K.; Matsumoto, Y.; Kanaoka, S.; Aoshima, S. Thermosensitive polyalcohols: Synthesis via living cationic polymerization of vinyl ethers with a silyloxy group. *J Polym Sci Pol Chem* **2003**, *41* (21), 3300-3312. DOI: DOI 10.1002/pola.10929.
- (58) Constantinou, A. P.; Tall, A.; Li, Q.; Georgiou, T. K. Liquid-liquid phase separation in aqueous solutions of poly(ethylene glycol) methacrylate homopolymers. *Journal of Polymer Science* **2021**, *60* (2), 188-198. DOI: 10.1002/pol.20210714.
- (59) Hironaka, K.; Yoshihara, E.; Nabil, A.; Lai, J. J.; Kikuchi, A.; Ebara, M. Conjugation of antibody with temperature-responsive polymer via in situ click reaction to enable biomarker enrichment for increased diagnostic sensitivity. *Biomater Sci* **2021**, *9* (14), 4870-4879. DOI: 10.1039/d1bm00349f From NLM Medline.
- (60) Raval, A.; Pillai, S. A.; Bahadur, A.; Bahadur, P. Systematic characterization of Pluronic® micelles and their application for solubilization and in vitro release of some hydrophobic anticancer drugs. *Journal of Molecular Liquids* **2017**, *230*, 473-481. DOI: 10.1016/j.molliq.2017.01.065.

References

- (61) Vicente, F. A.; Santos, J. H. P. M.; Pereira, I. M. M.; Gonçalves, C. V. M.; Dias, A. C. R. V.; Coutinho, J. A. P.; Ventura, S. P. M. Integration of aqueous (micellar) two-phase systems on the proteins separation. *BMC Chemical Engineering* **2019**, *1* (1). DOI: 10.1186/s42480-019-0004-x.
- (62) Uhlig, K.; Boerner, H.; Wischerhoff, E.; Lutz, J.-F.; Jaeger, M.; Laschewsky, A.; Duschl, C. On the Interaction of Adherent Cells with Thermoresponsive Polymer Coatings. *Polymers* **2014**, *6* (4), 1164-1177. DOI: 10.3390/polym6041164.
- (63) Işık, D.; Quaas, E.; Klinger, D. Thermo- and oxidation-sensitive poly(meth)acrylates based on alkyl sulfoxides: dual-responsive homopolymers from one functional group. *Polym Chem-Uk* **2020**, *11* (48), 7662-7676. DOI: 10.1039/d0py01321h.
- (64) Hechenbichler, M.; Laschewsky, A.; Gradzielski, M. Poly(N,N-bis(2-methoxyethyl)acrylamide), a thermoresponsive non-ionic polymer combining the amide and the ethyleneglycoether motifs. *Colloid and Polymer Science* **2020**, *299* (2), 205-219. DOI: 10.1007/s00396-020-04701-9.
- (65) He, T.; Wang, Y.; Xu, L.; Fu, X.; Narumi, A.; Sato, S.-i.; Shen, X.; Kakuchi, T. Poly[glycidyl oligo(oxyethylene)carbamate]s (PGn-EOMR' and R-PGn-EOMR'): controlled synthesis and effects of molecular parameters (n and m), side groups (R'), and end-groups (R) on thermoresponsive properties. *Polym Chem-Uk* **2021**, *12* (17), 2580-2591. DOI: 10.1039/d1py00070e.
- (66) Jung, S.-H.; Song, H.-Y.; Lee, Y.; Jeong, H. M.; Lee, H.-i. Novel Thermoresponsive Polymers Tunable by pH. *Macromolecules* **2011**, *44* (6), 1628-1634. DOI: 10.1021/ma102751p.
- (67) Jeffrey, G. A. *An Introduction to Hydrogen Bonding*; Oxford University Press, 1997.
- (68) Savoji, M. T.; Strandman, S.; Zhu, X. X. Block Random Copolymers of N-Alkyl-Substituted Acrylamides with Double Thermosensitivity. *Macromolecules* **2012**, *45* (4), 2001-2006. DOI: 10.1021/ma2027269.
- (69) Cao, Y.; Zhu, X. X.; Luo, J.; Liu, H. Effects of Substitution Groups on the RAFT Polymerization of N-Alkylacrylamides in the Preparation of Thermosensitive Block Copolymers. *Macromolecules* **2007**, *40* (18), 6481-6488. DOI: 10.1021/ma0628230.
- (70) Hoogenboom, R.; Thijs, H. M.; Jochems, M. J.; van Lankvelt, B. M.; Fijten, M. W.; Schubert, U. S. Tuning the LCST of poly(2-oxazoline)s by varying composition and molecular weight: alternatives to poly(N-isopropylacrylamide)? *Chem Commun (Camb)* **2008**, (44), 5758-5760. DOI: 10.1039/b813140f From NLM Medline.
- (71) Weaver, J. V. M.; Bannister, I.; Robinson, K. L.; Bories-Azeau, X.; Armes, S. P.; Smallridge, M.; McKenna, P. Stimulus-Responsive Water-Soluble Polymers Based on 2-Hydroxyethyl Methacrylate. *Macromolecules* **2004**, *37* (7), 2395-2403. DOI: 10.1021/ma0356358.
- (72) Ikemoto, Y.; Harada, Y.; Tanaka, M.; Nishimura, S. N.; Murakami, D.; Kurahashi, N.; Moriwaki, T.; Yamazoe, K.; Washizu, H.; Ishii, Y.; et al. Infrared Spectra and Hydrogen-Bond Configurations of Water Molecules at the Interface of Water-Insoluble Polymers under Humidified Conditions. *J Phys Chem B* **2022**, *126* (22), 4143-4151. DOI: 10.1021/acs.jpcc.2c01702 From NLM Medline.
- (73) Eggenhuisen, T. M.; Becer, C. R.; Fijten, M. W. M.; Eckardt, R.; Hoogenboom, R.; Schubert, U. S. Libraries of Statistical Hydroxypropyl Acrylate Containing Copolymers with LCST Properties Prepared by NMP. *Macromolecules* **2008**, *41* (14), 5132-5140. DOI: 10.1021/ma800469p.
- (74) Vo, C.-D.; Rosselgong, J.; Armes, S. P.; Tirelli, N. Stimulus-responsive polymers based on 2-hydroxypropyl acrylate prepared by RAFT polymerization. *J Polym Sci Pol Chem* **2010**, *48* (9), 2032-2043. DOI: 10.1002/pola.23973.
- (75) Schweigerdt, A.; Stöbener, D. D.; Schäfer, A.; Kara, S.; Weinhart, M. Impact of Amphiphilicity Balance in Hydroxy-Functional, Isomeric, Thermoresponsive Poly(meth)acrylates. *Macromolecules* **2023**, *56* (21), 8602-8613. DOI: 10.1021/acs.macromol.3c01251.
- (76) Weber, C.; Hoogenboom, R.; Schubert, U. S. Temperature responsive bio-compatible polymers based on poly(ethylene oxide) and poly(2-oxazoline)s. *Prog Polym Sci* **2012**, *37* (5), 686-714. DOI: 10.1016/j.progpolymsci.2011.10.002.
- (77) Vancoillie, G.; Frank, D.; Hoogenboom, R. Thermoresponsive poly(oligo ethylene glycol acrylates). *Prog Polym Sci* **2014**, *39* (6), 1074-1095. DOI: 10.1016/j.progpolymsci.2014.02.005.
- (78) Becherer, T.; Heinen, S.; Wei, Q.; Haag, R.; Weinhart, M. In-depth analysis of switchable glycerol based polymeric coatings for cell sheet engineering. *Acta Biomater* **2015**, *25*, 43-55. DOI: 10.1016/j.actbio.2015.06.036.
- (79) Li, J.; Mizutani, S.; Sato, S.-i.; Narumi, A.; Haba, O.; Kawaguchi, S.; Kikuchi, M.; Kakuchi, T.; Shen, X. Thermoresponsive properties of poly(N-isopropyl,N-methylacrylamide) and its statistical and block copolymers with poly(N,N-dimethylacrylamide) prepared by B(C6F5)3-catalyzed group transfer polymerization. *Polymer Chemistry* **2020**, *11* (13), 2346-2359, 10.1039/D0PY00015A. DOI: 10.1039/D0PY00015A.
- (80) Xia, Y.; Burke, N. A. D.; Stöver, H. D. H. End Group Effect on the Thermal Response of Narrow-Disperse Poly(N-isopropylacrylamide) Prepared by Atom Transfer Radical Polymerization. *Macromolecules* **2006**, *39* (6), 2275-2283. DOI: 10.1021/ma0519617.

References

- (81) Healy, D.; Nash, M.; Gorelov, A.; Thompson, K.; Dockery, P.; Belochapkin, S.; Madden, J.; Rochev, Y. Nanometer-scale physically adsorbed thermoresponsive films for cell culture. *International Journal of Polymeric Materials and Polymeric Biomaterials* **2016**, *66* (5), 221-234. DOI: 10.1080/00914037.2016.1201765.
- (82) Nash, M. E.; Carroll, W. M.; Nikoloskya, N.; Yang, R.; O'Connell, C.; Gorelov, A. V.; Dockery, P.; Liptrot, C.; Lyng, F. M.; Garcia, A.; et al. Straightforward, one-step fabrication of ultrathin thermoresponsive films from commercially available pNIPAm for cell culture and recovery. *ACS Appl Mater Interfaces* **2011**, *3* (6), 1980-1990. DOI: 10.1021/am200204j From NLM Medline.
- (83) Stobener, D. D.; Scholz, J.; Schedler, U.; Weinhart, M. Switchable Oligo(glycidyl ether) Acrylate Bottlebrushes "Grafted-from" Polystyrene Surfaces: A Versatile Strategy toward Functional Cell Culture Substrates. *Biomacromolecules* **2018**, *19* (11), 4207-4218. DOI: 10.1021/acs.biomac.8b00933.
- (84) Yamamoto, S.-i.; Pietrasik, J.; Matyjaszewski, K. ATRP Synthesis of Thermally Responsive Molecular Brushes from Oligo(ethylene oxide) Methacrylates. *Macromolecules* **2007**, *40* (26), 9348-9353. DOI: 10.1021/ma701970t.
- (85) Pan, Y. V.; Wesley, R. A.; Luginbuhl, R.; Denton, D. D.; Ratner, B. D. Plasma polymerized N-isopropylacrylamide: synthesis and characterization of a smart thermally responsive coating. *Biomacromolecules* **2001**, *2* (1), 32-36. DOI: 10.1021/bm0000642 From NLM Medline.
- (86) Nash, M. E.; Carroll, W. M.; Foley, P. J.; Maguire, G.; Connell, C. O.; Gorelov, A. V.; Beloshapkin, S.; Rochev, Y. A. Ultra-thin spin coated crosslinkable hydrogels for use in cell sheet recovery—synthesis, characterisation to application. *Soft Matter* **2012**, *8* (14). DOI: 10.1039/c2sm06466a.
- (87) Dalsin, J. L.; Lin, L.; Tosatti, S.; Vörös, J.; Textor, M.; Messersmith, P. B. Protein Resistance of Titanium Oxide Surfaces Modified by Biologically Inspired mPEG-DOPA. *Langmuir* **2004**, *21* (2), 640-646. DOI: 10.1021/la048626g.
- (88) Gon, S.; Kumar, K.-N.; Nüsslein, K.; Santore, M. M. How Bacteria Adhere to Brushy PEG Surfaces: Clinging to Flaws and Compressing the Brush. *Macromolecules* **2012**, *45* (20), 8373-8381. DOI: 10.1021/ma300981r.
- (89) Heinen, S.; Cuellar-Camacho, J. L.; Weinhart, M. Thermoresponsive poly(glycidyl ether) brushes on gold: Surface engineering parameters and their implication for cell sheet fabrication. *Acta Biomater* **2017**, *59*, 117-128. DOI: 10.1016/j.actbio.2017.06.029.
- (90) Takahashi, H.; Nakayama, M.; Yamato, M.; Okano, T. Controlled chain length and graft density of thermoresponsive polymer brushes for optimizing cell sheet harvest. *Biomacromolecules* **2010**, *11* (8), 1991-1999. DOI: 10.1021/bm100342e From NLM Medline.
- (91) Liu, G.; Zhang, G. Collapse and swelling of thermally sensitive poly(N-isopropylacrylamide) brushes monitored with a quartz crystal microbalance. *J Phys Chem B* **2005**, *109* (2), 743-747. DOI: 10.1021/jp046903m.
- (92) Laloyaux, X.; Mathy, B.; Nysten, B.; Jonas, A. M. Surface and bulk collapse transitions of thermoresponsive polymer brushes. *Langmuir* **2010**, *26* (2), 838-847. DOI: 10.1021/la902285t.
- (93) Adam, S.; Koenig, M.; Rodenhausen, K. B.; Eichhorn, K.-J.; Oertel, U.; Schubert, M.; Stamm, M.; Uhlmann, P. Quartz crystal microbalance with coupled spectroscopic ellipsometry-study of temperature-responsive polymer brush systems. *Appl Surf Sci* **2017**, *421*, 843-851. DOI: 10.1016/j.apsusc.2017.02.078.
- (94) Kim, M.; Schmitt, S.; Choi, J.; Krutty, J.; Gopalan, P. From Self-Assembled Monolayers to Coatings: Advances in the Synthesis and Nanobio Applications of Polymer Brushes. *Polymers* **2015**, *7* (7), 1346-1378. DOI: 10.3390/polym7071346.
- (95) Krishnamoorthy, M.; Hakobyan, S.; Ramstedt, M.; Gautrot, J. E. Surface-initiated polymer brushes in the biomedical field: applications in membrane science, biosensing, cell culture, regenerative medicine and antibacterial coatings. *Chem Rev* **2014**, *114* (21), 10976-11026. DOI: 10.1021/cr500252u From NLM Medline.
- (96) Khabibullin, A.; Mastan, E.; Matyjaszewski, K.; Zhu, S. Surface-Initiated Atom Transfer Radical Polymerization. In *Controlled Radical Polymerization at and from Solid Surfaces*, Advances in Polymer Science, 2015; pp 29-76.
- (97) Zoppe, J. O.; Ataman, N. C.; Mocny, P.; Wang, J.; Moraes, J.; Klok, H. A. Surface-Initiated Controlled Radical Polymerization: State-of-the-Art, Opportunities, and Challenges in Surface and Interface Engineering with Polymer Brushes. *Chem Rev* **2017**, *117* (3), 1105-1318. DOI: 10.1021/acs.chemrev.6b00314 From NLM PubMed-not-MEDLINE.
- (98) Sweat, D. P.; Kim, M.; Yu, X.; Gopalan, P. A single-component inimer containing cross-linkable ultrathin polymer coating for dense polymer brush growth. *Langmuir* **2013**, *29* (11), 3805-3812. DOI: 10.1021/la305060z.
- (99) Zou, Y.; Kizhakkedathu, J. N.; Brooks, D. E. Surface Modification of Polyvinyl Chloride Sheets via Growth of Hydrophilic Polymer Brushes. *Macromolecules* **2009**, *42* (9), 3258-3268. DOI: 10.1021/ma8025699.
- (100) Zamfir, M.; Rodriguez-Emmenegger, C.; Bauer, S.; Barner, L.; Rosenhahn, A.; Barner-Kowollik, C. Controlled growth of protein resistant PHEMA brushes via S-RAFT polymerization. *J Mater Chem B* **2013**, *1* (44). DOI: 10.1039/c3tb20880j.
- (101) Rakhmatullina, E.; Braun, T.; Kaufmann, T.; Spillmann, H.; Malinova, V.; Meier, W. Functionalization of Gold and Silicon Surfaces by Copolymer Brushes Using Surface-Initiated ATRP. *Macromolecular Chemistry and Physics* **2007**, *208* (12), 1283-1293. DOI: 10.1002/macp.200700119.

References

- (102) Balamurugan, S. S.; Subramanian, B.; Bolivar, J. G.; McCarley, R. L. Aqueous-based initiator attachment and ATRP grafting of polymer brushes from poly(methyl methacrylate) substrates. *Langmuir* **2012**, *28* (40), 14254-14260. DOI: 10.1021/la302922p From NLM Medline.
- (103) Wang, S.; Zhu, Y. Facile method to prepare smooth and homogeneous polymer brush surfaces of varied brush thickness and grafting density. *Langmuir* **2009**, *25* (23), 13448-13455. DOI: 10.1021/la901785t From NLM PubMed-not-MEDLINE.
- (104) Turgman-Cohen, S.; Genzer, J. Simultaneous bulk- and surface-initiated controlled radical polymerization from planar substrates. *J Am Chem Soc* **2011**, *133* (44), 17567-17569. DOI: 10.1021/ja2081636.
- (105) Morgese, G.; Benetti, E. M. Polyoxazoline biointerfaces by surface grafting. *European Polymer Journal* **2017**, *88*, 470-485. DOI: 10.1016/j.eurpolymj.2016.11.003.
- (106) Uhlig, K.; Boysen, B.; Lankenau, A.; Jaeger, M.; Wischerhoff, E.; Lutz, J. F.; Laschewsky, A.; Duschl, C. On the influence of the architecture of poly(ethylene glycol)-based thermoresponsive polymers on cell adhesion. *Biomicrofluidics* **2012**, *6* (2), 24129. DOI: 10.1063/1.4729130 From NLM PubMed-not-MEDLINE.
- (107) Su, X.; Shuai, Y.; Guo, Z.; Feng, Y. Functionalization of multi-walled carbon nanotubes with thermo-responsive azide-terminated poly(N-isopropylacrylamide) via click reactions. *Molecules* **2013**, *18* (4), 4599-4612. DOI: 10.3390/molecules18044599 From NLM Medline.
- (108) Biggs, C. I.; Walker, M.; Gibson, M. I. "Grafting to" of RAFTed Responsive Polymers to Glass Substrates by Thiol-Ene and Critical Comparison to Thiol-Gold Coupling. *Biomacromolecules* **2016**, *17* (8), 2626-2633. DOI: 10.1021/acs.biomac.6b00662 From NLM Medline.
- (109) Burgi, T. Properties of the gold-sulphur interface: from self-assembled monolayers to clusters. *Nanoscale* **2015**, *7* (38), 15553-15567. DOI: 10.1039/c5nr03497c From NLM PubMed-not-MEDLINE.
- (110) Vericat, C.; Vela, M. E.; Benitez, G.; Carro, P.; Salvarezza, R. C. Self-assembled monolayers of thiols and dithiols on gold: new challenges for a well-known system. *Chem Soc Rev* **2010**, *39* (5), 1805-1834. DOI: 10.1039/b907301a From NLM PubMed-not-MEDLINE.
- (111) Liu, G.; Cheng, H.; Yan, L.; Zhang, G. Study of the kinetics of the pancake-to-brush transition of poly(N-isopropylacrylamide) chains. *J Phys Chem B* **2005**, *109* (47), 22603-22607. DOI: 10.1021/jp0538417.
- (112) Olszewski, J. D.; Dorman, G.; Elliott, J. T.; Hong, Y.; Ahern, D. G.; Prestwich, G. D. Tethered benzophenone reagents for the synthesis of photoactivatable ligands. *Bioconjugate chemistry* **1995**, *6* (4), 395-400.
- (113) Farrell, I. S.; Toroney, R.; Hazen, J. L.; Mehl, R. A.; Chin, J. W. Photo-cross-linking interacting proteins with a genetically encoded benzophenone. *Nat Methods* **2005**, *2* (5), 377-384. DOI: 10.1038/nmeth0505-377 From NLM Medline.
- (114) Spighi, G.; Gaveau, M. A.; Mestdagh, J. M.; Poisson, L.; Soep, B. Gas phase dynamics of triplet formation in benzophenone. *Phys Chem Chem Phys* **2014**, *16* (20), 9610-9618. DOI: 10.1039/c4cp00423j From NLM PubMed-not-MEDLINE.
- (115) Takahashi, K.; Tezuka, H.; Kitamura, S.; Satoh, T.; Katoh, R. Reactions of excited-state benzophenone ketyl radical in a room-temperature ionic liquid. *Phys Chem Chem Phys* **2010**, *12* (8), 1963-1970. DOI: 10.1039/b920131a From NLM Medline.
- (116) Dorman, G.; Nakamura, H.; Pulsipher, A.; Prestwich, G. D. The Life of Pi Star: Exploring the Exciting and Forbidden Worlds of the Benzophenone Photophore. *Chem Rev* **2016**, *116* (24), 15284-15398. DOI: 10.1021/acs.chemrev.6b00342.
- (117) Demeter, A.; Horvath, K.; Boor, K.; Molnar, L.; Soos, T.; Lendvay, G. Substituent effect on the photoreduction kinetics of benzophenone. *J Phys Chem A* **2013**, *117* (40), 10196-10210. DOI: 10.1021/jp406269e From NLM PubMed-not-MEDLINE.
- (118) Ma, D.; Chen, H.; Shi, D.; Li, Z.; Wang, J. Preparation and characterization of thermo-responsive PDMS surfaces grafted with poly(N-isopropylacrylamide) by benzophenone-initiated photopolymerization. *J Colloid Interface Sci* **2009**, *332* (1), 85-90. DOI: 10.1016/j.jcis.2008.12.046 From NLM Medline.
- (119) Kecici, Z.; Babaoglu, S.; Temel, G. Methacrylated benzophenone as triple functional compound for the synthesis of partially crosslinked copolymers. *Progress in Organic Coatings* **2018**, *115*, 138-142. DOI: 10.1016/j.porgcoat.2017.11.015.
- (120) Healy, D.; Nash, M. E.; Gorelov, A.; Thompson, K.; Dockery, P.; Beloshapkin, S.; Rochev, Y. Fabrication and Application of Photocrosslinked, Nanometer-Scale, Physically Adsorbed Films for Tissue Culture Regeneration. *Macromol Biosci* **2017**, *17* (2). DOI: 10.1002/mabi.201600175 From NLM Medline.
- (121) Convertine, A. J.; Ayres, N.; Scales, C. W.; Lowe, A. B.; McCormick, C. L. Facile, controlled, room-temperature RAFT polymerization of N-isopropylacrylamide. *Biomacromolecules* **2004**, *5* (4), 1177-1180. DOI: 10.1021/bm049825h From NLM Medline.
- (122) Perrier, S. 50th Anniversary Perspective: RAFT Polymerization—A User Guide. *Macromolecules* **2017**, *50* (19), 7433-7447. DOI: 10.1021/acs.macromol.7b00767.

References

- (123) Kim, C. S.; Cho, S.; Lee, J. H.; Cho, W. K.; Son, K. S. Open-to-Air RAFT Polymerization on a Surface under Ambient Conditions. *Langmuir* **2020**, *36* (39), 11538-11545. DOI: 10.1021/acs.langmuir.0c01947 From NLM PubMed-not-MEDLINE.
- (124) Boyer, C.; Corrigan, N. A.; Jung, K.; Nguyen, D.; Nguyen, T. K.; Adnan, N. N.; Oliver, S.; Shanmugam, S.; Yeow, J. Copper-Mediated Living Radical Polymerization (Atom Transfer Radical Polymerization and Copper(0) Mediated Polymerization): From Fundamentals to Bioapplications. *Chem Rev* **2016**, *116* (4), 1803-1949. DOI: 10.1021/acs.chemrev.5b00396 From NLM Medline.
- (125) Keddie, D. J.; Moad, G.; Rizzardo, E.; Thang, S. H. RAFT Agent Design and Synthesis. *Macromolecules* **2012**, *45* (13), 5321-5342. DOI: 10.1021/ma300410v.
- (126) Yang, L.; Fan, X.; Zhang, J.; Ju, J. Preparation and Characterization of Thermoresponsive Poly(N-Isopropylacrylamide) for Cell Culture Applications. *Polymers (Basel)* **2020**, *12* (2). DOI: 10.3390/polym12020389 From NLM PubMed-not-MEDLINE.
- (127) Murad Bhayo, A.; Yang, Y.; He, X. Polymer brushes: Synthesis, characterization, properties and applications. *Progress in Materials Science* **2022**, *130*. DOI: 10.1016/j.pmatsci.2022.101000.
- (128) Israelachvili, J. N. Surface forces. In *The Handbook of Surface Imaging and Visualization*, CRC Press, 2022; pp 793-816.
- (129) Baulin, V. A.; Zhulina, E. B.; Halperin, A. Self-consistent field theory of brushes of neutral water-soluble polymers. *J Chem Phys* **2003**, *119* (20), 10977-10988. DOI: 10.1063/1.1619934.
- (130) Yim, H.; Kent, M. S.; Satija, S.; Mendez, S.; Balamurugan, S. S.; Balamurugan, S.; Lopez, G. P. Evidence for vertical phase separation in densely grafted, high-molecular-weight poly(-isopropylacrylamide) brushes in water. *Phys Rev E* **2005**, *72* (5 Pt 1), 051801. DOI: 10.1103/PhysRevE.72.051801.
- (131) Ma, H.; Textor, M.; Clark, R. L.; Chilkoti, A. Monitoring kinetics of surface initiated atom transfer radical polymerization by quartz crystal microbalance with dissipation. *Biointerphases* **2006**, *1* (1), 35. DOI: 10.1116/1.2190697 From NLM PubMed-not-MEDLINE.
- (132) Plunkett, K. N.; Zhu, X.; Moore, J. S.; Leckband, D. E. PNIPAM chain collapse depends on the molecular weight and grafting density. *Langmuir* **2006**, *22* (9), 4259-4266. DOI: 10.1021/la0531502.
- (133) Ishida, N.; Biggs, S. Direct observation of the phase transition for a poly(N-isopropylacrylamide) layer grafted onto a solid surface by AFM and QCM-D. *Langmuir* **2007**, *23* (22), 11083-11088. DOI: 10.1021/la701461b.
- (134) Arima, Y.; Iwata, H. Effect of wettability and surface functional groups on protein adsorption and cell adhesion using well-defined mixed self-assembled monolayers. *Biomaterials* **2007**, *28* (20), 3074-3082. DOI: 10.1016/j.biomaterials.2007.03.013 From NLM Medline.
- (135) Xue, C.; Yonet-Tanyeri, N.; Brouette, N.; Sferrazza, M.; Braun, P. V.; Leckband, D. E. Protein adsorption on poly(N-isopropylacrylamide) brushes: dependence on grafting density and chain collapse. *Langmuir* **2011**, *27* (14), 8810-8818. DOI: 10.1021/la2001909 From NLM Medline.
- (136) Zhang, G. Study on Conformation Change of Thermally Sensitive Linear Grafted Poly(N-isopropylacrylamide) Chains by Quartz Crystal Microbalance. *Macromolecules* **2004**, *37* (17), 6553-6557. DOI: 10.1021/ma035937+.
- (137) Bittrich, E.; Burkert, S.; Muller, M.; Eichhorn, K. J.; Stamm, M.; Uhlmann, P. Temperature-sensitive swelling of poly(N-isopropylacrylamide) brushes with low molecular weight and grafting density. *Langmuir* **2012**, *28* (7), 3439-3448. DOI: 10.1021/la204230a.
- (138) Zhuang, P.; Dirani, A.; Glinel, K.; Jonas, A. M. Temperature Dependence of the Surface and Volume Hydrophilicity of Hydrophilic Polymer Brushes. *Langmuir* **2016**, *32* (14), 3433-3444. DOI: 10.1021/acs.langmuir.6b00448.
- (139) Ruoslahti, E.; Reed, J. C. Anchorage dependence, integrins, and apoptosis. *Cell* **1994**, *77* (4), 477-478. DOI: 10.1016/0092-8674(94)90209-7 From NLM Medline.
- (140) Conzatti, G.; Cavalie, S.; Combes, C.; Torrisani, J.; Carrere, N.; Tourrette, A. PNIPAM grafted surfaces through ATRP and RAFT polymerization: Chemistry and bioadhesion. *Colloids Surf B Biointerfaces* **2017**, *151*, 143-155. DOI: 10.1016/j.colsurfb.2016.12.007 From NLM Medline.
- (141) Wilson, C. J.; Clegg, R. E.; Leavesley, D. I.; Pearcy, M. J. Mediation of biomaterial-cell interactions by adsorbed proteins: a review. *Tissue Eng* **2005**, *11* (1-2), 1-18. DOI: 10.1089/ten.2005.11.1 From NLM Medline.
- (142) Pertsin, A. J.; Grunze, M. Computer Simulation of Water near the Surface of Oligo(ethylene glycol)-Terminated Alkanethiol Self-Assembled Monolayers. *Langmuir* **2000**, *16* (23), 8829-8841. DOI: 10.1021/la000340y.
- (143) Ma, Z.; Mao, Z.; Gao, C. Surface modification and property analysis of biomedical polymers used for tissue engineering. *Colloids Surf B Biointerfaces* **2007**, *60* (2), 137-157. DOI: 10.1016/j.colsurfb.2007.06.019 From NLM Medline.
- (144) Aiyelabegan, H. T.; Sadroddiny, E. Fundamentals of protein and cell interactions in biomaterials. *Biomed Pharmacother* **2017**, *88*, 956-970. DOI: 10.1016/j.biopha.2017.01.136 From NLM Medline.

References

- (145) Verdanova, M.; Sauerova, P.; Hempel, U.; Kalbacova, M. H. Initial cell adhesion of three cell types in the presence and absence of serum proteins. *Histochem Cell Biol* **2017**, *148* (3), 273-288. DOI: 10.1007/s00418-017-1571-7 From NLM Medline.
- (146) Horbett, T. A.; Schway, M. B. Correlations between mouse 3T3 cell spreading and serum fibronectin adsorption on glass and hydroxyethylmethacrylate-ethylmethacrylate copolymers. *J Biomed Mater Res* **1988**, *22* (9), 763-793. DOI: 10.1002/jbm.820220903 From NLM Medline.
- (147) Engler, A.; Bacakova, L.; Newman, C.; Hategan, A.; Griffin, M.; Discher, D. Substrate compliance versus ligand density in cell on gel responses. *Biophysical Journal* **2004**, *86* (1), 617-628.
- (148) Bacakova, L.; Filova, E.; Kubies, D.; Machova, L.; Proks, V.; Malinova, V.; Lisa, V.; Rypacek, F. Adhesion and growth of vascular smooth muscle cells in cultures on bioactive RGD peptide-carrying polylactides. *J Mater Sci Mater Med* **2007**, *18* (7), 1317-1323. DOI: 10.1007/s10856-006-0074-1 From NLM Medline.
- (149) Lee, J.; Lee, H.; Andrade, J. Blood compatibility of polyethylene oxide surfaces. *Progress in Polymer Science* **1995**, *20* (6), 1043-1079. DOI: 10.1016/0079-6700(95)00011-4.
- (150) Pei, J.; Hall, H.; Spencer, N. D. The role of plasma proteins in cell adhesion to PEG surface-density-gradient-modified titanium oxide. *Biomaterials* **2011**, *32* (34), 8968-8978. DOI: 10.1016/j.biomaterials.2011.08.034 From NLM Medline.
- (151) Mei, Y.; Wu, T.; Xu, C.; Langenbach, K. J.; Elliott, J. T.; Vogt, B. D.; Beers, K. L.; Amis, E. J.; Washburn, N. R. Tuning cell adhesion on gradient poly(2-hydroxyethyl methacrylate)-grafted surfaces. *Langmuir* **2005**, *21* (26), 12309-12314. DOI: 10.1021/la050668x From NLM Medline.
- (152) Pelton, R. Poly(N-isopropylacrylamide) (PNIPAM) is never hydrophobic. *J Colloid Interface Sci* **2010**, *348* (2), 673-674. DOI: 10.1016/j.jcis.2010.05.034 From NLM PubMed-not-MEDLINE.
- (153) Fukumori, K.; Akiyama, Y.; Kumashiro, Y.; Kobayashi, J.; Yamato, M.; Sakai, K.; Okano, T. Characterization of ultra-thin temperature-responsive polymer layer and its polymer thickness dependency on cell attachment/detachment properties. *Macromol Biosci* **2010**, *10* (10), 1117-1129. DOI: 10.1002/mabi.201000043 From NLM Medline.
- (154) Baume, A. S.; Boughton, P. C.; Coleman, N. V.; Ruys, A. J. Sterilization of tissue scaffolds. In *Characterisation and Design of Tissue Scaffolds*, 2016; pp 225-244.
- (155) Lakhani, P.; Faoagali, J.; Steinhardt, R.; Olesen, D. Shelf life of sterilized packaged items stored in acute care hospital settings: factors for consideration. *Healthcare Infection* **2013**, *18* (3), 121-129. DOI: 10.1071/hi13002.
- (156) 96 Well Plate, UpCell Temperature Responsive Surface, Pack of 1. <https://www.thermofisher.com/order/catalog/product/174897> (accessed 2024-07-02).
- (157) Hadar, J.; Tirosh, T.; Grafstein, O.; Korabelnikov, E. Autoclave Emissions—Hazardous or Not. *Journal of the American Biological Safety Association* **2016**, *2* (3), 44-51. DOI: 10.1177/109135059700200309.
- (158) Nair, P. D. Morphological changes of poly(ethylene terephthalate) on multiple steam sterilization. *Clin Mater* **1990**, *5* (1), 43-46. DOI: 10.1016/0267-6605(90)90070-c From NLM Medline.
- (159) Kanemitsu, K.; Imasaka, T.; Ishikawa, S.; Kunishima, H.; Harigae, H.; Ueno, K.; Takemura, H.; Hirayama, Y.; Kaku, M. A comparative study of ethylene oxide gas, hydrogen peroxide gas plasma, and low-temperature steam formaldehyde sterilization. *Infect Control Hosp Epidemiol* **2005**, *26* (5), 486-489. DOI: 10.1086/502572 From NLM Medline.
- (160) Sedlacek, O.; Kucka, J.; Monnery, B. D.; Slouf, M.; Vetric, M.; Hoogenboom, R.; Hruby, M. The effect of ionizing radiation on biocompatible polymers: From sterilization to radiolysis and hydrogel formation. *Polym Degrad Stab* **2017**, *137*, 1-10. DOI: 10.1016/j.polymdegradstab.2017.01.005.
- (161) Parsons, B. J. Sterilisation of healthcare products by ionising radiation: principles and standards. In *Sterilisation of Biomaterials and Medical Devices*, 2012; pp 56-70.
- (162) Sharma, S.; Johnson, R. W.; Desai, T. A. Evaluation of the stability of nonfouling ultrathin poly(ethylene glycol) films for silicon-based microdevices. *Langmuir* **2004**, *20* (2), 348-356. DOI: 10.1021/la034753l From NLM Medline.
- (163) Pidhatika, B.; Rodenstein, M.; Chen, Y.; Rakhmatullina, E.; Muhlebach, A.; Acikgoz, C.; Textor, M.; Konradi, R. Comparative stability studies of poly(2-methyl-2-oxazoline) and poly(ethylene glycol) brush coatings. *Biointerphases* **2012**, *7* (1-4), 1. DOI: 10.1007/s13758-011-0001-y From NLM Medline.
- (164) Iqbal, Z.; Moses, W.; Kim, S.; Kim, E. J.; Fissell, W. H.; Roy, S. Sterilization effects on ultrathin film polymer coatings for silicon-based implantable medical devices. *J Biomed Mater Res B Appl Biomater* **2018**, *106* (6), 2327-2336. DOI: 10.1002/jbm.b.34039.
- (165) Bretagnol, F.; Rauscher, H.; Hasiwa, M.; Kylian, O.; Ceccone, G.; Hazell, L.; Paul, A. J.; Lefranc, O.; Rossi, F. The effect of sterilization processes on the bioadhesive properties and surface chemistry of a plasma-polymerized polyethylene glycol film: XPS characterization and L929 cell proliferation tests. *Acta Biomater* **2008**, *4* (6), 1745-1751. DOI: 10.1016/j.actbio.2008.06.013.

References

- (166) Kikuchi, A.; Okuhara, M.; Karikusa, F.; Sakurai, Y.; Okano, T. Two-dimensional manipulation of confluent cultured vascular endothelial cells using temperature-responsive poly(N-isopropylacrylamide)-grafted surfaces. *J Biomater Sci Polym Ed* **1998**, *9* (12), 1331-1348. DOI: 10.1163/156856298x00424 From NLM Medline.
- (167) Berry, D. J.; Currier, B. H.; Mayor, M. B.; Collier, J. P. Gamma-irradiation sterilization in an inert environment: a partial solution. *Clin Orthop Relat Res* **2012**, *470* (7), 1805-1813. DOI: 10.1007/s11999-011-2150-1 From NLM Medline.
- (168) Seitz, J. M.; Durisin, M.; Goldman, J.; Drelich, J. W. Recent advances in biodegradable metals for medical sutures: a critical review. *Adv Healthc Mater* **2015**, *4* (13), 1915-1936. DOI: 10.1002/adhm.201500189 From NLM Medline.
- (169) Deng, J.; Ren, T.; Zhu, J.; Mao, Z.; Gao, C. Adsorption of plasma proteins and fibronectin on poly(hydroxyethyl methacrylate) brushes of different thickness and their relationship with adhesion and migration of vascular smooth muscle cells. *Regen Biomater* **2014**, *1* (1), 17-25. DOI: 10.1093/rb/rbu008 From NLM PubMed-not-MEDLINE.
- (170) Benhabbour, S. R.; Sheardown, H.; Adronov, A. Cell adhesion and proliferation on hydrophilic dendritically modified surfaces. *Biomaterials* **2008**, *29* (31), 4177-4186. DOI: 10.1016/j.biomaterials.2008.07.016 From NLM Medline.

8. Publications and conference contributions

Peer-reviewed publications

(1) Schweigerdt, A.; Heinen, S.; Stobener, D. D.; Weinhart, M. Grafting Density-Dependent Phase Transition Mechanism of Thermoresponsive Poly(glycidyl ether) Brushes: A Comprehensive QCM-D Study. *Langmuir* **2021**, *37* (23), 7087-7096. DOI: 10.1021/acs.langmuir.1c00695.

(2) Schweigerdt, A.; Stöbener, D. D.; Schäfer, A.; Kara, S.; Weinhart, M. Impact of Amphiphilicity Balance in Hydroxy-Functional, Isomeric, Thermoresponsive Poly(meth)acrylates. *Macromolecules* **2023**, *56* (21), 8602-8613. DOI: 10.1021/acs.macromol.3c01251.

(3) Schweigerdt, A.; Stöbener, D. D.; Scholz, J.; Schäfer, A.; Weinhart, M. Thermoresponsive brush coatings for cell sheet engineering with low protein adsorption below and above the polymers' phase transition temperature. *ACS Biomater Sci Eng* **2024**, *submitted*.

Posters

Schweigerdt, A.; Stöbener, D. D.; Scholz, J.; Weinhart, M. „Poly(glycidyl ether)brushes for Cell Sheet Fabrication” at *Materialinnovationen für gesundes Leben: ProMatLeben – Polymere, Berlin, Germany, 2019*.

Schweigerdt, A.; Stöbener, D. D.; Weinhart, M. „Bulk vs. Surface Phase Transition of Thermoresponsive Poly(glycidyl ether) Brushes - Impact on Cell Adhesion and Cell Sheet Detachment” at *Makromolekulares Kolloquium, Freiburg, Germany, 2020*.

Schweigerdt, A.; Schäfer, A.; Weinhart, M. „The influence of hydrophobicity balance in novel glycerol-containing poly(meth acrylates) on their phase transition properties” at *EPF European Polymer Congress, Prague, Czech Republic, 2022*.